Appendix H

Spectral Analysis of Surface Waves

Hanford Site-Wide Probabilistic Seismic Hazard Analysis (PSHA): Seismic Shear Wave Velocity Profiling at Hanford, WA

SASW Testing and Analysis Procedures, V_s Profiles, Sensitivity Studies and Responses to Technical Integration Team Questions

for

Pacific Northwest National Laboratory
Richland, WA

by

Kenneth H. Stokoe, II
Yin-Cheng Lin
Sungmoon Hwang, and
Julia Roberts

May 7, 2014

Geotechnical Engineering Report GR14-1
Geotechnical Engineering Center
Civil Engineering Department
The University of Texas at Austin

DCN: GR14-1
Revision 0, May 7, 2014

TABLE OF CONTENTS

LIST OF TABLES iii
LIST OF FIGURES iv
1.0 INTRODUCTION 1
2.0 OVERVIEW OF THE SASW TEST METHOD 4
3.0 SUMMARY OF PROCEDURES USED AT THE HANFORD SITES 10
3.1 Field Equipment and Testing Procedure 10
3.2 Spectral Calculations 14
3.3 Data Reduction and Forward Modeling Procedure 15
3.3.1 Constructing the Individual and Composite Field Dispersion Curves 17
3.3.2 Matching the Composite Field and Theoretical Dispersion Curves 17
3.3.3 Additional Considerations 21
4.0 DISCUSSION OF V_S PROFILES AT 12 DEEP TEST LOCATIONS 23
5.0 SUMMARY AND CONCLUSIONS 32
6.0 REFERENCES 33
APPENDIX A Field Dispersion Data and Associated V_S Profiles at the 13 Sites ..... A-1 through A-55
APPENDIX B Sensitivity Study: Impact on the Theoretical Dispersion Curve of Changing V_S of the Bottom Layer ..... B-1 through B-13
APPENDIX C Sensitivity Study: Impact on the V_S Profiles of Changing the Water Table Depth ..... C-1 through C-25
APPENDIX D Responses to Questions from Technical Integration Team ..... D-1 through D-24

Appendix H

SASW Testing and Analysis Procedures, V_s Profiles, Sensitivity Studies and Responses to Technical Integration Team Questions

Hanford Site-Wide Probabilistic Seismic Hazard Analysis (PSHA): Seismic Shear Wave Velocity Profiling at Hanford, WA

SASW Testing and Analysis Procedures, V_s Profiles, Sensitivity Studies and Responses to Technical Integration Team Questions

for

Pacific Northwest National Laboratory
Richland, WA

by

Kenneth H. Stokoe, II
Yin-Cheng Lin
Sungmoon Hwang, and
Julia Roberts

May 7, 2014

Geotechnical Engineering Report GR14-1
Geotechnical Engineering Center
Civil Engineering Department
The University of Texas at Austin

DCN: GR14-1
Revision 0, May 7, 2014

TABLE OF CONTENTS

LIST OF TABLES iii
LIST OF FIGURES iv
1.0 INTRODUCTION 1
2.0 OVERVIEW OF THE SASW TEST METHOD 4
3.0 SUMMARY OF PROCEDURES USED AT THE HANFORD SITES 10
3.1 Field Equipment and Testing Procedure 10
3.2 Spectral Calculations 14
3.3 Data Reduction and Forward Modeling Procedure 15
3.3.1 Constructing the Individual and Composite Field Dispersion Curves 17
3.3.2 Matching the Composite Field and Theoretical Dispersion Curves 17
3.3.3 Additional Considerations 21
4.0 DISCUSSION OF V_S PROFILES AT 12 DEEP TEST LOCATIONS 23
5.0 SUMMARY AND CONCLUSIONS 32
6.0 REFERENCES 33
APPENDIX A Field Dispersion Data and Associated V_S Profiles at the 13 Sites ..... A-1 through A-55
APPENDIX B Sensitivity Study: Impact on the Theoretical Dispersion Curve of Changing V_S of the Bottom Layer ..... B-1 through B-13
APPENDIX C Sensitivity Study: Impact on the V_S Profiles of Changing the Water Table Depth ..... C-1 through C-25
APPENDIX D Responses to Questions from Technical Integration Team ..... D-1 through D-24

LIST OF TABLES

Table 1 Example Source-Receiver Spacings and Associated Information Used in SASW Testing at the Hanford Test Sites 11

Table 2 Parameters Used to Obtain the Vs Profile of Site H3A Shown in Figure 15 20

LIST OF FIGURES

Figure 1 Map of the 12, Deep SASW Testing Locations around the Hanford Site.....3

Figure 2 Illustration of Surface Waves with Different Wavelengths Sampling Different Materials in a Layered System which Results in Dispersion in Wave Velocities 5

Figure 3 Schematic Diagram of the Generalized Equipment Arrangement Used in Spectral-Analysis-of-Surface-Waves (SASW) Testing 5

Figure 4 Comparison of Shear Wave Velocity Profiles from SASW and Crosshole Measurements Performed at a Site on Treasure Island in California (Joh, 1996; Fuhriman and Stokoe, 1993) 7

Figure 5 Comparison between SASW and Downhole Vs profiles at Site H2 in Hanford, WA (Stokoe et al., 2005) 8

Figure 6 Comparison of SASW and Downhole Median Profiles of Both Sand and Gravel Sequences in the Hanford Formation (Stokoe et al., 2005).....9

Figure 7 Common-Middle-Receiver Geometry Used in SASW Testing at Hanford Sites.....11

Figure 8 Photograph of 1-Hz Geophone Semi-embedded in the Gravel Surface and the Pre-test Check for Plumbness at Site H1K.....12

Figure 9 Photograph of Professor Kenneth Stokoe, Using the Sledge Hammer Source and Mr. Sungmoon Hwang and Ms. Julia Roberts(inside the van) Recording the Seismic Signals at Site H3A 13

Figure 10 Photograph of Liquidator Operating in Stepped-Sine Mode at Site WIAB.....14

Figure 11 Phase of the Cross Power Spectrum Measured at Site H3A with the Liquidator as the Seismic Source and a 700-ft Spacing between the Receivers 16

Figure 12 Individual Experimental Dispersion Curve Created from the Wrapped Phase Record in Figure 11b Measured with a 700-ft Receiver Spacing at Site H3A 18

Figure 13 Composite Experimental Dispersion Curve Created from Phase Measurements Performed at all Receiver Spacings at Site H3A 18

Figure 14 Comparison of the Fit of the Theoretical Dispersion Curve to the Composite Experimental Dispersion Curve at Site H3A 19

Figure 15 Final Shear Wave Velocity Profile Determined at Site H3A 20

Figure 16 Summary of all 12 Deep V_S Profiles at the Hanford Site.....24

Figure 17 Portions of the 12 Deep V_S Profiles with $V_S \leq 2600$ fps ft/sec 25

Figure 18 Portions of the 12 Deep V_S Profiles with 3000 ft/sec $\leq V_S <$ 4600 ft/sec 26

Figure 19 Portions of the 12 Deep V_S Profiles with 5000 ft/sec $\leq V_S <$ 8000 ft/sec 27

Figure 20 Portions of the 12 Deep V_S Profiles with $V_S <$ 8000 ft/sec 28

Figure 21 Map of SASW Near-by Test Locations in 2004 and 2013.....29

Figure 22 Comparison of the V_S Profiles of Site H2E (2013) and Site H3 (2004) 30

Figure 23 Comparison of the V_S Profiles of Site 100B (2013) and Site H10 (2004) 31

1.0 INTRODUCTION

This report presents the findings from field seismic tests that were performed at 12 sites of deep profiling and one site of shallow profiling at the Hanford Site. The Spectral-Analysis-of-Surface-Waves (SASW) method was employed in this work. The primary objective of the seismic testing was to determine shear wave velocity (V_S) profiles to depths exceeding 600 ft, termed "deep" profiling herein, around the Hanford Site. The general locations of the 12 SASW test sites are shown in Figure 1. Testing was conducted between April 8 and 14, 2013. Professor Kenneth H. Stokoe, II and personnel from the University of Texas at Austin (Ms. Julia Roberts, Mr. Sungmoon Hwang and Mr. Cecil Hoffpauir) performed the SASW tests in the field. Analyses of the SASW data and comparisons of the V_S profiles were performed by Dr. Yin-Cheng Lin and Prof. Stokoe.

The objective of the 12 deep seismic investigations was to develop shear wave velocity profiles to depths of 600 feet or more at each test site. This objective was achieved or exceeded at all 12 sites. The shallowest of these profiles (Site WIXX) extends to a depth of 604 ft. The deepest profile (Site 100B) extends to a depth of 1068 ft. The second objective was simply to develop a shallow V_S profile through the concrete floor in the missile bunker. The missile bunker is next to Site HAWA 2 in Figure 1. This objective was not achieved on the first site visit in April, 2013. Therefore, a second site visit was conducted by Mr. Sungmoon Hwang on July 29, 2013 using hand-held hammer sources and accelerometers as seismic receivers. The second site visit was successful.

The report documenting the SASW testing and results is presented herein. The report contains a discussion of the SASW test method as applied at the Hanford Site. The SASW field testing and data analysis procedures are described, a brief discussion of additional considerations entering the data analysis is given, and results of the measurements at each test location are presented in graphical and tabular forms. The 12 deep V_S profiles are compared with each other and portions of the profiles with similar wave velocities are grouped together. V_s profiles at two near-by locations where SASW testing was conducted in 2004 are also compared with the profiles in this study.

This report also contains four appendices as follows. In Appendix A, the complete sets of "raw" data (wrapped phase plot versus frequency) for all 13 sites are presented. The final fits of the theoretical and experimental dispersion curves using 3-D global forward modeling and 3-D array-based forward modeling are shown for each site. The resulting V_S profile for each site is then presented. In Appendix B, the results of a sensitivity study of the impact on the theoretical dispersion curve of changing the V_S value of the bottom layer by multiplying or dividing by a factor of 1.25 are presented. In Appendix C, the results of a sensitivity study of the impact on the V_S profiles of changing the depth of the water table by +/- 25% are presented. The work presented in Appendices B and C was conducted at the request of the Hanford PSHA Ground Motion Characterization (GMC) Technical Integration (TI) Team. The last appendix, Appendix D, contains answers to six questions posed by the TI Team.

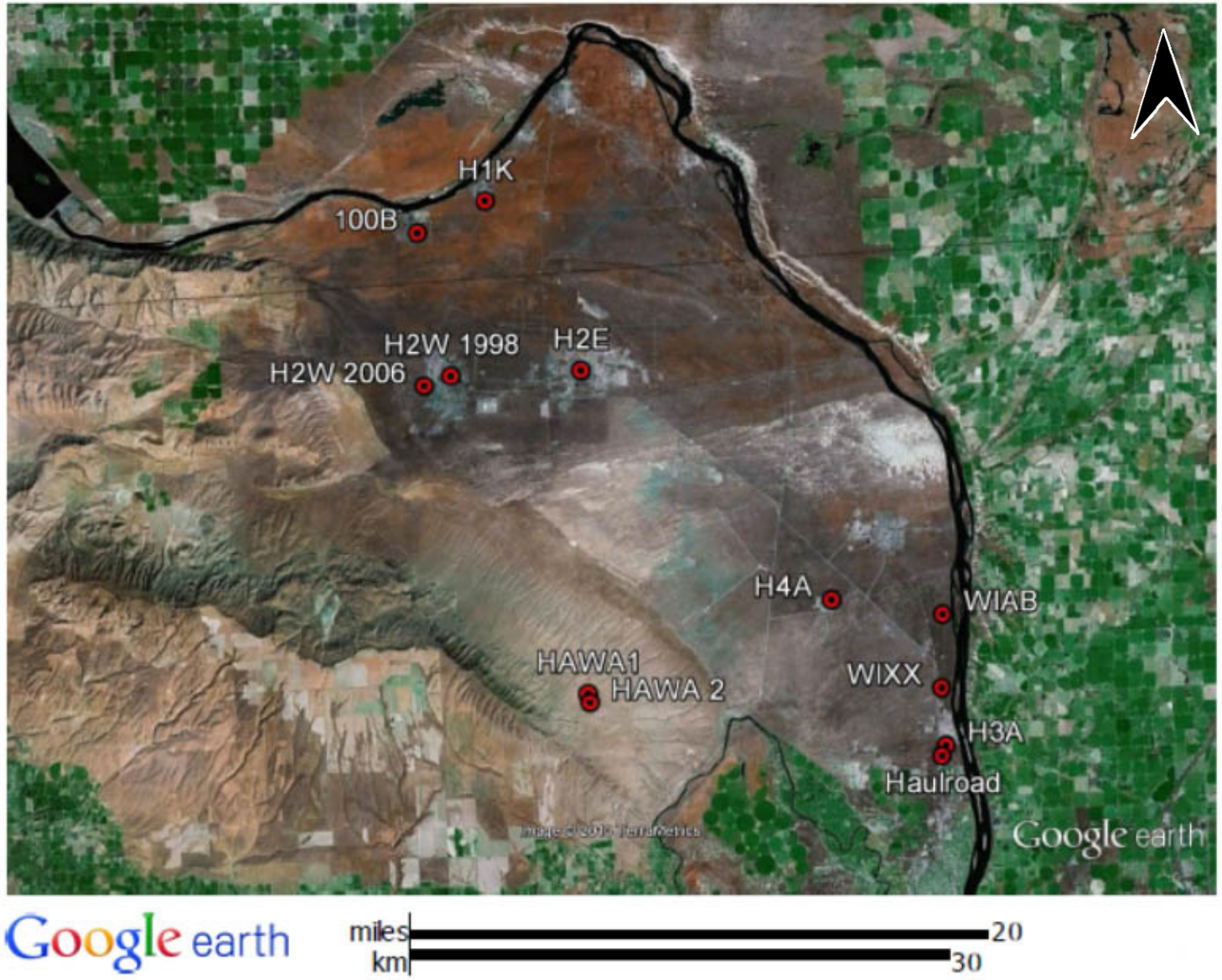

Figure 1 Map of the 12, Deep SASW Testing Locations around the Hanford Site

2.0 OVERVIEW OF THE SASW TEST METHOD

The SASW test method is a nondestructive and nonintrusive seismic method. The method utilizes the dispersive nature of Rayleigh-type surface waves propagating through a layered material to determine the shear wave velocity profile of the material (Stokoe et al., 1994). In this context, dispersion arises when surface wave velocity varies with wavelength or frequency. Dispersion in surface wave velocity arises from changing stiffness properties of the soil and rock layers with depth. This phenomenon is illustrated in Figure 2 for a multi-layered solid. A high-frequency surface wave, which propagates with a short wavelength, only stresses material near the exposed surface and thus only samples the properties of the shallow, near-surface material (Figure 2b). A lower-frequency surface wave, which has a longer wavelength, stresses material to a greater depth and thus samples the properties of the shallower and deeper materials (Figure 2c). Spectral analysis is used to separate the waves by frequency and wavelength to determine the experimental ("field") dispersion curve for the site. An analytical, forward - modeling procedure is then used to theoretically match the field dispersion curve with a one-dimensional layered system of varying layer stiffnesses and thicknesses (Joh, 1996). The one-dimensional shear wave velocity profile that generates a dispersion curve that most closely matches the field dispersion curve is presented as the shear wave velocity profile at the site.

SASW testing involves generating surface waves at one location on the exposed material surface and simultaneously measuring the motions perpendicular to the surface created by the passage of surface waves between pairs of receiver locations. This general testing configuration for one source/receiver set-up is illustrated in Figure 3. In this example, a source and one pair of receivers are used. The distance between the source and first receiver (d) is kept equal to the distance between the pair of receivers (d) as shown in Figure 3. All measurement points are arranged on the exposed surface along a single radial path from the source. Successively longer spacings between the receivers and between the source and first receiver are typically used to measure progressively longer and longer wavelengths. Testing is performed with several (typically 7 or more) sets of source-receiver spacings, depending on the profiling depth. The totality of all sets of source-receiver spacings is called an SASW array.

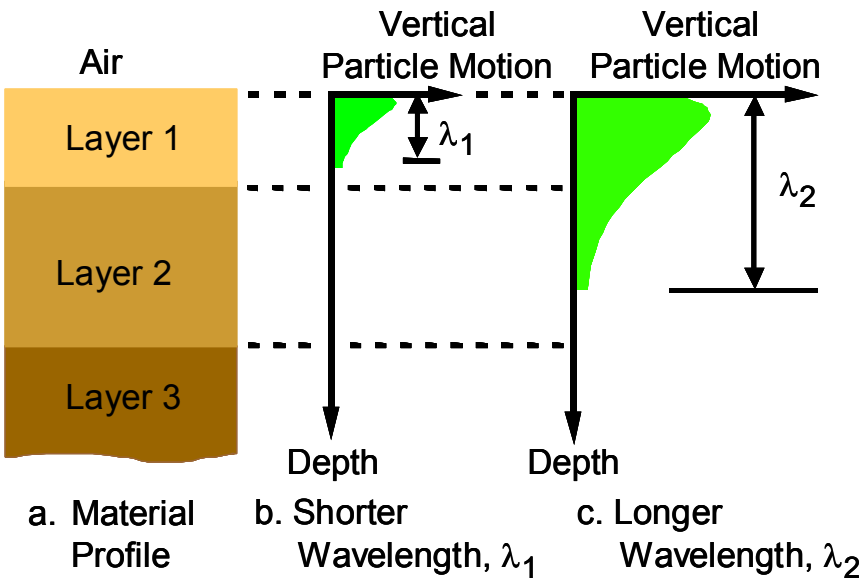

Figure 2 Illustration of Surface Waves with Different Wavelengths Sampling Different Materials in a Layered System which Results in Dispersion in Wave Velocities

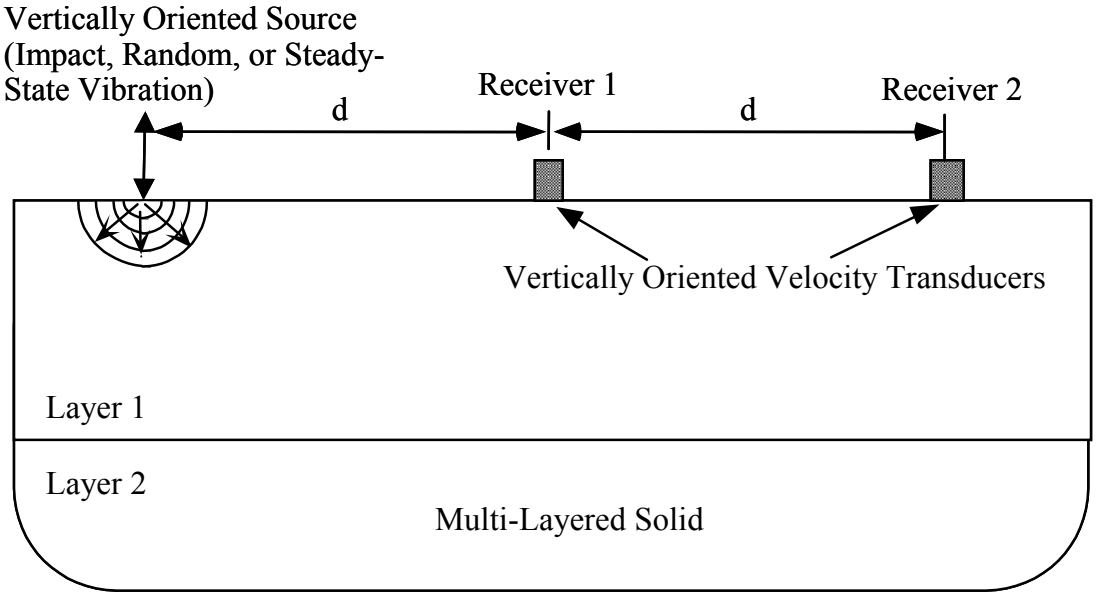

Figure 3 Schematic Diagram of the Generalized Equipment Arrangement Used in Spectral-Analysis-of-Surface-Waves (SASW) Testing

The variation in phase shift with frequency for surface waves propagating between receiver pairs is recorded for each source and receiver pair. With each receiver pair, the phase velocity of the surface wave is calculated at each frequency from:

$$V_R = f \bullet \frac{360}{\phi} \bullet d \qquad (1)$$

where V_R is the phase velocity in ft/sec or m/s, f is the frequency in Hertz (cycles per sec), ϕ is the phase angle in degrees (at frequency f), and d is the distance between the receivers in the pair in the same length units as used to represent V_R. From this calculation, a plot of phase velocity versus frequency, called an individual dispersion curve, is generated. This procedure is repeated for all source-receiver spacings used at the site and typically involves significant overlapping in the dispersion data between adjacent receiver pairs. The individual dispersion curves from all receiver pairs are combined into a single composite dispersion curve called the "experimental" or "field" dispersion curve.

Once the composite field dispersion curve is generated for the site, an iterative forward modeling procedure is used to create a theoretical dispersion curve to match the experimental curve (Joh, 1996). The stiffness profile that provides the best match to the experimental dispersion curve is presented as the shear wave velocity profile at the site. Typical comparisons between V_s profiles measured by SASW testing and by independent crosshole and downhole seismic tests are presented in Figures 4, 5 and 6 for work conducted in earlier studies (Joh, 1996; Fuhriman and Stokoe, 1993; Stokoe et al, 2005).

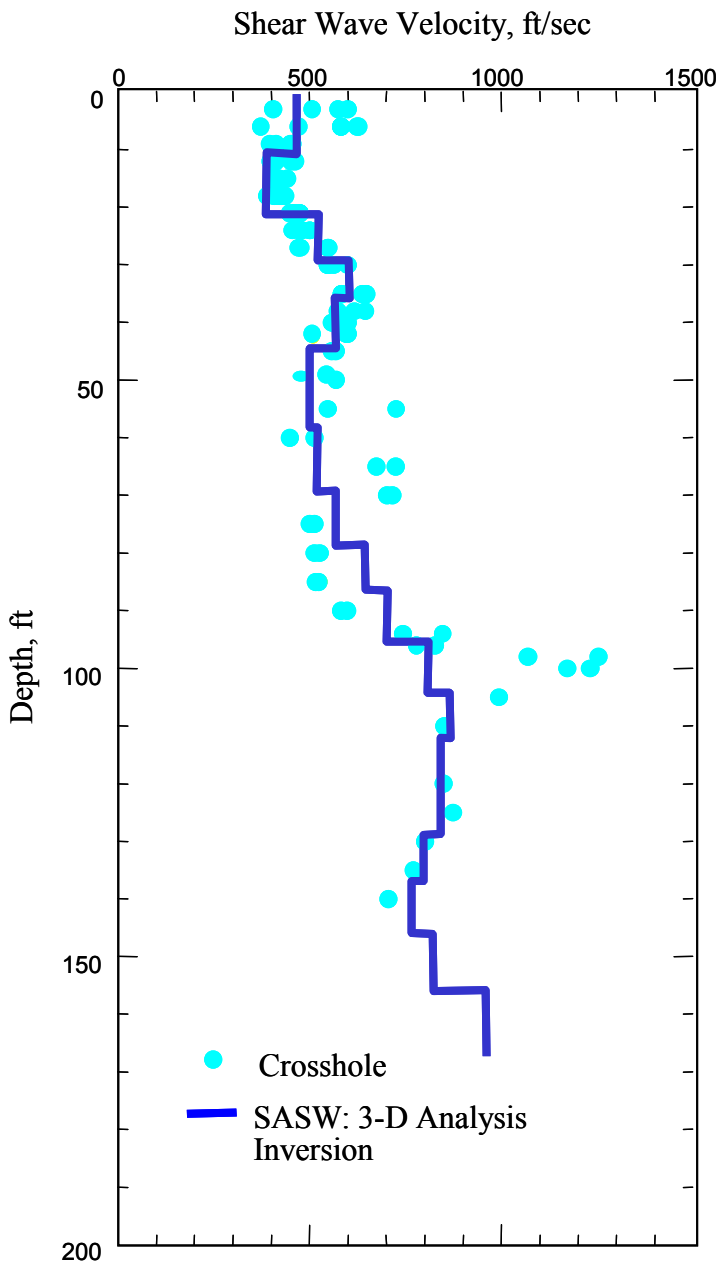

Figure 4 Comparison of Shear Wave Velocity Profiles from SASW and Crosshole Measurements Performed at a Site on Treasure Island in California (Joh, 1996; Fuhriman and Stokoe, 1993)

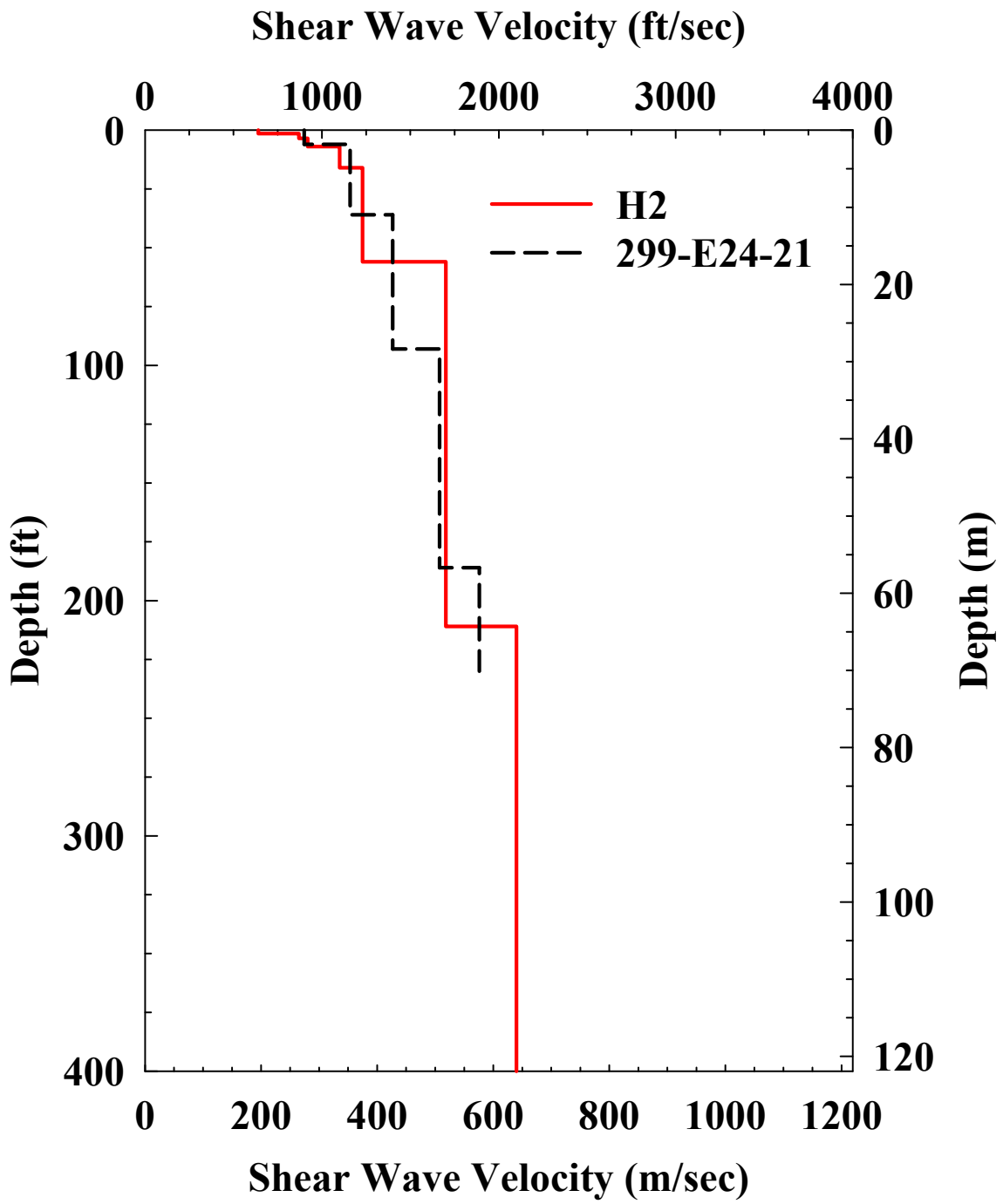

Figure 5 Comparison between SASW and Downhole V_s profiles at Site H2 in Hanford, WA (Stokoe et al., 2005)

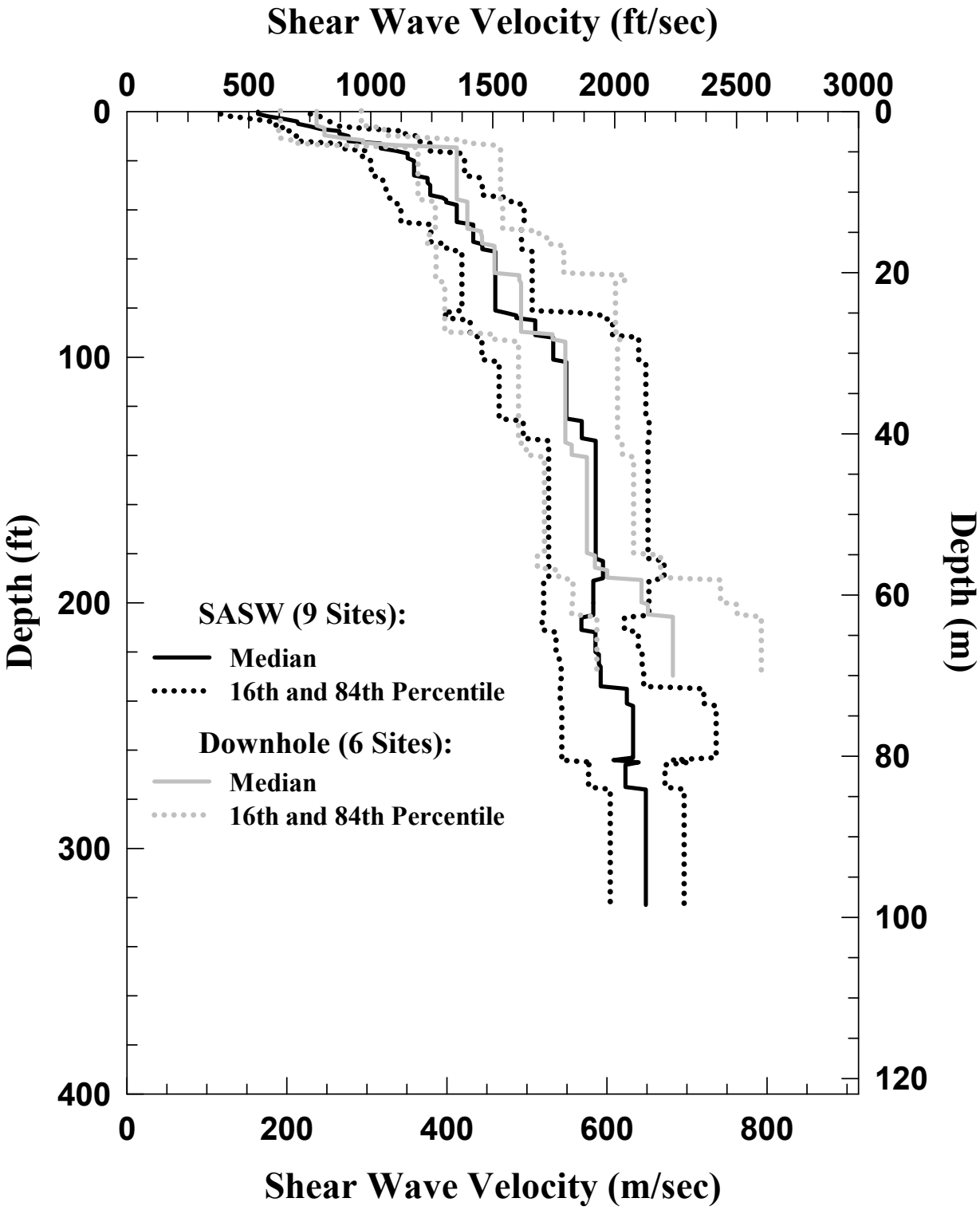

Figure 6 Comparison of SASW and Downhole Median Profiles of Both Sand and Gravel Sequences in the Hanford Formation (Stokoe et al., 2005)

3.0 SUMMARY OF PROCEDURES USED AT THE HANFORD SITES

3.1 Field Equipment and Testing Procedure

A total of 12 SASW test arrays were evaluated at locations around the Hanford Site. The basic configuration of the source and receivers used in field testing at each array location is illustrated in Figure 7. Three receivers were used at each source/receiver set-up. This arrangement enabled two sets of SASW test results to be obtained at the same time, thereby cutting testing time in half as compared to using only two receivers (as illustrated in Figure 3). The middle receiver (receiver #2) was located at the center line of the test array at all times. When different spacings were used and/or reverse directions were tested, only receivers #1 and #3 and the source were moved. For the shorter spacings, usually source-to-receiver spacings of 24 ft or less, tests were performed in both the forward and reverse directions using a sledge hammer for an impact source. For the larger spacings, usually source-to-receiver spacings of 30 ft and greater, testing was performed only in the forward direction using a large vibroseis truck (called "Liquidator") as the source. Reverse direction testing was not performed with Liquidator due to the difficulty of finding multiple locations to place this large machine (weight of about 70,000 lb).

Distances between receivers of 4, 8, 12, 24, 30, 60, 75, 150, 250, 350, 500, 700, and 1000 ft were typically used (see Table 1) when space considerations allowed. This number and progression of receiver spacings resulted in extensive overlapping of the individual dispersion curves used to develop a composite field curve, thereby enhancing the test reliability and confirming global lateral uniformity over the test array. The longest spacing used in the SASW arrays at Hanford was 1000 ft at Sites HAWA 1 and HAWA 3. Regardless of the spacing between receivers, at no point in the data analyses were wavelengths considered that were longer than twice the distance between the source and the first receiver in the receiver pair. This geometry results in minimizing near-field effects while simultaneously recording long wavelengths.

Vertical velocity transducers were used as receivers. The majority of the tests were conducted with Mark Products Model L-4C transducers which have a natural frequency of 1 Hz. Figure 8 shows one L-4C receiver being placed in the field. The key points with regard to these

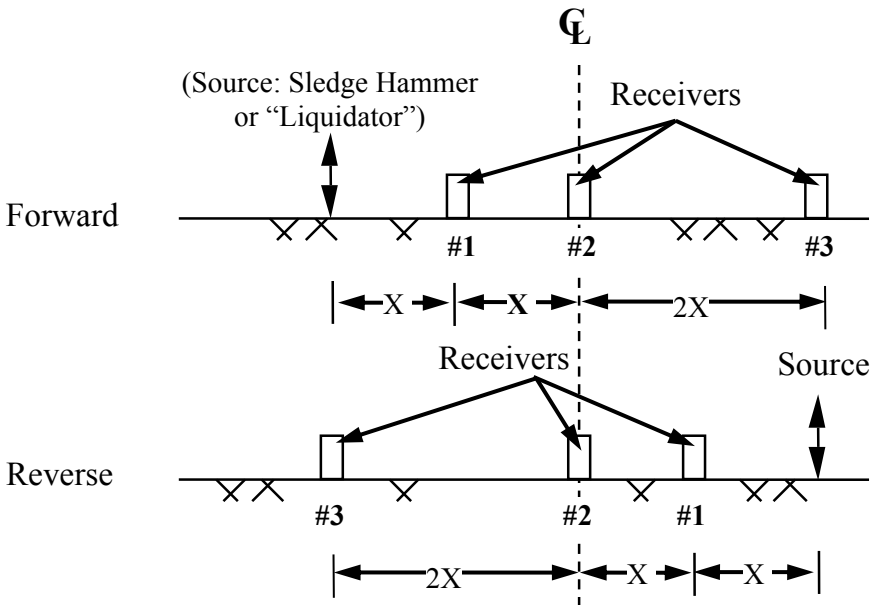

Figure 7 Common-Middle-Receiver Geometry Used in SASW Testing at Hanford Sites

Table 1 Example Source-Receiver Spacings and Associated Information Used in SASW Testing at the Hanford Test Sites

Distance, ft (m)			Impact Direction		Source
S-R1*	R1-R2#	R2-R3Δ	Forward	Reverse	
4	4	8	√	√	Sledge Hammer +Small Hammer
12	12	24	√	√	Sledge Hammer +Small Hammer
30	30	60	√		Sledge Hammer +Small Hammer or Liquidator♦
75	75	150	√		Liquidator
90	90	180	√▲		Liquidator
250	250	500	√		Liquidator
300	300	600	√		Liquidator
350	350	700	√		Liquidator
500	500	1000	√		Liquidator

*S-R1: Distance from source to first receiver
#R1-R2: Distance from first receiver to second receiver
ΔR2-R3: Distance from second receiver to third receiver
♦ Sledge Hammer +Small Hammer only used at Sites 4A, WIXX, H2W2006 and H1K
▲ Only at Site HAWA 2

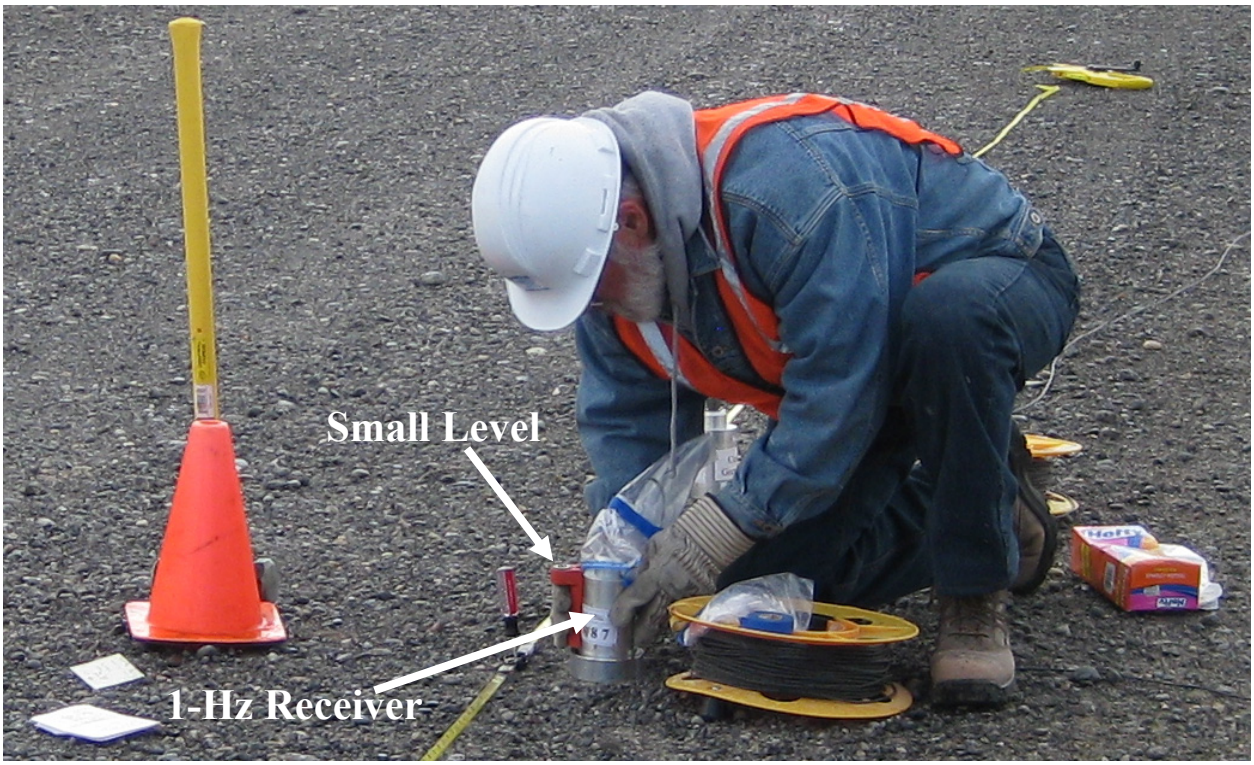

Figure 8 Photograph of 1-Hz Geophone Semi-embedded in the Gravel Surface and the Pre-test Check for Plumbness at Site H1Ks

receivers are that: (1) they have significant output over the measurement frequency range at Hanford (2 Hz to 200 Hz), (2) they are matched so that any differences in phase are negligible over the measurement frequency range, (3) they are coupled well to the soil, (4) the coupling is similar for each receiver, and (5) ambient temperatures were low enough (below 85°F) so as not to impact geophone performance. These 1-Hz geophones have outputs in excess of 10 volts/(in./sec) and phase shifts between receivers of less than +/- 5 degrees for frequencies from 2 Hz to 200 Hz, the range used in testing with these receivers.

The two types of seismic sources that were used to generate energy over the required frequency ranges at Hanford were a sledge hammer and a vibroseis. At the shorter receiver spacings (typically less than or equal to 24 ft), a sledge hammer was employed as shown in Figure 9. For receiver spacings equal to and greater than 30 ft, Liquidator, a one-of-a-kind vibroseis that is owned and operated by The University of Texas at Austin (UT), was used. Figure 10 is a photograph of Liquidator in use at Hanford, WA. Liquidator has proven to be an

excellent source of surface wave energy in previous work (Reference 5). Liquidator can excite energy in the low-frequency range of 0.5 to 4 Hz which allows V_s profiling to greater depths than any other active source.

The recording device used in these tests was a Dataphysics Quattro Dynamic Signal Analyzer, a four-channel analyzer (No photo available for this site). The dynamic signal analyzer was used to record the geophone output and to perform calculations in the frequency domain so that the relative phase of the cross-power spectrum (discussed below) could be reviewed in the field during data collection.

Figure 9 Photograph of Professor Kenneth Stokoe, Using the Sledge Hammer Source and Mr. Sungmoon Hwang and Ms. Julia Roberts(inside the van) Recording the Seismic Signals at Site H3A

Figure 10 Photograph of Liquidator Operating in Stepped-Sine Mode at Site WIAB

3.2 Spectral Calculations

The dynamic signal analyzer was used to measure time-domain records (x(t) and y(t)) from the two receivers at each receiver spacing. These time records were then transformed into the frequency domain (X (f) and Y (f)) and used to calculate the power spectra (G_{XX} and G_{YY}), the cross power spectrum (G_{XY}) and the coherence function (γ^2). Expressions for these quantities are:

$$G_{XX} = X^*(f) \bullet X(f) \tag{2}$$

$$G_{YY} = Y^*(f) \bullet Y(f) \tag{3}$$

$$G_{XY} = X^*(f) \bullet Y(f) \tag{4}$$

$$\phi(f) = \arctan \bullet \frac{\mathrm{Im}(G_{XY})}{\mathrm{Re}(G_{XY})} \tag{5}$$

$$\gamma^2(f) = \frac{\left|G_{XY}(f)\right|^2}{G_{XX}(f) \bullet G_{YY}(f)} \tag{6}$$

where $G_{XY}(f) = \frac{1}{N}\sum_{i=1}^{N} X^*(f) \bullet Y_i(f)$ is the cross power spectrum from coherent signal averaging, (*) represents the complex conjugate of the quantity, Im signifies the imaginary part of the expression, Re signifies the real part of the expression, and $\phi(f)$ is the relative phase between two receivers of the cross power spectrum.

The relative phase from the cross spectrum $\phi(f)$ is the key spectral quantity in SASW testing. The coherence function of averaged measurements is also important as an indicator of the quality of the measurement over the monitored frequency range. Low values of coherence indicate a possible decrease in data quality. The spectral functions were determined using signal averaging. The number of averages and integration time was adjusted in the field to control how long the source remained at each frequency. Typically 3 to 5 averages were used at each frequency in the determination of the spectral functions when Liquidator was used as the source. Five averages were typically used when the impact source (sledge hammer) was employed. The relative phase of the cross spectrum, simply called the phase hereafter, represents the phase difference between the motions measured by the receiver pair. One set of spectral functions was measured for each receiver spacing and testing direction.

As an example, the wrapped phase spectrum from one receiver pair is shown in Figure 11. These data were collected with a 180-ft (55-m) spacing between the receiver pair at Site H3A. Construction of individual dispersion curves from each receiver pair and combining them into composite dispersion curves are discussed below.

3.3 Data Reduction and Forward Modeling Procedure

The data collected in the field, in the form of phase plots, were transferred from the original laptop hard disk that was connected to the analyzer in the field to a desktop computer for analysis. The data were then reduced and interpreted using the program WinSASW, developed by Professor Sung Ho Joh at the University of Texas at Austin (Joh, 1996).

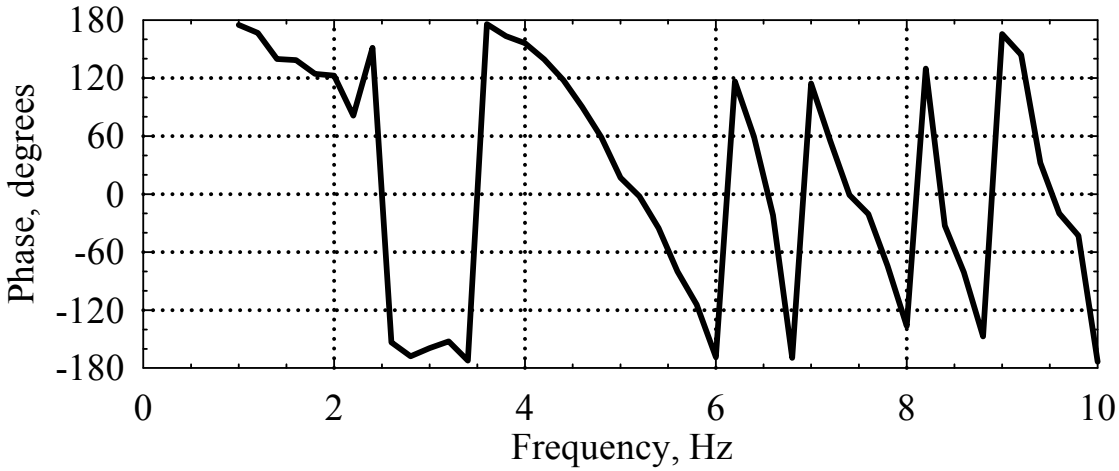

a. Wrapped Phase Calculated from Cross Power Spectrum

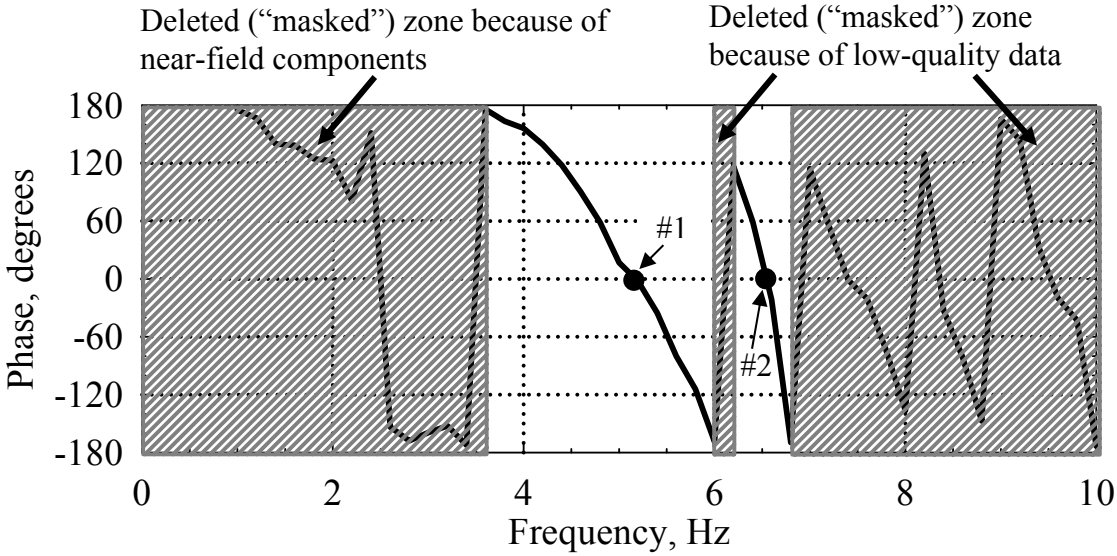

b. Masked Wrapped Phase to Minimize Near-Field Components and to Remove Low-Quality Data

Figure 11 Phase of the Cross Power Spectrum Measured at Site H3A with the Liquidator as the Seismic Source and a 700-ft Spacing between the Receivers

3.3.1 Constructing the Individual and Composite Field Dispersion Curves

Data reduction consisted of the following steps. For each receiver spacing, the phase plot was loaded into WinSASW. A masking procedure was then performed to manually eliminate portions of the data with poor signal quality and/or portions of the data contaminated by near-field waveform components. Figure 11b shows the masking applied to the phase plot collected with a Liquidator and the 700-ft receiver spacing at Site H3A. The WinSASW program uses the masking information to unwrap the phase plot, and then calculate the individual dispersion curve using the relationships presented in Equations 1 through 6.

As an example of the process followed in constructing an individual dispersion curve, consider Points #1 and #2 in Figure 11b which were measured using the Liquidator. Points #1 and #2 represent seismic waves with one and two wavelengths between the receivers, respectively. The unwrapped phase angles are 360° (one wavelength) and 720° (two wavelengths). The frequencies associated with Points #1 and #2 are 5.20 and 6.55 Hz, respectively, which results in phase velocities of 3640 and 2293 fps, respectively. The complete individual dispersion curve calculated from the unmasked portion of the wrapped phase record in Figure 11b is shown in Figure 12. This process is repeated for all receiver spacings which results in a composite experimental field dispersion curve that covers a wide range of wavelengths. Figure 13 shows the composite experimental dispersion curve created at Site H3A using the sledge hammer and Liquidator as the seismic sources. The maximum wavelength, λ_{max}, measured at Site H3A was 1282 ft. This wavelength was measured with S-R2 = 700 ft and R2 - R3 = 700 ft. The maximum depth to which the V_s profile was determined with the Liquidator at this site is λ_{max} /2 or 641 ft as discussed below.

3.3.2 Matching the Composite Field and Theoretical Dispersion Curves

The next step in the data reduction process is the creation of a theoretical dispersion curve which matches the field dispersion curve. The software program WinSASW is used for this purpose. WinSASW uses an algorithm developed by Professor Jose Roesset using the stiffness matrix approach to generate a theoretical dispersion curve for a given shear wave velocity profile (Kausel and Roesset, 1981). The theoretical dispersion curve is generated using either the first-mode Rayleigh wave solution (termed 2D approach) or a complete solution that

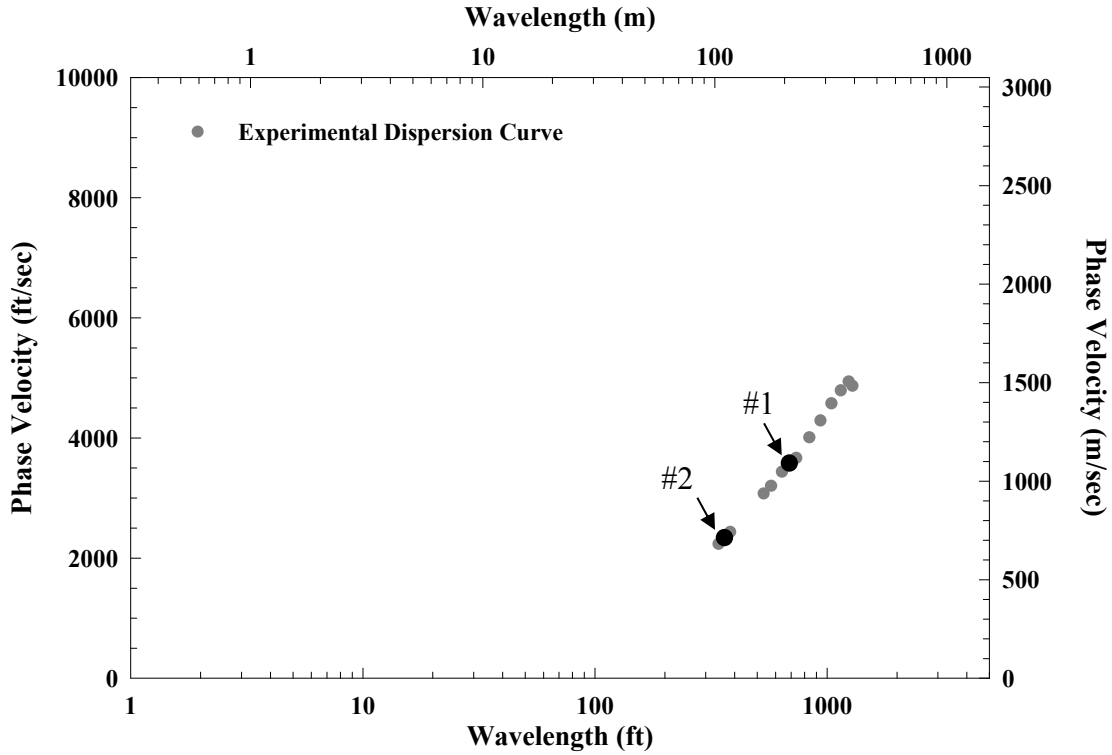

Figure 12 Individual Experimental Dispersion Curve Created from the Wrapped Phase Record in Figure 11b Measured with a 700-ft Receiver Spacing at Site H3A

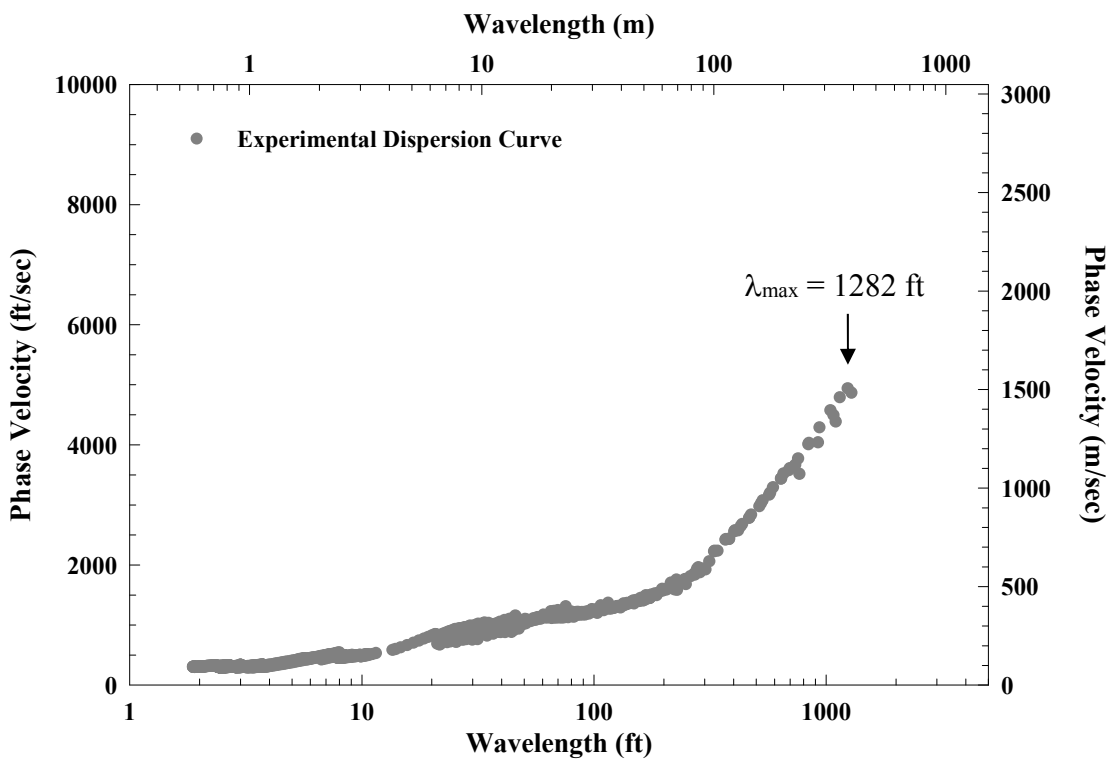

Figure 13 Composite Experimental Dispersion Curve Created from Phase Measurements Performed at all Receiver Spacings at Site H3A

includes all modes and both surface and body waves (termed 3D approach) (Foinquinos, 1991, and Roesset et al, 1991). For these analyses, the more accurate 3D approach was employed. With this approach, an initial shear wave velocity profile is first assumed based on the characteristics of the measured experimental dispersion curve. The theoretical dispersion curve is generated and compared with the experimental curve. The features of the shear wave velocity profile (shear wave velocities and layer thicknesses) are iteratively changed until an acceptable fit to the experimental curve is achieved. The goodness of the fit is based on visually determining a best fit which, in this study, was based on Dr. Lin's judgment followed by a review by Professor Stokoe.

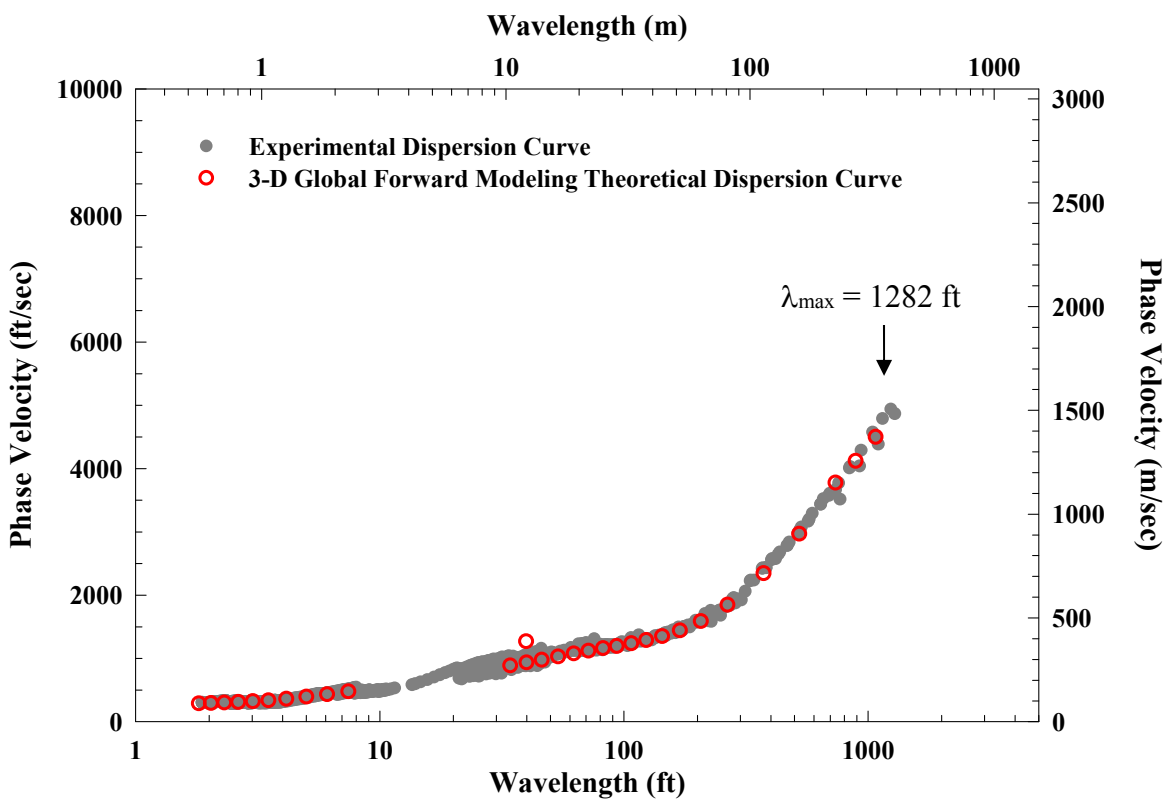

Figure 14 Comparison of the Fit of the Theoretical Dispersion Curve to the Composite Experimental Dispersion Curve at Site H3A

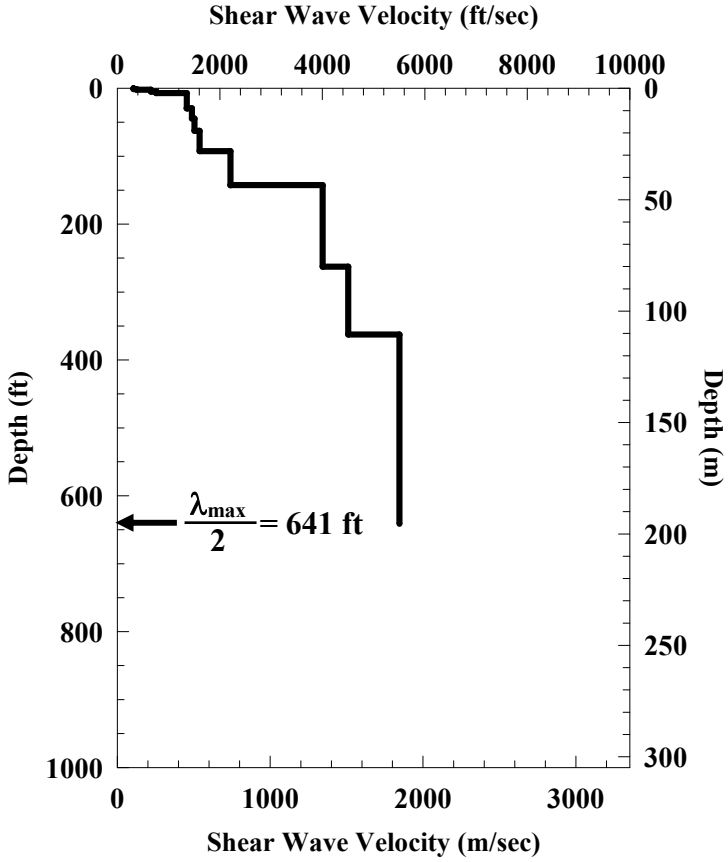

Figure 15 Final Shear Wave Velocity Profile Determined at Site H3A

Table 2 Parameters Used to Obtain the V_s Profile of Site H3A Shown in Figure 15

Layer No.	Layer Thickness, ft	Depth of the Top of the Layer, ft	V_S, fps	Poisson's Ratio	V_P, fps	Total Unit Weight, pcf
1	1	0	310	0.25	537	125
2	0.9	1	370	0.25	641	125
3	2.8	1.9	650	0.25	1126	125
4	2.2	4.7	750	0.25	1299	125
5	22.5	6.9	1350	0.25	2338	125
6	15	29	1450	0.25	2511	125
7	18	44	1500	0.46	5000	135
8	30	62	1600	0.45	5000	135
9	50	92	2200	0.40	5000	135
10	120	142	4000	0.33	7941	145
11	100	262	4500	0.33	8934	145
12	279	362	5500	0.33	10919	145
13*	Half Space	641	5500	0.33	10919	145

* Layer extends below maximum depth of the V_s Profile.
$^{\nabla}$ Water table reported at a depth of 44 ft

The matching process is shown using the composite experimental dispersion curve for Site H3A that is presented in Figure 13. The theoretical dispersion curve which is considered to best match (fit) the composite field dispersion curve is shown in Figure 14. The final shear wave velocity profile for the site is presented in Figure 15. The parameters used to generate the theoretical dispersion curve in Figure 14 are listed in Table 2. As shown in Figure 15, the maximum profile depth is λ_{max} /2 which is 641 ft.

3.3.3 Additional Considerations

For the theoretical analysis, some assumptions have to be made. First, the unit weight and Poisson's ratio of the material must be assumed. Poisson's ratio was assumed to be 0.25 for all materials above the water table. This value of Poisson's ratio is a reasonable assumption for soil when no water table exists in the profiling depth. When no water table is present, the value of Poisson's ratio (which may vary from 0.22 to 0.38) has only a minor influence on the calculated dispersion curve. The unit weight of the soil was assumed to be 125 pcf. Relative changes in unit weight with depth affect the dispersion curve, but the effect on the final shear wave velocity profile is also minor. Therefore, precise knowledge of the unit weights at all depths is not required. However, the values of Poisson's ratio of the soil layers under the water table were calculated by WinSASW. The P-wave velocities of soil layers beneath the water table were assumed to be 5500 fps and values of Poisson's ratio were calculated from the assumed P-wave and S-wave velocities. The unit weight of the soil under water table was assumed to be 135 pcf. For the basalt layers, Poisson's ratio was assumed to be 0.33 and the unit weight was assumed to be 145 pcf. Table 2 shows the parameters used to obtain the shear wave velocity profile of Site H3A.

Theoretical dispersion curves can also be generated using different assumptions of receiver locations. For these analyses, the theoretical dispersion curve was calculated assuming Source-to-Receiver #1 spacing of two wavelengths, and Source-to-Receiver #2 spacing of four wavelengths. These receiver locations represent far-field motions. Past studies have shown that the range in wavelengths collected in the SASW test does not differ significantly from the far-field motions (Foinquinos, 1991; Roesset et al, 1991; Sanchez-Salinero, 1987; and Jathal, 2003).

Lastly, the final shear wave velocity profile is generally presented to a depth of approximately 0.5 times the maximum wavelength ($\lambda_{max}/2$) in the experimental dispersion curve. This cutoff depth is based on the fact that most of the particle motion occurs at depths less than one-half of the wavelength, as shown in Figure 2. Past experience has shown this maximum depth to be an acceptable cut-off depth for most shear wave velocity profiles. However, at eight sites (HAWA 1, HAWA 2+HAWA3, 4A, Haulroad, H2W1998, H2W2006, 100B and H1K), wavelengths that extended slightly into the near-field zone were used in an attempt to determine if an increase in V_s occurred just below a depth equal to $\lambda_{max}/2$. In these eight cases, the portions of the V_s profiles evaluated using near-field data are shown by dashed lines in the figures in Appendix A.

4.0 DISCUSSION OF V_S PROFILES AT 12 DEEP TEST LOCATIONS

A summary of all 12 deep V_S profiles is presented in Figure 16. Clearly, a wide range in V_S values has been determined, beginning at a depth around 50 ft. To view this variability in more detail, the V_S values have been subdivided into ranges so that portions of the profiles with similar V_S values can be grouped together as discussed below.

The first subdivision in the V_S profiles is Group 1. Material in Group 1 has $V_S \leq 2600$ ft/sec. This V_S group is shown in Figure 17. As expected, all 12 profiles have material in this range. It is also interesting to observe that test locations HAWA 1, HAWA 2 + HAWA 3, WIXX and WIAB exhibit the least amount of softer material in the top portion of the profiles. In addition, it is interesting to compare the V_S profiles in Group 1 with profiles of dense sand and dense gravel. This comparison is also shown in Figure 17 and indicates that the Group 1 profiles are generally equal to or are slightly above the V_S profile predicted for dense gravel.

The second subdivision of V_S profiles, Group 2, is presented in Figure 18. These materials represent rock with 3000 ft/sec $\leq V_S <$ 4600 ft/sec. All SASW testing locations except Site H1K are represented.

The other two subdivisions of the V_S profiles are Groups 3 and 4. In Group 3, the V_S values range from 5000 to 6500 ft/sec. Four test locations are present in this group as shown in Figure 19. In Group 4, the V_S values are above 8000 fps and, as seen in Figure 20, only one test location, Site HAWA 1, is in Group 4. Interestingly, four of the five test locations in Groups 3 and 4 are located in the south-eastern quadrant of the Hanford Site.

SASW testing was also performed in 2004 at the Hanford Site (Stokoe et al., 2005). A map of the SASW near-by test locations in 2004 and 2013 is shown in Figure 21. The comparisons of each set of near-by V_S profiles are shown in Figures 22 and 23. Clearly, the comparison is excellent in Figure 22 and shows large differences in Figure 23.

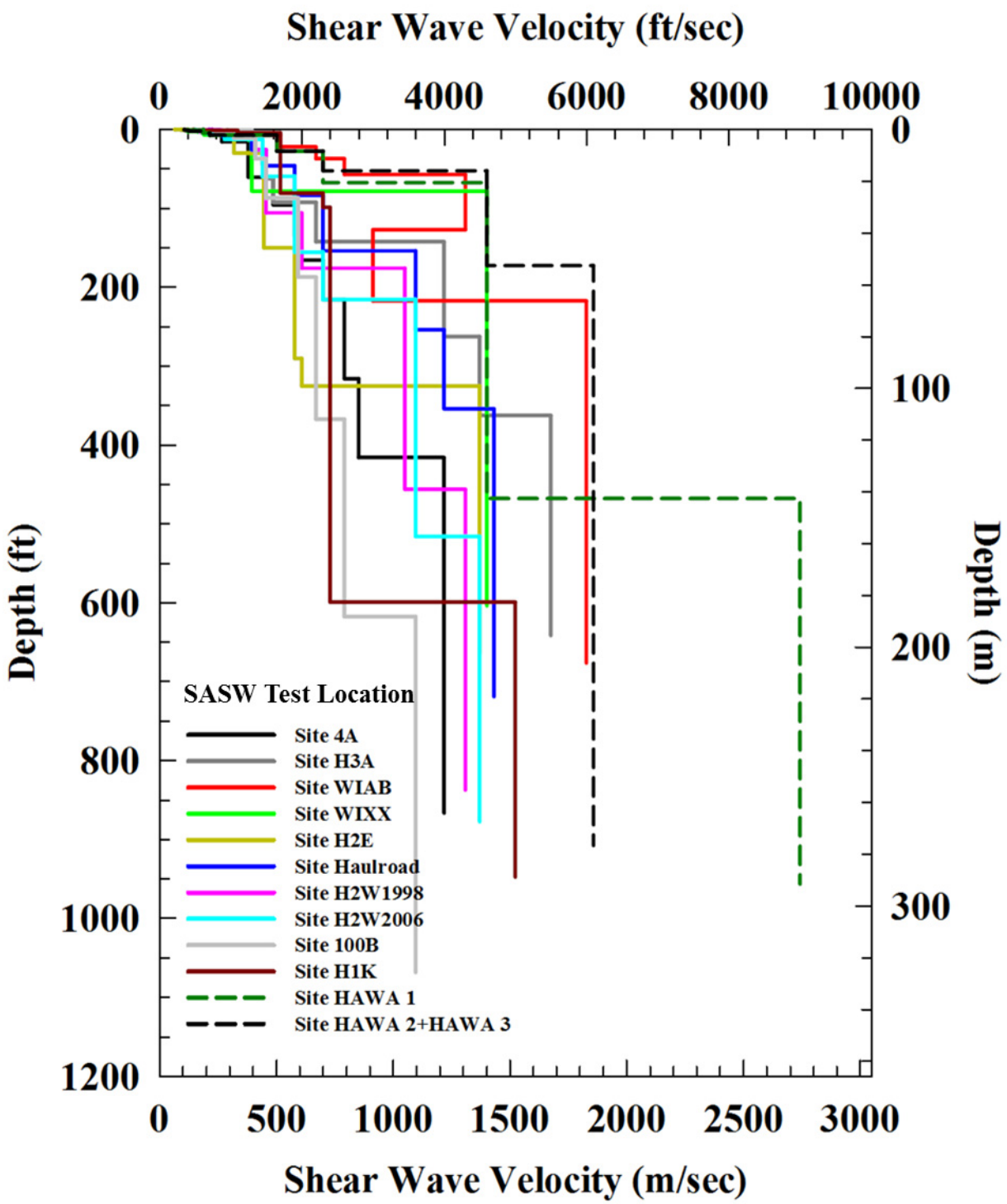

Figure 16 Summary of all 12 Deep Vs Profiles at the Hanford Site

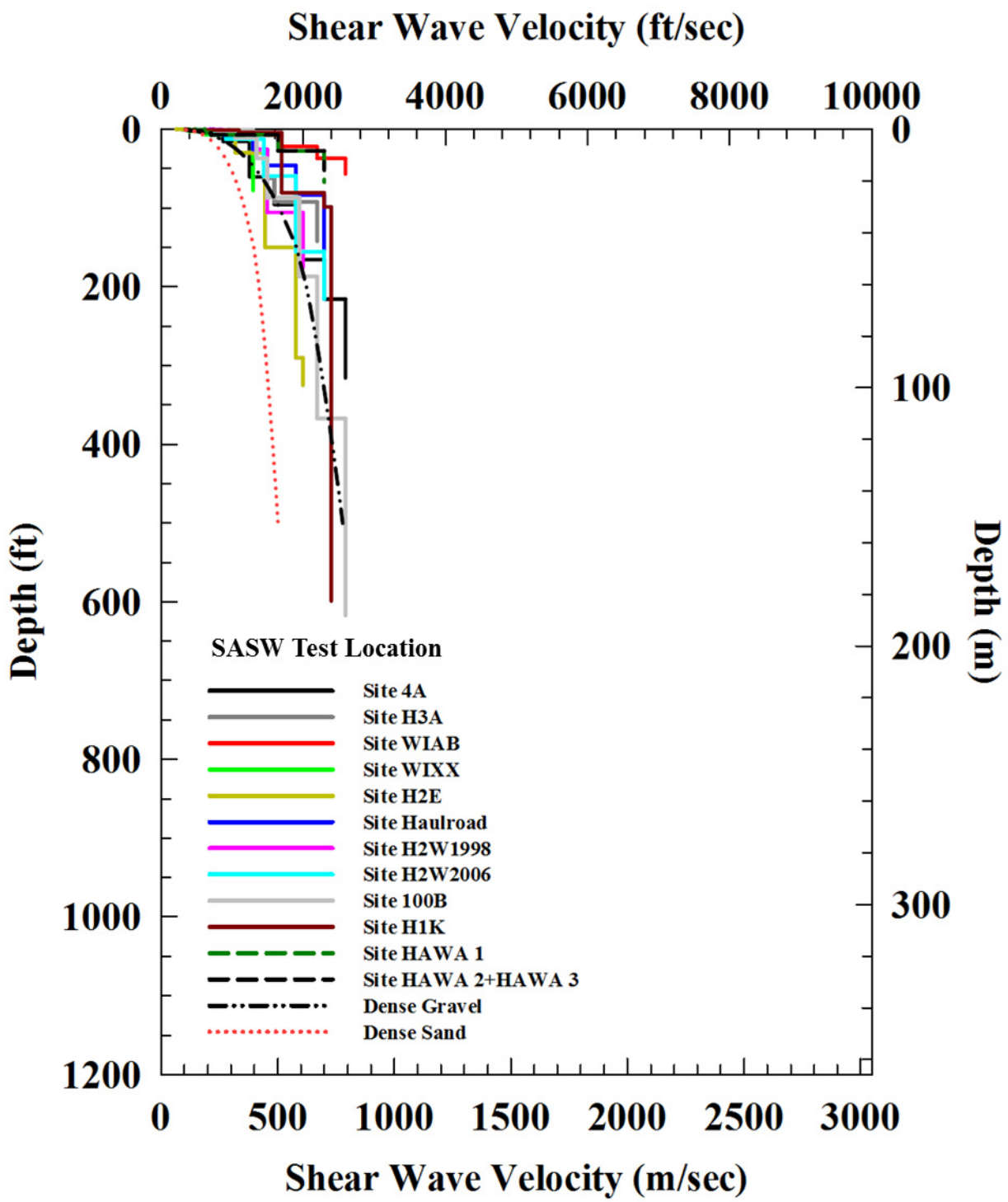

Figure 17 Portions of the 12 Deep V_S Profiles with $V_S \leq 2600$ fps ft/sec

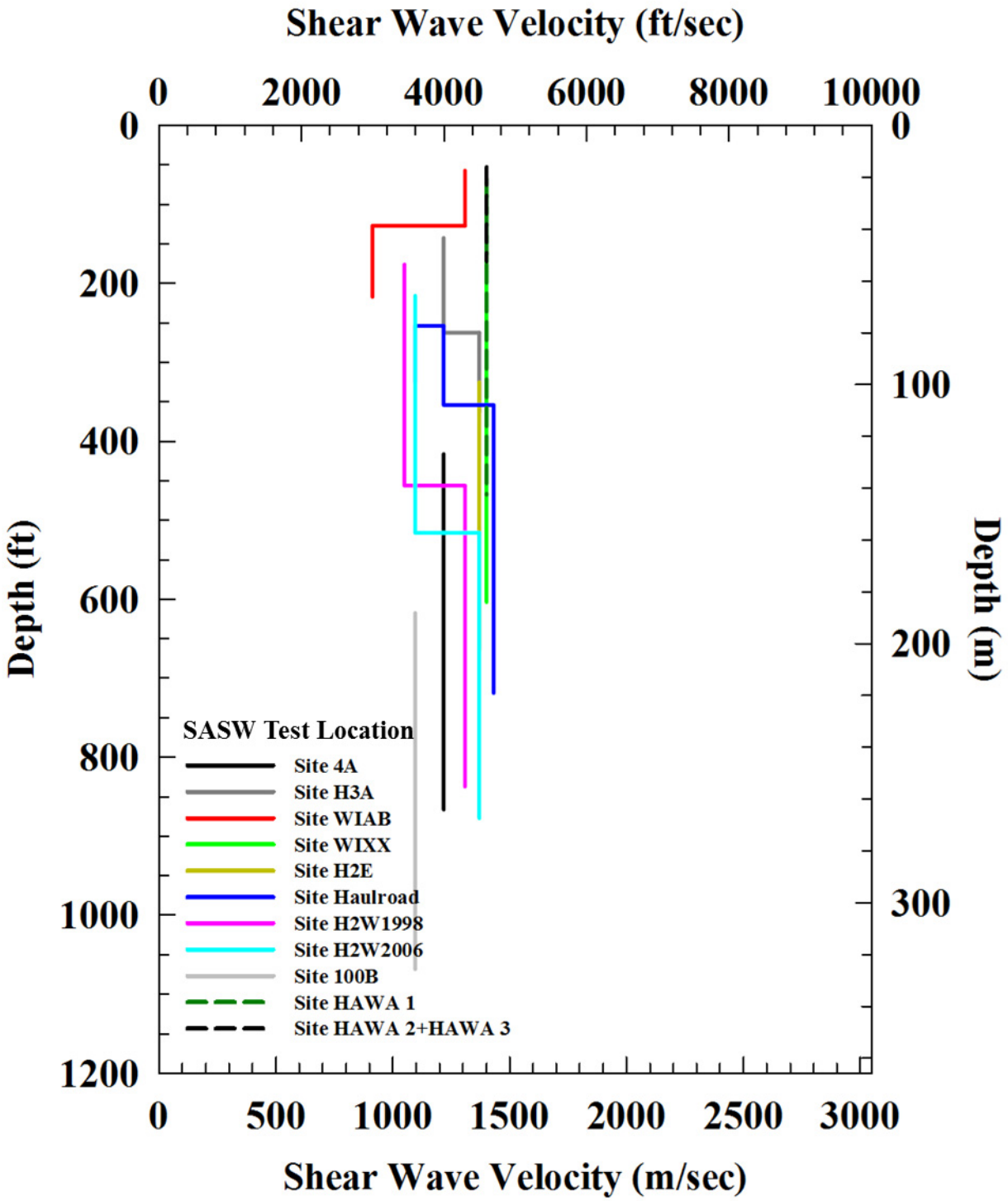

Figure 18 Portions of the 12 Deep V_S Profiles with 3000 ft/sec ≤ V_S < 4600 ft/sec

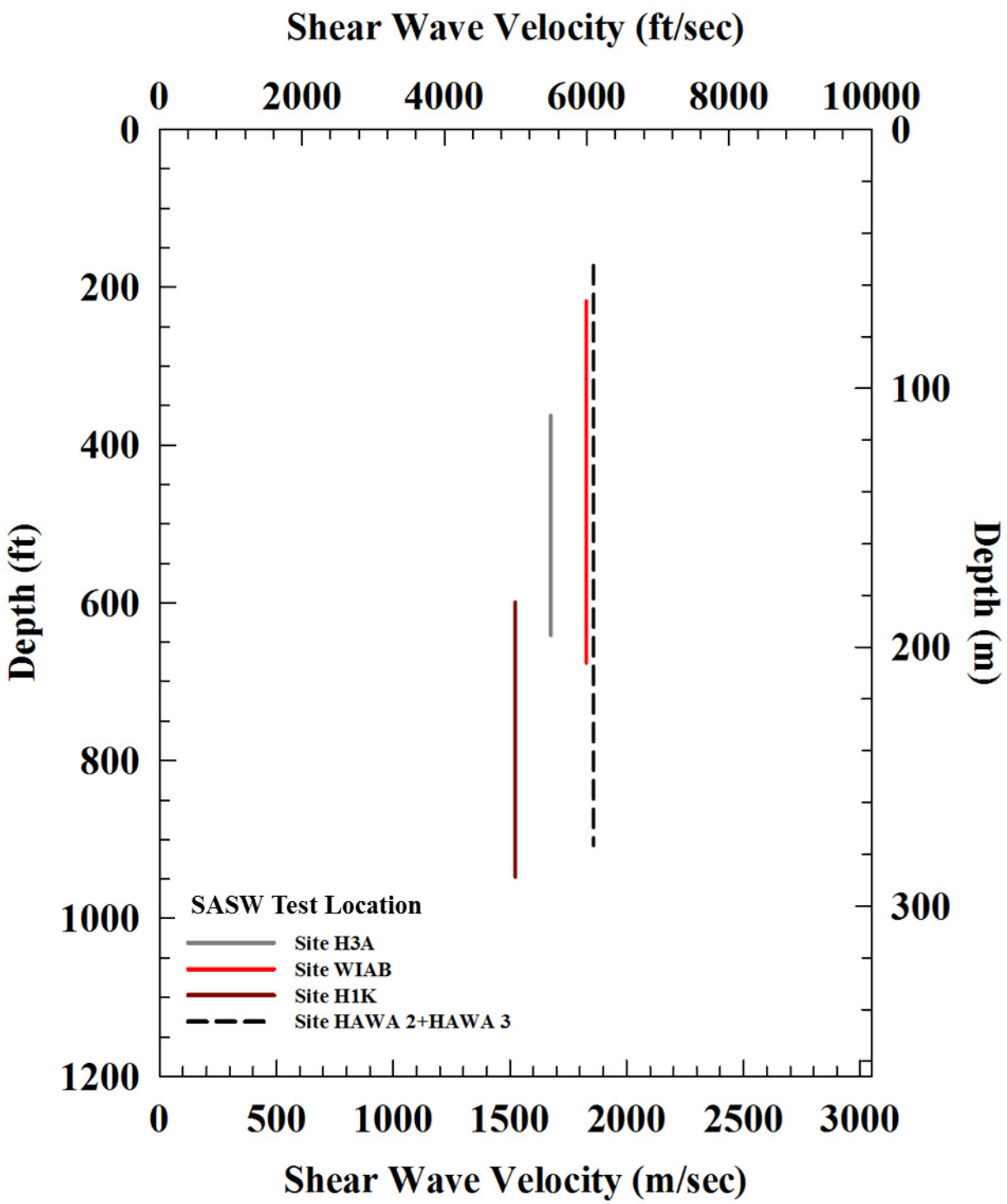

Figure 19 Portions of the 12 Deep V_S Profiles with 5000 ft/sec ≤ V_S < 8000 ft/sec

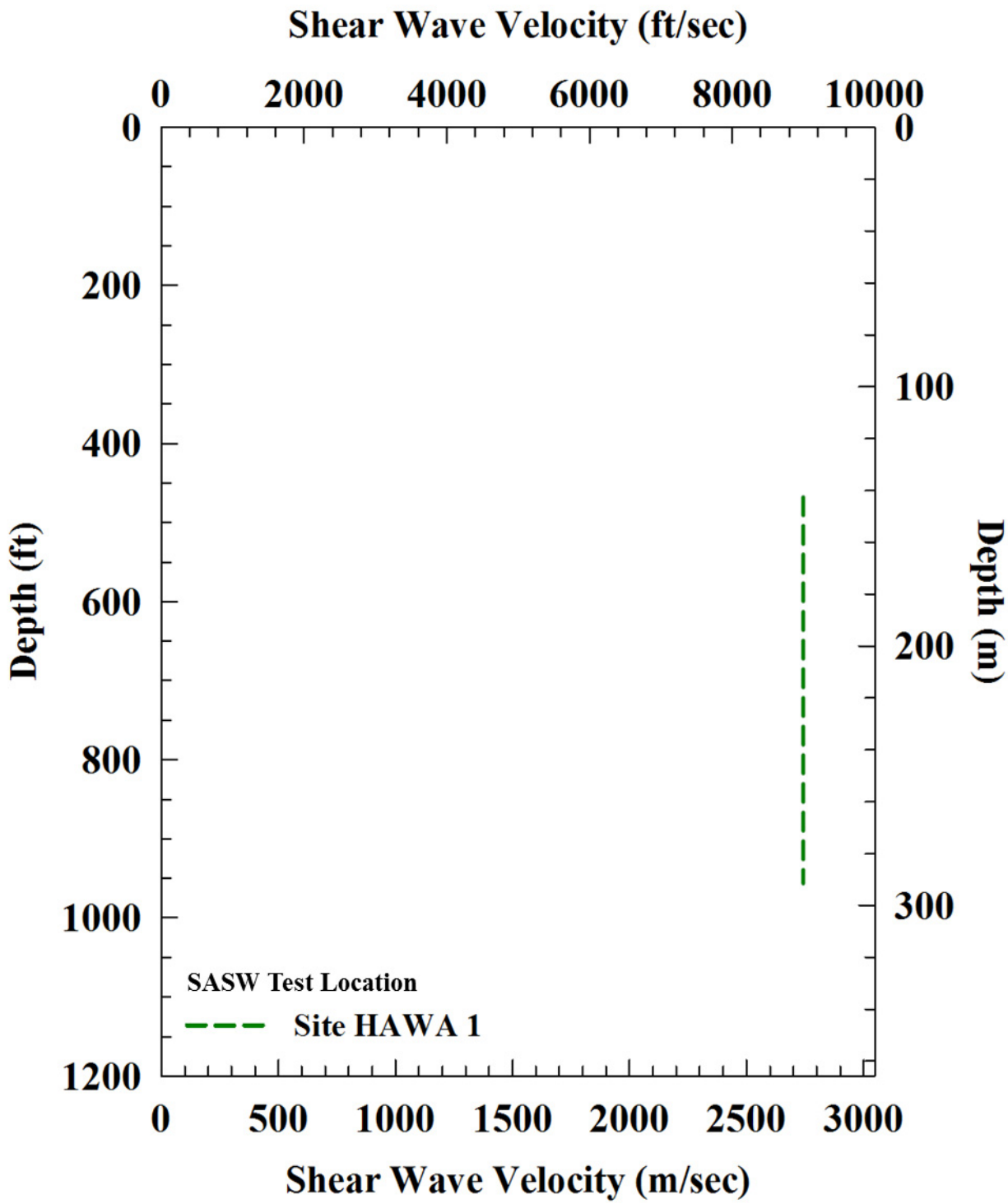

Figure 20 Portions of the 12 Deep V_S Profiles with V_S > 8000 ft/sec

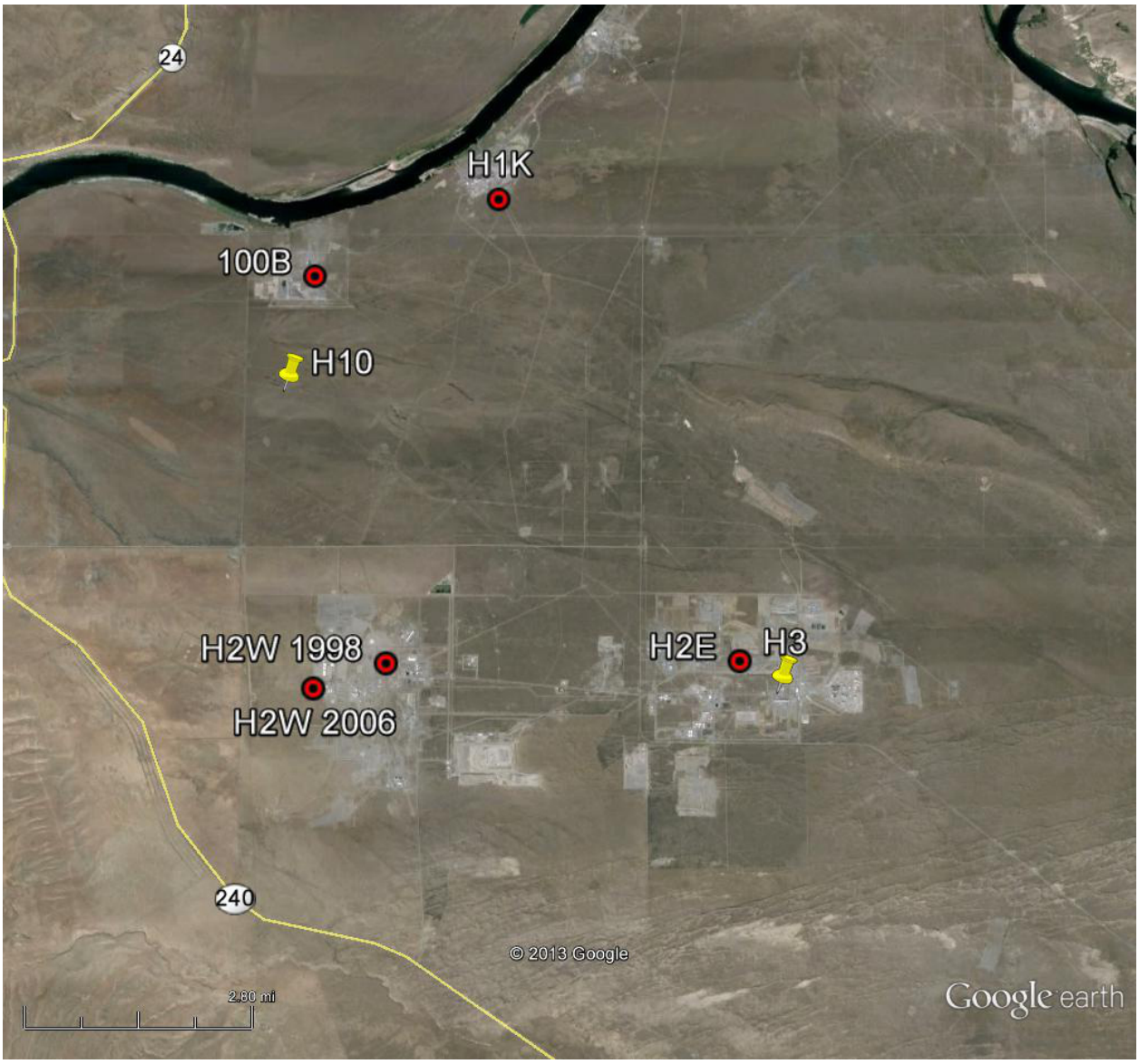

Figure 21 Map of SASW Near-by Test Locations in 2004 and 2013

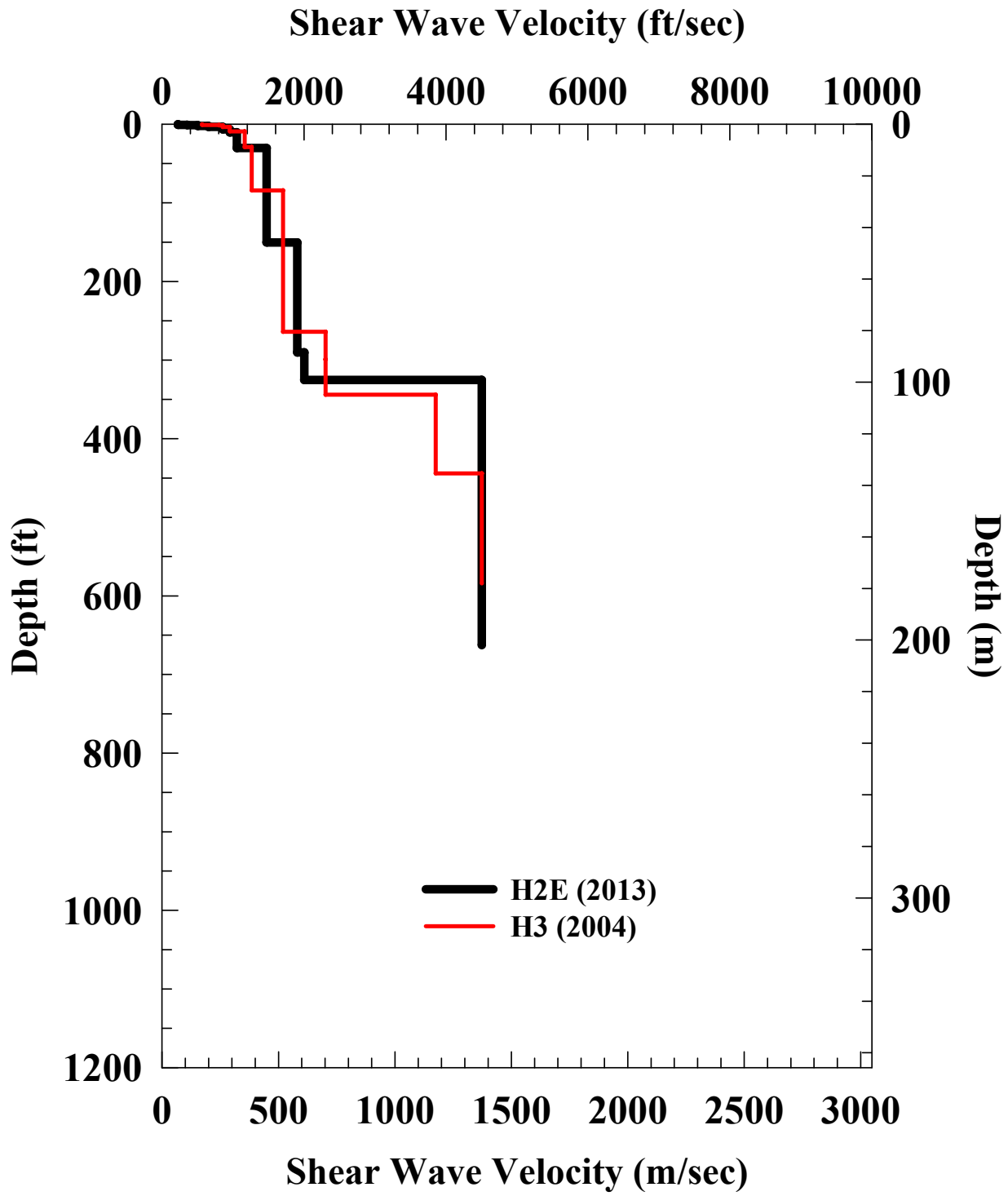

Figure 22 Comparison of the V_S Profiles of Site H2E (2013) and Site H3 (2004)

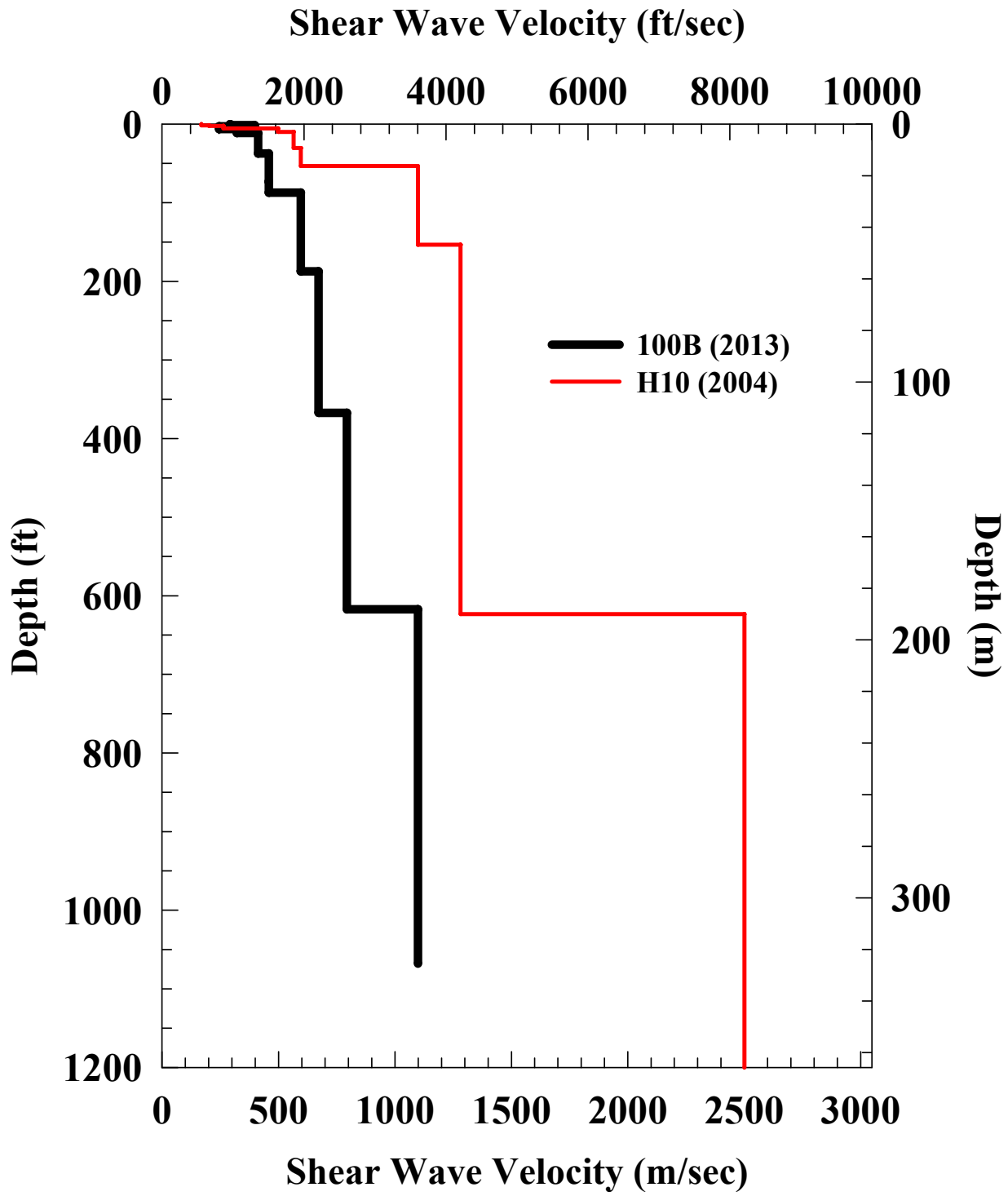

Figure 23 Comparison of the V_S Profiles of Site 100B (2013) and Site H10 (2004)

5.0 SUMMARY AND CONCLUSIONS

Profiles of V_S were evaluated using the SASW method at 13 test locations at the Hanford Site. Twelve profiles were deep; that is V_S values were determined to depths ranging from 604 ft to 1068 ft. These 12 test locations are shown in Figure 1. All SASW results and data analyses associated with these sites are presented in Appendix A. The 12 V_S profiles are presented in Figure 16 and briefly discussed in Section 4. The SASW field testing at these sites went smoothly, the data analyses were normal for such deep profiles and the deepest portion of the profiles were supported by additional 3-D array-based forward modeling.

Profiling at the 13th site was shallow. The 13th site was the missile bunker which is next to Site HAWA 2 in Figure 1. The objective was to develop a shallow V_S profile through the concrete floor inside the bunker. This effort required two field visits, and the testing was rather difficult due to the confined space in the bunker and the large velocity contrast between the concrete floor and the supporting subgrade. After several analyses, the recommended V_S profile is presented in Appendix A, Figure A.15.1 and Table A.15.1. A response to the TI Team's Question #3 about this V_S profile is presented in Appendix D.

6.0 REFERENCES

1. Foinquinos, M.R., (1991), "Analytical Study of Inversion for the Spectral Analysis of Surface Waves Method," Master's Thesis, The University of Texas at Austin, 119 pgs.
2. Fuhriman, M.D. and Stokoe, K.H., II (1993), "Crosshole Seismic Test at the Gilroy No. 2 and Treasure Island Sites Affected by the 1989 Loma Prieta Earthquake," Geotechnical Engineering Report GR93-1, Civil Engineering Department, University of Texas at Austin, Austin, TX, January, 259 pgs.
3. Jathal, J.K. (2003), "Investigation of V_s Profiles Measured by Borehole and Surface-Wave Seismic Techniques," Master's Thesis, The University of Texas at Austin, 348 pgs.
4. Joh, S.-H. (1996), "Advances in the Data Interpretation Technique for Spectral- Analysis-of-Surface-Waves (SASW) Measurements," Ph.D. Dissertation, The University of Texas at Austin, 240 pgs.
5. Kausel, E. and Roesset, J.M. (1981), "Stiffness Matrices for Layered Soils," *Bulletin of the Seismological Society of America*, 71, pp. 1743-1761.
6. Lin, Y.-C, Stokoe, K. H., II, and Rosenblad, B. L., (2008), "Variability in V_s Profiles and Consistency between Seismic Profiling Methods: A Case Study in Imperial Valley, California", the 3rd International Conference on Site Characterization (ISC'3), Taipei, Taiwan. April, 2008.
7. Menq, F.-Y. (2003), "Dynamic Properties of Sandy and Gravely Soils," Ph.D. Dissertation, The University of Texas at Austin, 390 pgs.
8. Roesset, J.M., Chang D.-W., and Stokoe, K.H., II (1991), "Comparison of 2D and 3D Models for Analysis of Surface Wave Tests," *Proceedings of the 5th International Conference on Soil Dynamics and Earthquake Engineering*, pp. 111-126.
9. Sanchez-Salinero, I. (1987), "Analytical Investigation of Seismic Methods used for Engineering Applications," Ph.D. Dissertation, The University of Texas at Austin, 401 pgs.

10. Stokoe, II, K.H., Lin, Y.C., Cox, B., Kurtulus, A., Jung, M.J. (2005). "Shear Wave Profiling at the Waste Treatment Plant Site, Hanford, WA," Vols. I and II, Geotechnical Engineering Report GR05-1, University of Texas at Austin, July, 243 pgs.

11. Stokoe, K.H., II, Wright, S.G., Bay, J.A. and J.M. Roesset (1994), "Characterization of Geotechnical Sites by SASW Method," *ISSMFE Technical Committee 10 for XIII ICSMFE*, Geophysical Characteristics of Sites, A.A. Balkema Publishers/Rotterdam & Brookfield, Netherlands, pp. 785-816.

Appendix A

Field Dispersion Data and Associated V_S Profiles at the 12, Deep-Profiling Sites (Pages A-2 through A-49) and at the Missile Bunker Site (Pages A-50 through A-53) and Recommended Bunker V_S Profile (Pages A-54 and A-55)

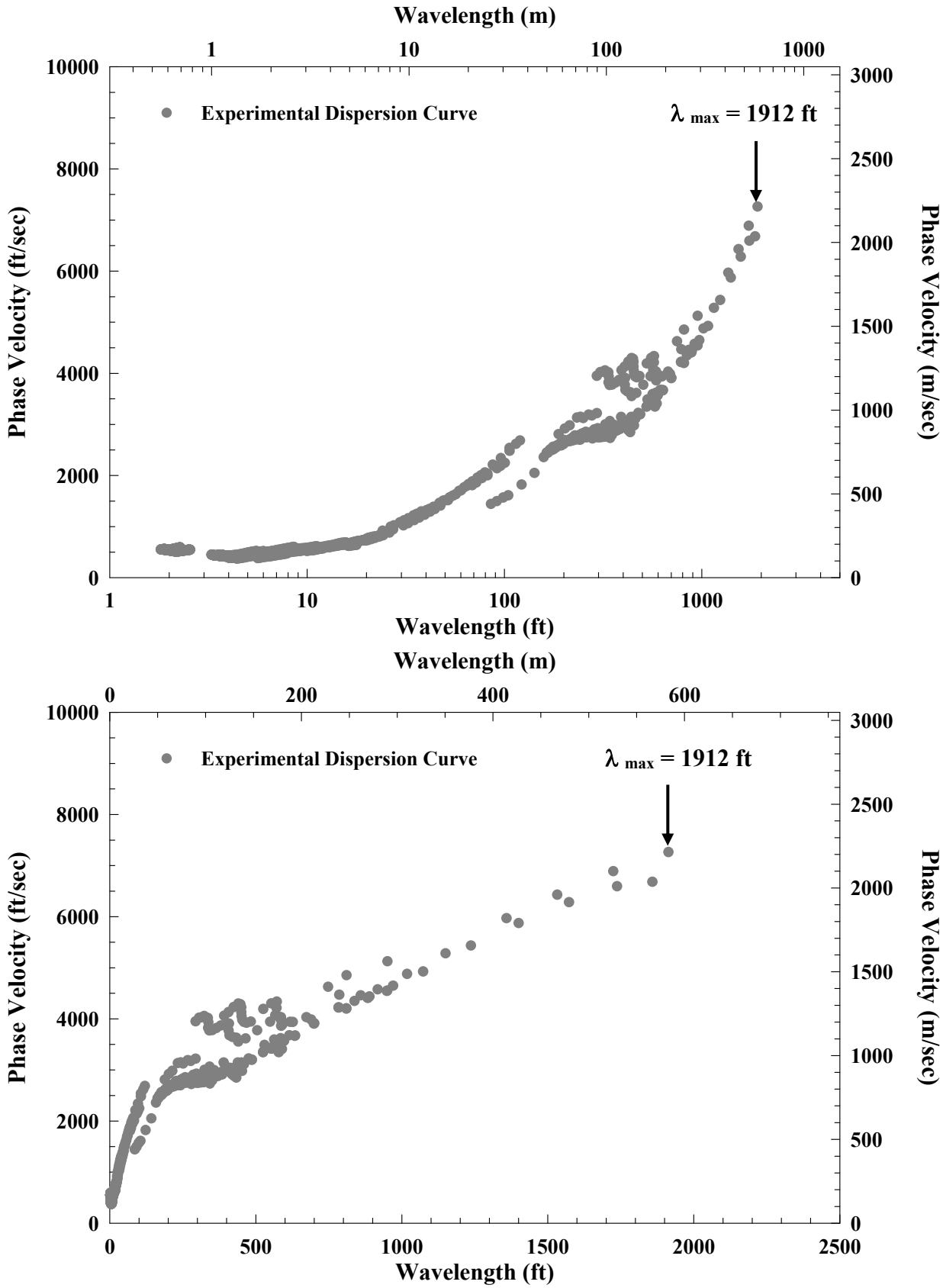

Figure A.1.1 Experimental Dispersion Curve Measured at Site HAWA 1; Logarithmic (Top) and Linear (Bottom) Wavelength Axes

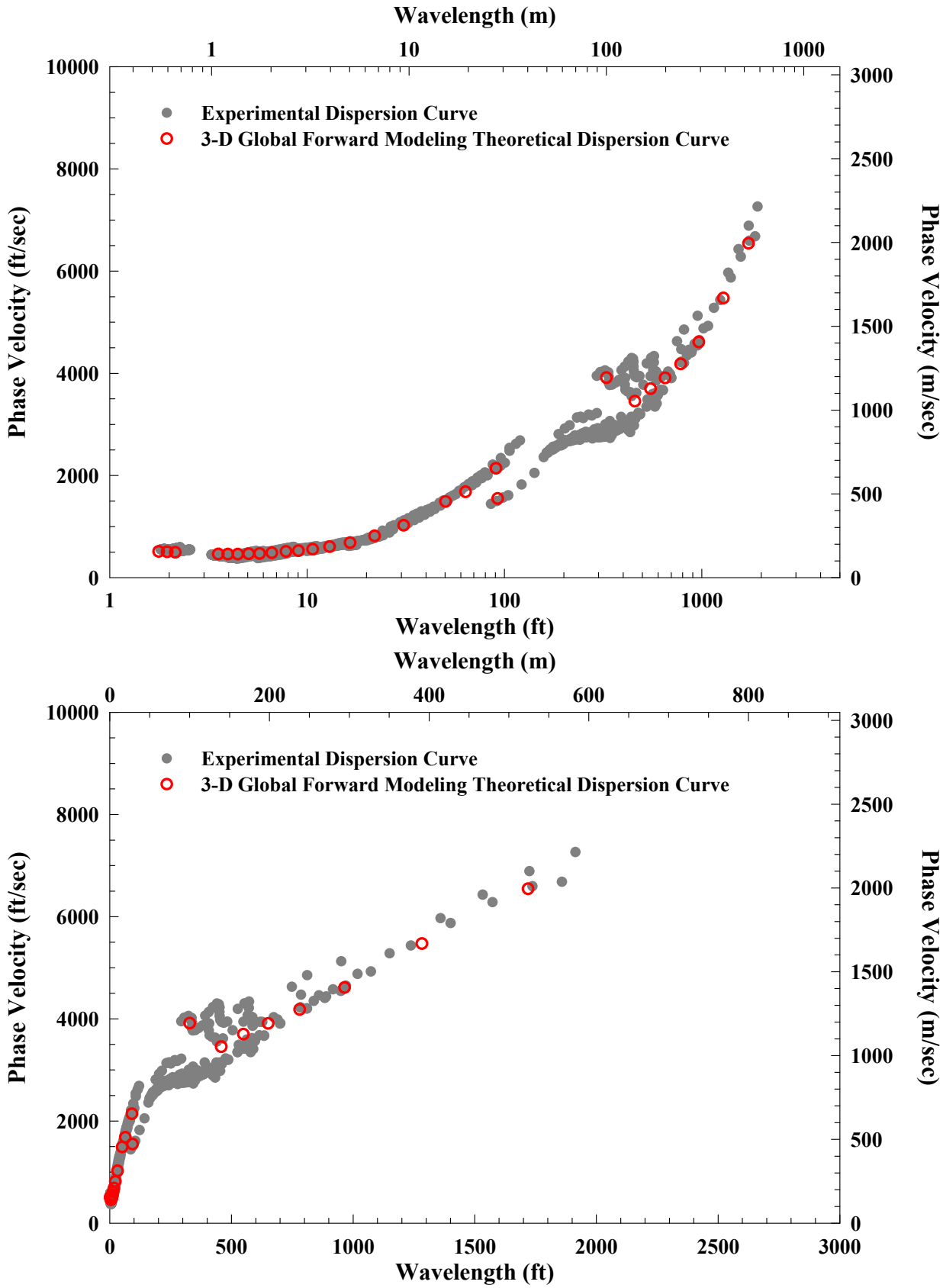

Figure A.1.2 Experimental (Field) and Global Forward Modeling Theoretical Dispersion Curves from Site HAWA 1; Logarithmic (Top) and Linear (Bottom) Wavelength Axes

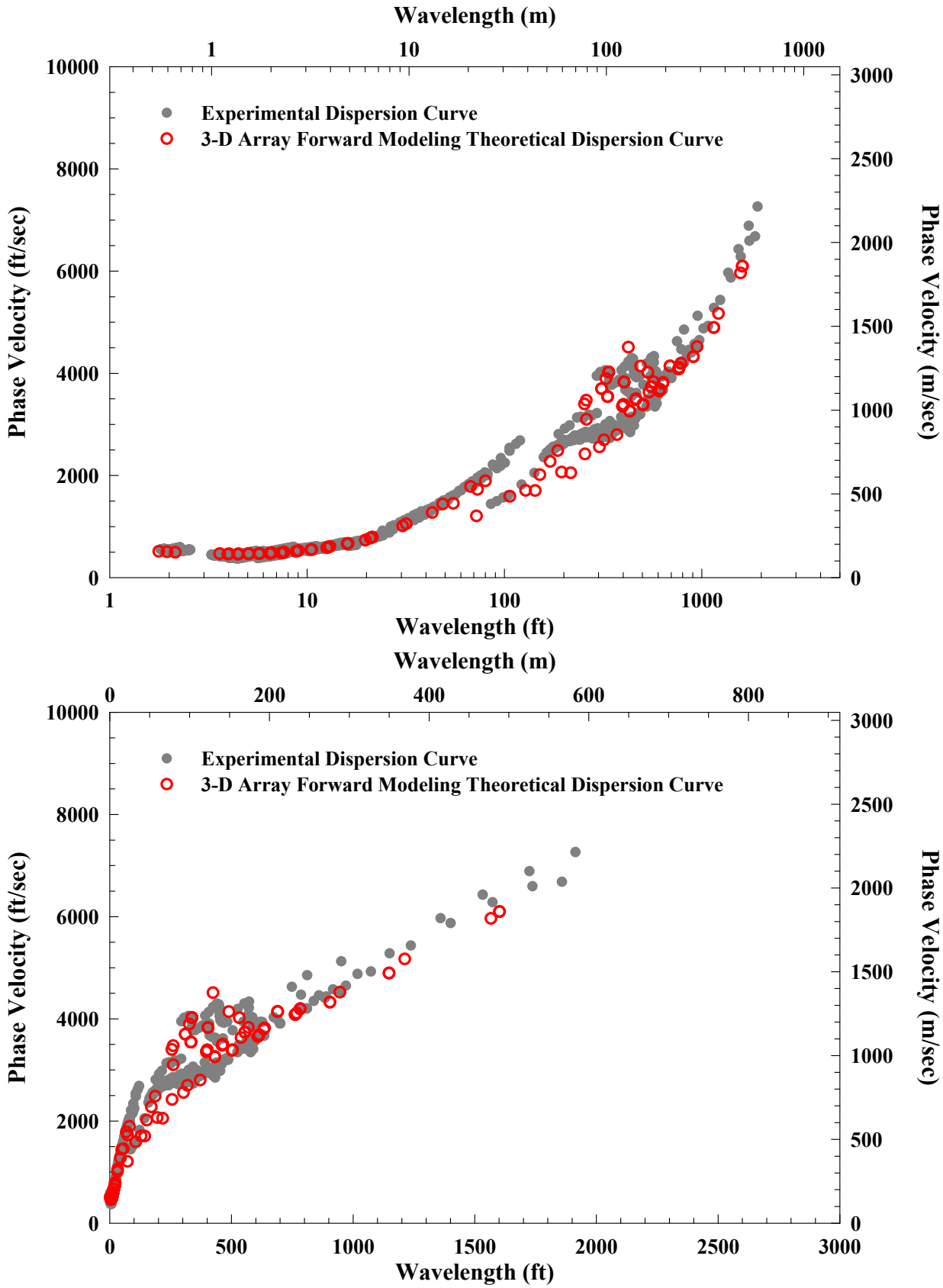

Figure A.1.3 Experimental (Field) and Array Forward Modeling Theoretical Dispersion Curves from Site HAWA 1; Logarithmic (Top) and Linear (Bottom) Wavelength Axes

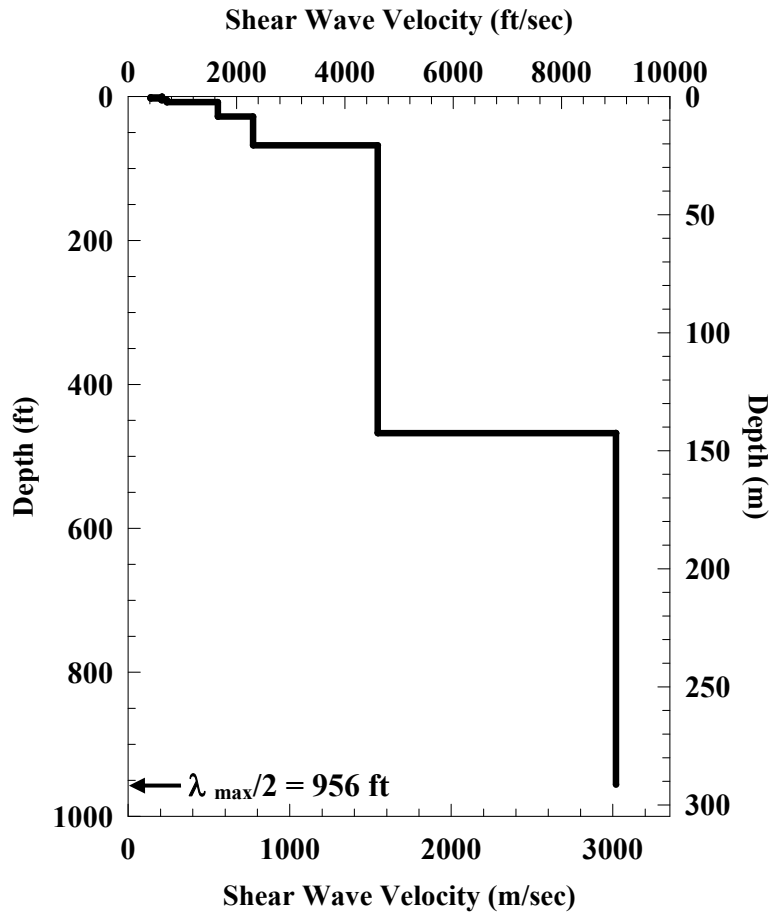

Figure A.1.4 Shear Wave Velocity Profile Determined at Site HAWA 1

Table A.1.1 Profile Parameters Used to Develop Theoretical Dispersion Curve at Site HAWA 1

Layer No.	Layer Thickness, ft	Depth of the Top of the Layer, ft	Vs, fps	Poisson's Ratio	Vp, fps	Total Unit Weight, pcf
1	1	0	620	0.25	1074	125
2	1.3	1	410	0.25	710	125
3	2.4	2.3	610	0.25	1057	125
4	2.8	4.7	710	0.25	1230	125
5	20	7.5	1650	0.25	2858	125
6	40	28	2300	0.25	3984	125
7	400	68	4600	0.33	9132	145
8	489	468	9000	0.33	17867	145
9*	Half Space	956	9000	0.33	17867	145

* Layer deeper than the maximum recommended profiling depth (λ_{max}/ 2).

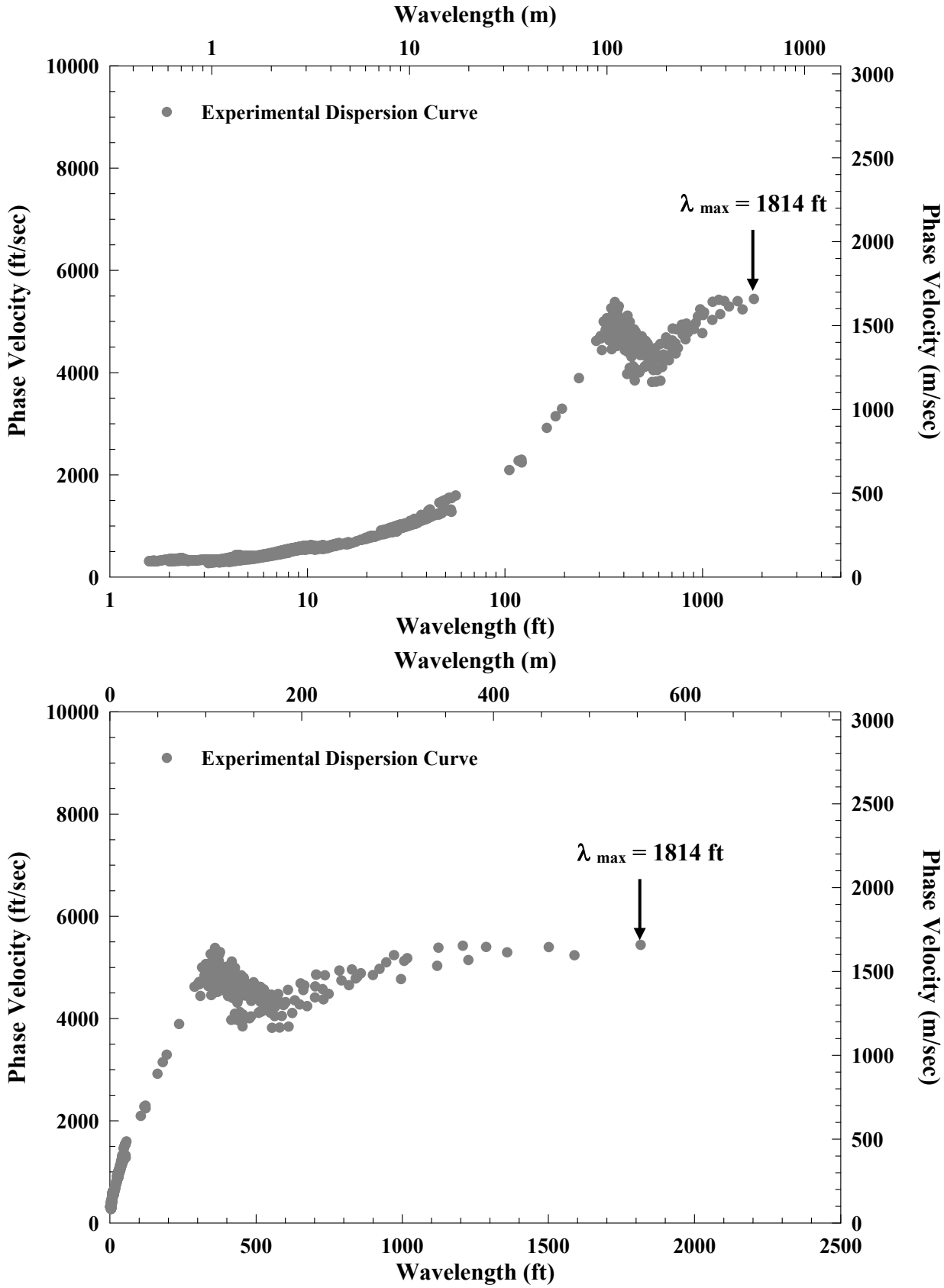

Figure A.2.1 Experimental Dispersion Curve Measured at Site HAWA 2+3; Logarithmic (Top) and Linear (Bottom) Wavelength Axes

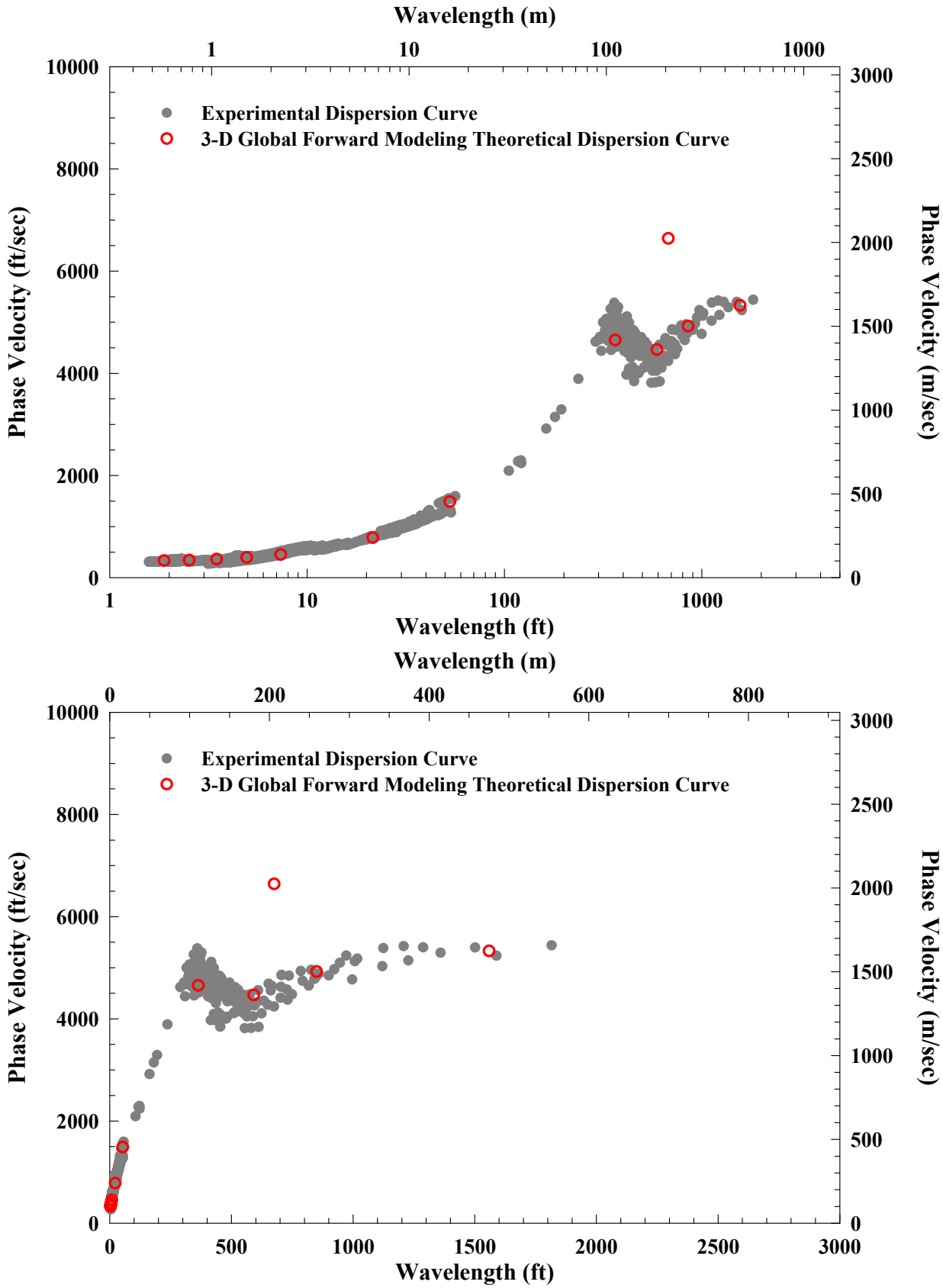

Figure A.2.2 Experimental (Field) and Global Forward Modeling Theoretical Dispersion Curves from Site HAWA 2+3; Logarithmic (Top) and Linear (Bottom) Wavelength Axes

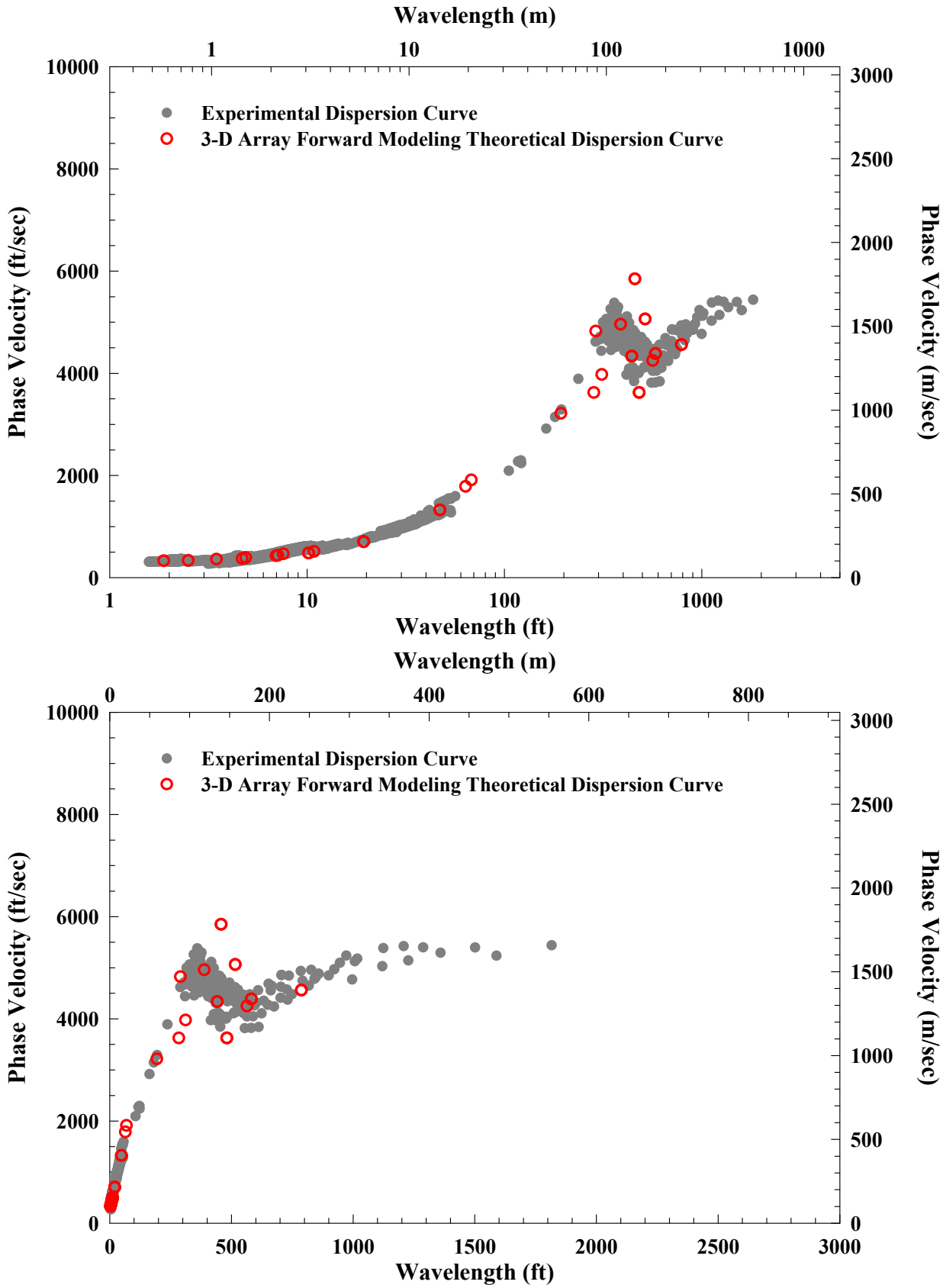

Figure A.2.3 Experimental (Field) and Array Forward Modeling Theoretical Dispersion Curves from Site HAWA 2+3; Logarithmic (Top) and Linear (Bottom) Wavelength Axes

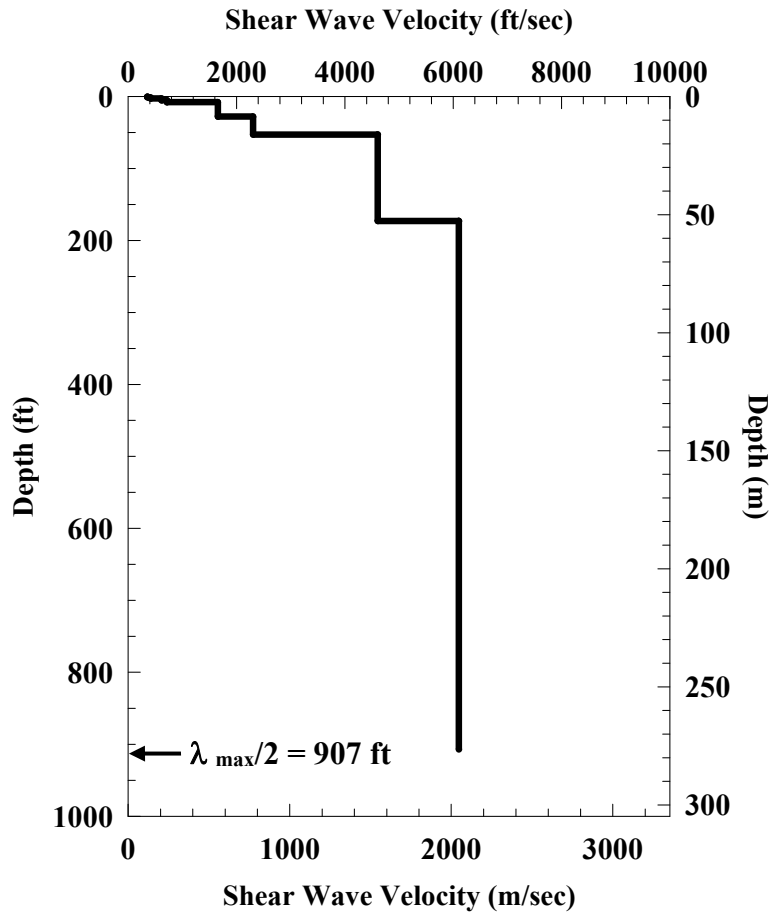

Figure A.2.4 Shear Wave Velocity Profile Determined at Site HAWA 2+3

Table A.2.1 Profile Parameters Used to Develop Theoretical Dispersion Curve at Site HAWA 2+3

Layer No.	Layer Thickness, ft	Depth of the Top of the Layer, ft	Vs, fps	Poisson's Ratio	Vp, fps	Total Unit Weight, pcf
1	0.8	0	350	0.25	606	125
2	0.25	0.8	380	0.25	658	125
3	1.3	1.05	410	0.25	710	125
4	2.4	2.35	610	0.25	1057	125
5	2.8	4.75	710	0.25	1230	125
6	20	7.55	1650	0.25	2858	125
7	25	28	2300	0.25	3984	125
8	120	53	4600	0.33	9132	145
9	734	173	6100	0.33	12110	145
10*	Half Space	907	6100	0.33	12110	145

* Layer deeper than the maximum recommended profiling depth (λ_{max}/ 2).

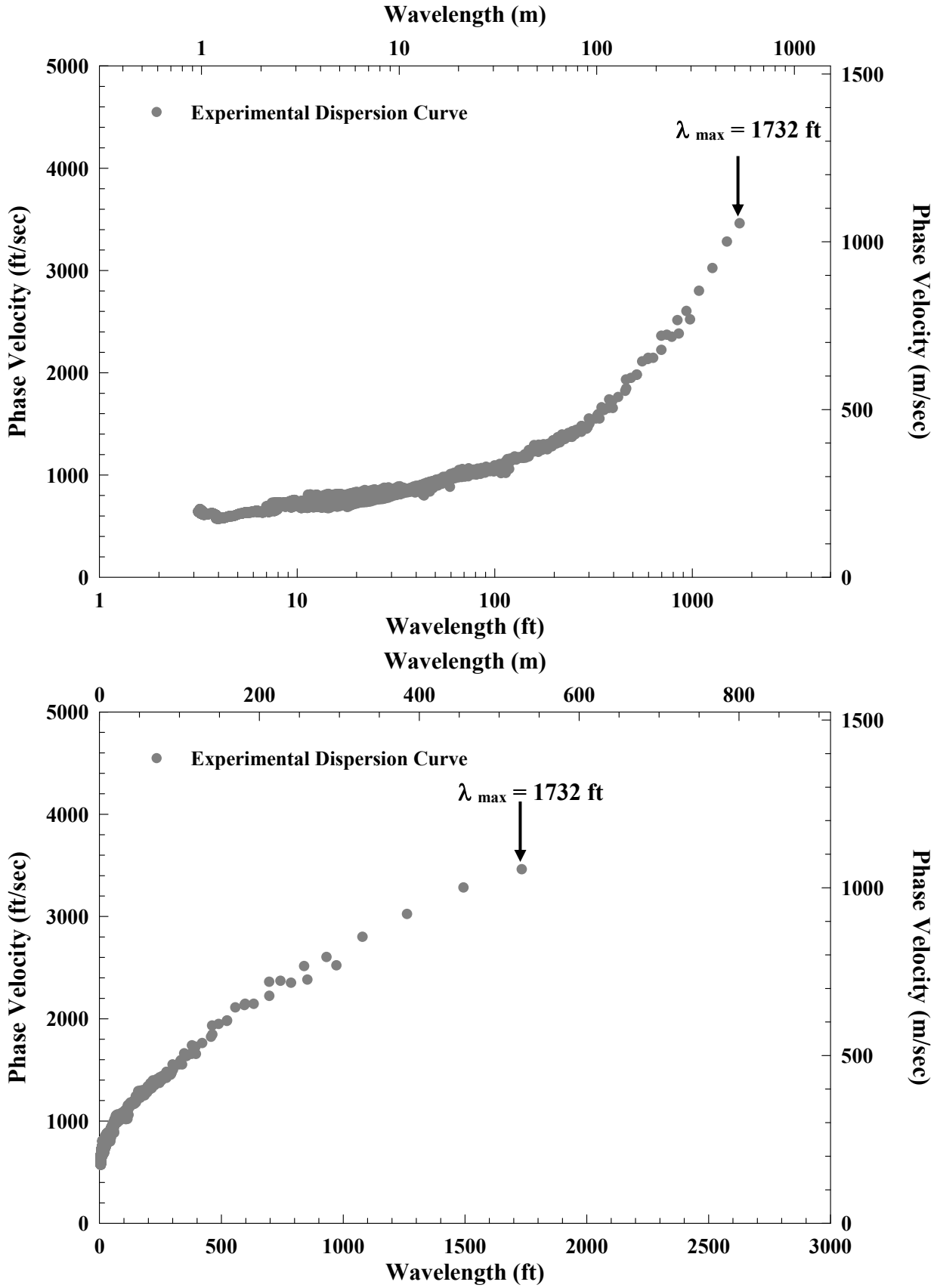

Figure A.3.1 Experimental Dispersion Curve Measured at Site 4A; Logarithmic (Top) and Linear (Bottom) Wavelength Axes

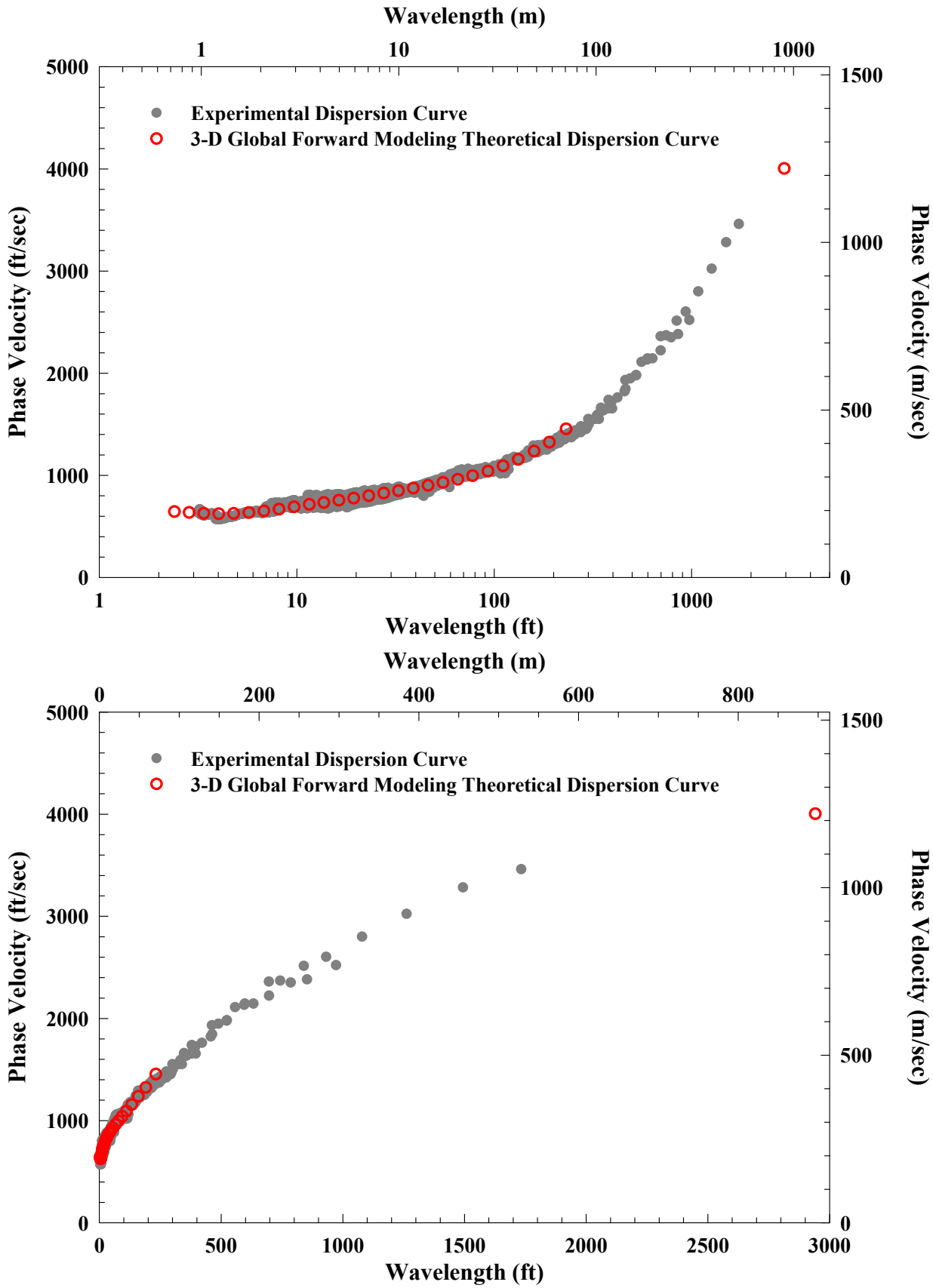

Figure A.3.2 Experimental (Field) and Global Forward Modeling Theoretical Dispersion Curves from Site 4A; Logarithmic (Top) and Linear (Bottom) Wavelength Axes

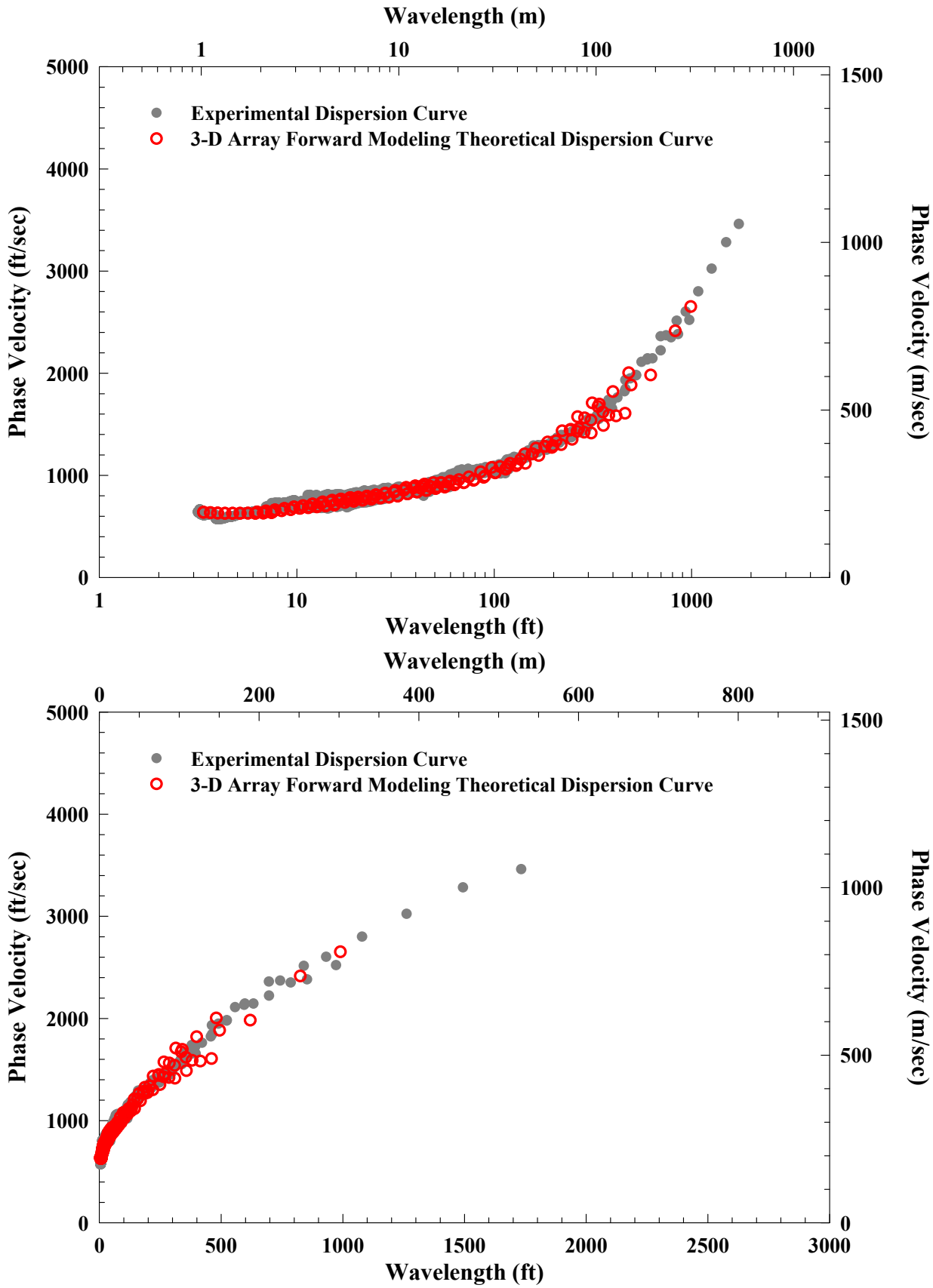

Figure A.3.3 Experimental (Field) and Array Forward Modeling Theoretical Dispersion Curves from Site 4A; Logarithmic (Top) and Linear (Bottom) Wavelength Axes

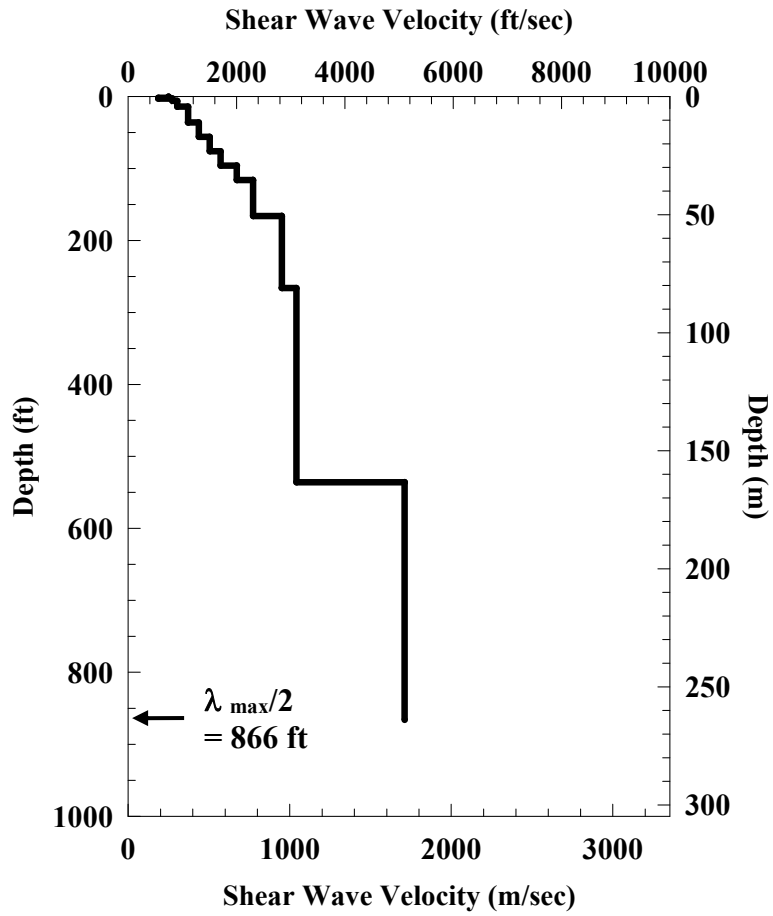

Figure A.3.4 Shear Wave Velocity Profile Determined at Site 4A

Table A.3.1 Profile Parameters Used to Develop Theoretical Dispersion Curve at Site 4A

Layer No.	Layer Thickness, ft	Depth of the Top of the Layer, ft	Vs, fps	Poisson's Ratio	Vp, fps	Total Unit Weight, pcf
1	1.5	0	740	0.25	1282	125
2	1	1.5	550	0.25	953	125
3	3.2	2.5	810	0.25	1403	125
4	8	5.7	900	0.25	1559	125
5	22	13.7	1100	0.25	1905	125
6	20	36	1300	0.25	2252	125
7	20	56	1500	0.25	2598	125
8	20	76	1700	0.25	2944	125
9	20	96	2000	0.25	3464	125
10	50	116	2300	0.25	3984	125
11	100	166	2830	0.33	5618	145
12	270	266	3100	0.33	6154	145
13	330	536	5100	0.33	10125	145
14*	Half Space	866	5100	0.33	10125	145

* Layer deeper than the maximum recommended profiling depth (λ_{max}/ 2).

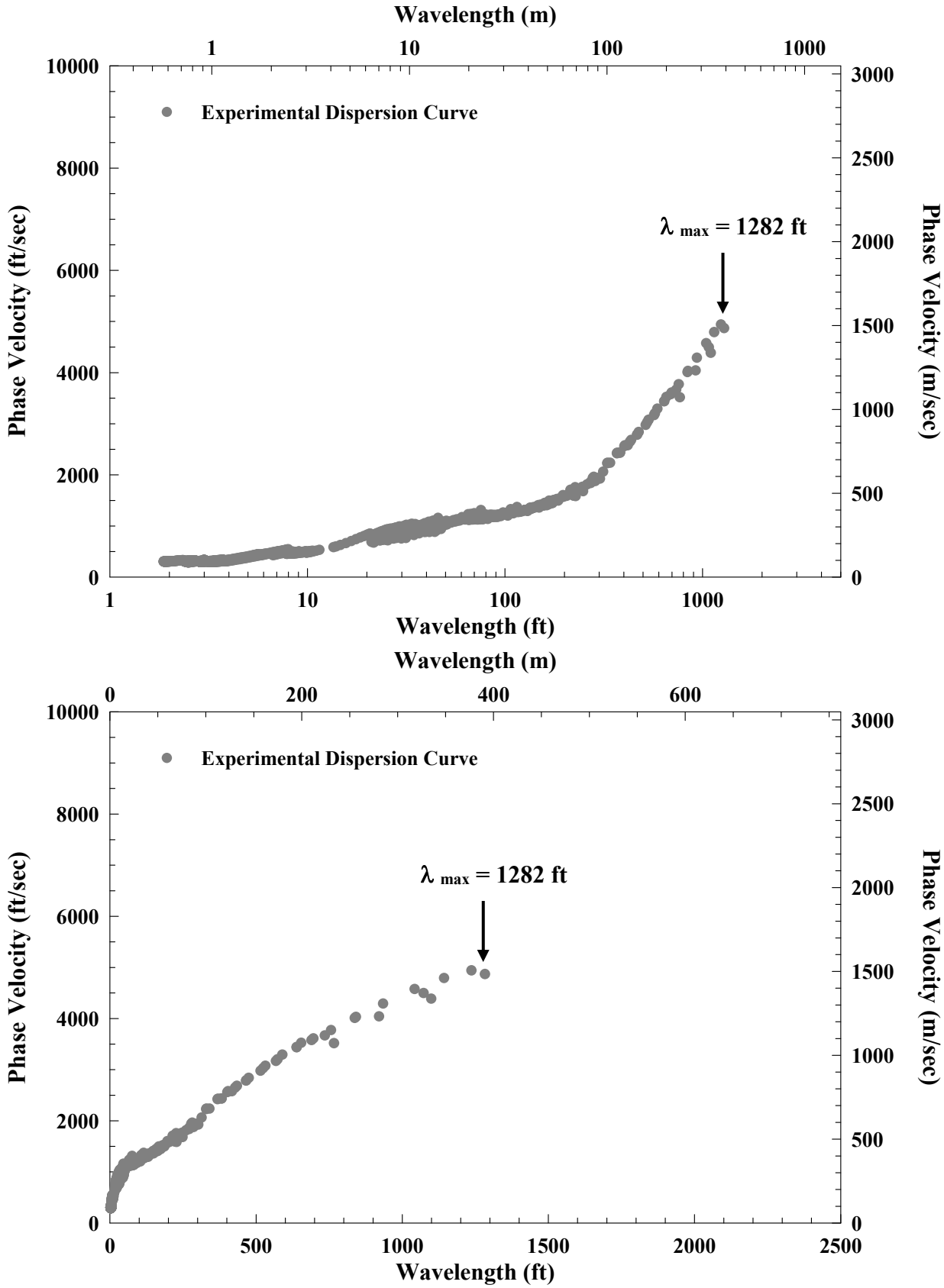

Figure A.4.1 Experimental Dispersion Curve Measured at Site H3A; Logarithmic (Top) and Linear (Bottom) Wavelength Axes

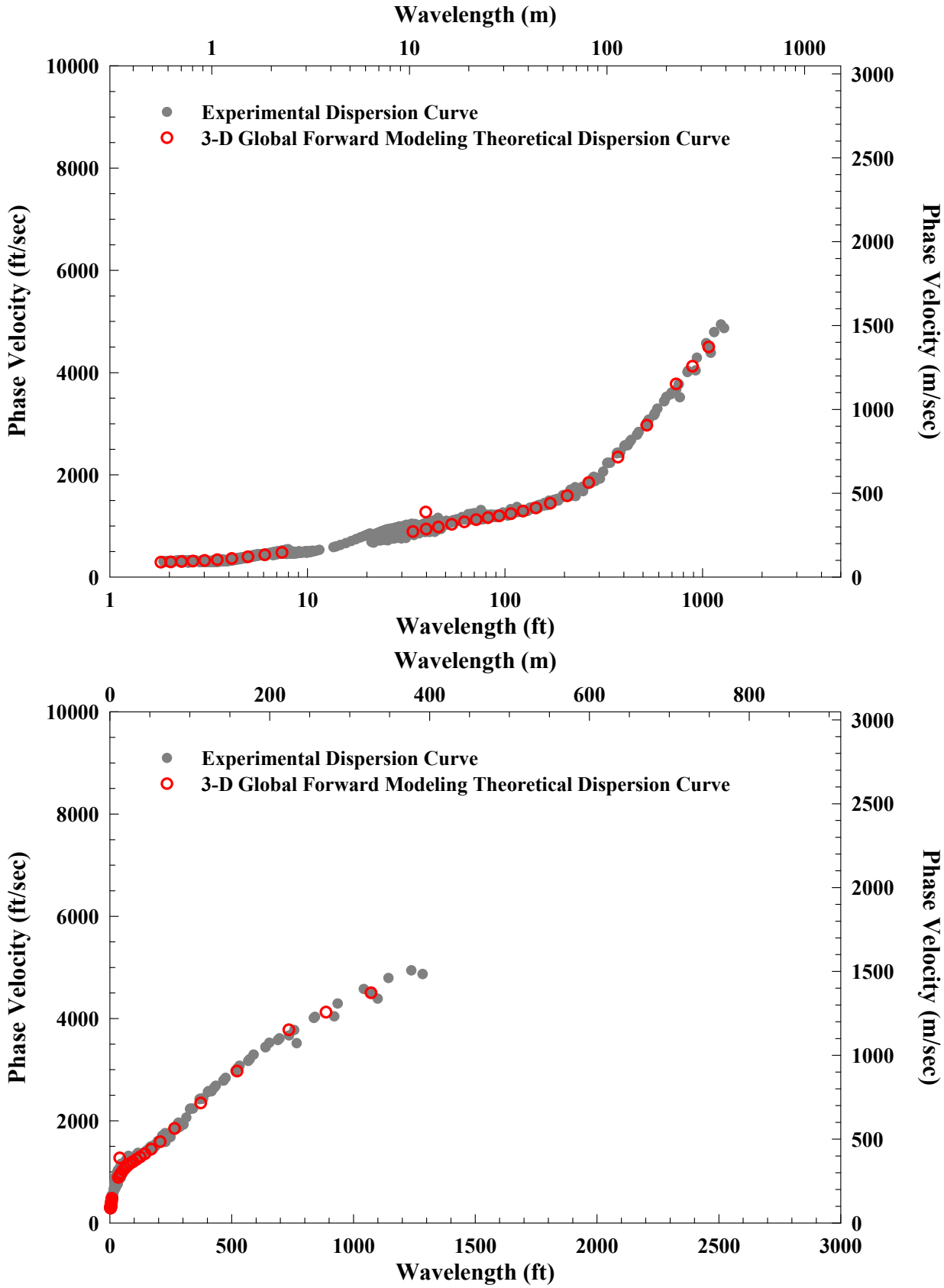

Figure A.4.2 Experimental (Field) and Global Forward Modeling Theoretical Dispersion Curves from Site H3A; Logarithmic (Top) and Linear (Bottom) Wavelength Axes

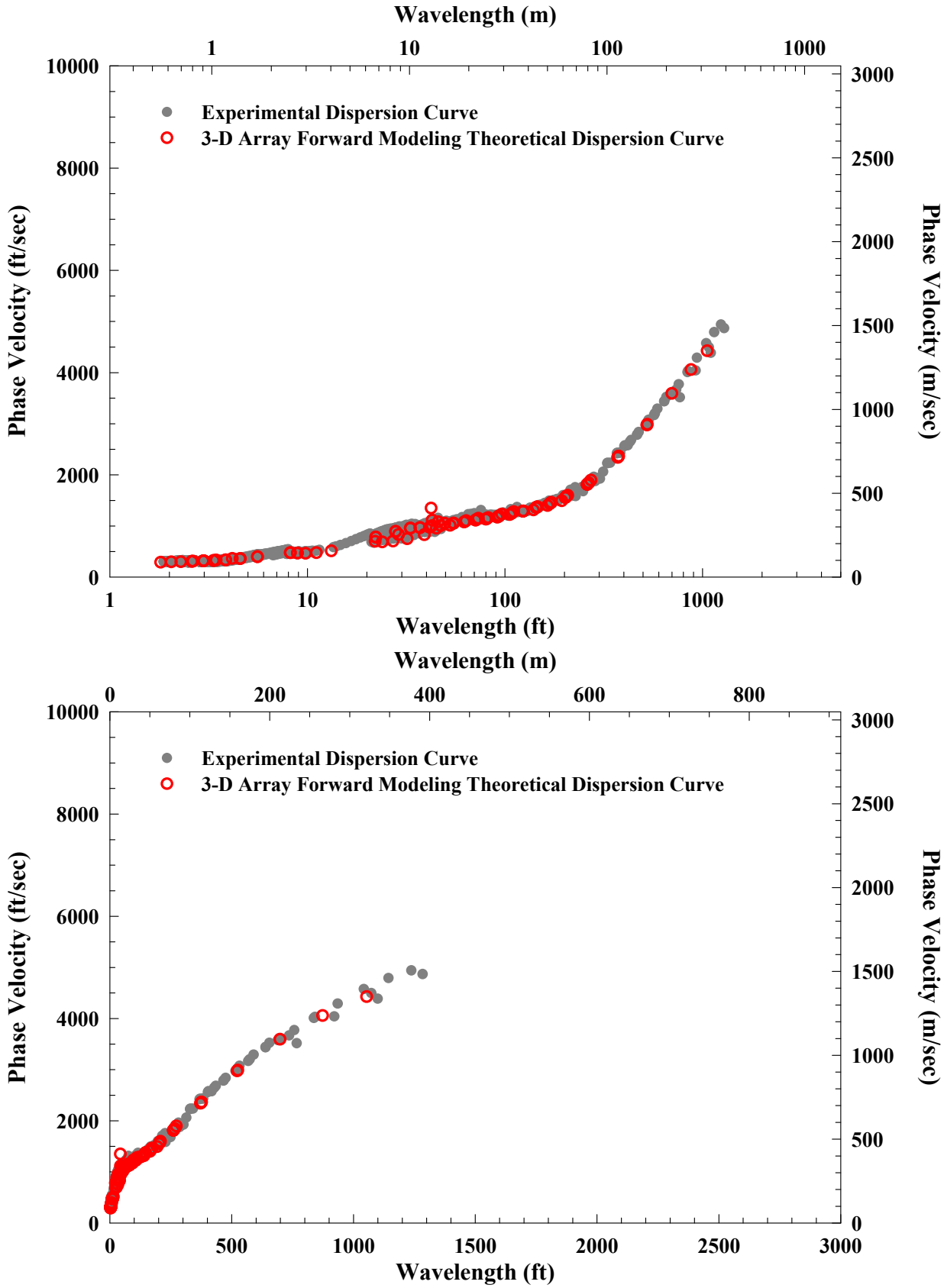

Figure A.4.3 Experimental (Field) and Array Forward Modeling Theoretical Dispersion Curves from Site H3A; Logarithmic (Top) and Linear (Bottom) Wavelength Axes

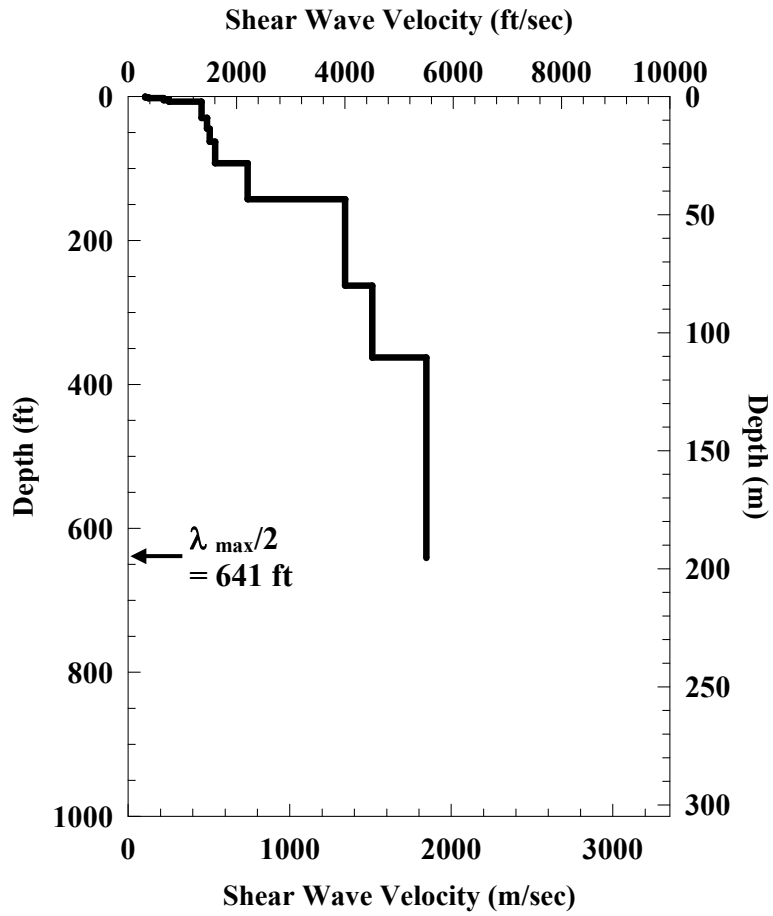

Figure A.4.4 Shear Wave Velocity Profile Determined at Site H3A

Table A.4.1 Profile Parameters Used to Develop Theoretical Dispersion Curve at Site H3A

Layer No.	Layer Thickness, ft	Depth of the Top of the Layer, ft	Vs, fps	Poisson's Ratio	Vp, fps	Total Unit Weight, pcf
1	1	0	310	0.25	537	125
2	0.9	1	370	0.25	641	125
3	2.8	1.9	650	0.25	1126	125
4	2.2	4.7	750	0.25	1299	125
5	22.5	6.9	1350	0.25	2338	125
6	15	29	1450	0.25	2511	125
7	18	44	1500	0.46	5000	135
8	30	62	1600	0.45	5000	135
9	50	92	2200	0.40	5000	135
10	120	142	4000	0.33	7941	145
11	100	262	4500	0.33	8934	145
12	279	362	5500	0.33	10919	145
13*	Half Space	641	5500	0.33	10919	145

* Layer deeper than the maximum recommended profiling depth (λ_{max}/ 2).

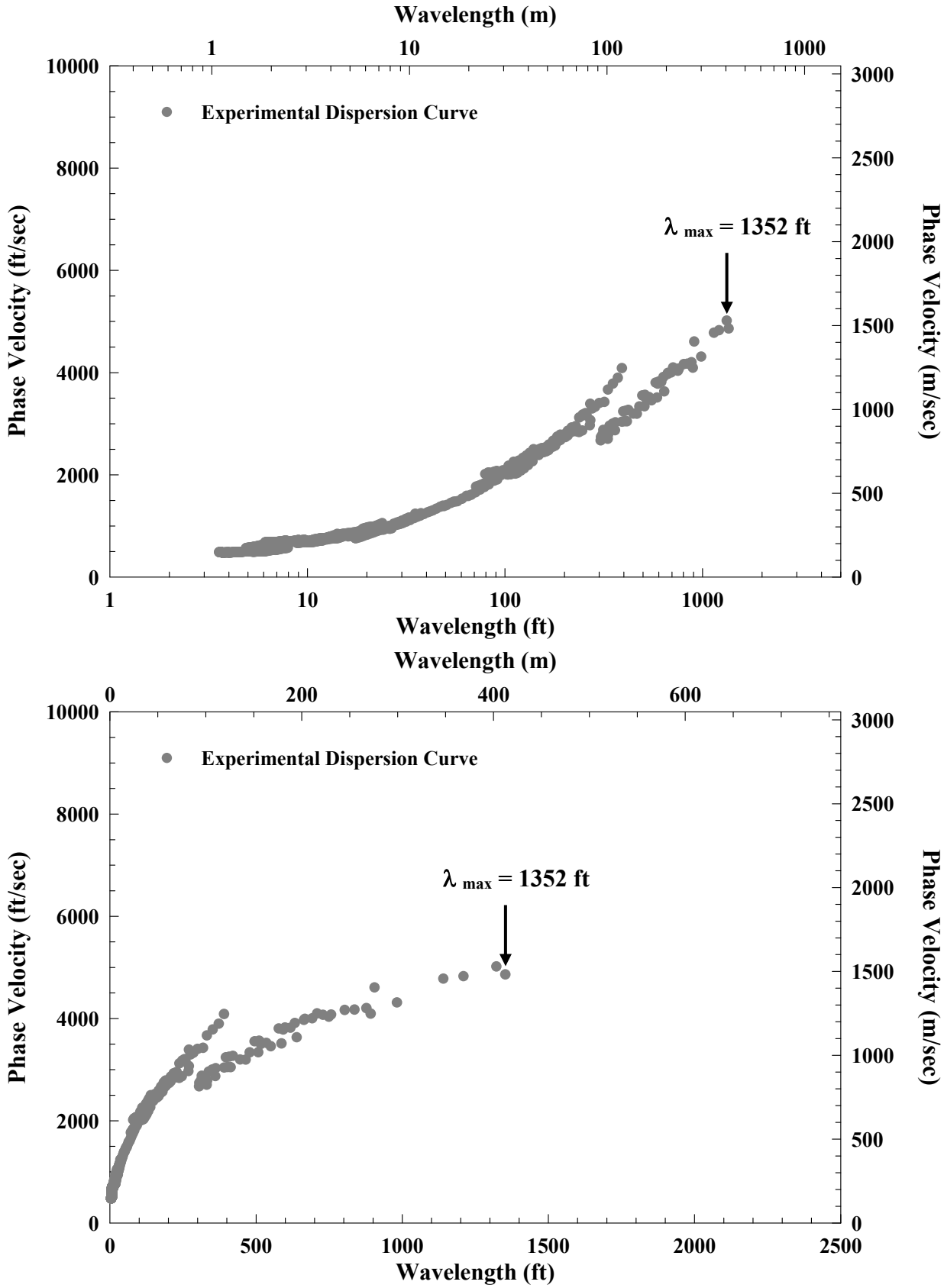

Figure A.5.1 Experimental Dispersion Curve Measured at Site WIAB; Logarithmic (Top) and Linear (Bottom) Wavelength Axes

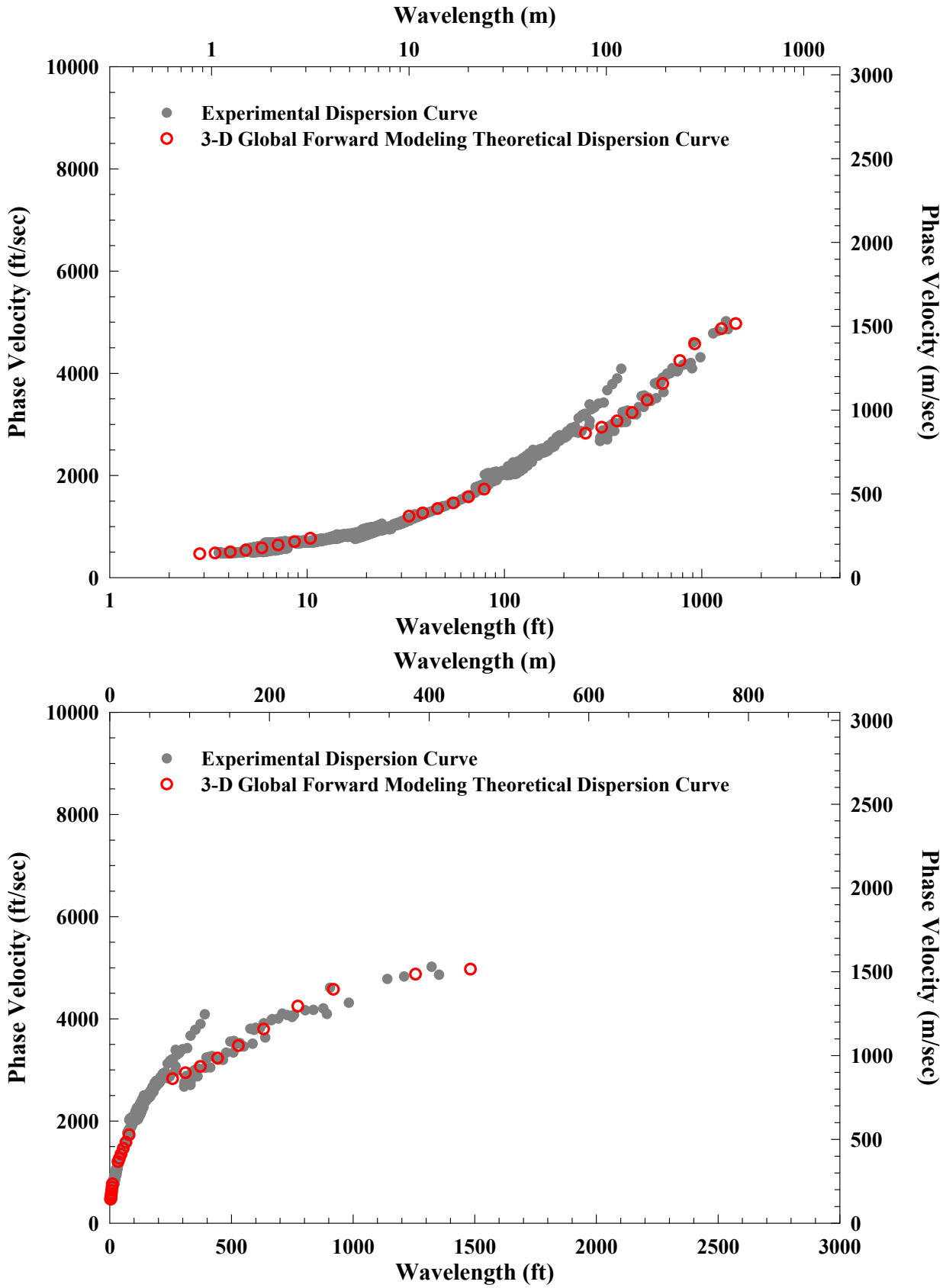

Figure A.5.2 Experimental (Field) and Global Forward Modeling Theoretical Dispersion Curves from Site WIAB; Logarithmic (Top) and Linear (Bottom) Wavelength Axes

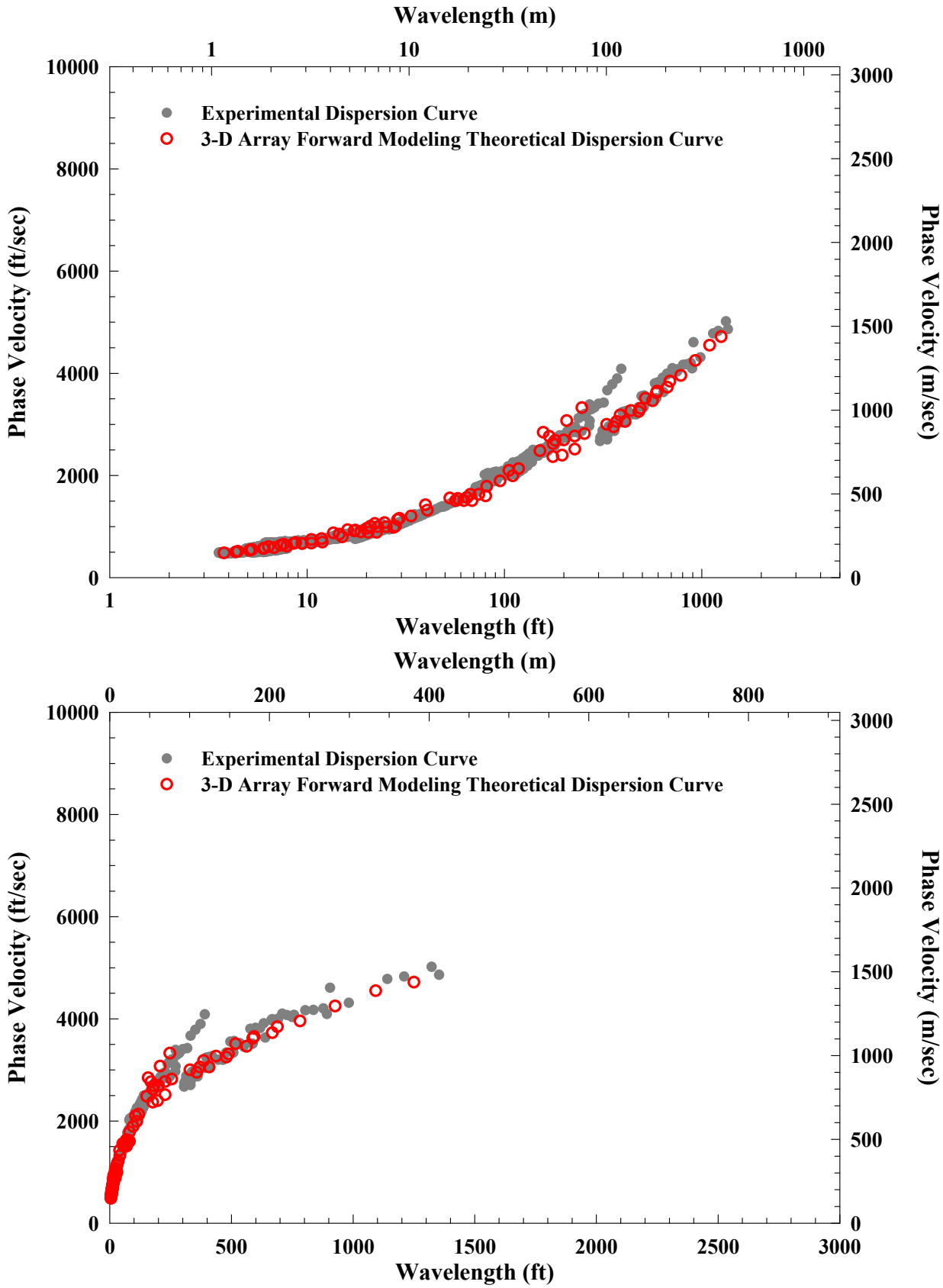

Figure A.5.3 Experimental (Field) and Array Forward Modeling Theoretical Dispersion Curves from Site WIAB; Logarithmic (Top) and Linear (Bottom) Wavelength Axes

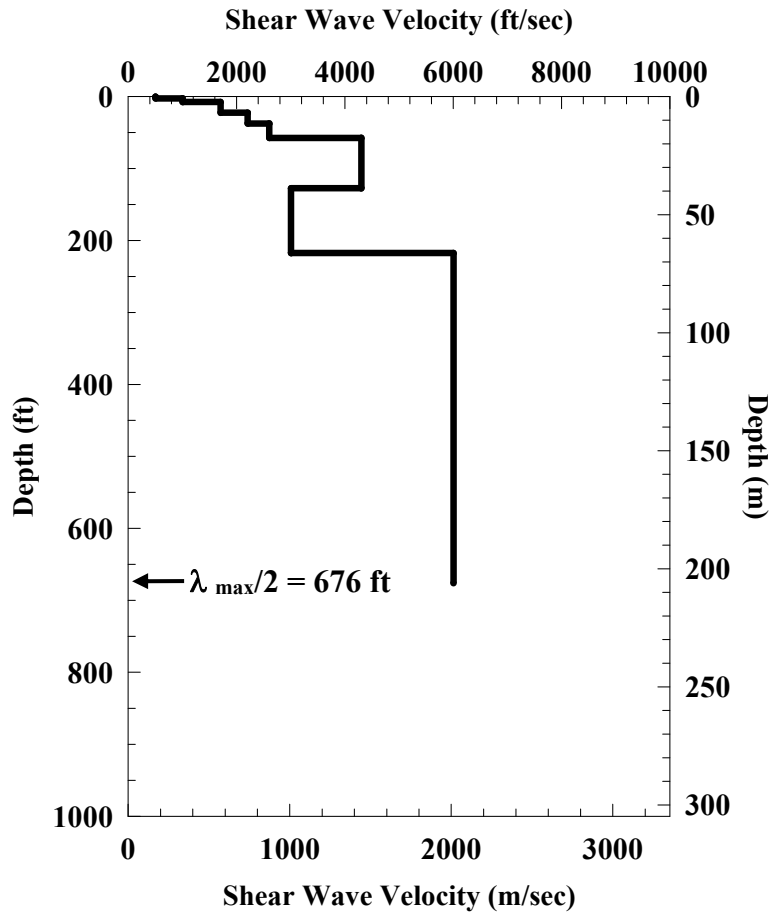

Figure A.5.4 Shear Wave Velocity Profile Determined at Site WIAB

Table A.5.1 Profile Parameters Used to Develop Theoretical Dispersion Curve at Site WIAB

Layer No.	Layer Thickness, ft	Depth of the Top of the Layer, ft	Vs, fps	Poisson's Ratio	Vp, fps	Total Unit Weight, pcf
1	2.2	0	500	0.25	866	125
2	5	2.2	1000	0.25	1732	125
3	15	7.2	1700	0.25	2944	125
4	15	22	2200	0.25	3811	125
5	20	37	2600	0.33	5162	145
6	70	57	4300	0.33	8537	145
7	90	127	3000	0.33	5956	145
8	459	217	6000	0.33	11911	145
9*	Half Space	676	6000	0.33	11911	145

* Layer deeper than the maximum recommended profiling depth (λ_{max}/ 2).

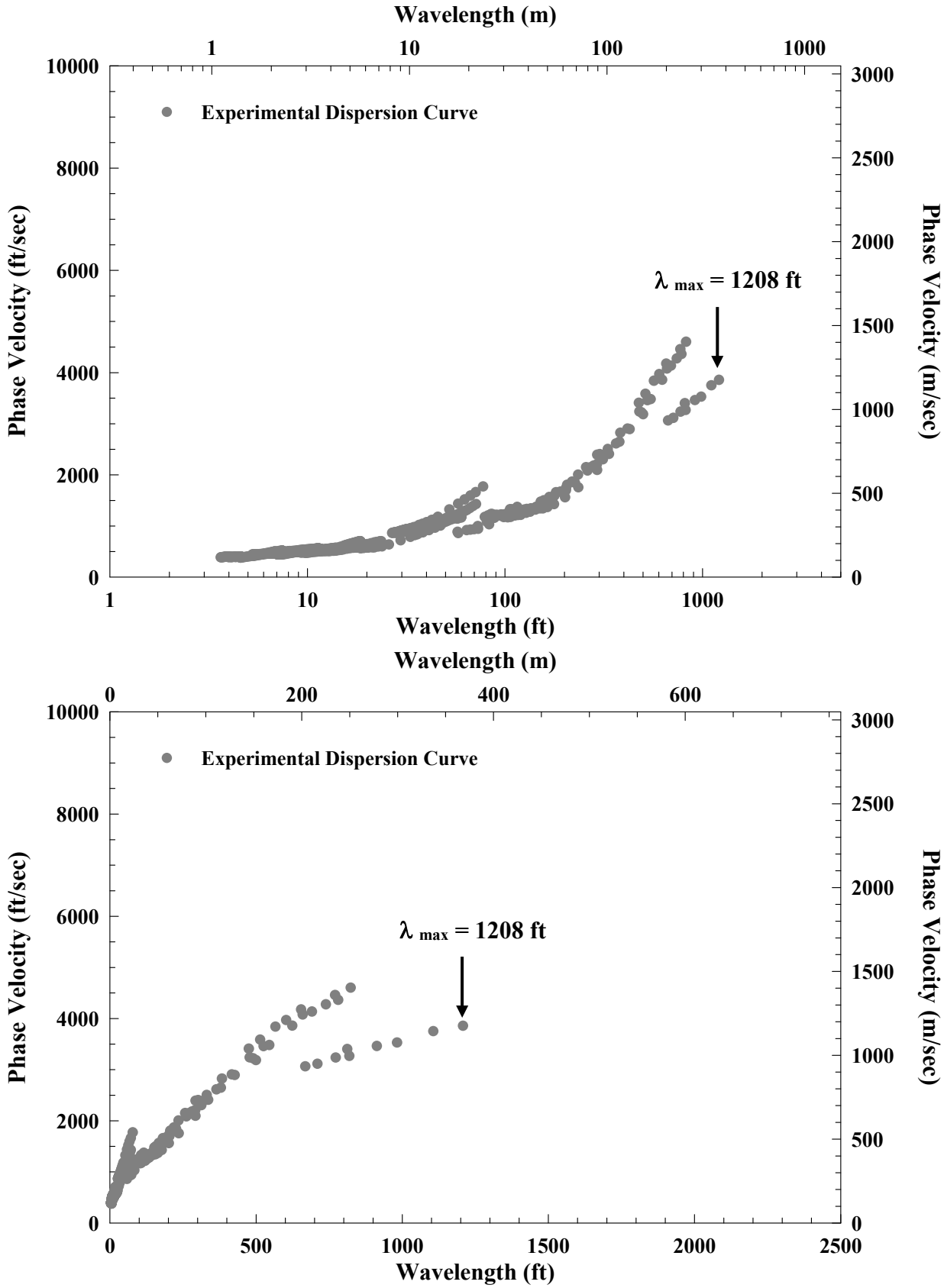

Figure A.6.1 Experimental Dispersion Curve Measured at Site WIXX; Logarithmic (Top) and Linear (Bottom) Wavelength Axes

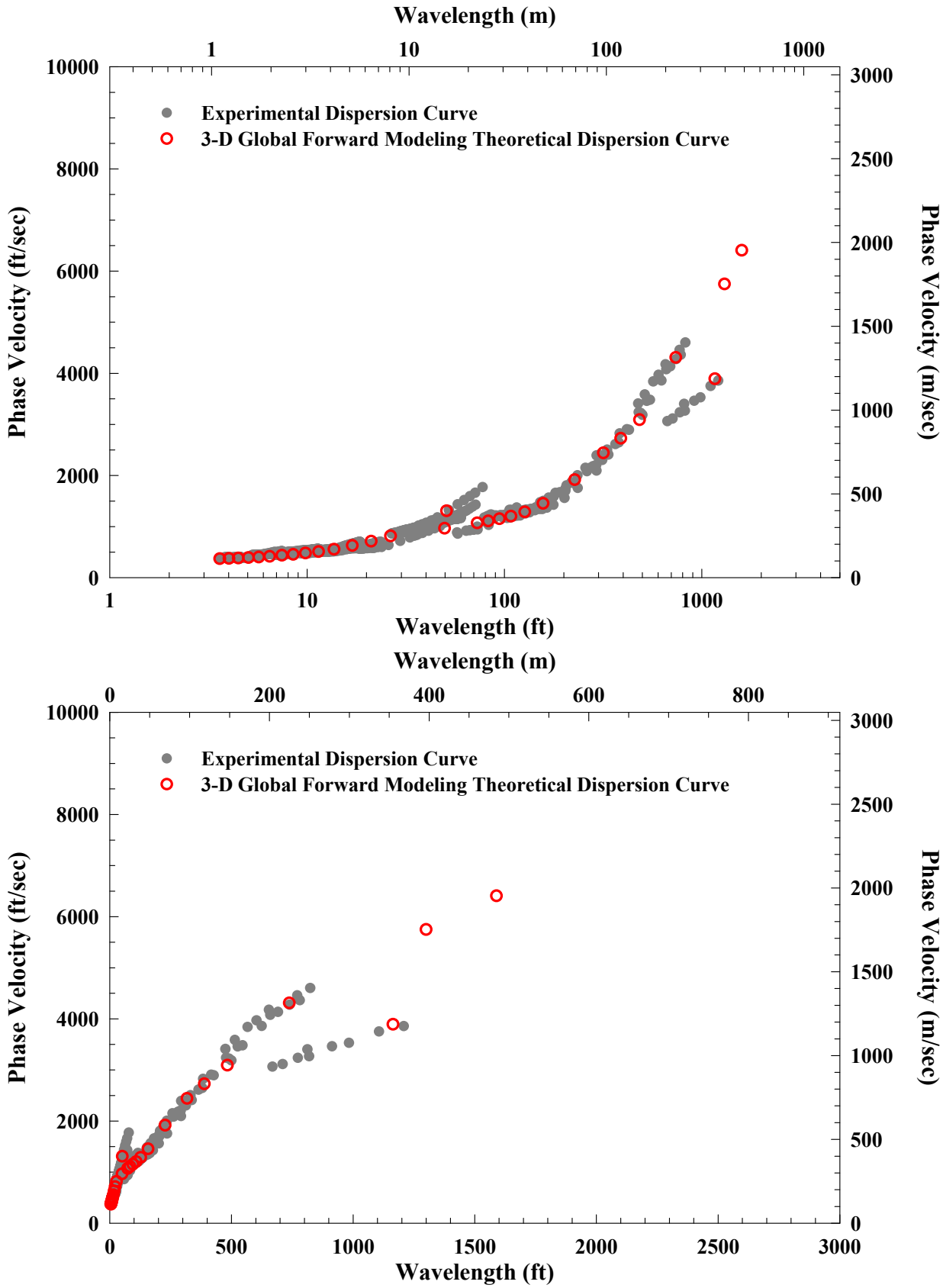

Figure A.6.2 Experimental (Field) and Global Forward Modeling Theoretical Dispersion Curves from Site WIXX; Logarithmic (Top) and Linear (Bottom) Wavelength Axes

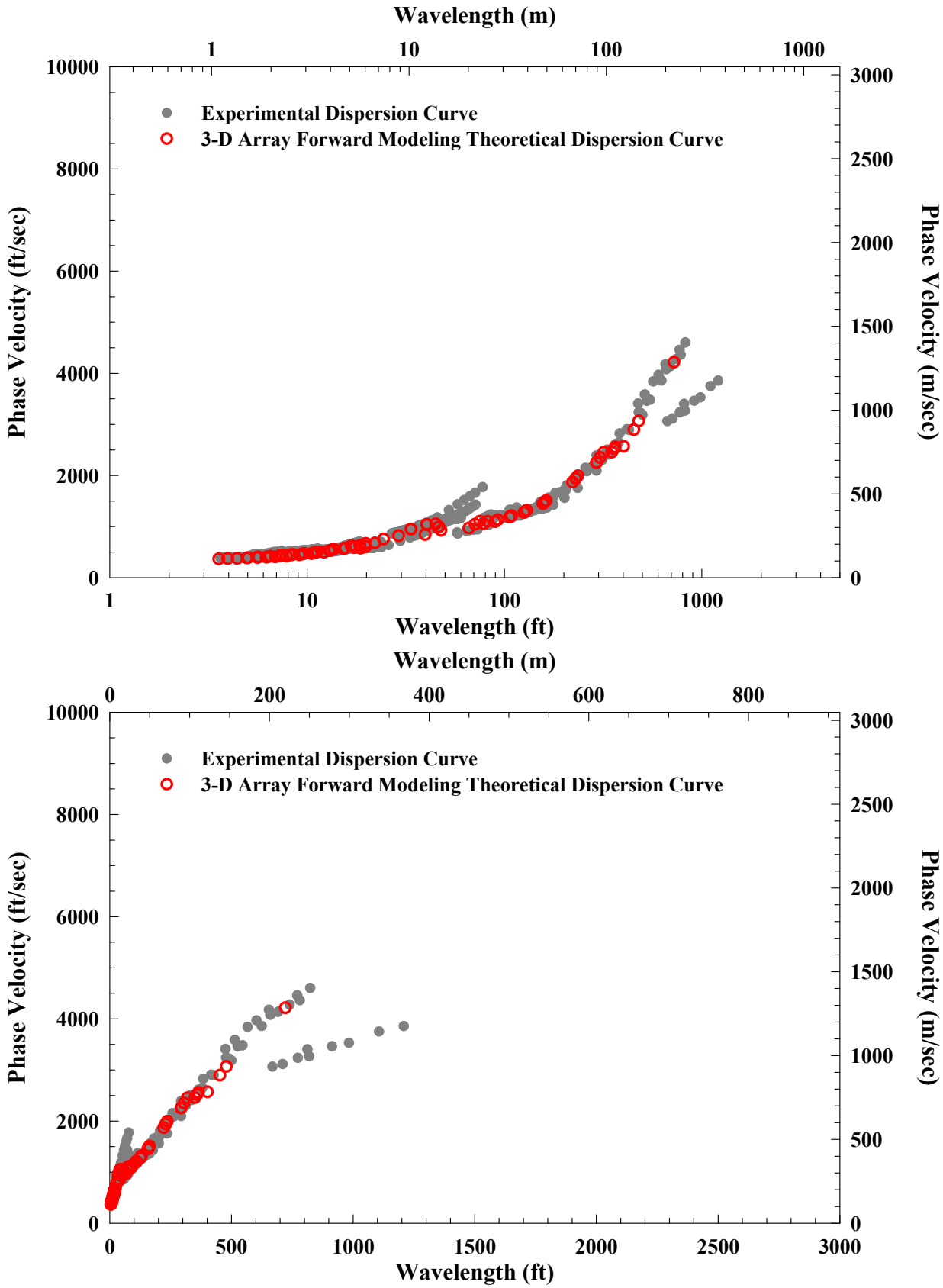

Figure A.6.3 Experimental (Field) and Array Forward Modeling Theoretical Dispersion Curves from Site WIXX; Logarithmic (Top) and Linear (Bottom) Wavelength Axes

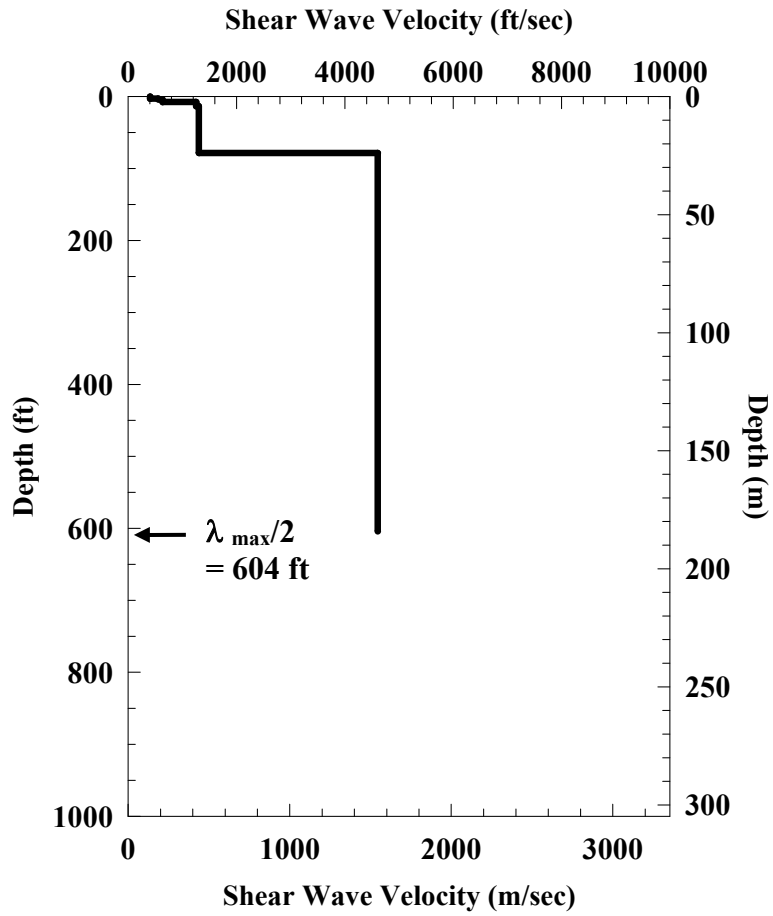

Figure A.6.4 Shear Wave Velocity Profile Determined at Site WIXX

Table A.6.1 Profile Parameters Used to Develop Theoretical Dispersion Curve at Site WIXX

Layer No.	Layer Thickness, ft	Depth of the Top of the Layer, ft	Vs, fps	Poisson's Ratio	Vp, fps	Total Unit Weight, pcf
1	2.6	0	400	0.25	693	125
2	1.1	2.6	550	0.25	953	125
3	3.5	3.7	630	0.25	1091	125
4	6	7.2	1250	0.25	2165	125
5	65	13.2	1300	0.46	5000	135
6	526	78	4600	0.33	9132	145
7*	Half Space	604	4600	0.33	9132	145

* Layer deeper than the maximum recommended profiling depth (λ_{max}/ 2).

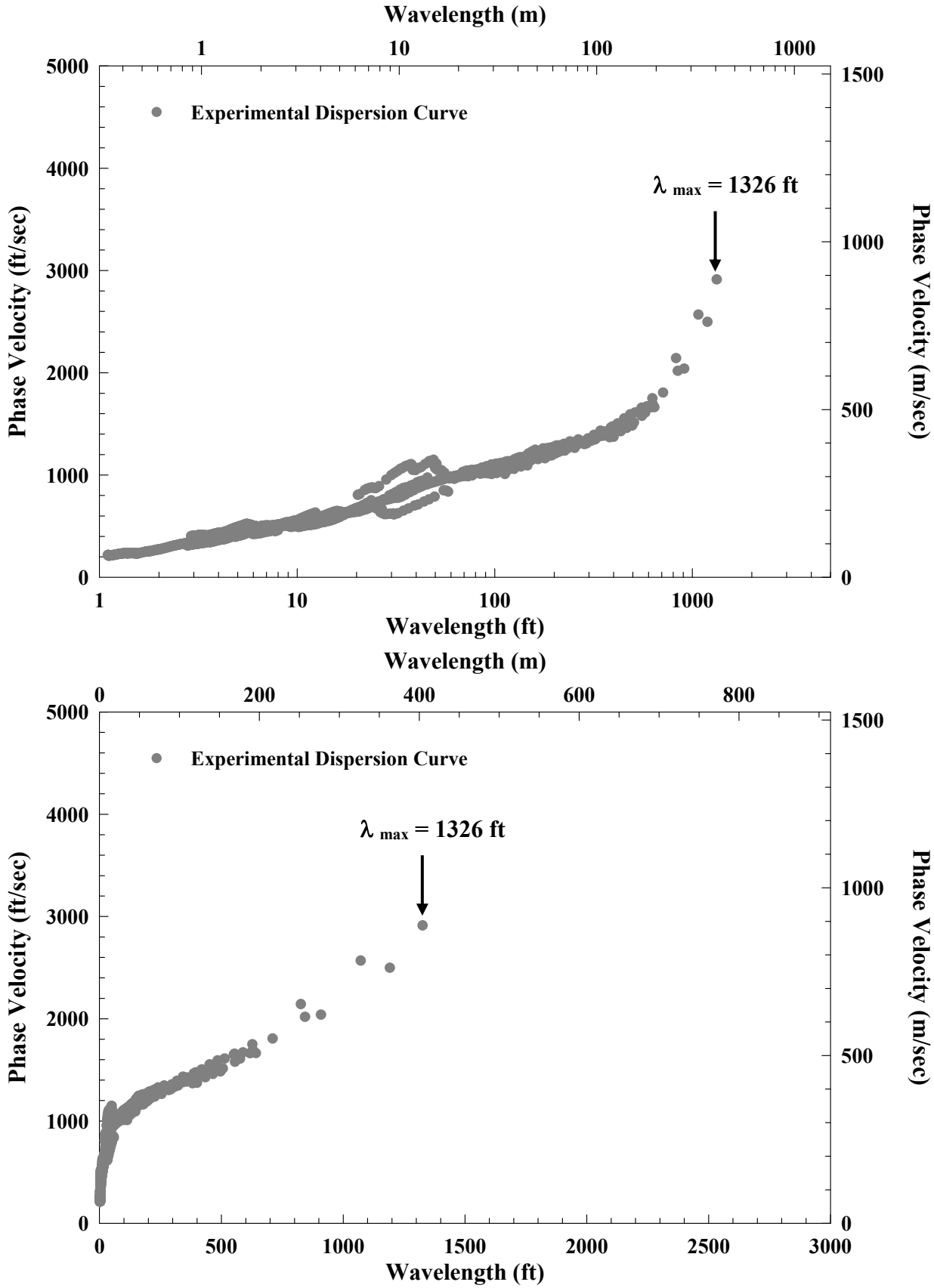

Figure A.7.1 Experimental Dispersion Curve Measured at Site H2E; Logarithmic (Top) and Linear (Bottom) Wavelength Axes

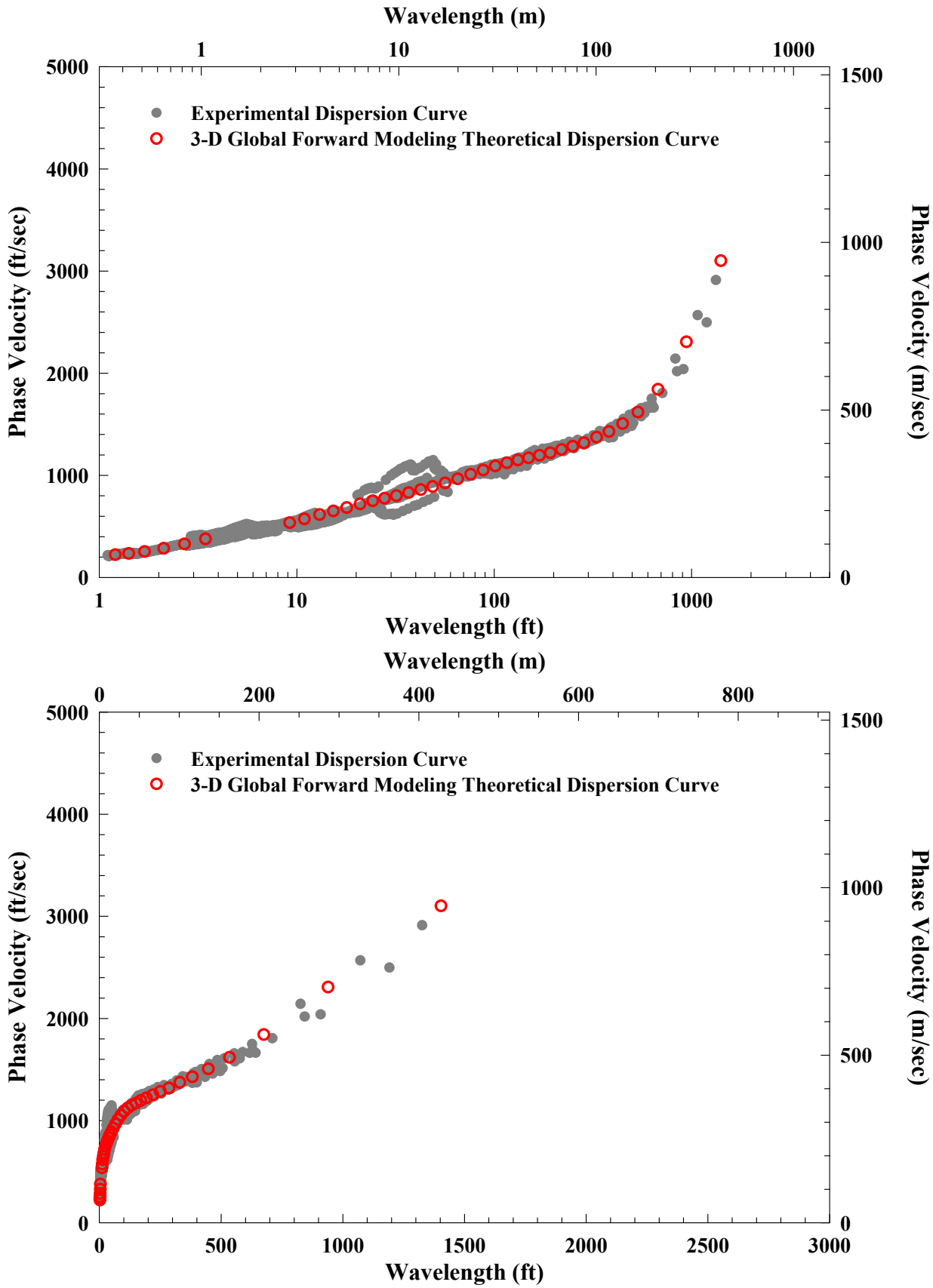

Figure A.7.2 Experimental (Field) and Global Forward Modeling Theoretical Dispersion Curves from Site H2E; Logarithmic (Top) and Linear (Bottom) Wavelength Axes

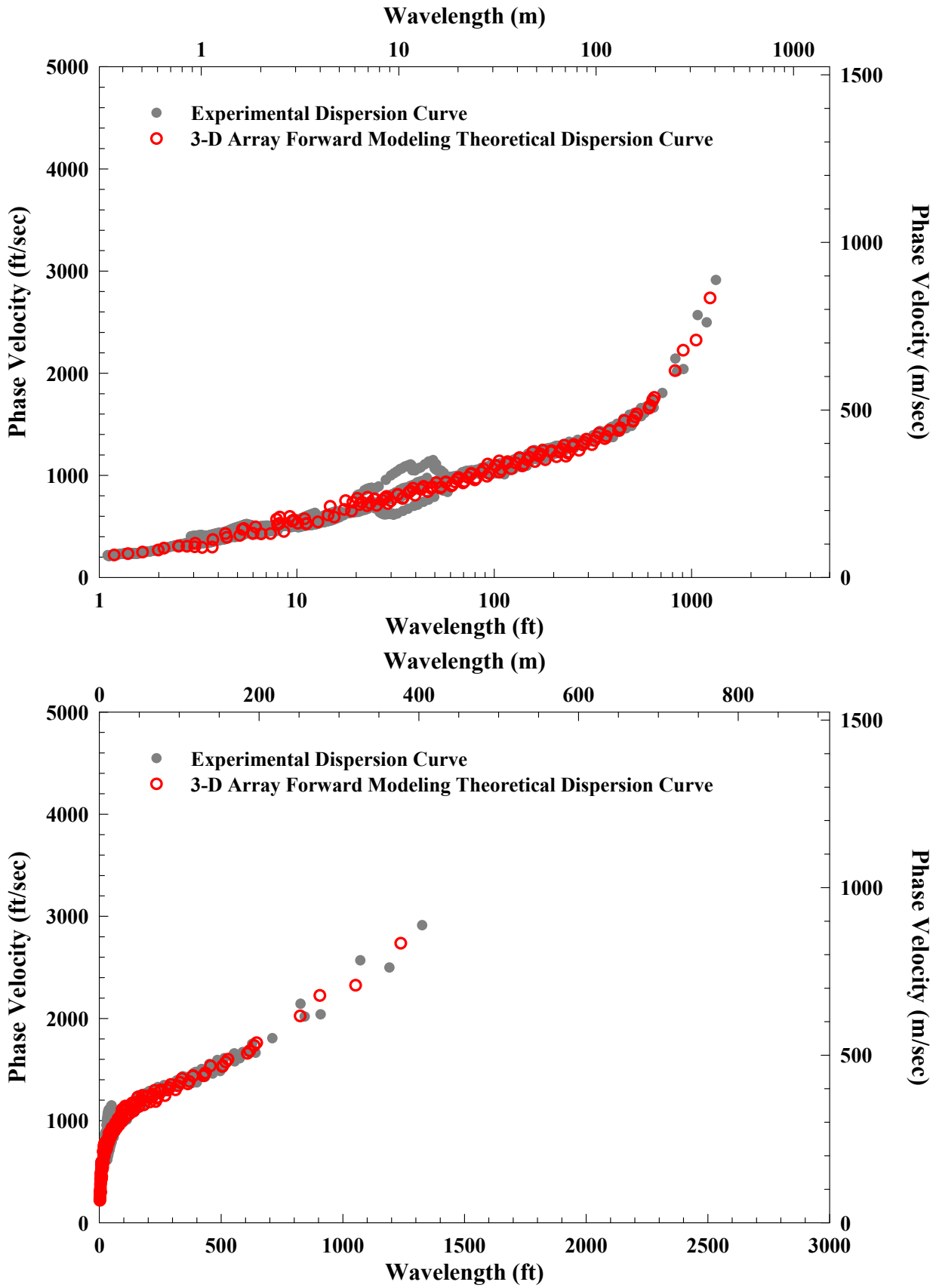

Figure A.7.3 Experimental (Field) and Array Forward Modeling Theoretical Dispersion Curves from Site H2E; Logarithmic (Top) and Linear (Bottom) Wavelength Axes

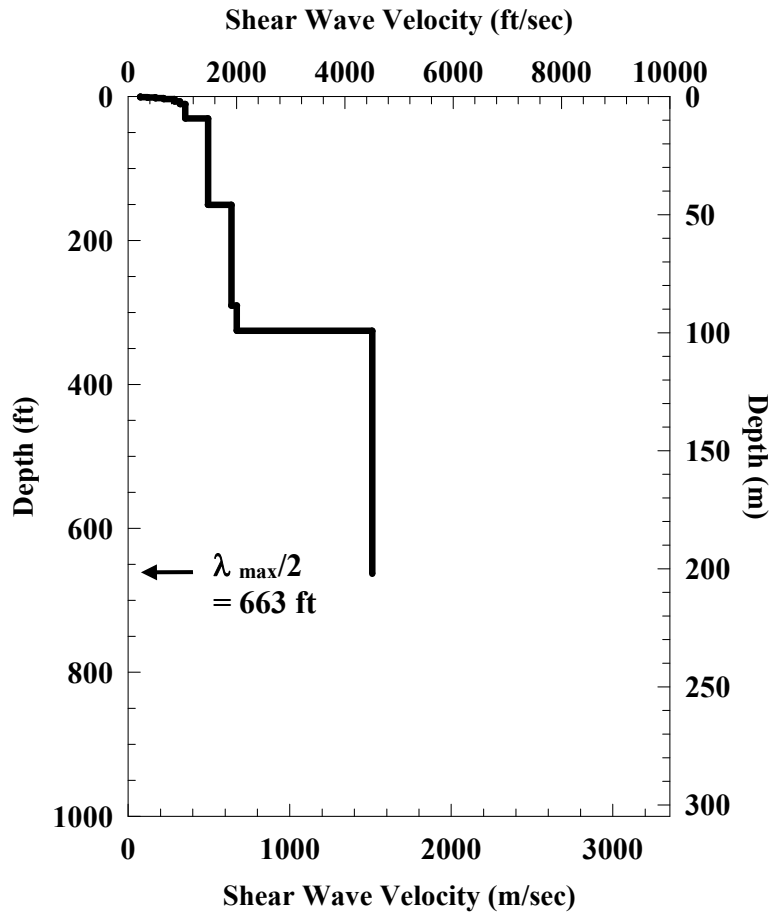

Figure A.7.4 Shear Wave Velocity Profile Determined at Site H2E

Table A.7.1 Profile Parameters Used to Develop Theoretical Dispersion Curve at Site H2E

Layer No.	Layer Thickness, ft	Depth of the Top of the Layer, ft	Vs, fps	Poisson's Ratio	Vp, fps	Total Unit Weight, pcf
1	0.6	0	220	0.25	381	125
2	0.3	0.6	350	0.25	606	125
3	1.08	0.9	500	0.25	866	125
4	1.2	1.98	650	0.25	1126	125
5	3.2	3.18	850	0.25	1472	125
6	3.75	6.38	950	0.25	1645	125
7	20	10.13	1050	0.25	1819	125
8	120	30	1470	0.25	2546	125
9	140	150	1900	0.25	3291	125
10	35	290	2000	0.40	5000	135
11	338	325	4500	0.33	8934	145
12*	Half Space	663	4500	0.33	8934	145

* Layer deeper than the maximum recommended profiling depth (λ_{max}/ 2).

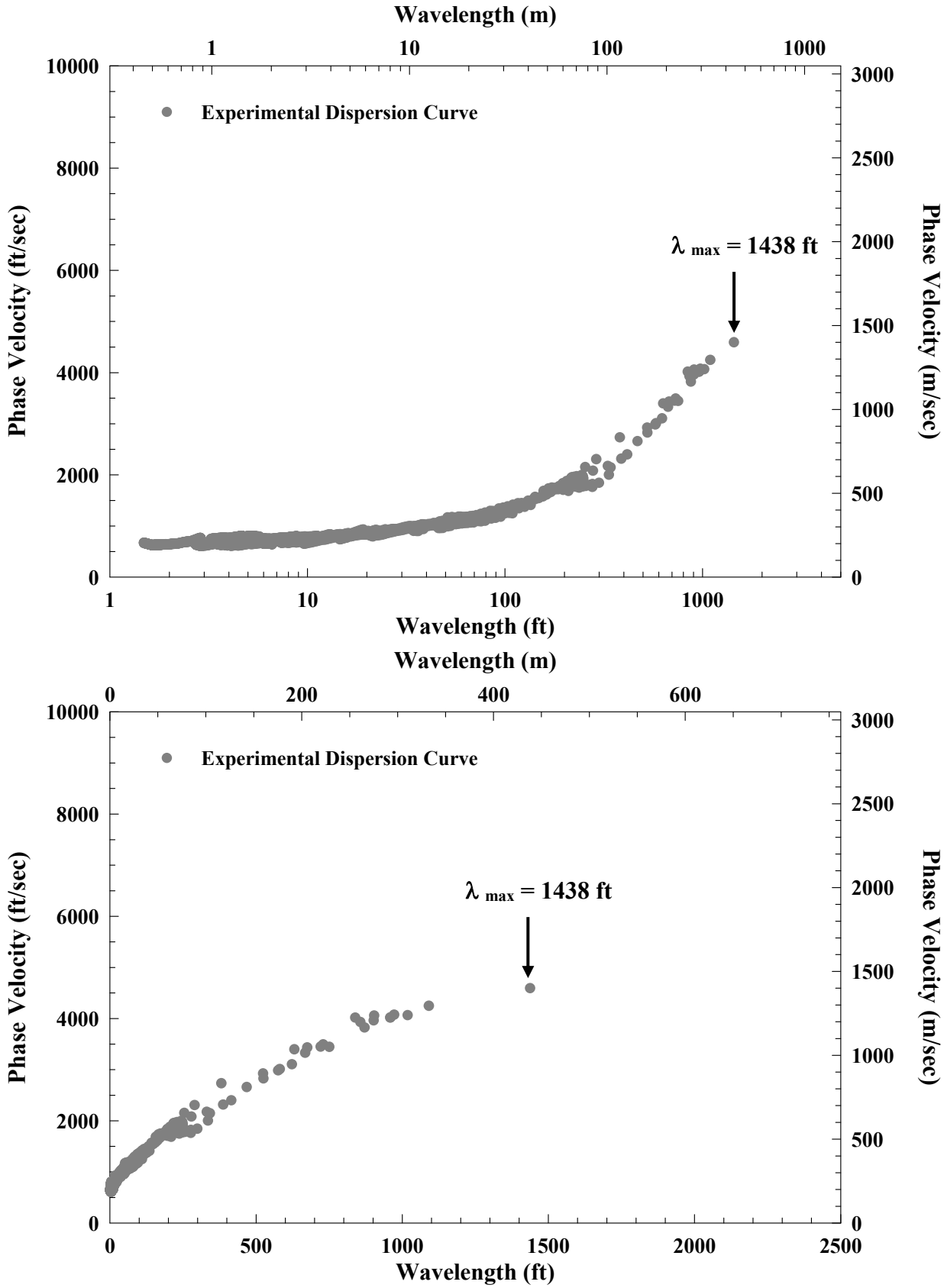

Figure A.8.1 Experimental Dispersion Curve Measured at Site Haulroad; Logarithmic (Top) and Linear (Bottom) Wavelength Axes

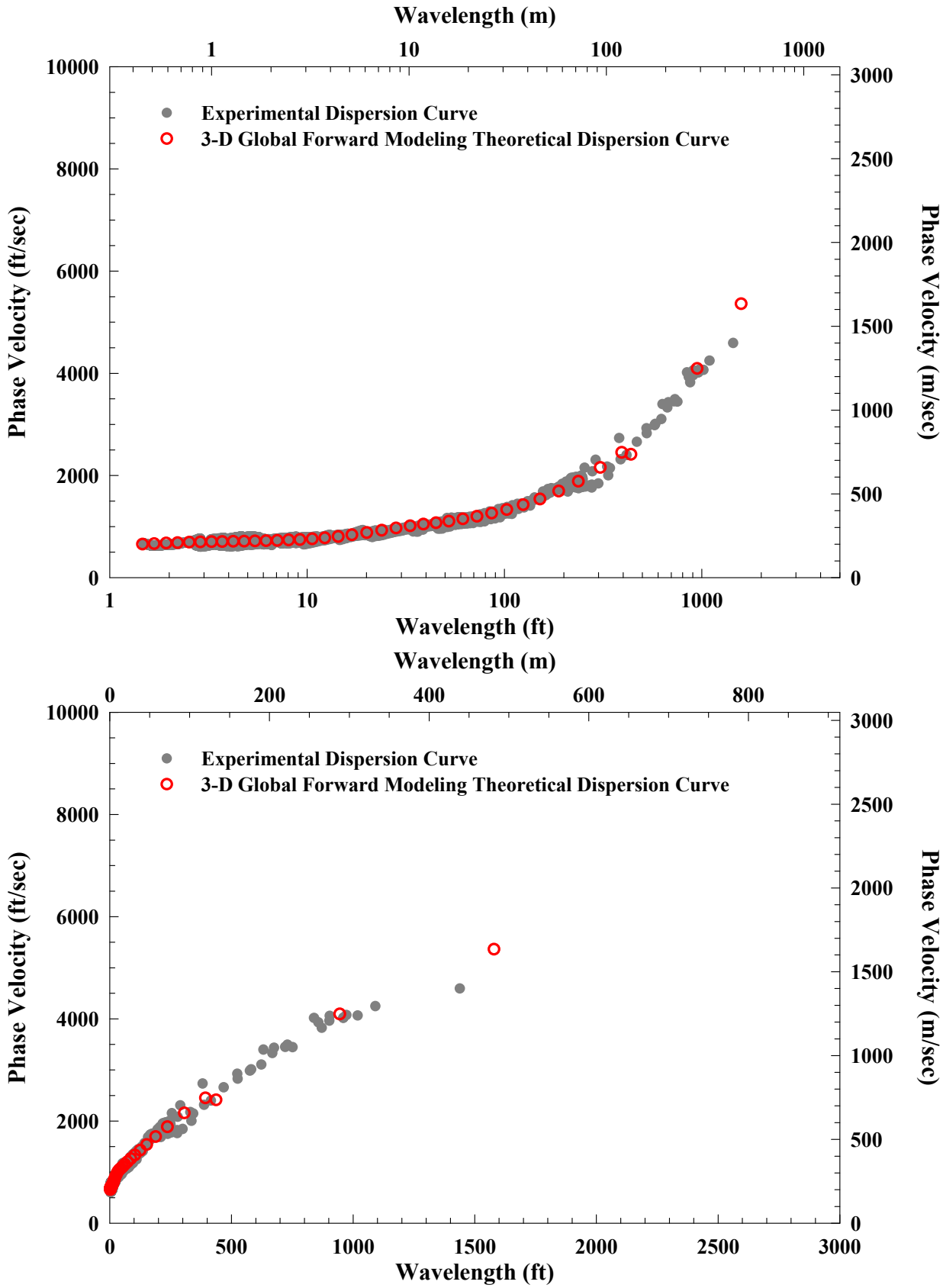

Figure A.8.2 Experimental (Field) and Global Forward Modeling Theoretical Dispersion Curves from Site Haulroad; Logarithmic (Top) and Linear (Bottom) Wavelength Axes

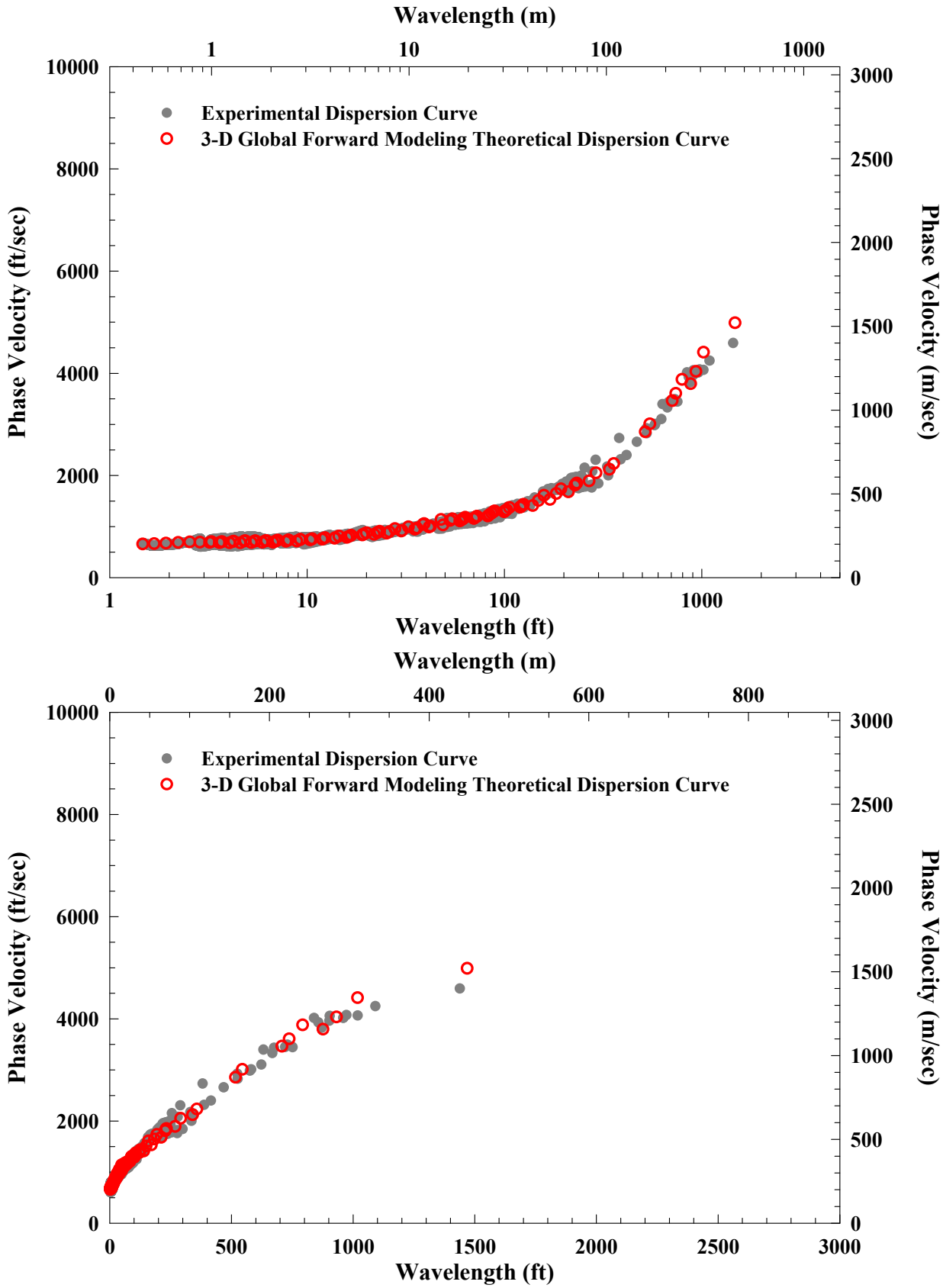

Figure A.8.3 Experimental (Field) and Array Forward Modeling Theoretical Dispersion Curves from Site Haulroad; Logarithmic (Top) and Linear (Bottom) Wavelength Axes

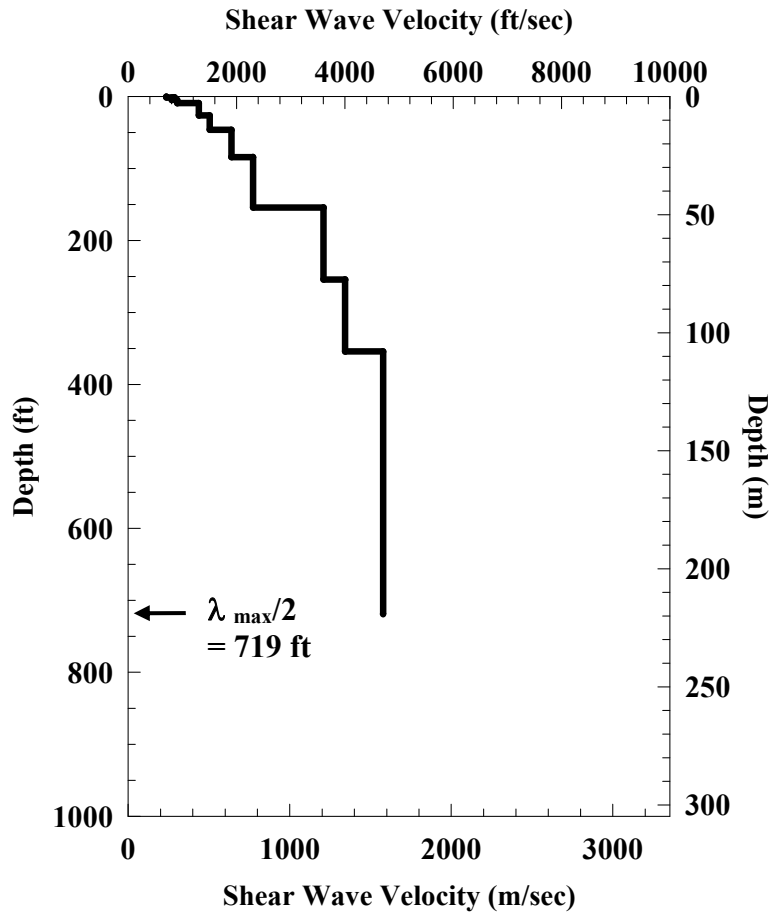

Figure A.8.4 Shear Wave Velocity Profile Determined at Site Haulroad

Table A.8.1 Profile Parameters Used to Develop Theoretical Dispersion Curve at Site Haulroad

Layer No.	Layer Thickness, ft	Depth of the Top of the Layer, ft	Vs, fps	Poisson's Ratio	Vp, fps	Total Unit Weight, pcf
1	0.9	0	700	0.25	1212	125
2	0.5	0.9	850	0.25	1472	125
3	3	1.4	800	0.25	1386	125
4	4.5	4.4	900	0.25	1559	125
5	17	8.9	1300	0.25	2252	125
6	20	26	1500	0.25	2598	125
7	38	46	1900	0.43	5000	135
8	70	84	2300	0.39	5000	135
9	100	154	3600	0.33	7147	145
10	100	254	4000	0.33	7941	145
11	365	354	4700	0.33	9331	145
12*	Half Space	719	4700	0.33	9331	145

* Layer deeper than the maximum recommended profiling depth (λ_{max}/ 2).

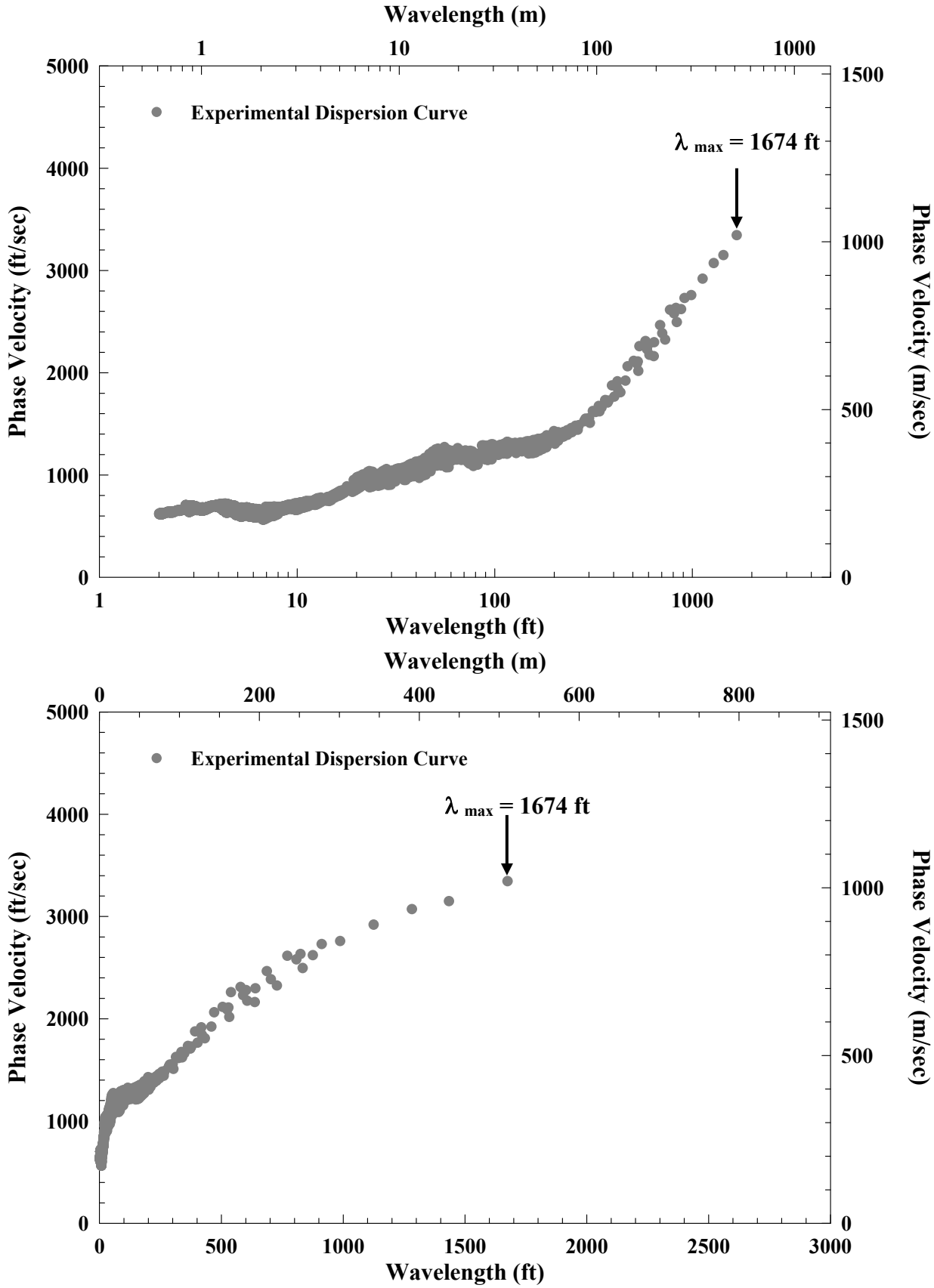

Figure A.9.1 Experimental Dispersion Curve Measured at Site H2W1998; Logarithmic (Top) and Linear (Bottom) Wavelength Axes

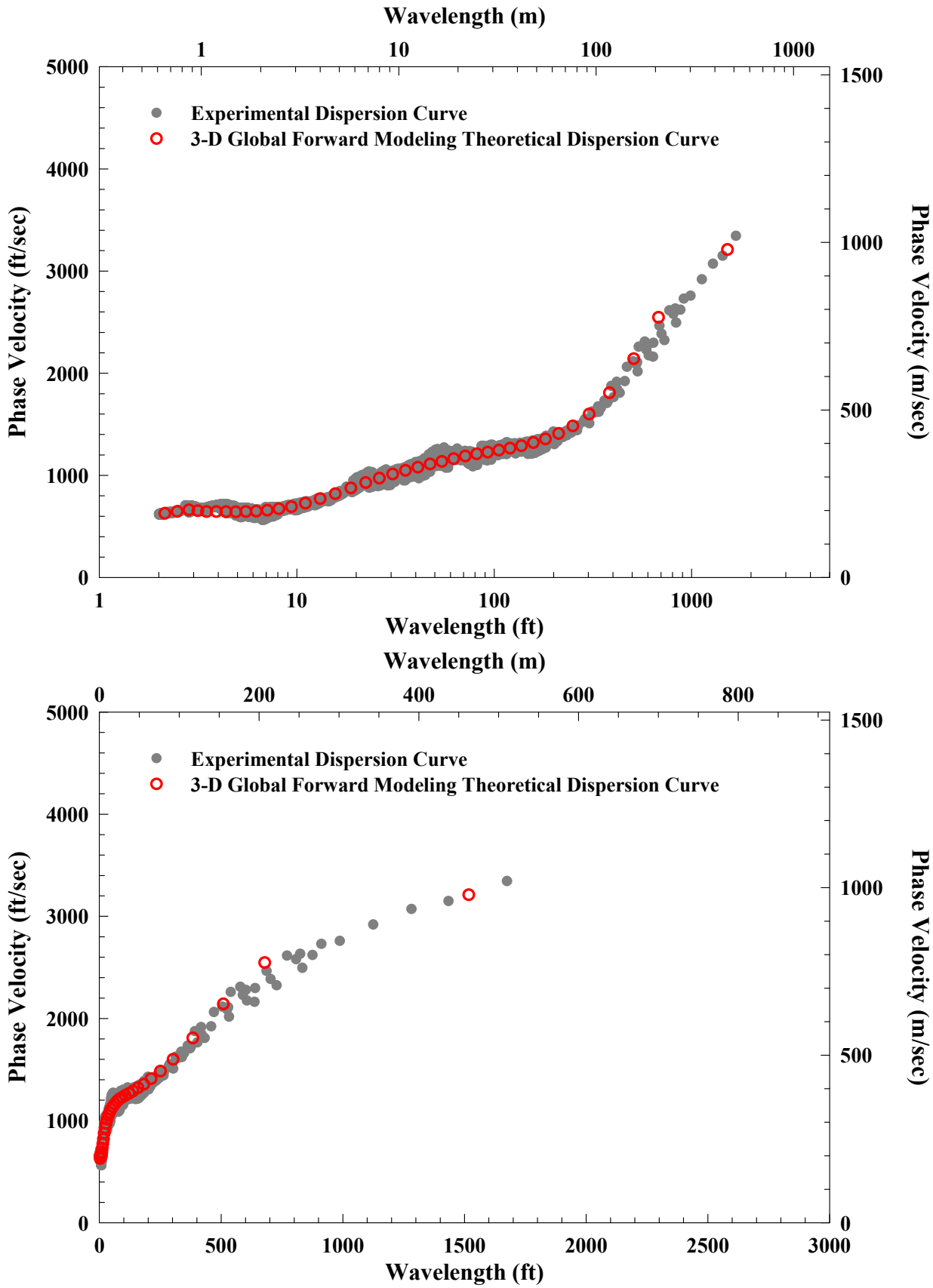

Figure A.9.2 Experimental (Field) and Global Forward Modeling Theoretical Dispersion Curves from Site H2W1998; Logarithmic (Top) and Linear (Bottom) Wavelength Axes

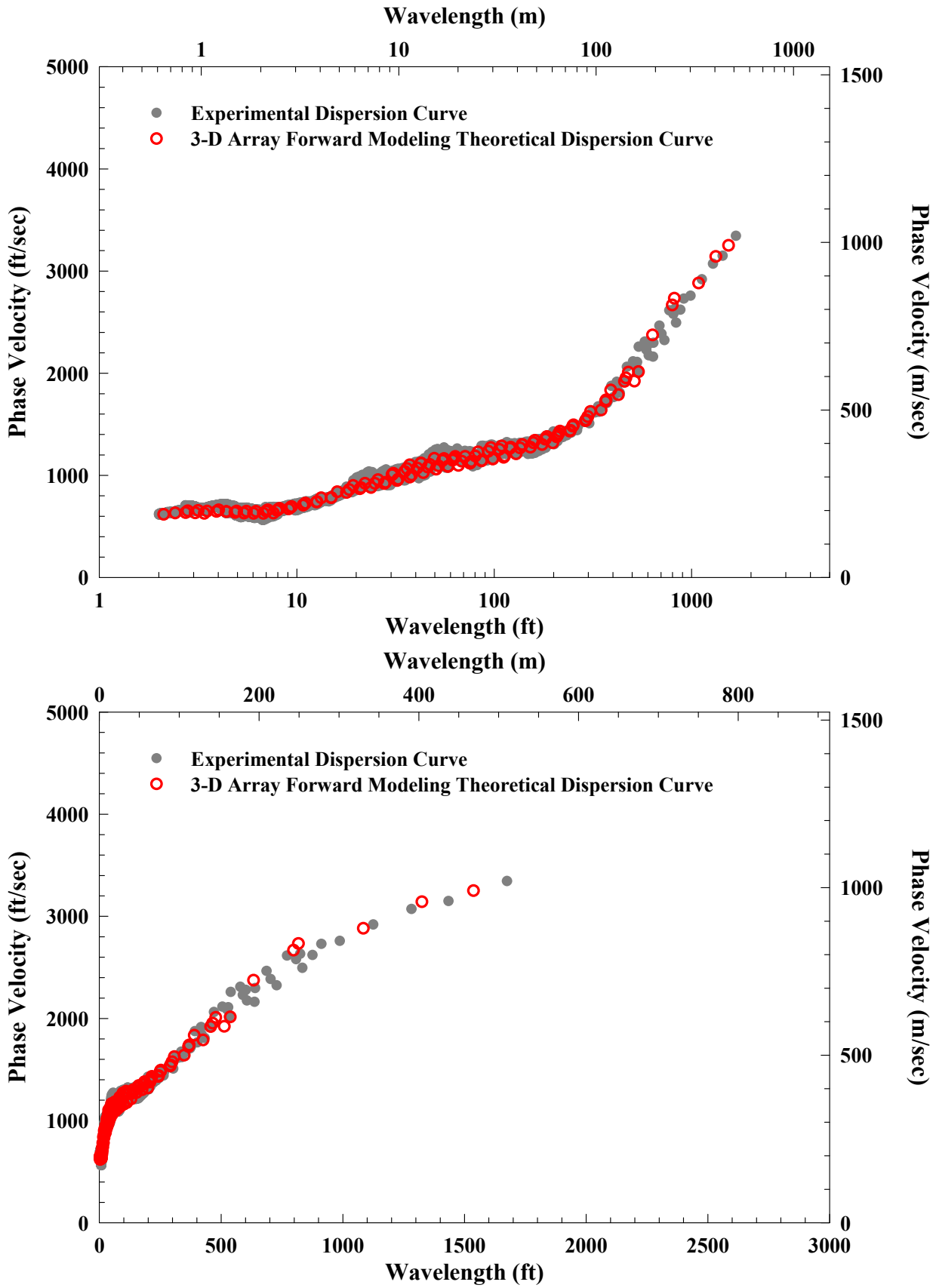

Figure A.9.3 Experimental (Field) and Array Forward Modeling Theoretical Dispersion Curves from Site H2W1998; Logarithmic (Top) and Linear (Bottom) Wavelength Axes

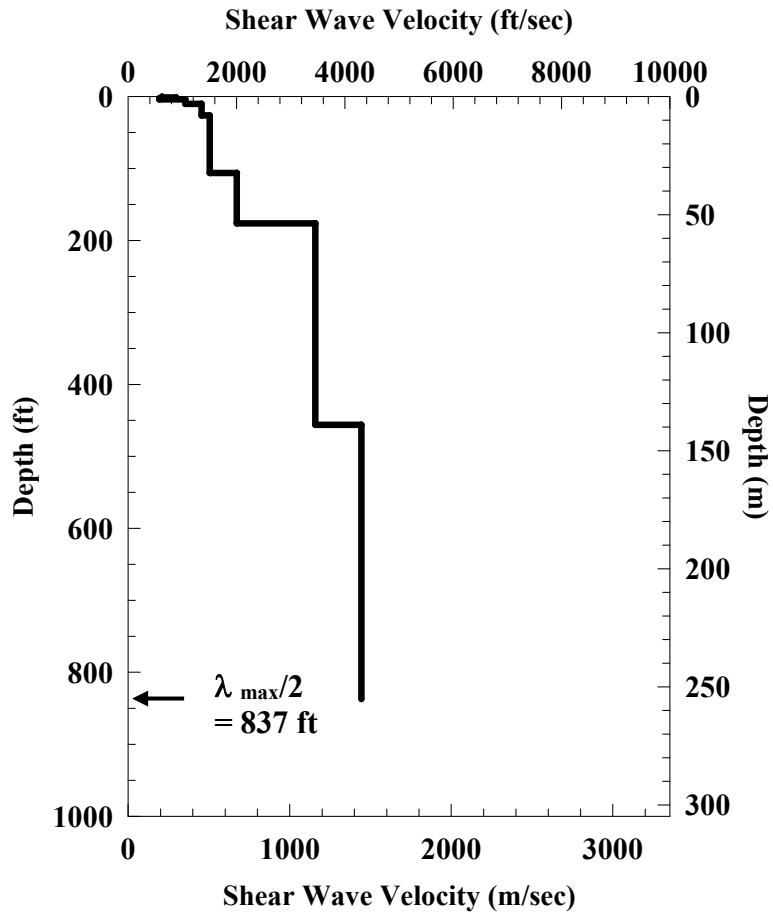

Figure A.9.4 Shear Wave Velocity Profile Determined at Site H2W1998

Table A.9.1 Profile Parameters Used to Develop Theoretical Dispersion Curve at Site H2W1998

Layer No.	Layer Thickness, ft	Depth of the Top of the Layer, ft	Vs, fps	Poisson's Ratio	Vp, fps	Total Unit Weight, pcf
1	1	0	620	0.25	1074	125
2	1.2	1	880	0.25	1524	125
3	1.5	2.2	570	0.25	987	125
4	6.2	3.7	1050	0.25	1819	125
5	16	9.9	1350	0.25	2338	125
6	80	26	1500	0.25	2598	125
7	70	106	2000	0.25	3464	125
8	280	176	3450	0.33	6849	145
9	381	456	4300	0.33	8537	145
10*	Half Space	837	4300	0.33	8537	145

* Layer deeper than the maximum recommended profiling depth (λ_{max}/ 2).

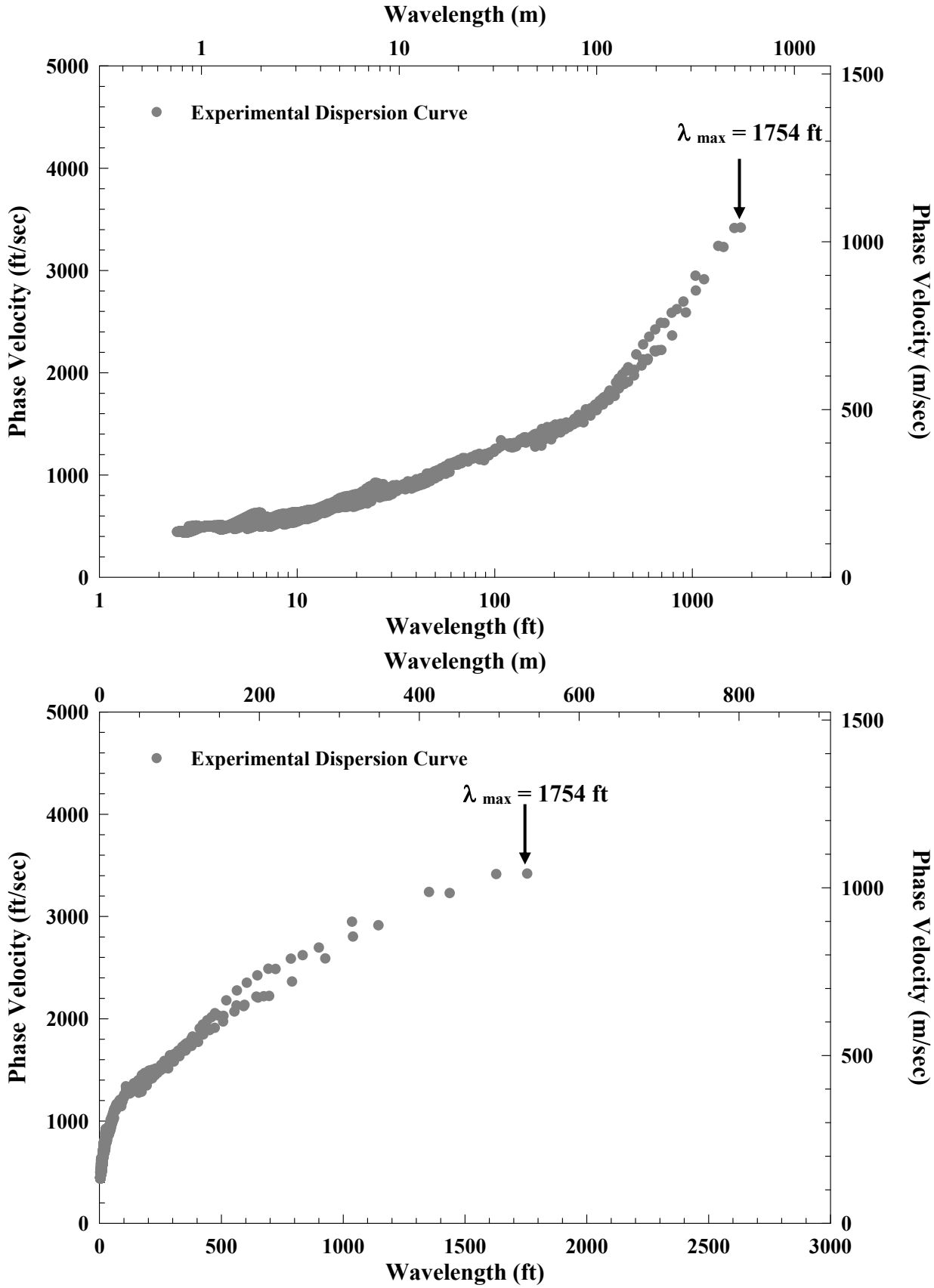

Figure A.10.1 Experimental Dispersion Curve Measured at Site H2W2006; Logarithmic (Top) and Linear (Bottom) Wavelength Axes

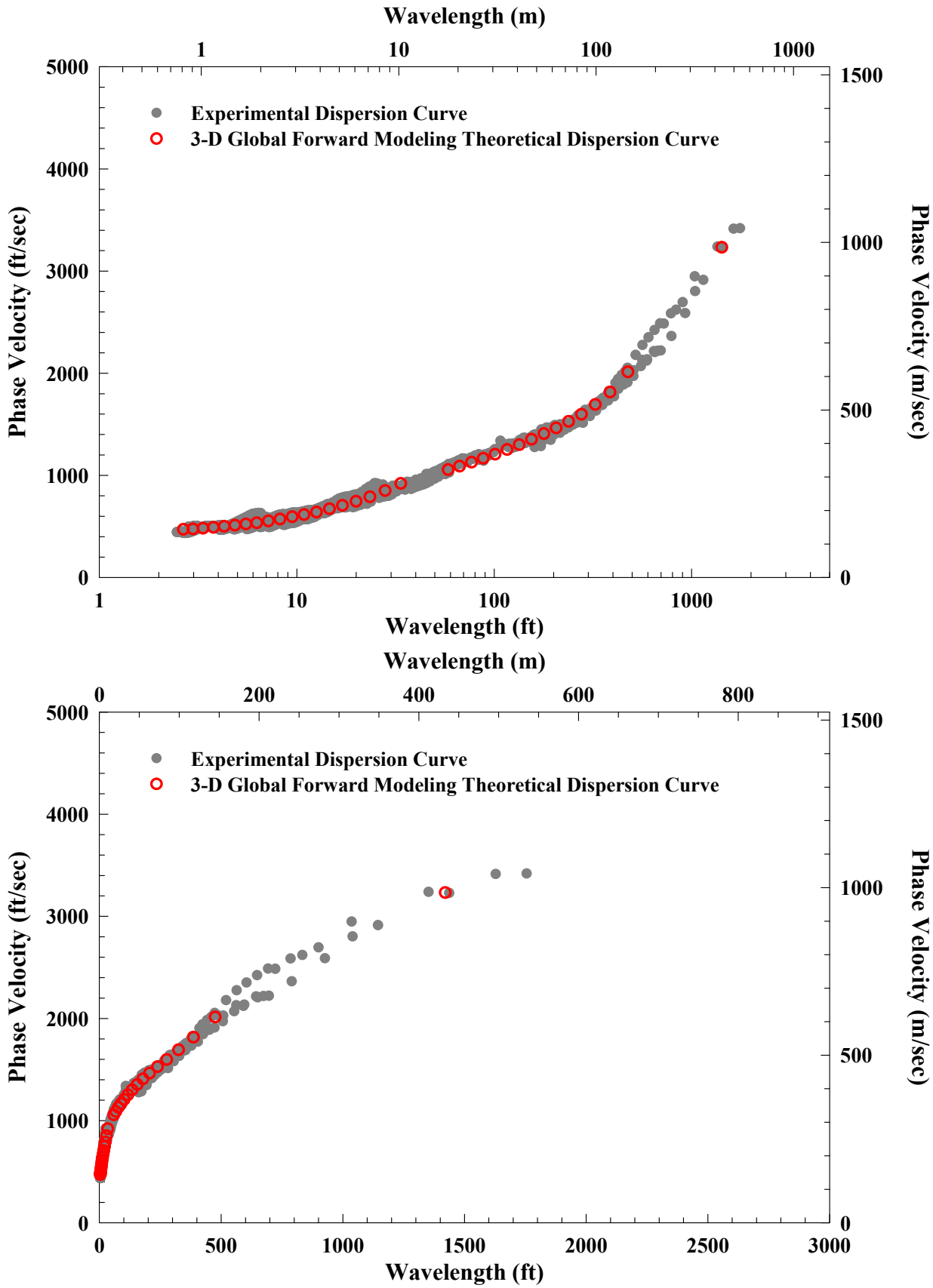

Figure A.10.2 Experimental (Field) and Global Forward Modeling Theoretical Dispersion Curves from Site H2W2006; Logarithmic (Top) and Linear (Bottom) Wavelength Axes

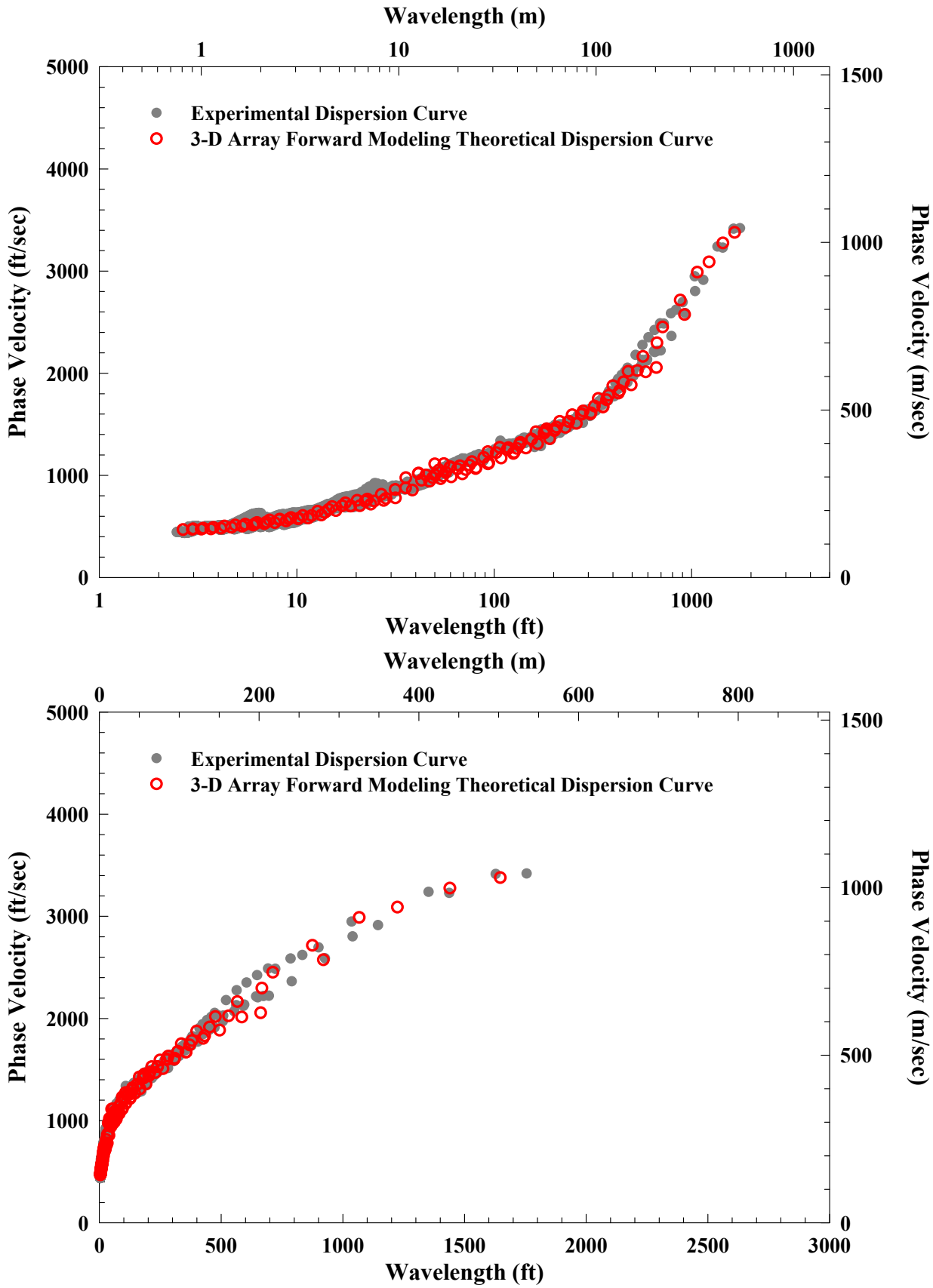

Figure A.10.3 Experimental (Field) and Array Forward Modeling Theoretical Dispersion Curves from Site H2W2006; Logarithmic (Top) and Linear (Bottom) Wavelength Axes

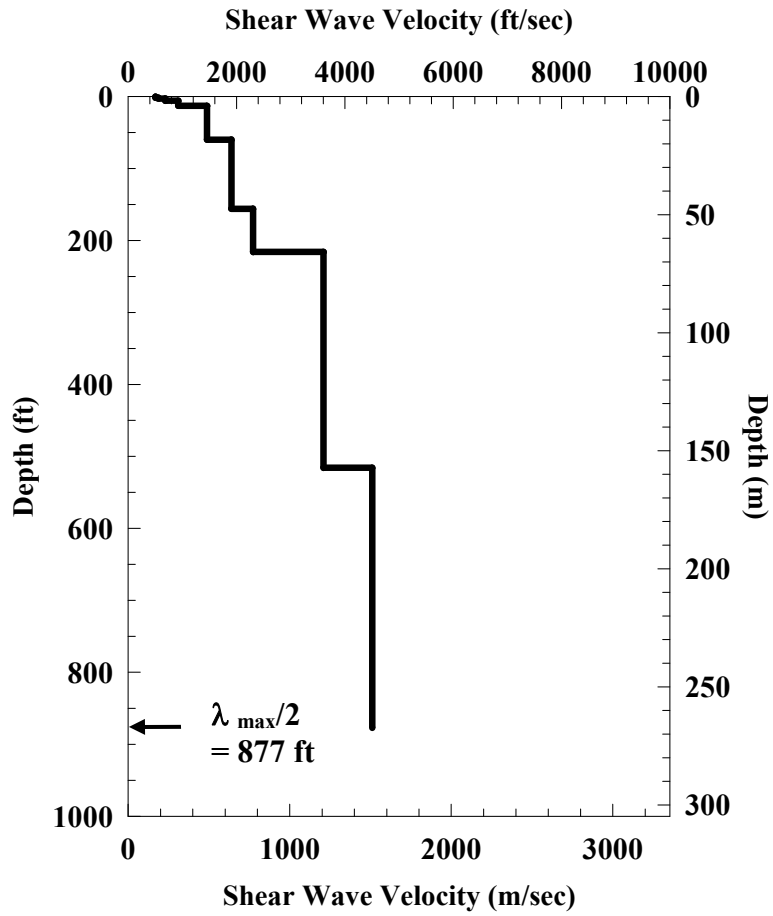

Figure A.10.4 Shear Wave Velocity Profile Determined at Site H2W2006

Table A.10.1 Profile Parameters Used to Develop Theoretical Dispersion Curve at Site H2W2006

Layer No.	Layer Thickness, ft	Depth of the Top of the Layer, ft	Vs, fps	Poisson's Ratio	Vp, fps	Total Unit Weight, pcf
1	1.4	0	500	0.25	866	125
2	1.05	1.4	550	0.25	953	125
3	3.1	2.5	680	0.25	1178	125
4	7	5.6	920	0.25	1593	125
5	47	12.6	1450	0.25	2511	125
6	96	60	1900	0.25	3291	125
7	60	156	2300	0.25	3984	125
8	300	216	3600	0.33	7147	145
9	361	516	4500	0.33	8934	145
10*	Half Space	877	4500	0.33	8934	145

* Layer deeper than the maximum recommended profiling depth (λ_{max}/ 2).

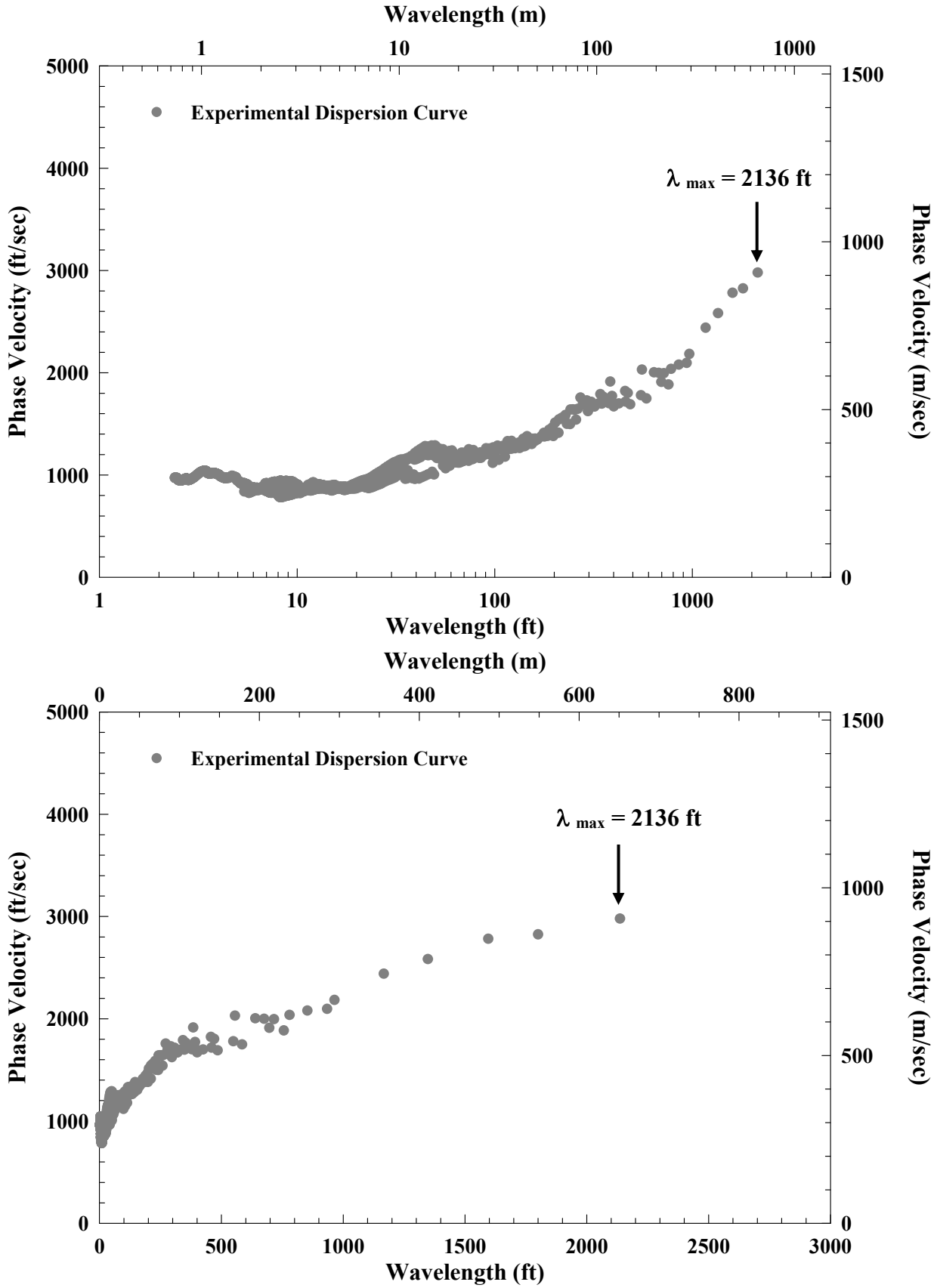

Figure A.11.1 Experimental Dispersion Curve Measured at Site 100B; Logarithmic (Top) and Linear (Bottom) Wavelength Axes

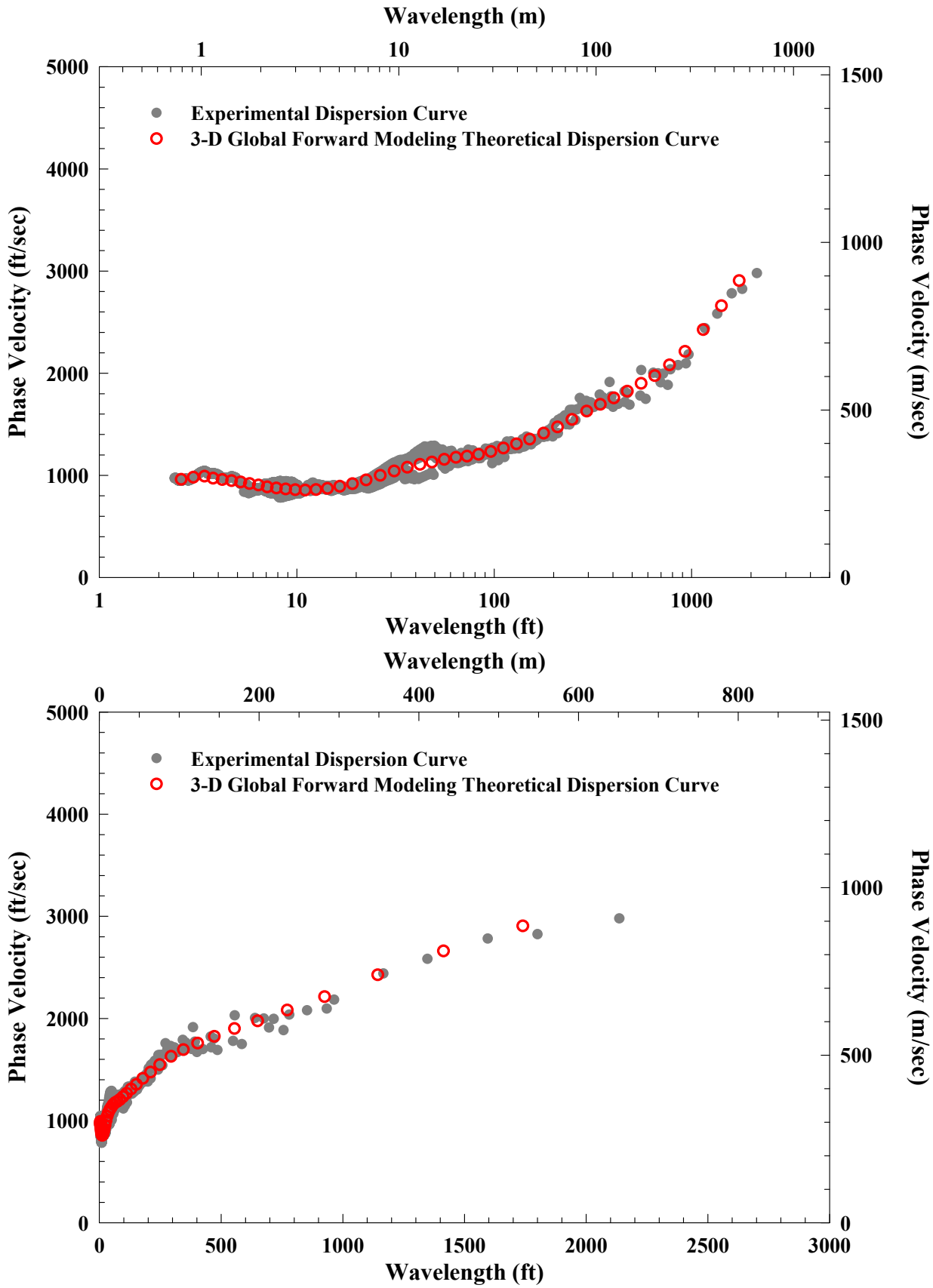

Figure A.11.2 Experimental (Field) and Global Forward Modeling Theoretical Dispersion Curves from Site 100B; Logarithmic (Top) and Linear (Bottom) Wavelength Axes

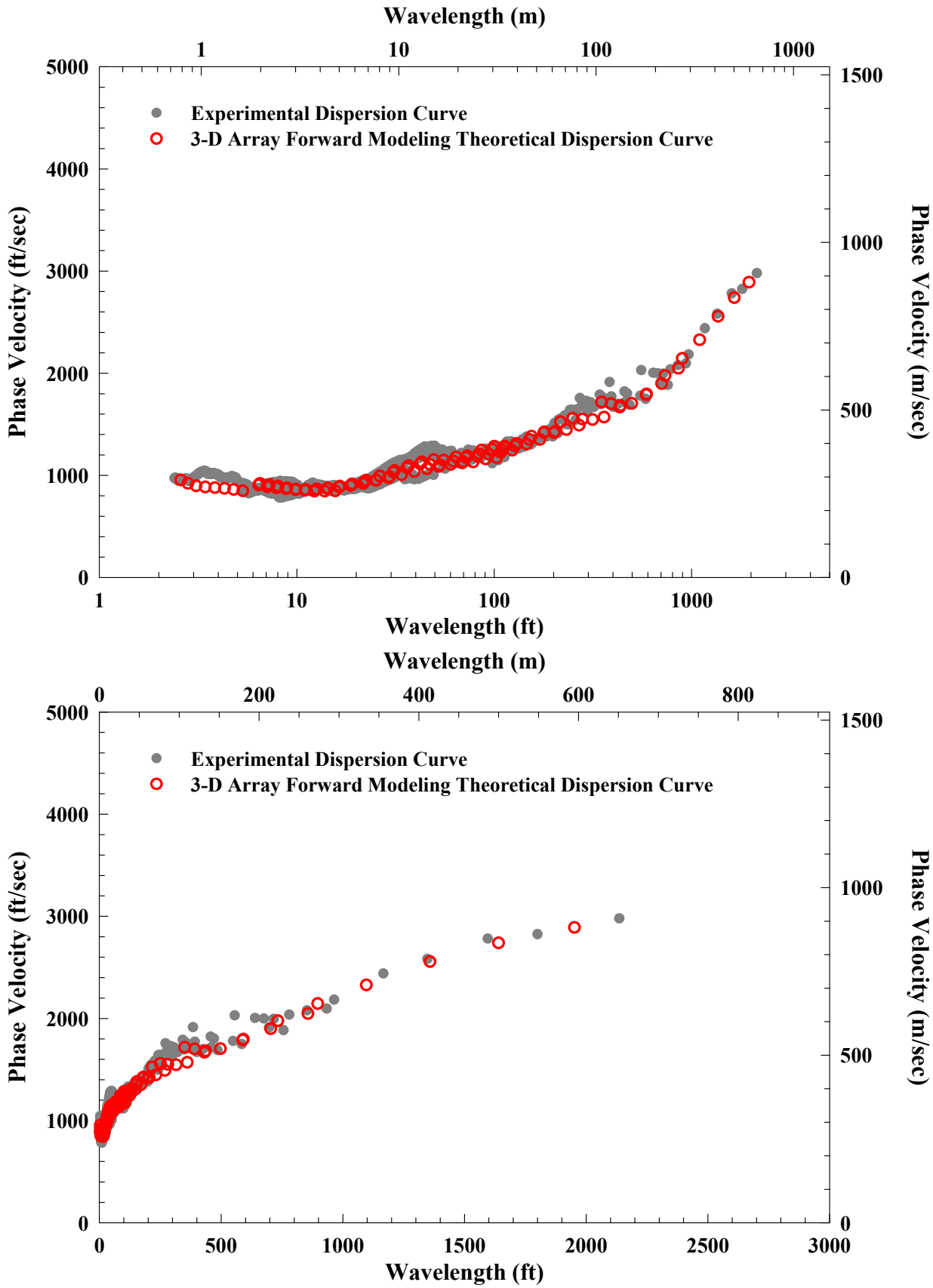

Figure A.11.3 Experimental (Field) and Array Forward Modeling Theoretical Dispersion Curves from Site 100B; Logarithmic (Top) and Linear (Bottom) Wavelength Axes

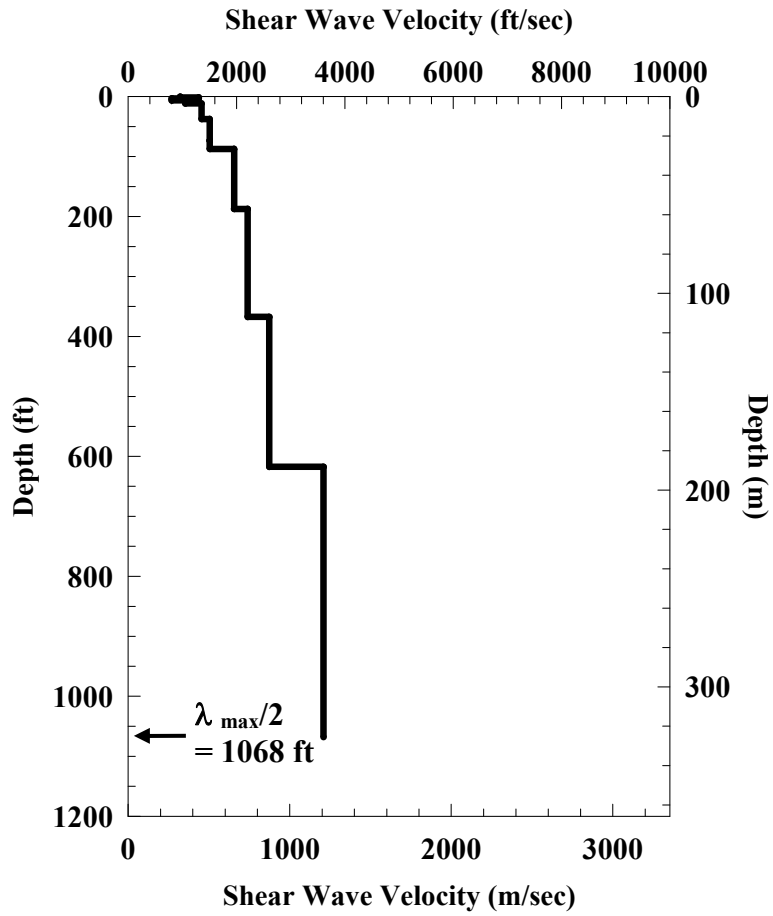

Figure A.11.4 Shear Wave Velocity Profile Determined at Site 100B

Table A.11.1 Profile Parameters Used to Develop Theoretical Dispersion Curve at Site 100B

Layer No.	Layer Thickness, ft	Depth of the Top of the Layer, ft	Vs, fps	Poisson's Ratio	Vp, fps	Total Unit Weight, pcf
1	1.2	0	955	0.25	1654	125
2	1.4	1.2	1300	0.25	2252	125
3	3.5	2.6	800	0.25	1386	125
4	5	6.1	1050	0.25	1819	125
5	26	11.1	1350	0.25	2338	125
6	36	37	1500	0.25	2598	125
7	14	73	1500	0.45	5000	135
8	100	87	1950	0.41	5000	135
9	180	187	2200	0.38	5000	135
10	250	367	2600	0.33	5162	145
11	451	617	3600	0.33	7147	145
12*	Half Space	1068	3600	0.33	7147	145

* Layer deeper than the maximum recommended profiling depth (λ_{max}/ 2).

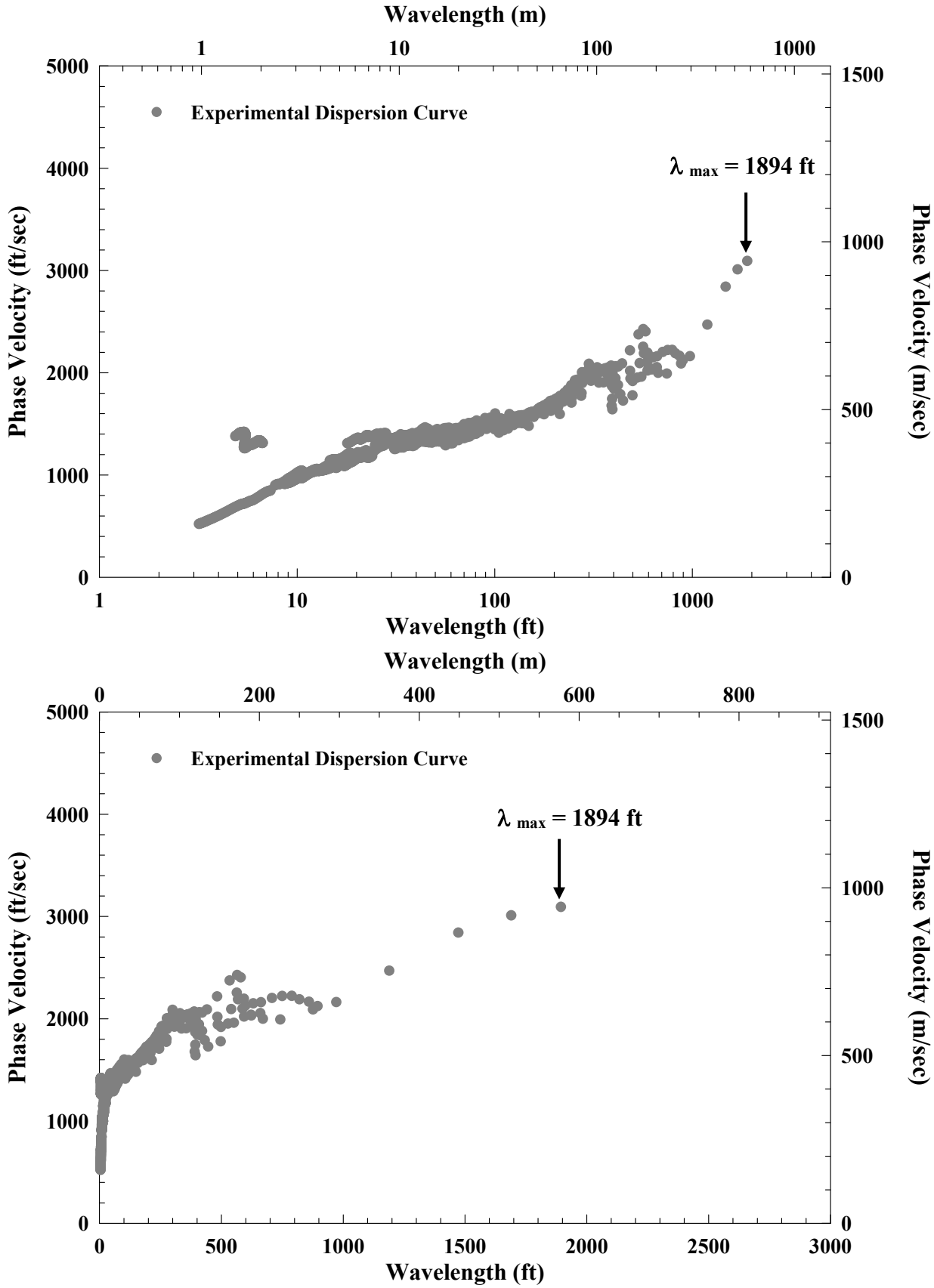

Figure A.12.1 Experimental Dispersion Curve Measured at Site H1K; Logarithmic (Top) and Linear (Bottom) Wavelength Axes

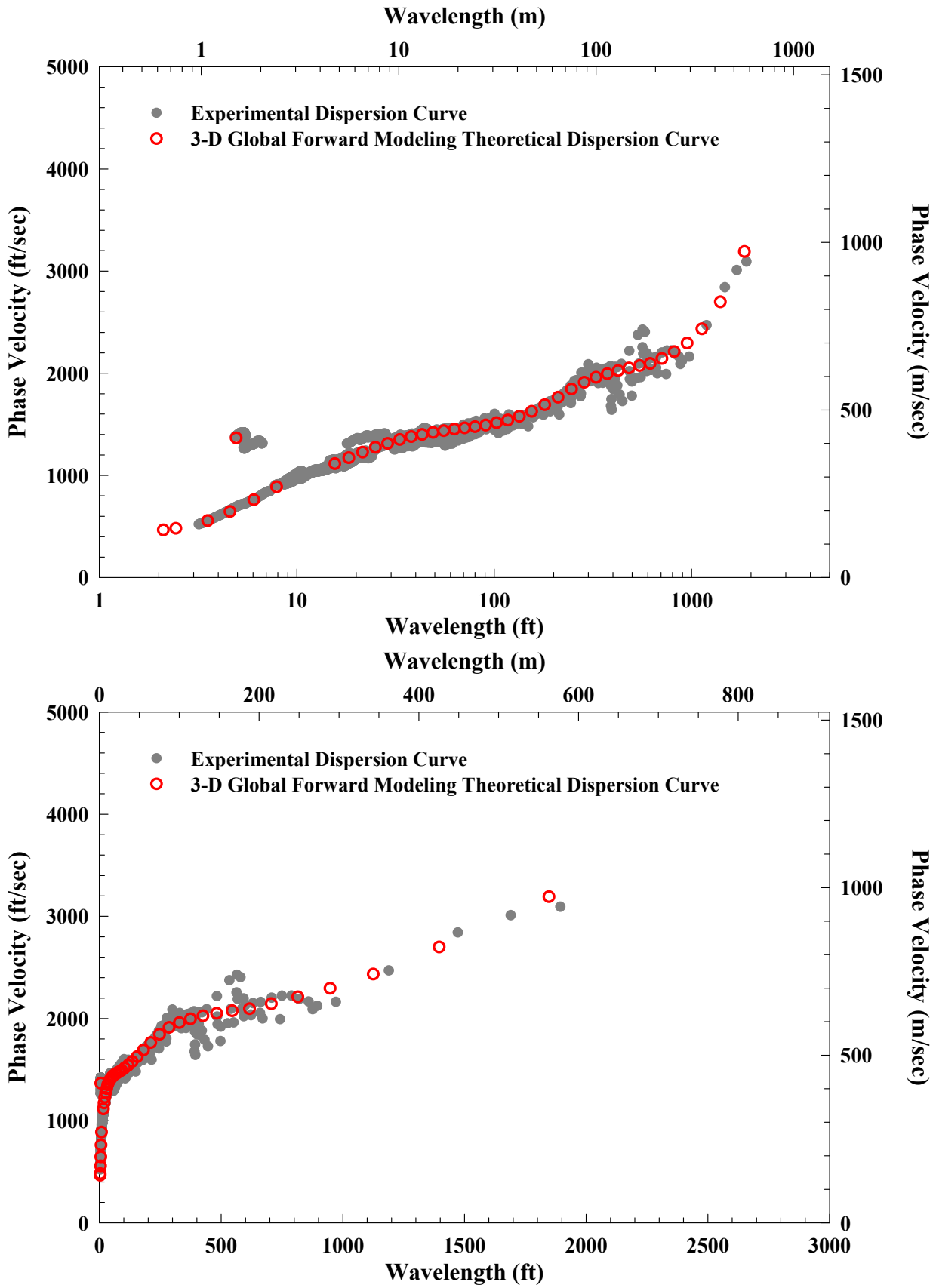

Figure A.12.2 Experimental (Field) and Global Forward Modeling Theoretical Dispersion Curves from Site H1K; Logarithmic (Top) and Linear (Bottom) Wavelength Axes

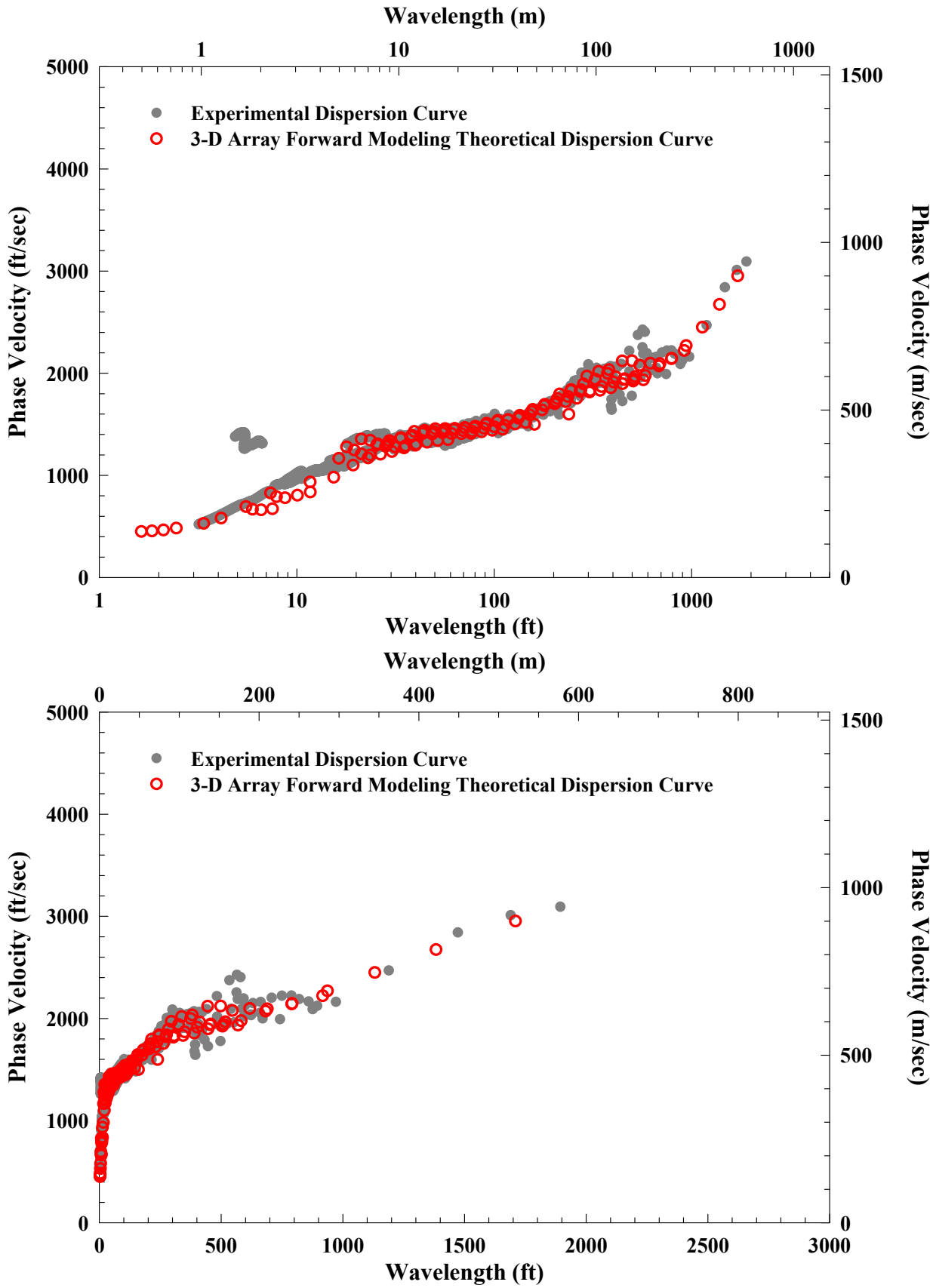

Figure A.12.3 Experimental (Field) and Array Forward Modeling Theoretical Dispersion Curves from Site H1K; Logarithmic (Top) and Linear (Bottom) Wavelength Axes

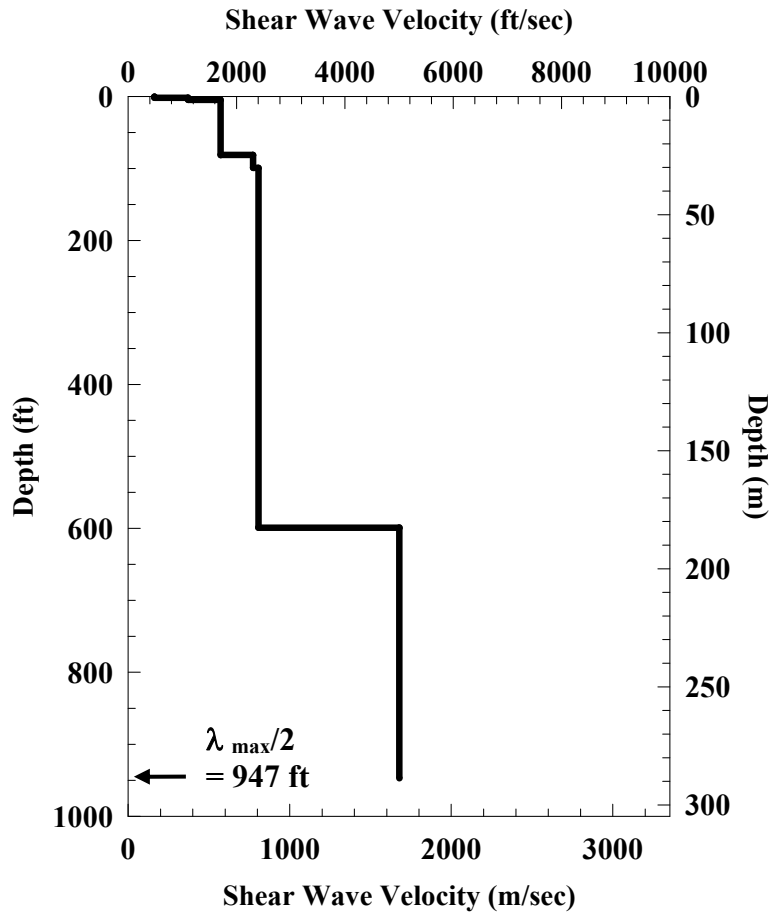

Figure A.12.4 Shear Wave Velocity Profile Determined at Site H1K

Table A.12.1 Profile Parameters Used to Develop Theoretical Dispersion Curve at Site H1K

Layer No.	Layer Thickness, ft	Depth of the Top of the Layer, ft	Vs, fps	Poisson's Ratio	Vp, fps	Total Unit Weight, pcf
1	1.4	0	480	0.25	831	125
2	2.9	1.4	1100	0.25	1905	125
3	76.5	4.3	1700	0.25	2944	125
4	18	80.8	2300	0.25	3984	125
5	500	98.8	2400	0.35	5000	135
6	348	598.8	5000	0.33	9926	145
7*	Half Space	947	5000	0.33	9926	145

* Layer deeper than the maximum recommended profiling depth (λ_{max}/ 2).

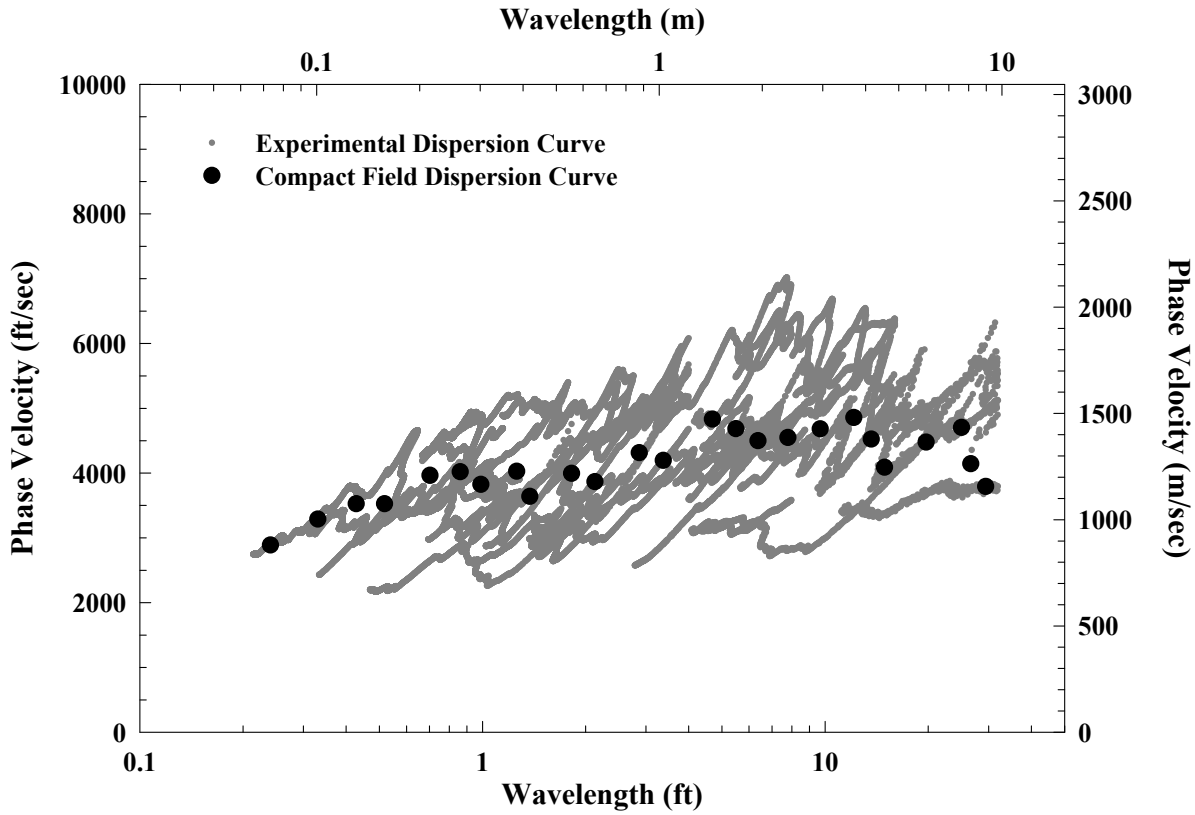

Figure A.13.1 Experimental Dispersion Curve Measured at Bunker (Including Near-Field Data) and the Compact Dispersion Curve; Logarithmic Wavelength Axes

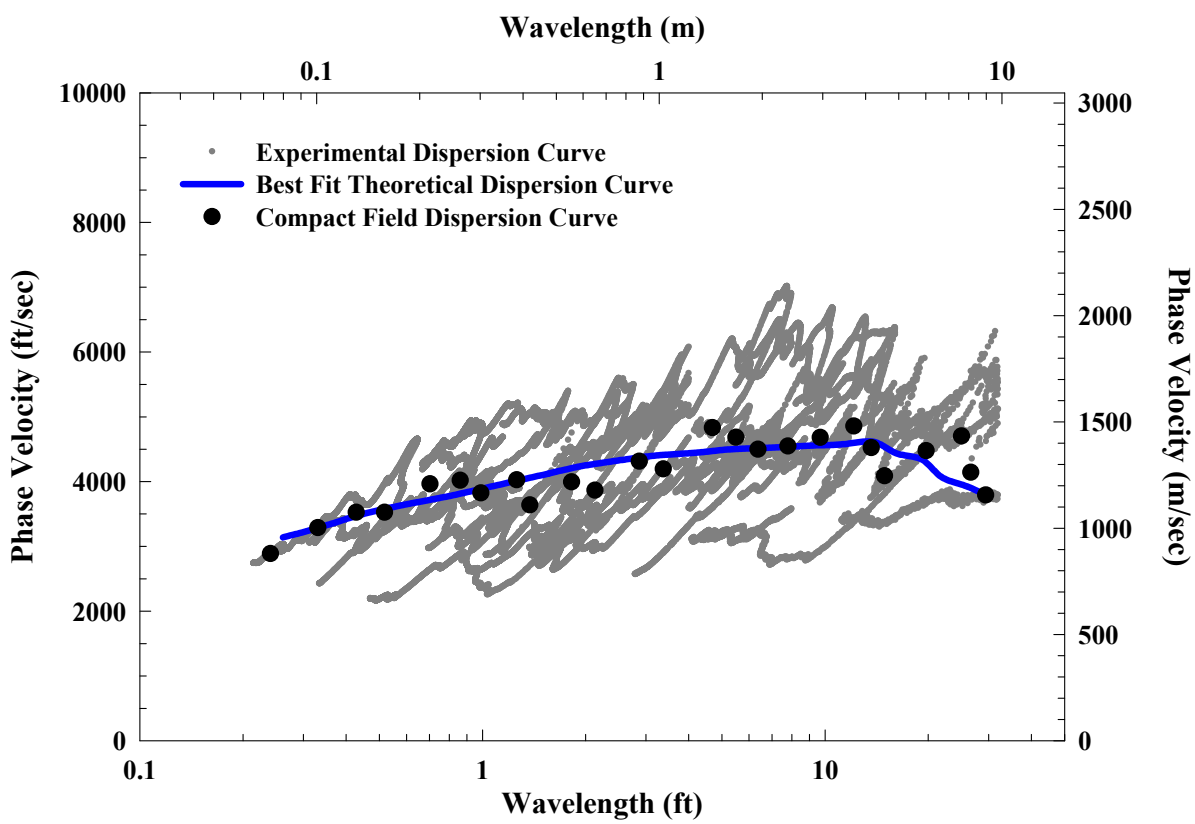

Figure A.13.2 Experimental (Field) and Global Forward Modeling Theoretical Dispersion Curves from Bunker Site (Near-Field Data was taken into Account); Logarithmic Wavelength Axes

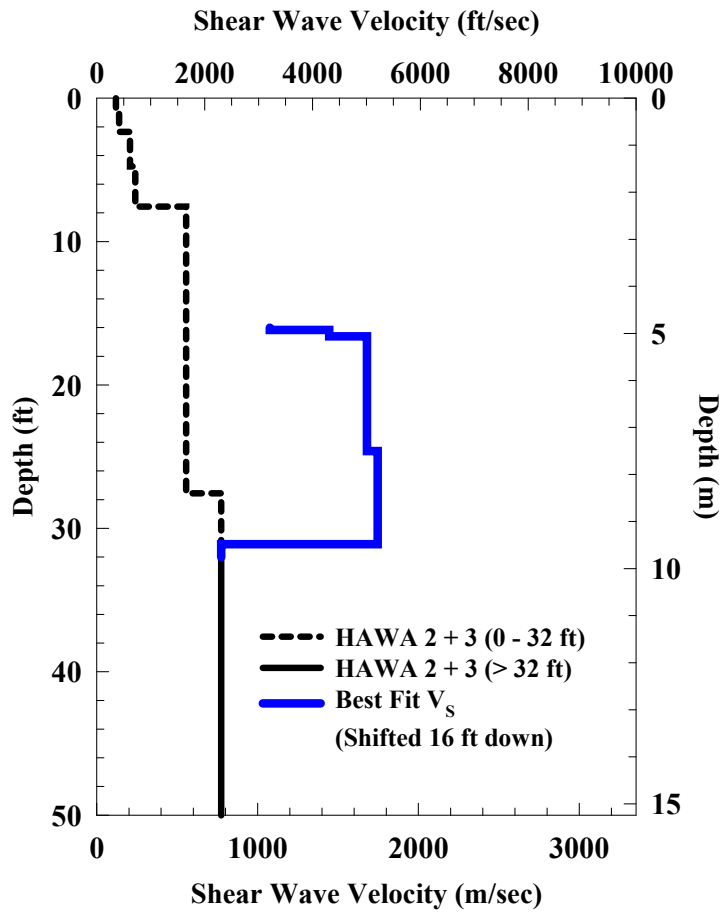

Figure A.13.3 Shear Wave Velocity Profile (Blue Line; Shifted Down 16 ft) Determined at Bunker Site (Near-Field Data was taken into Account)

Table A.13.1 Profile Parameters Used to Develop Theoretical Dispersion Curve at Bunker Site (Near-Field Data was taken into Account)

Layer No.	Layer Thickness, ft	Depth of the Top of the	Vs, fps	Poisson's Ratio	Vp, fps	Total Unit Weight, pcf
1	0.15	0	3200	0.30	5987	150
2	0.45	0.15	4300	0.30	8045	150
3	8	0.6	5000	0.30	9354	150
4	6.5	8.6	5200	0.30	9728	150
5	0.9	15.1	2300	0.25	4303	125
6*	Half Space	16	2300	0.25	4303	125

* Layer below maximum depth of the V_S Profile

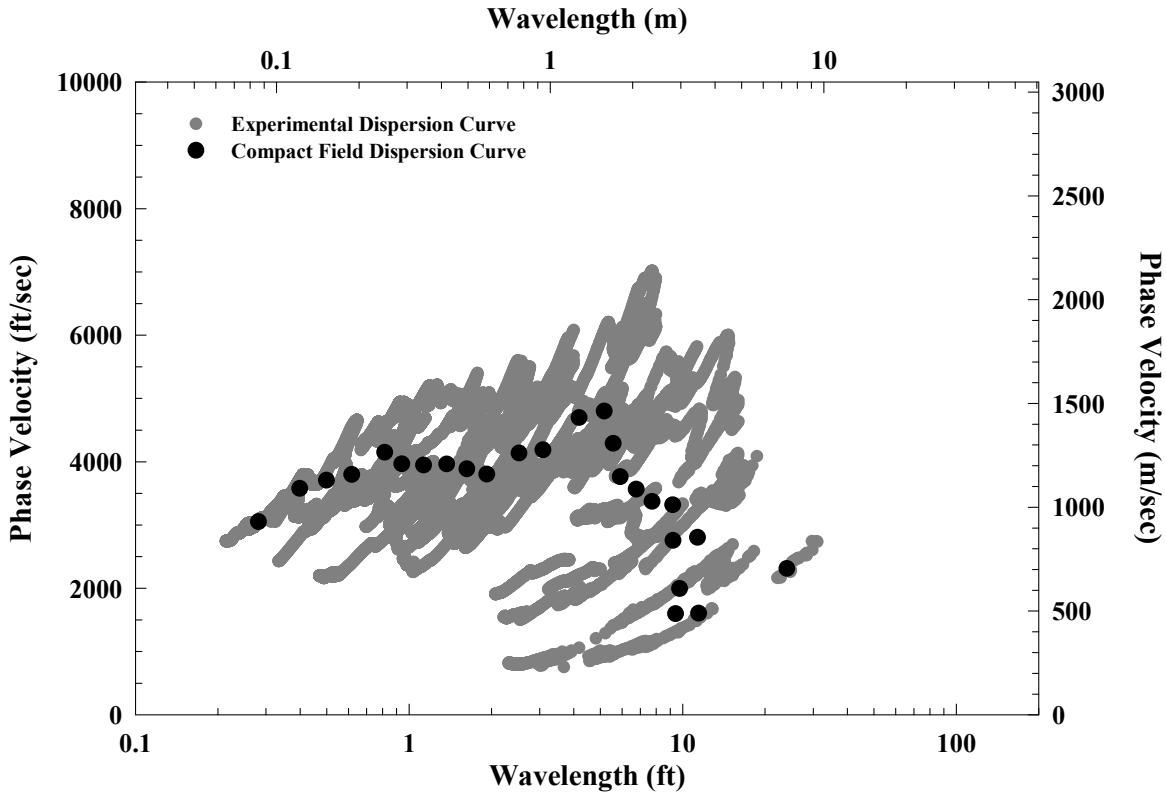

Figure A.14.1 Experimental Dispersion Curve Measured at Bunker (Excluding Near-Field Data) and the Compact Dispersion Curve; Logarithmic Wavelength Axes

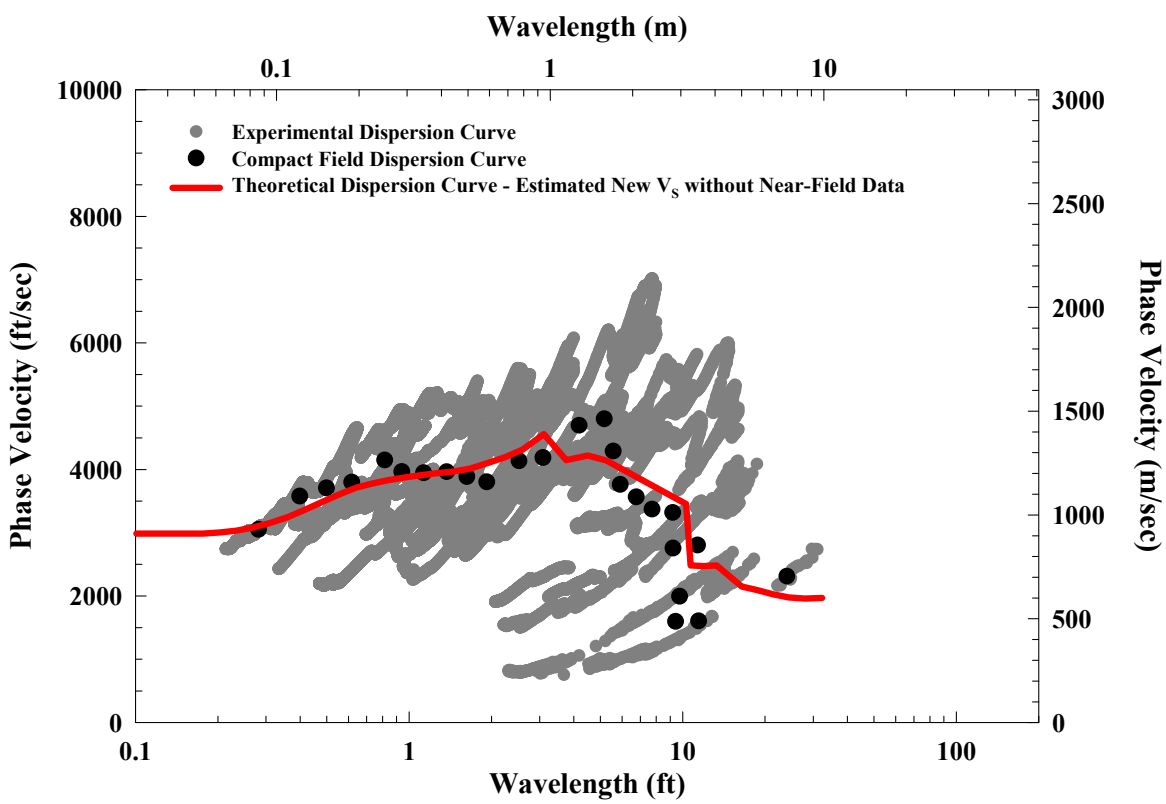

Figure A.14.2 Experimental (Field) and Global Forward Modeling Theoretical Dispersion Curves from Bunker Site (without Near-Field Data); Logarithmic Wavelength Axes

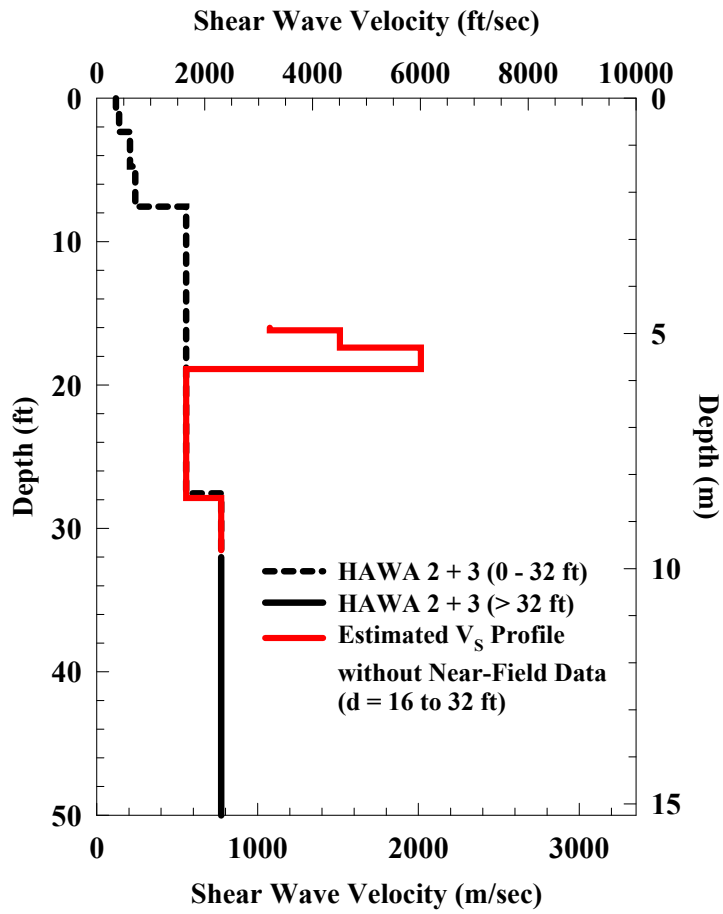

Figure A.14.3 Shear Wave Velocity Profile (Red Line; Shifted Down 16 ft) Determined at Bunker Site (No Near-Field Data was taken into Account)

Table A.14.1 Profile Parameters Used to Develop Theoretical Dispersion Curve at Bunker Site (No Near-Field Data was taken into Account)

Layer No.	Layer Thickness, ft	Depth of the Top of the	Vs, fps	Poisson's Ratio	Vp, fps	Total Unit Weight, pcf
1	0.18	0	3200	0.30	5987	150
2	1.2	0.18	4500	0.30	8419	150
3	1.5	1.38	6000	0.30	11225	150
4	9	2.88	1650	0.25	2858	125
5	3.64	11.88	2300	0.30	4303	150
6*	Half Space	15.52	2300	0.30	4303	150

* Layer deeper than the maximum recommended profiling depth (λ_{max}/ 2).

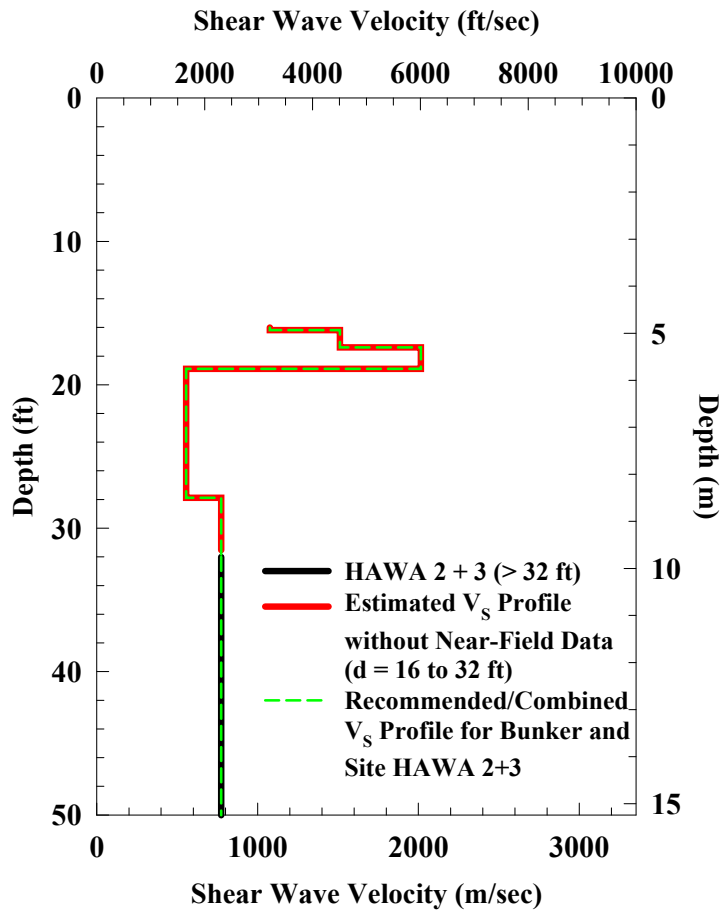

Figure A.15.1 Recommended Shear Wave Velocity Profile (Green Dashed Line) by Combining Shifted V_S Profile from Bunker and Trimmed V_S Profile from Site HAWA 2+3 in Figure A.14.3 (Solid Red and Black Lines)

Table A.15.1 Parameters of Recommended Shear Wave Velocity Profile in Figure A.15.1 (Green Dashed Line)

Layer No.	Layer Thickness, ft	Depth of the Top of the	Vs, fps	Poisson's Ratio	Vp, fps	Total Unit Weight, pcf
1	0.18	0	3200	0.30	5987	150
2	1.2	0.18	4500	0.30	8419	150
3	1.5	1.38	6000	0.30	11225	150
4	9	2.88	1650	0.25	2858	125
5	25	11.88	2300	0.25	3984	125
6	120	37	4600	0.33	9132	145
7	734	157	6100	0.33	12110	145
8*	Half Space	891	6100	0.33	12110	145

* Layer deeper than the maximum recommended profiling depth (λ_{max}/ 2).

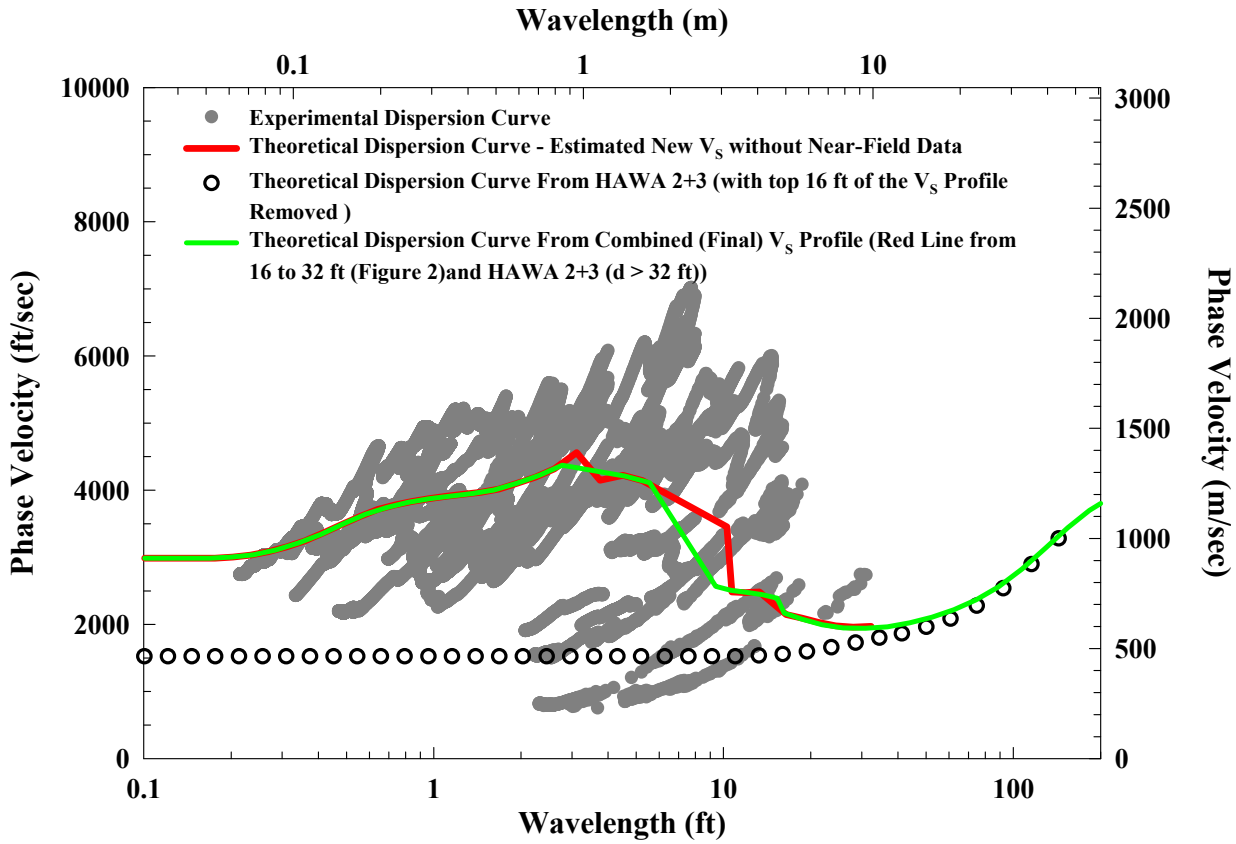

Figure A.15.2 Comparison of Experimental (Field) Dispersion Curve from Bunker Site and Global Forward Modeling Theoretical Dispersion Curves Generated Based on V_S Profiles (Soild Red and Black, and Dashed Green lines) from Figure A.15.1; Logarithmic Wavelength Axes

Appendix B

Sensitivity Study of the Impact on the Theoretical Dispersion Curve by Changing the V_S Value of the Bottom Layer by Multipling or Dividing by a Factor of 1.25

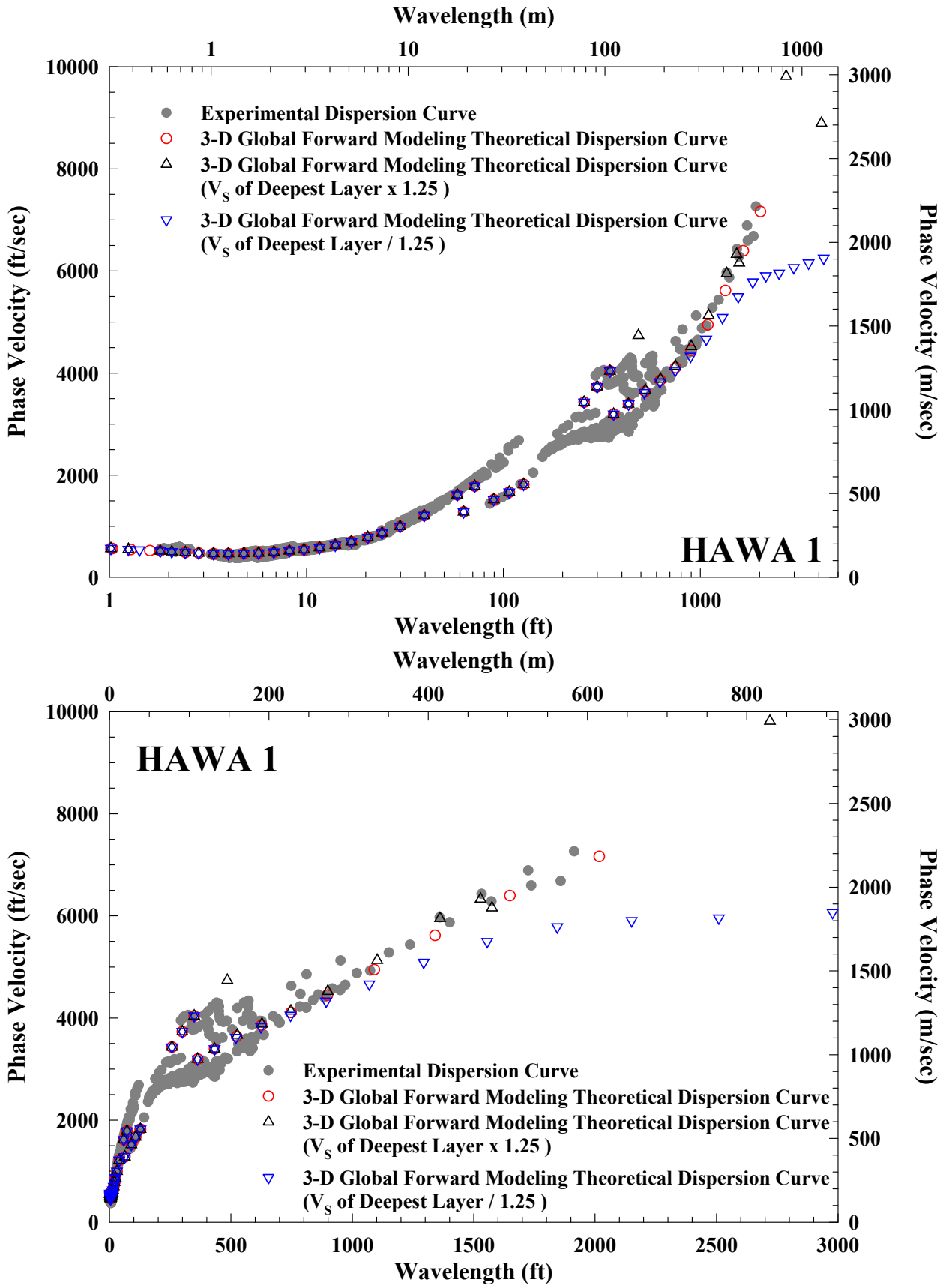

Figure B.1.1 Comparison of Experimental (Field) and Global Forward Modeling Theoretical Dispersion Curves from Site HAWA 1 Before and After Changing the Vs Value of the Bottom Layer; Logarithmic (Top) and Linear (Bottom) Wavelength Axes

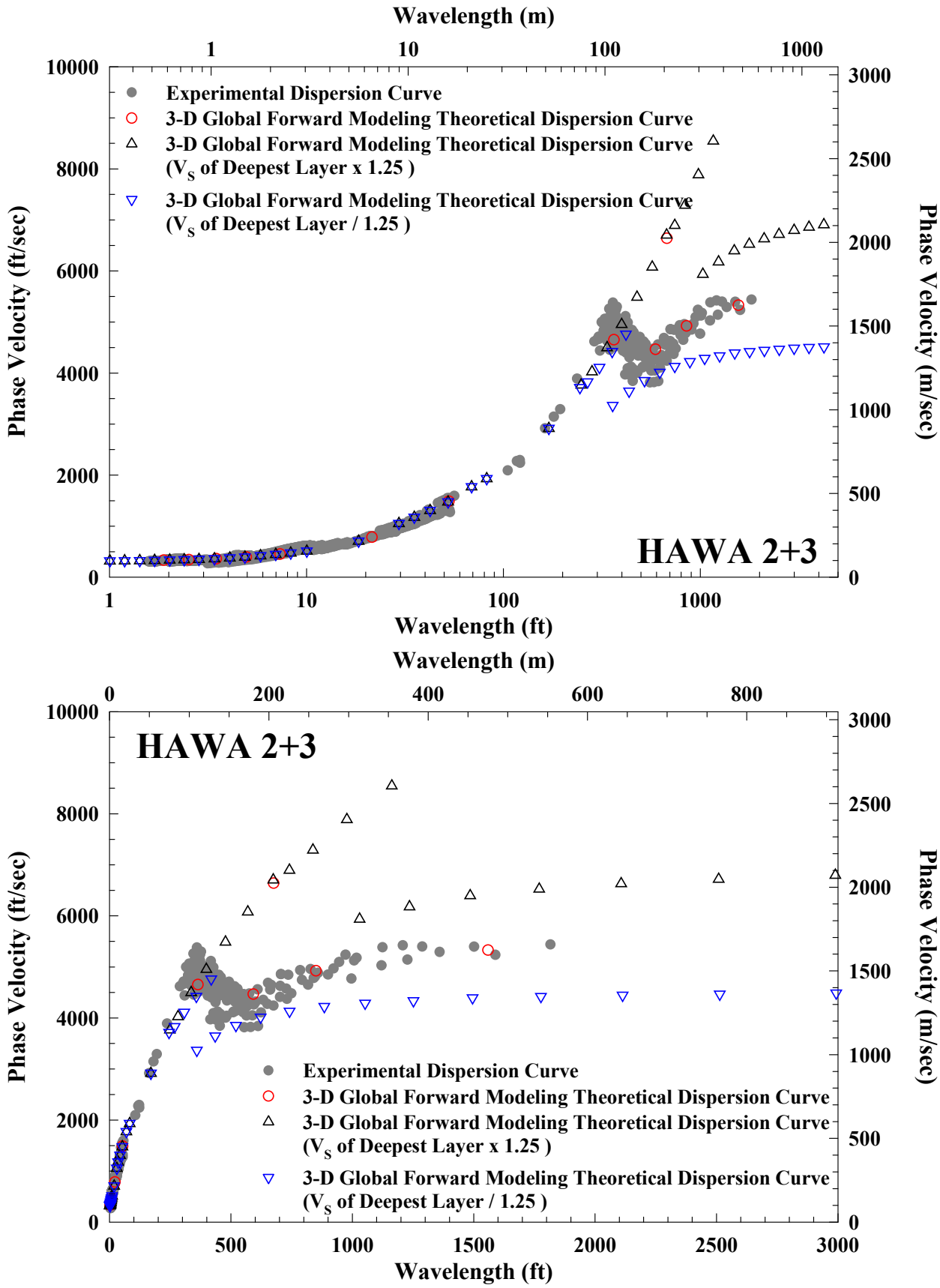

Figure B.2.1 Comparison of Experimental (Field) and Global Forward Modeling Theoretical Dispersion Curves from Site HAWA 2+3 Before and After Changing the V_S Value of the Bottom Layer; Logarithmic (Top) and Linear (Bottom) Wavelength Axes

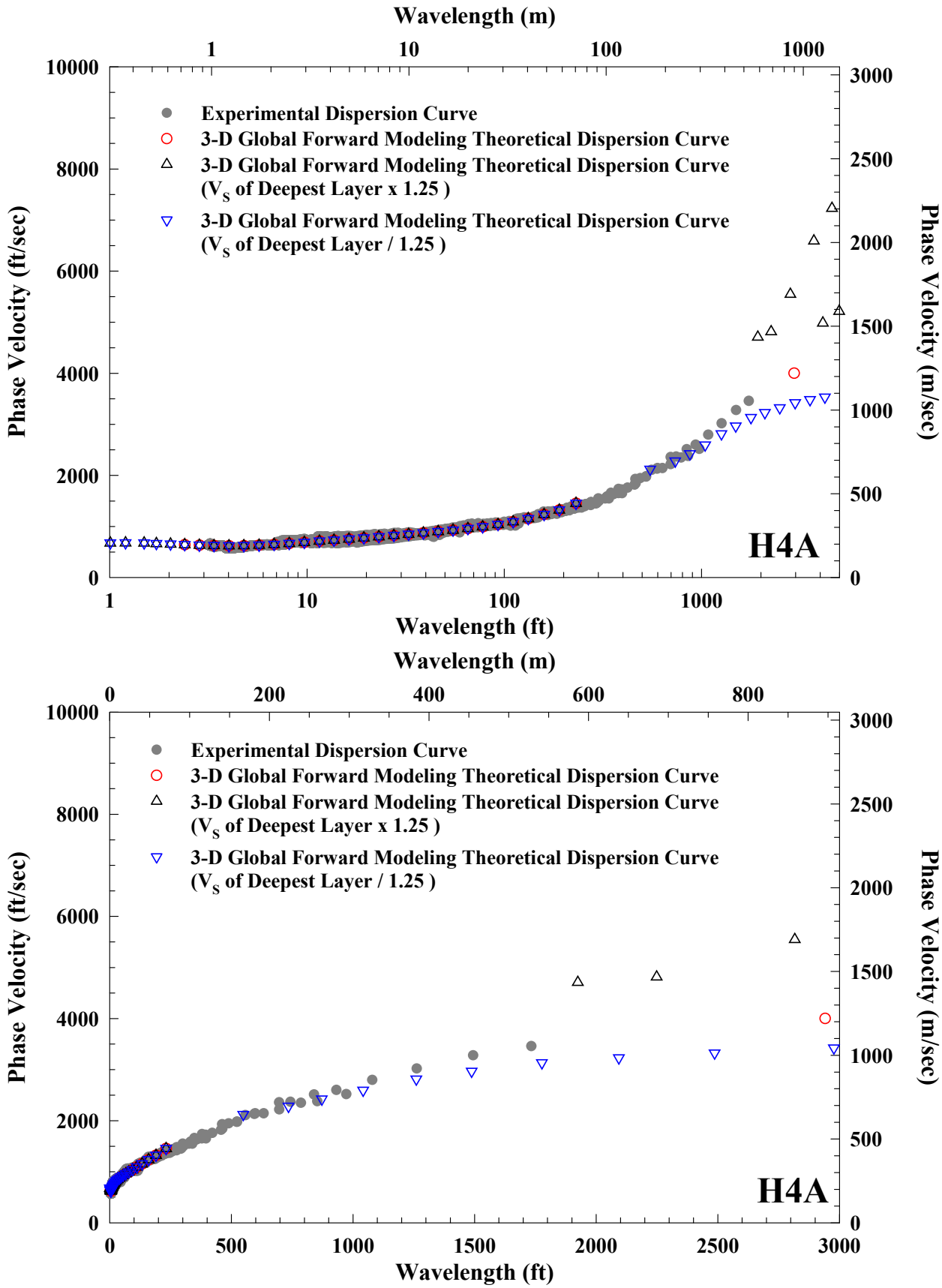

Figure B.3.1 Comparison of Experimental (Field) and Global Forward Modeling Theoretical Dispersion Curves from Site H4A Before and After Changing the V_S Value of the Bottom Layer; Logarithmic (Top) and Linear (Bottom) Wavelength Axes

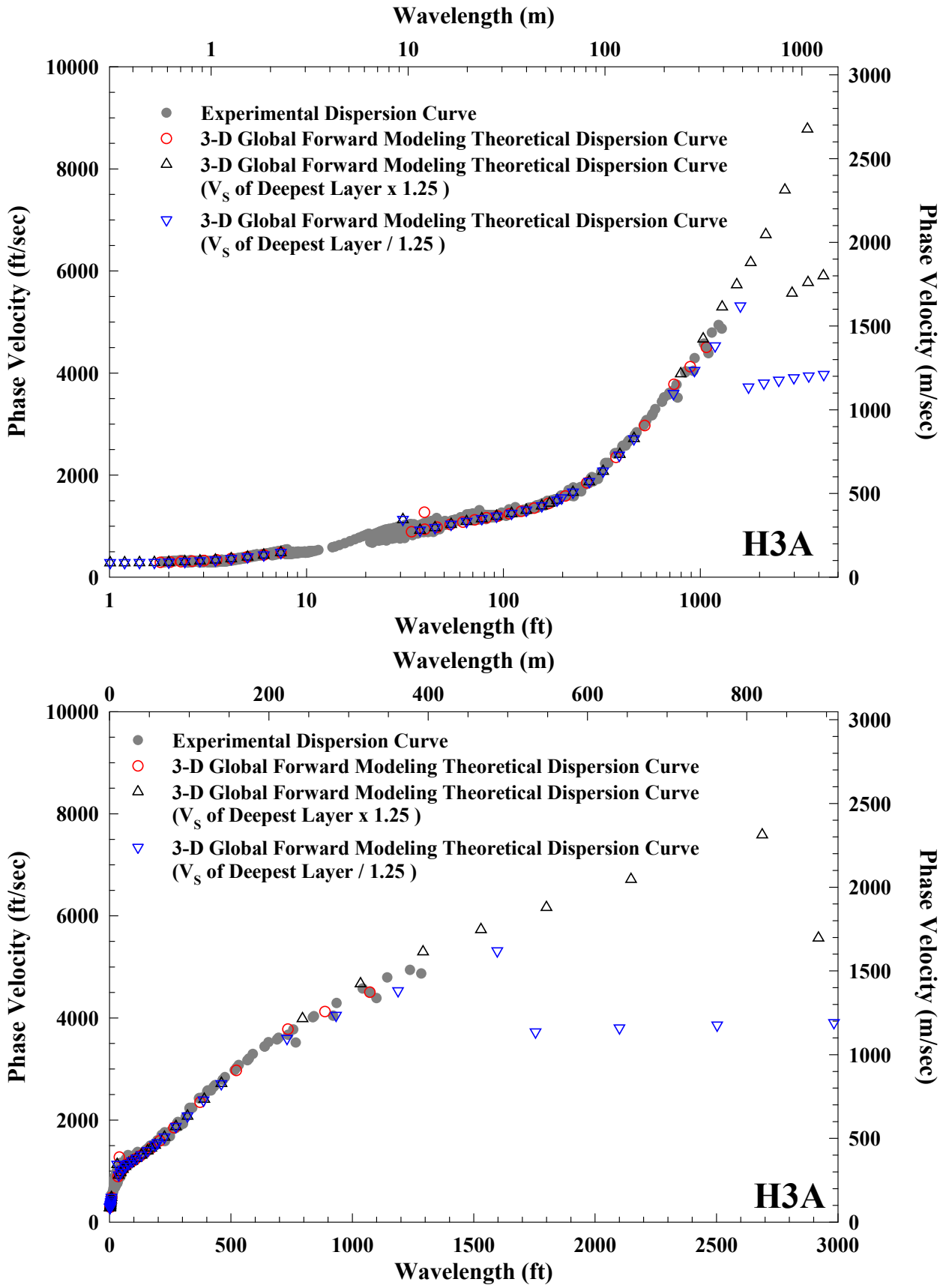

Figure B.4.1 Comparison of Experimental (Field) and Global Forward Modeling Theoretical Dispersion Curves from Site H3A Before and After Changing the V_S Value of the Bottom Layer; Logarithmic (Top) and Linear (Bottom) Wavelength Axes

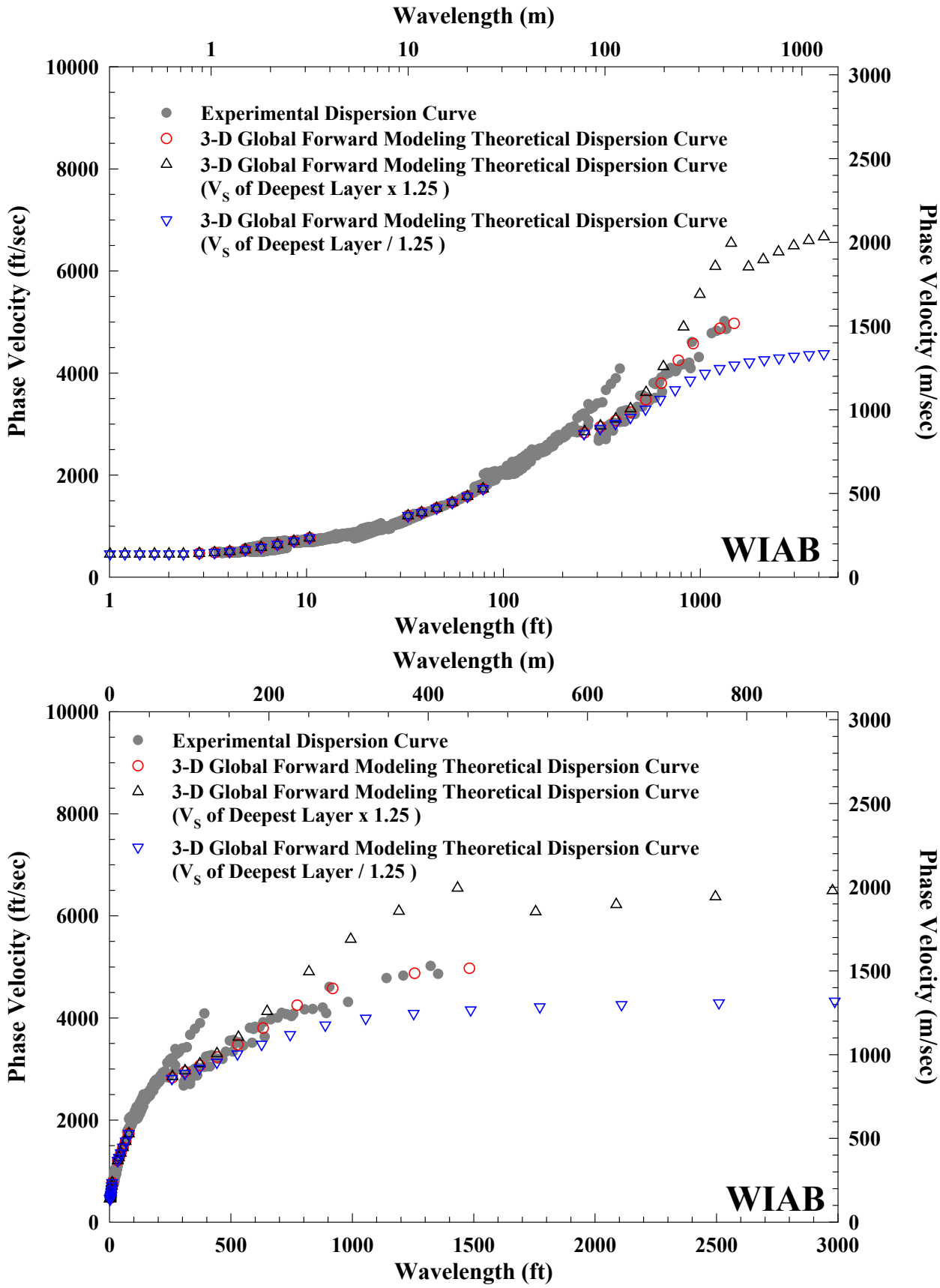

Figure B.5.1 Comparison of Experimental (Field) and Global Forward Modeling Theoretical Dispersion Curves from Site WIAB Before and After Changing the Vs Value of the Bottom Layer; Logarithmic (Top) and Linear (Bottom) Wavelength Axes

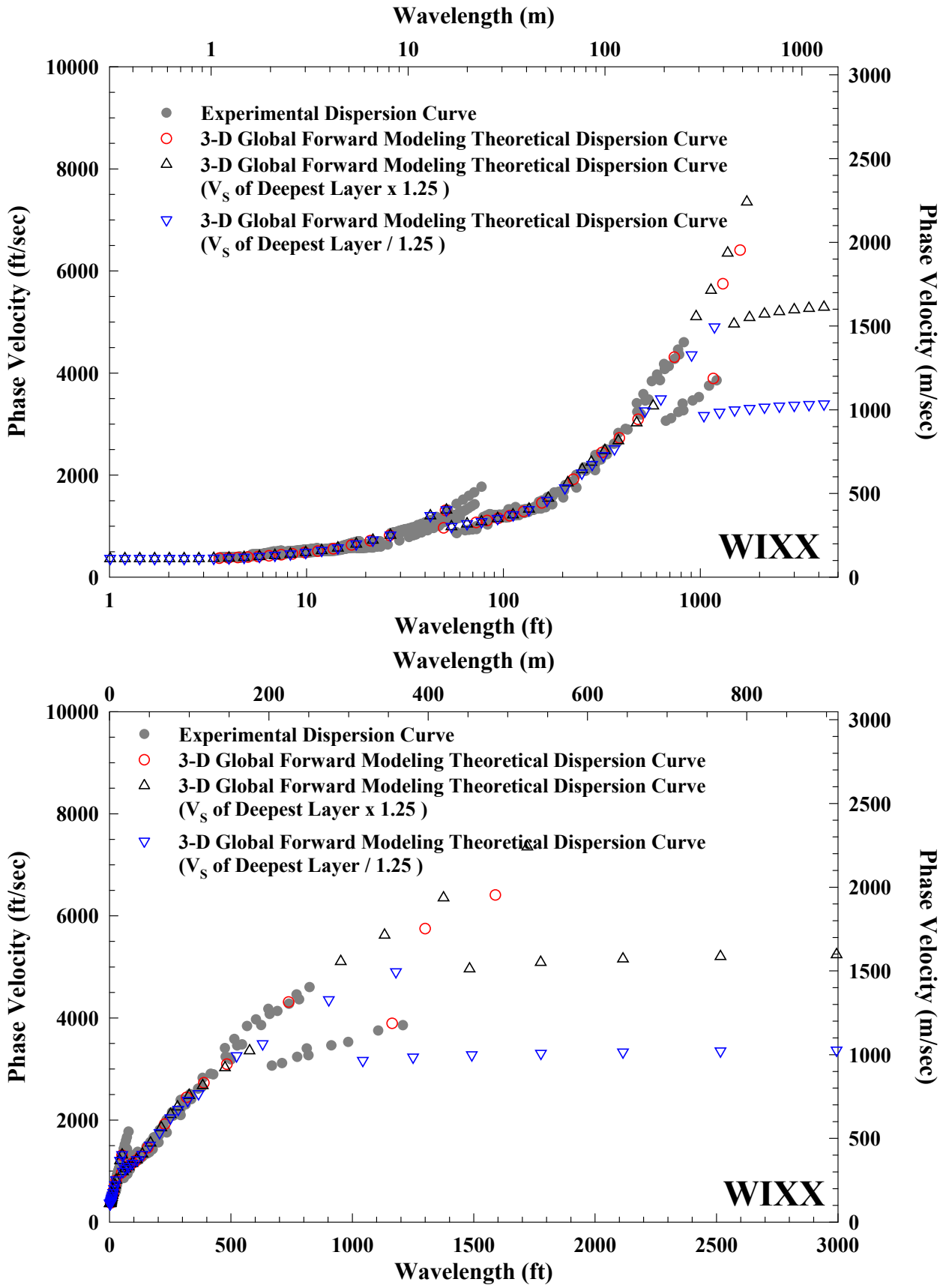

Figure B.6.1 Comparison of Experimental (Field) and Global Forward Modeling Theoretical Dispersion Curves from Site WIXX Before and After Changing the Vs Value of the Bottom Layer; Logarithmic (Top) and Linear (Bottom) Wavelength Axes

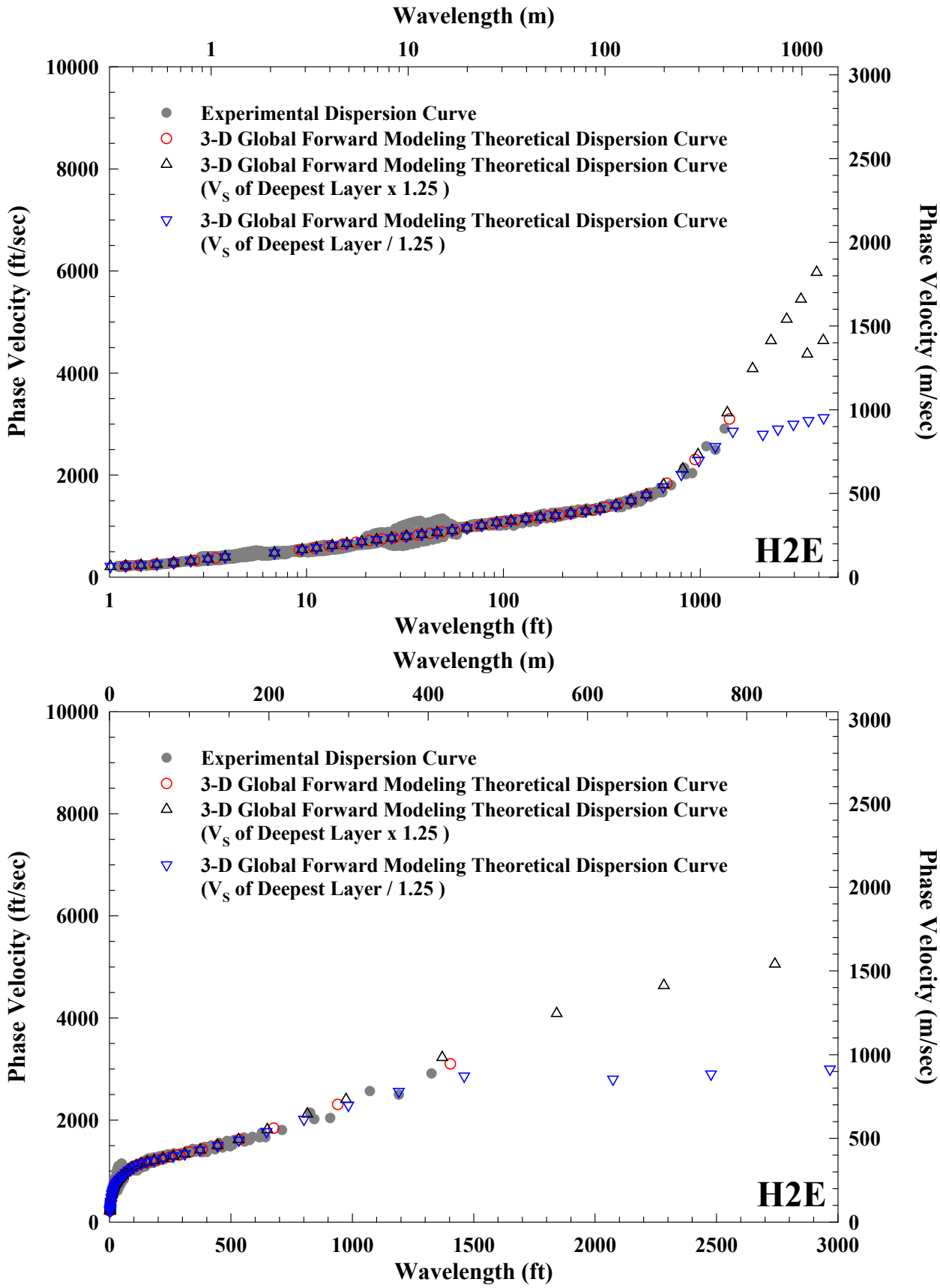

Figure B.7.1 Comparison of Experimental (Field) and Global Forward Modeling Theoretical Dispersion Curves from Site H2E Before and After Changing the Vs Value of the Bottom Layer; Logarithmic (Top) and Linear (Bottom) Wavelength Axes

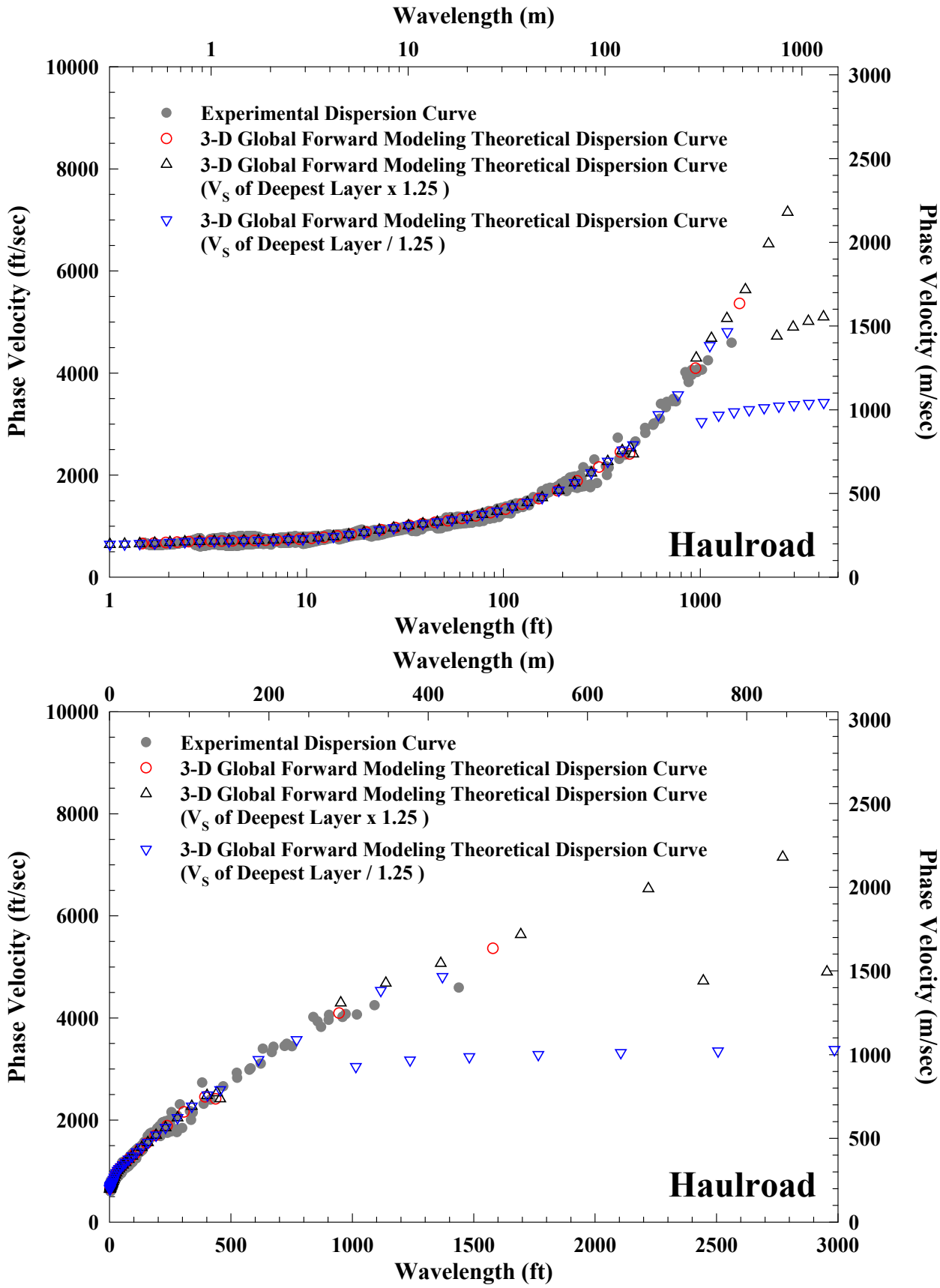

Figure B.8.1 Comparison of Experimental (Field) and Global Forward Modeling Theoretical Dispersion Curves from Site Haulroad Before and After Changing the Vs Value of the Bottom Layer; Logarithmic (Top) and Linear (Bottom) Wavelength Axes

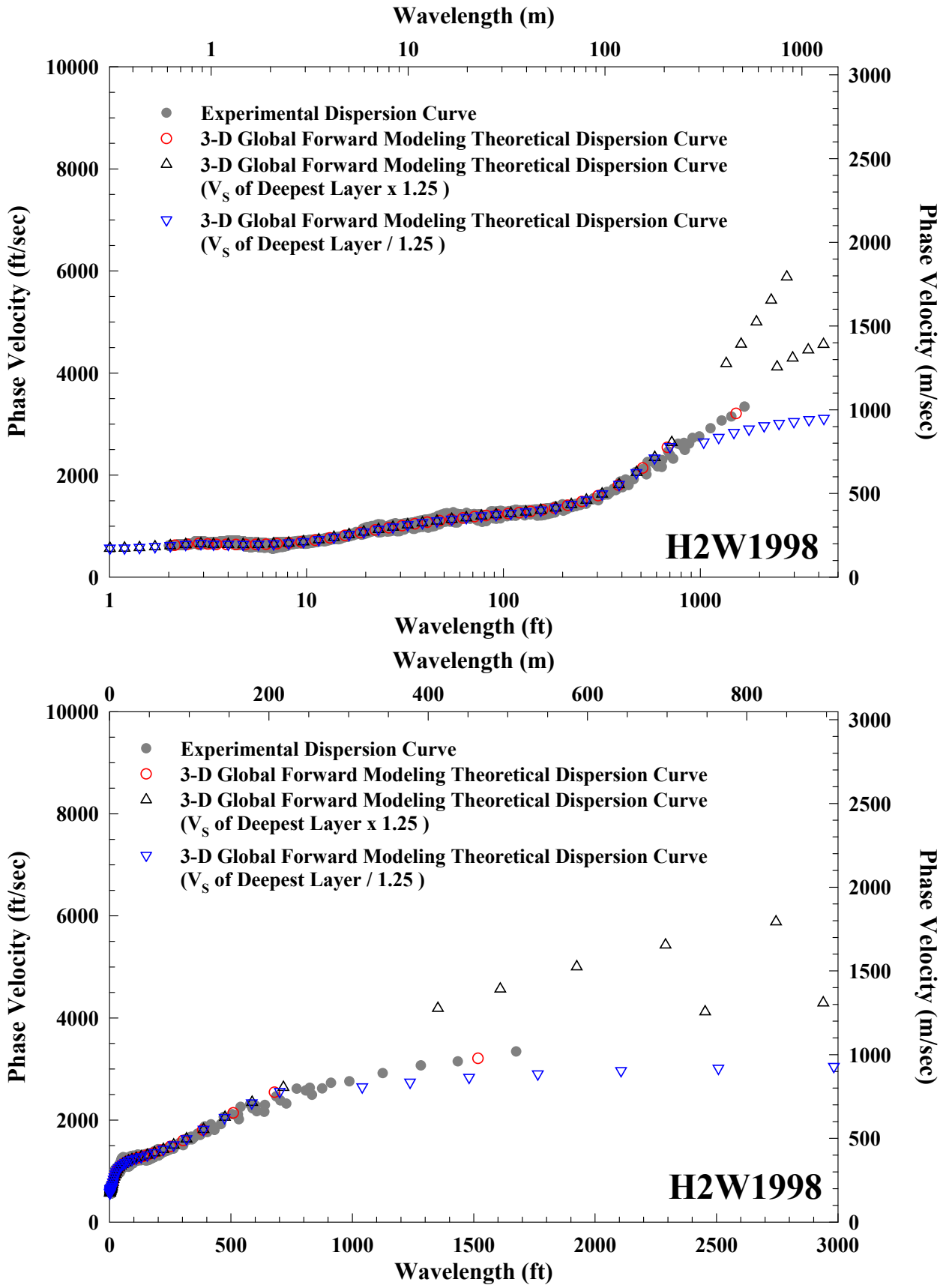

Figure B.9.1 Comparison of Experimental (Field) and Global Forward Modeling Theoretical Dispersion Curves from Site H2W1998 Before and After Changing the Vs Value of the Bottom Layer; Logarithmic (Top) and Linear (Bottom) Wavelength Axes

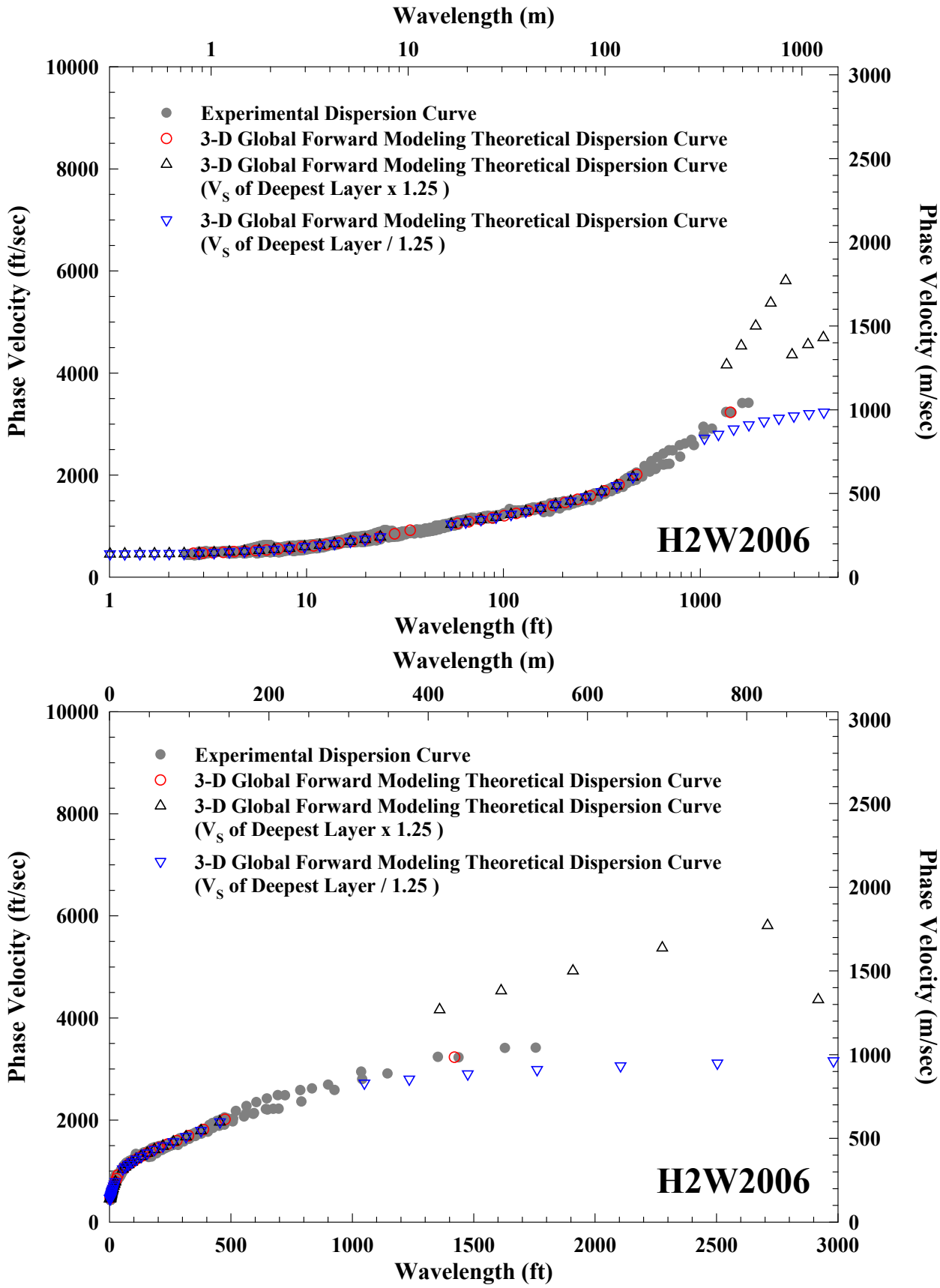

Figure B.10.1 Comparison of Experimental (Field) and Global Forward Modeling Theoretical Dispersion Curves from Site H2W2006 Before and After Changing the Vs Value of the Bottom Layer; Logarithmic (Top) and Linear (Bottom) Wavelength Axes

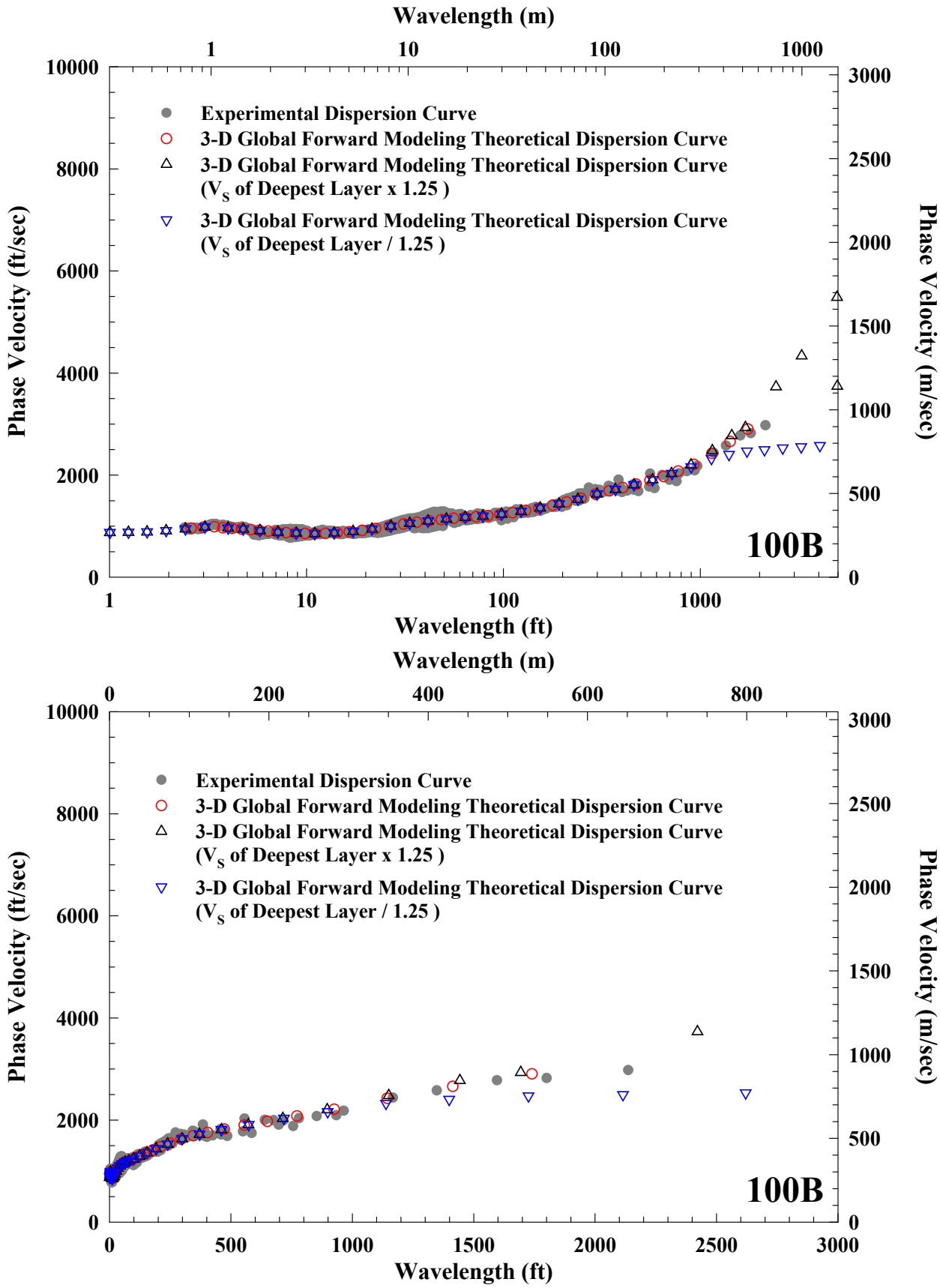

Figure B.11.1 Comparison of Experimental (Field) and Global Forward Modeling Theoretical Dispersion Curves from Site 100B Before and After Changing the Vs Value of the Bottom Layer; Logarithmic (Top) and Linear (Bottom) Wavelength Axes

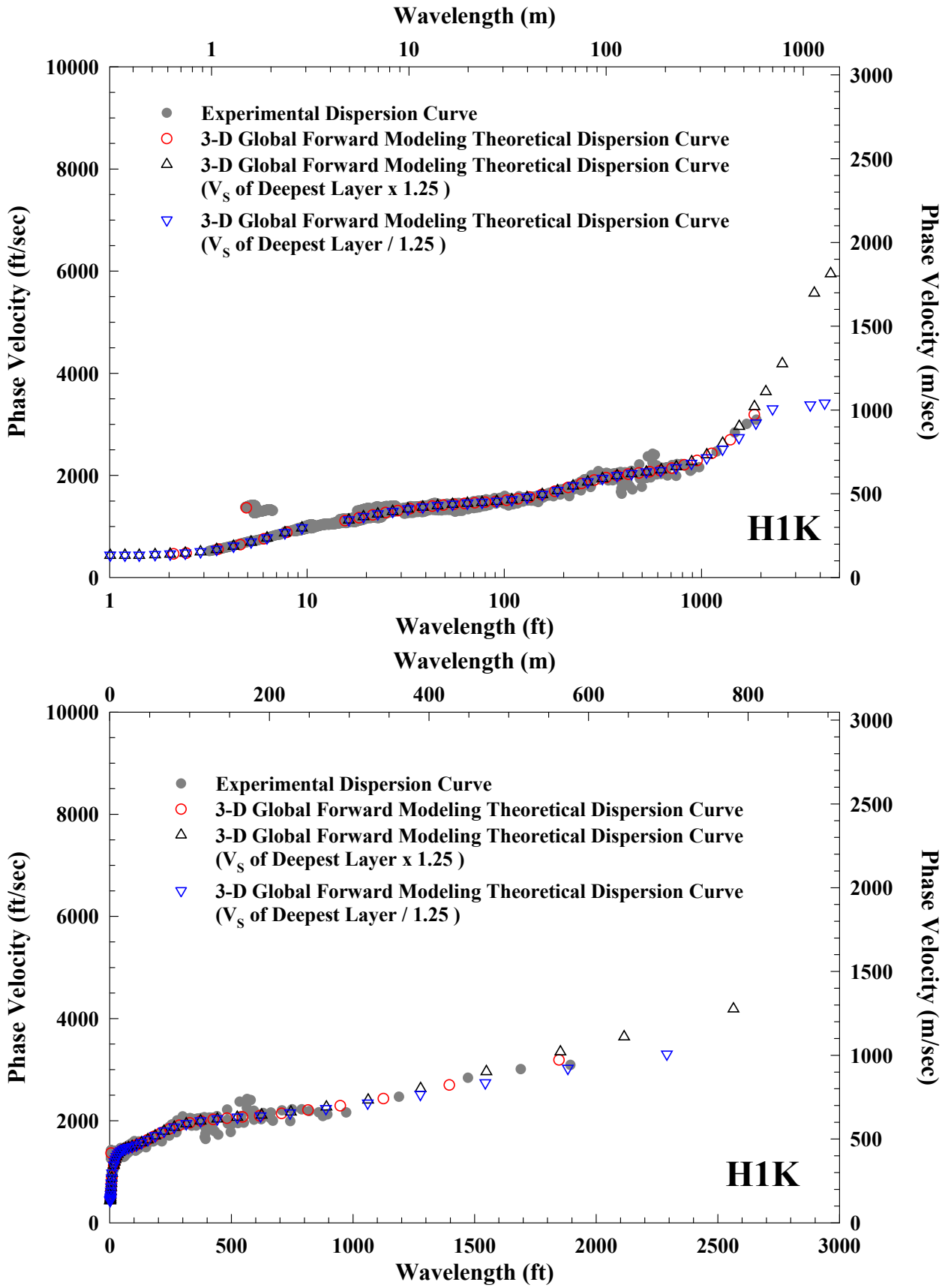

Figure B.12.1 Comparison of Experimental (Field) and Global Forward Modeling Theoretical Dispersion Curves from Site H1K Before and After Changing the V_S Value of the Bottom Layer; Logarithmic (Top) and Linear (Bottom) Wavelength Axes

Appendix C

Sensitivity Study of the Impact on the V_S Profiles of Changing the Water Table Depth by +/- 25%

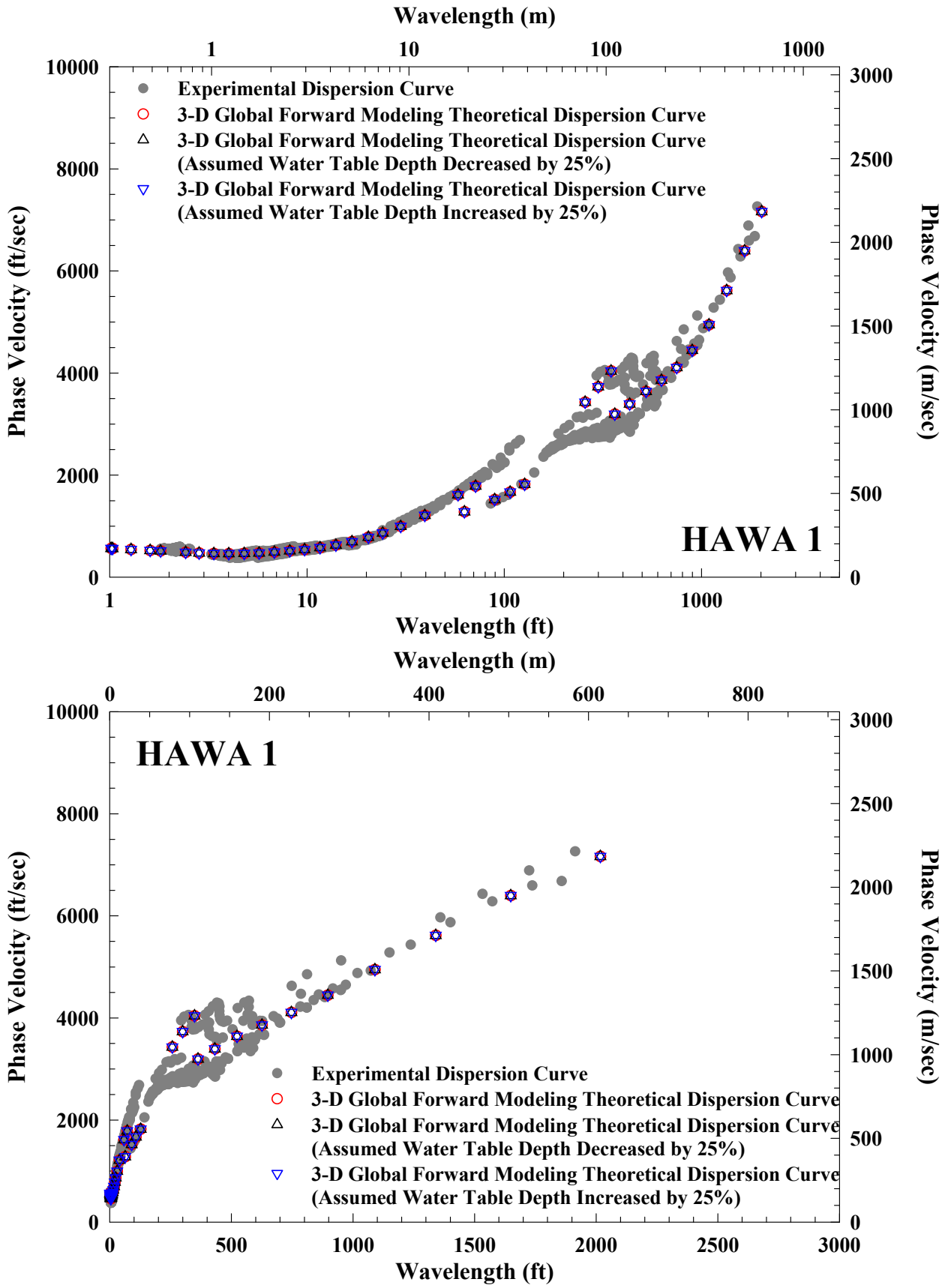

Figure C.1.1 Comparison of Experimental (Field) and Global Forward Modeling Theoretical Dispersion Curves from Site HAWA 1 Before and After Changing the Water Table Depth by +/- 25%; Logarithmic (Top) and Linear (Bottom) Wavelength Axes

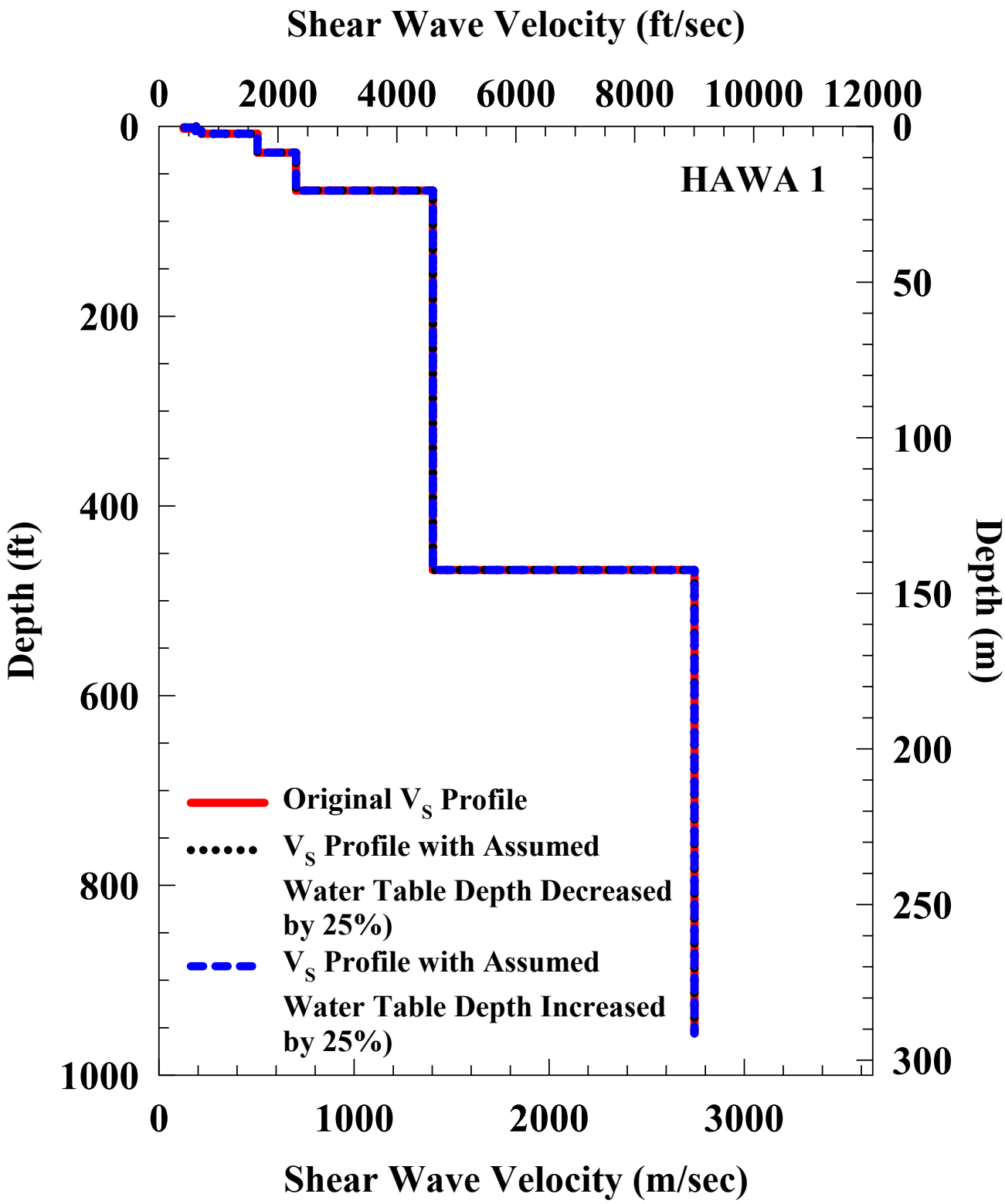

Figure C.1.2 Comparison of Vs Profiles from Site HAWA 1 Before and After Changing the Water Table Depth by +/- 25%

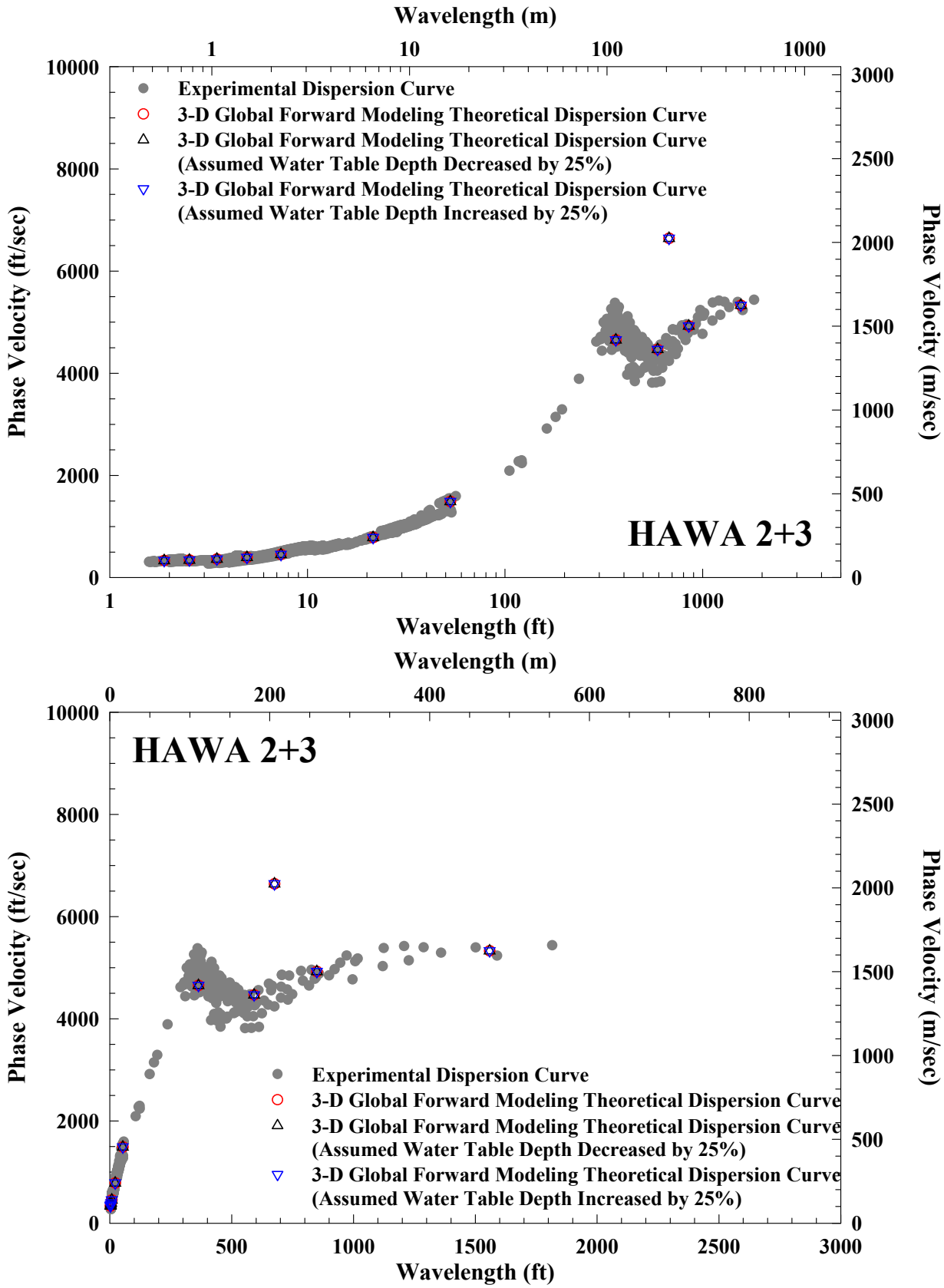

Figure C.2.1 Comparison of Experimental (Field) and Global Forward Modeling Theoretical Dispersion Curves from Site HAWA 2+3 Before and After Changing the Water Table Depth by +/- 25%; Logarithmic (Top) and Linear (Bottom) Wavelength Axes

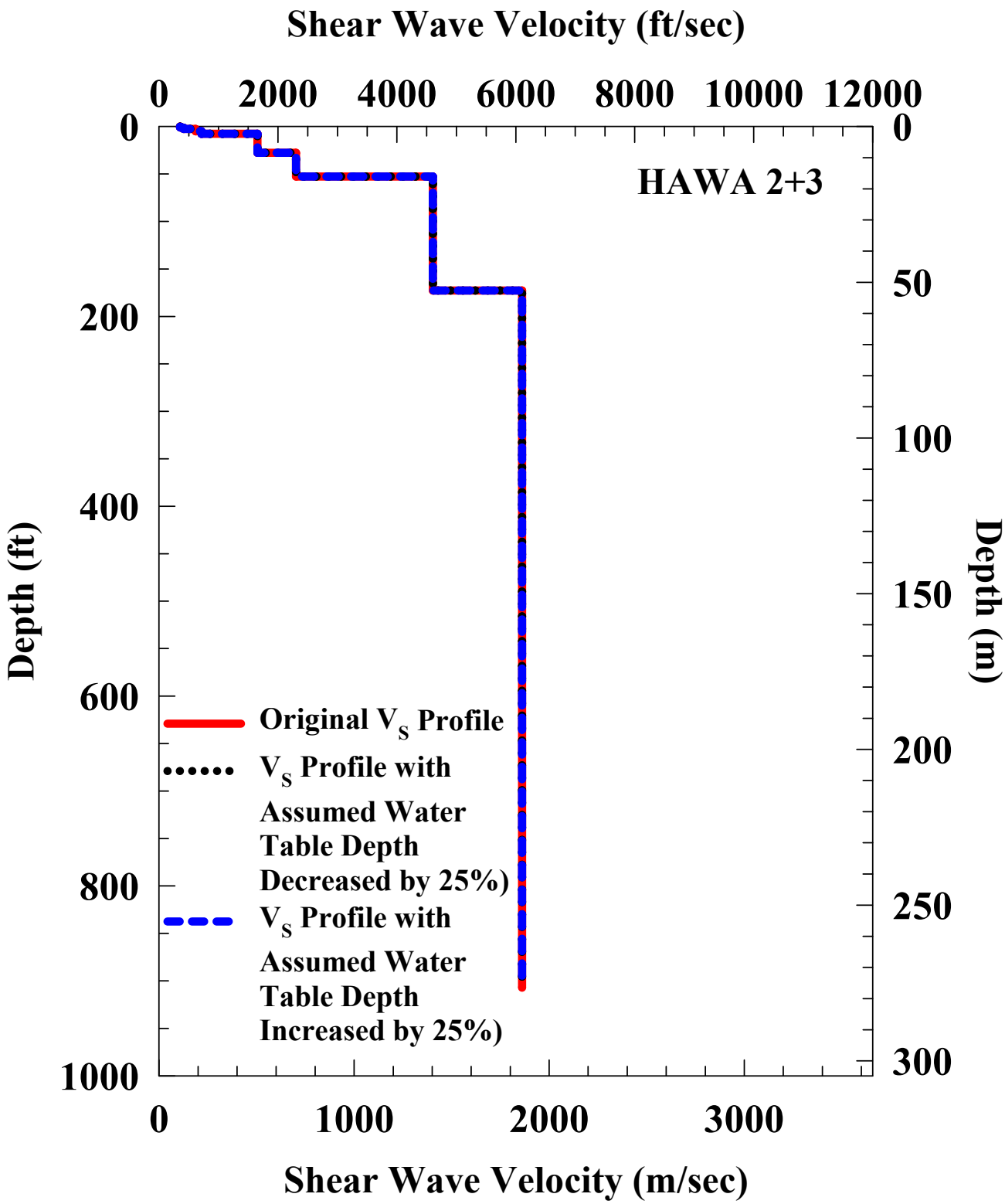

Figure C.2.2 Comparison of V_S Profiles from Site HAWA 2+3 Before and After Changing the Water Table Depth by +/- 25%

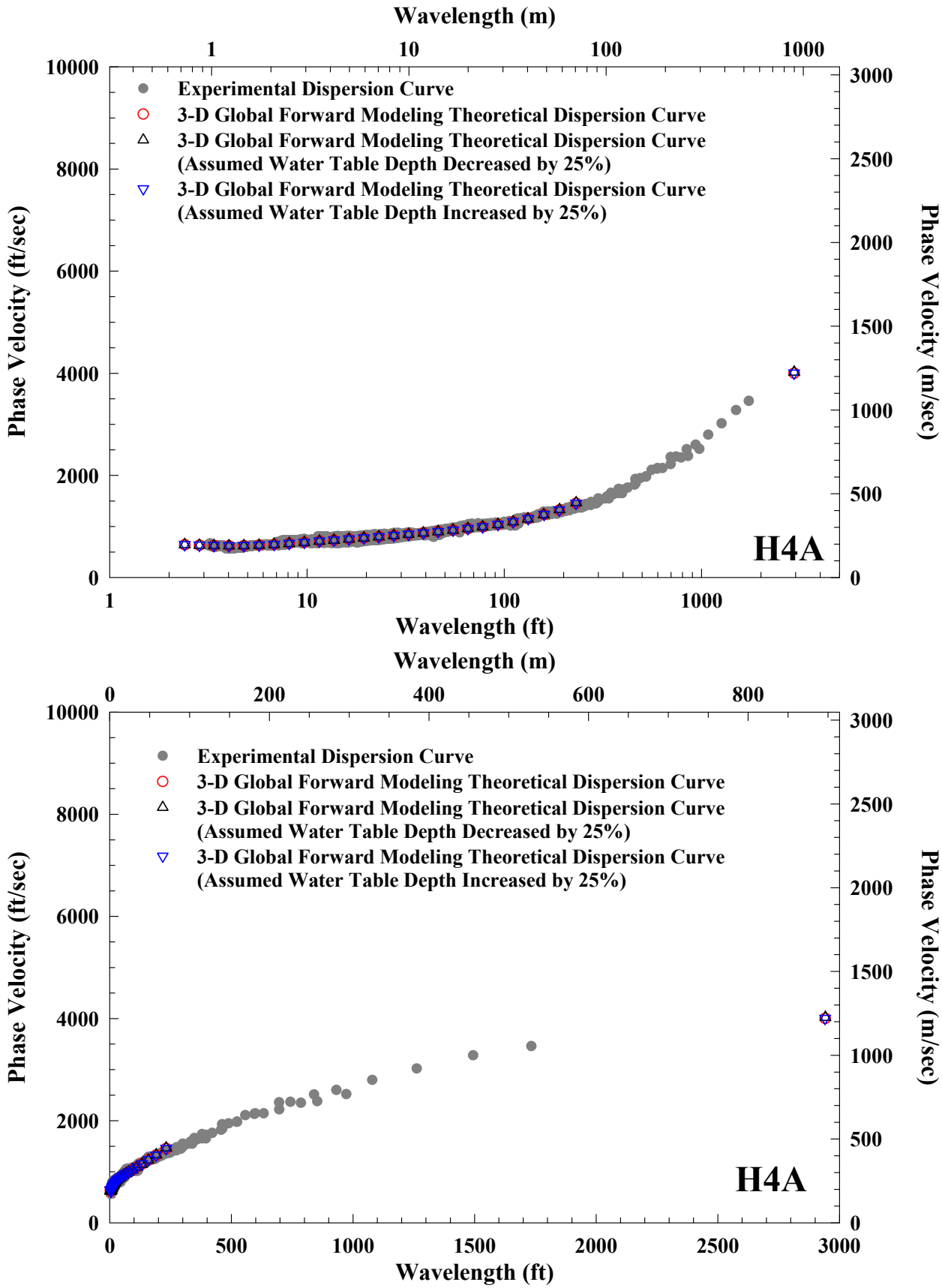

Figure C.3.1 Comparison of Experimental (Field) and Global Forward Modeling Theoretical Dispersion Curves from Site H4A Before and After Changing the Water Table Depth by +/- 25%; Logarithmic (Top) and Linear (Bottom) Wavelength Axes

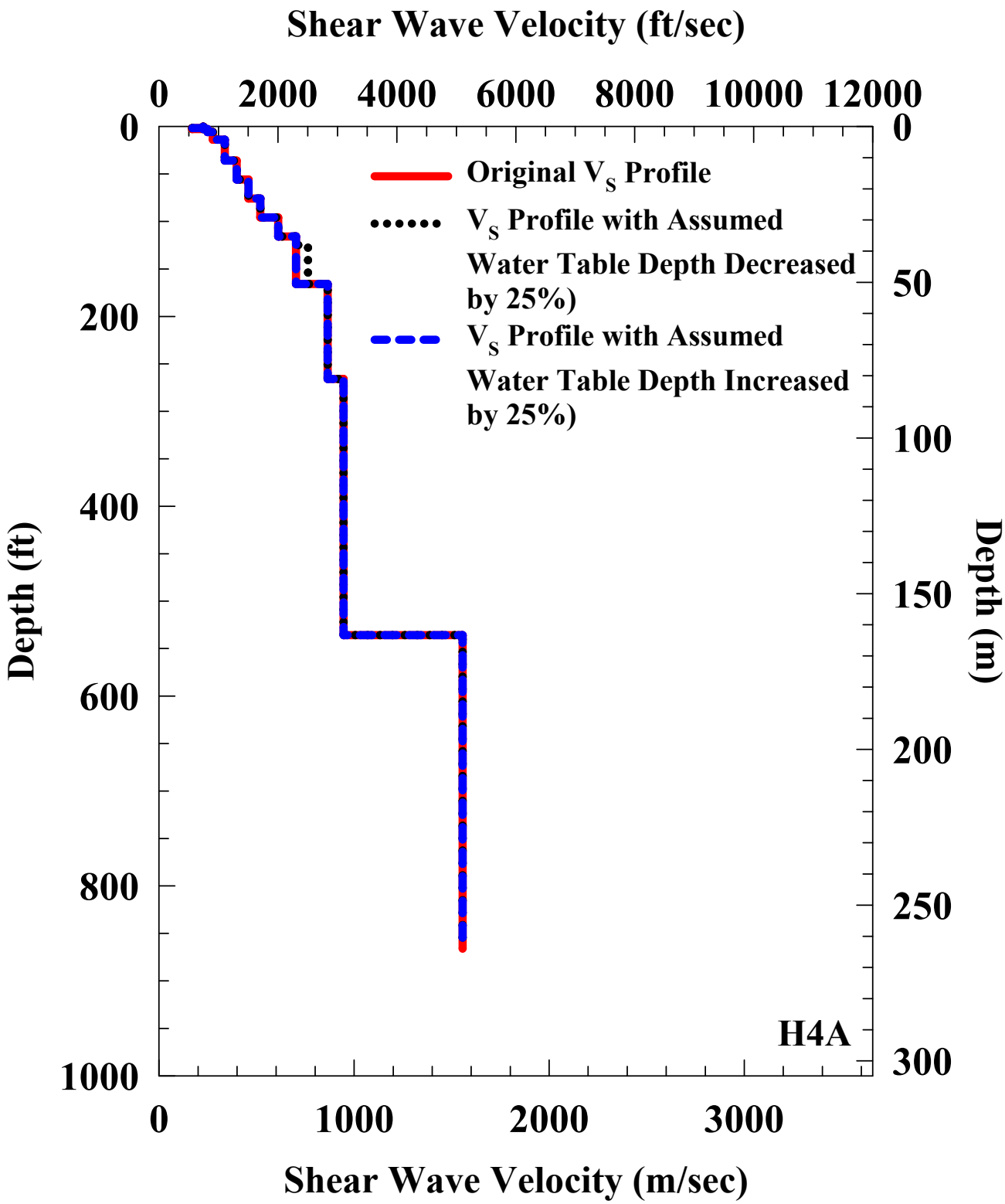

Figure C.3.2 Comparison of V_S Profiles from Site H4A Before and After Changing the Water Table Depth by +/- 25%

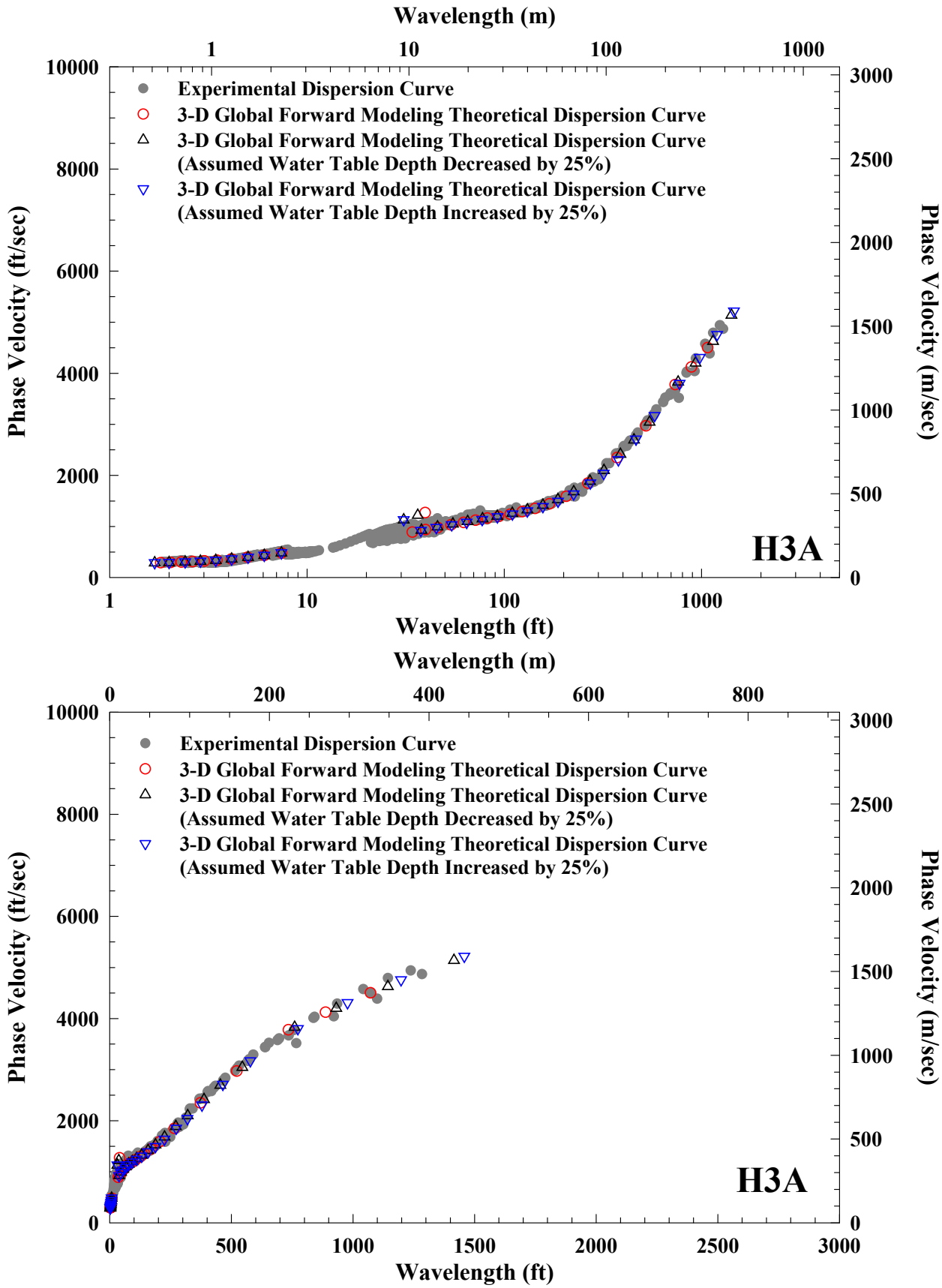

Figure C.4.1 Comparison of Experimental (Field) and Global Forward Modeling Theoretical Dispersion Curves from Site H3A Before and After Changing the Water Table Depth by +/- 25%; Logarithmic (Top) and Linear (Bottom) Wavelength Axes

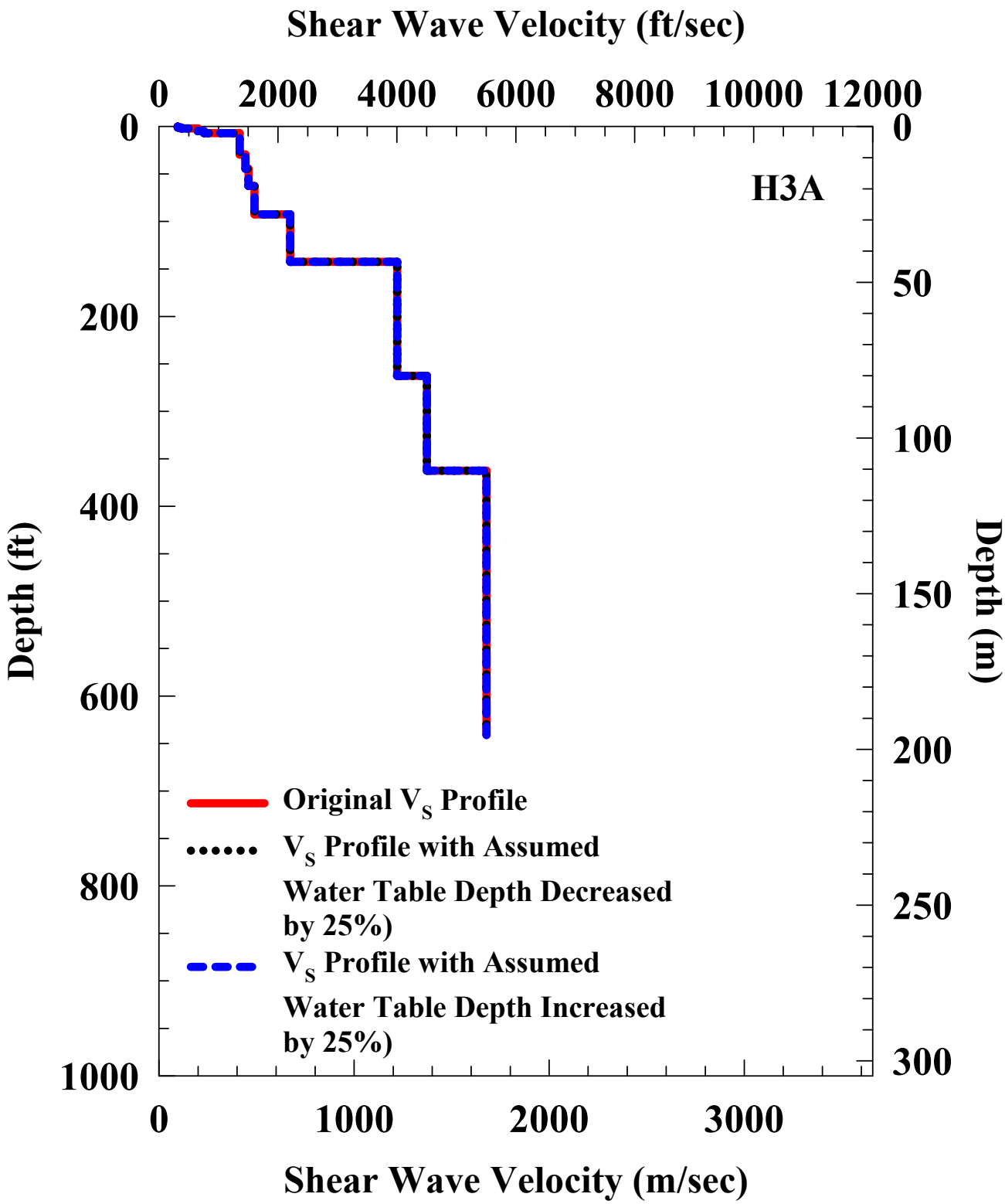

Figure C.4.2 Comparison of V_S Profiles from Site H3A Before and After Changing the Water Table Depth by +/- 25%

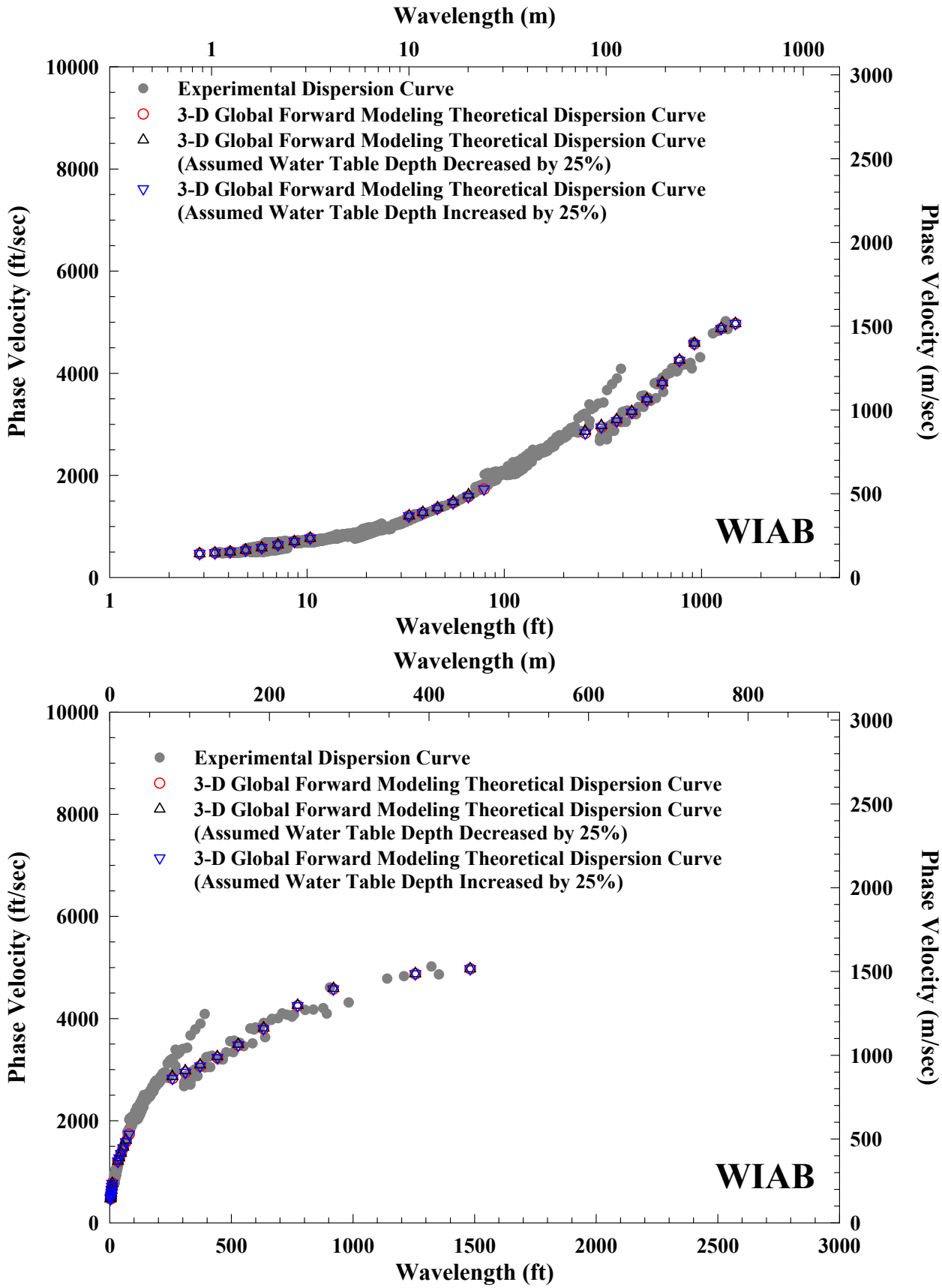

Figure C.5.1 Comparison of Experimental (Field) and Global Forward Modeling Theoretical Dispersion Curves from Site WIAB Before and After Changing the Water Table Depth by +/- 25%; Logarithmic (Top) and Linear (Bottom) Wavelength Axes

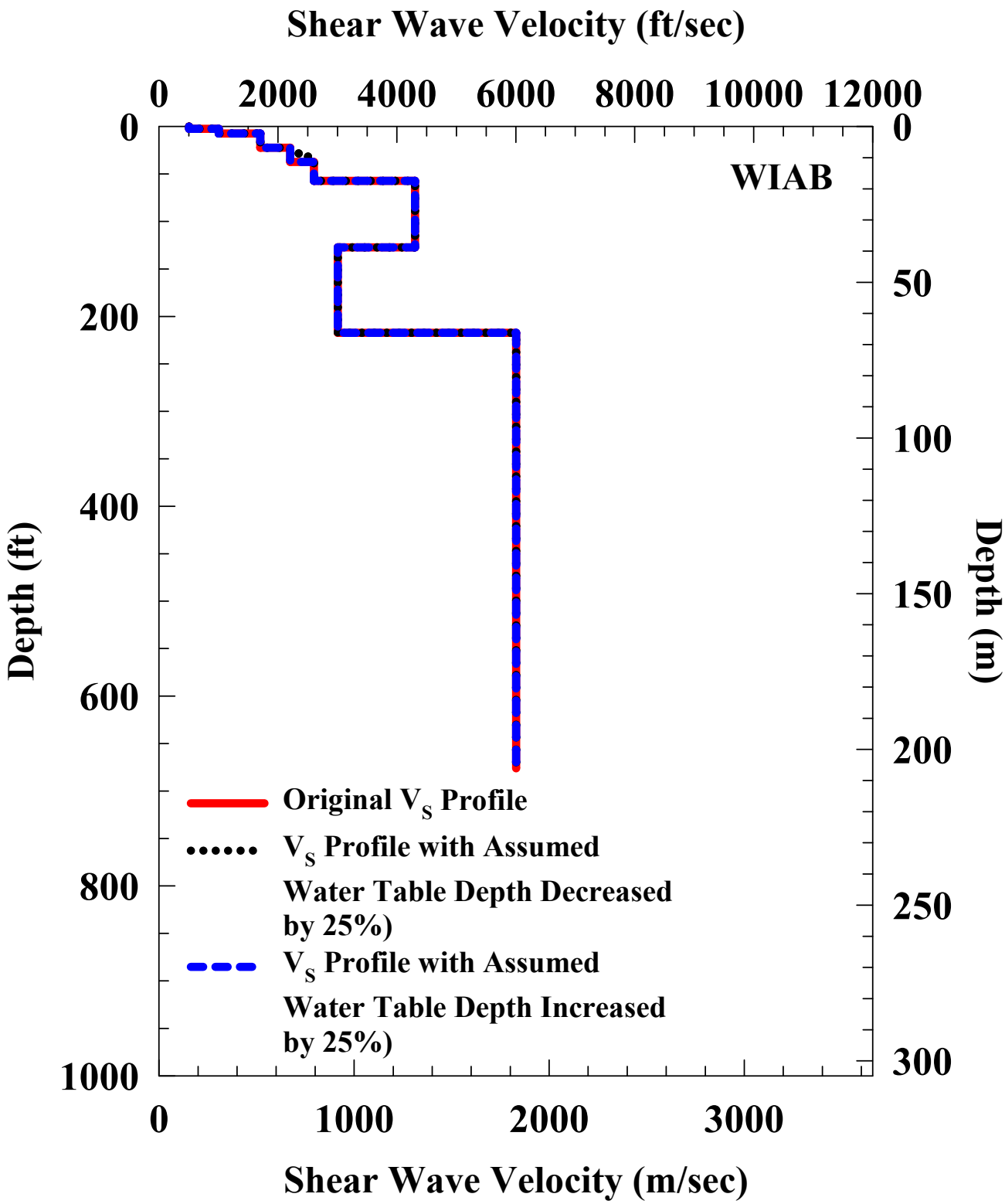

Figure C.5.2 Comparison of V_S Profiles from Site WIAB Before and After Changing the Water Table Depth by +/- 25%

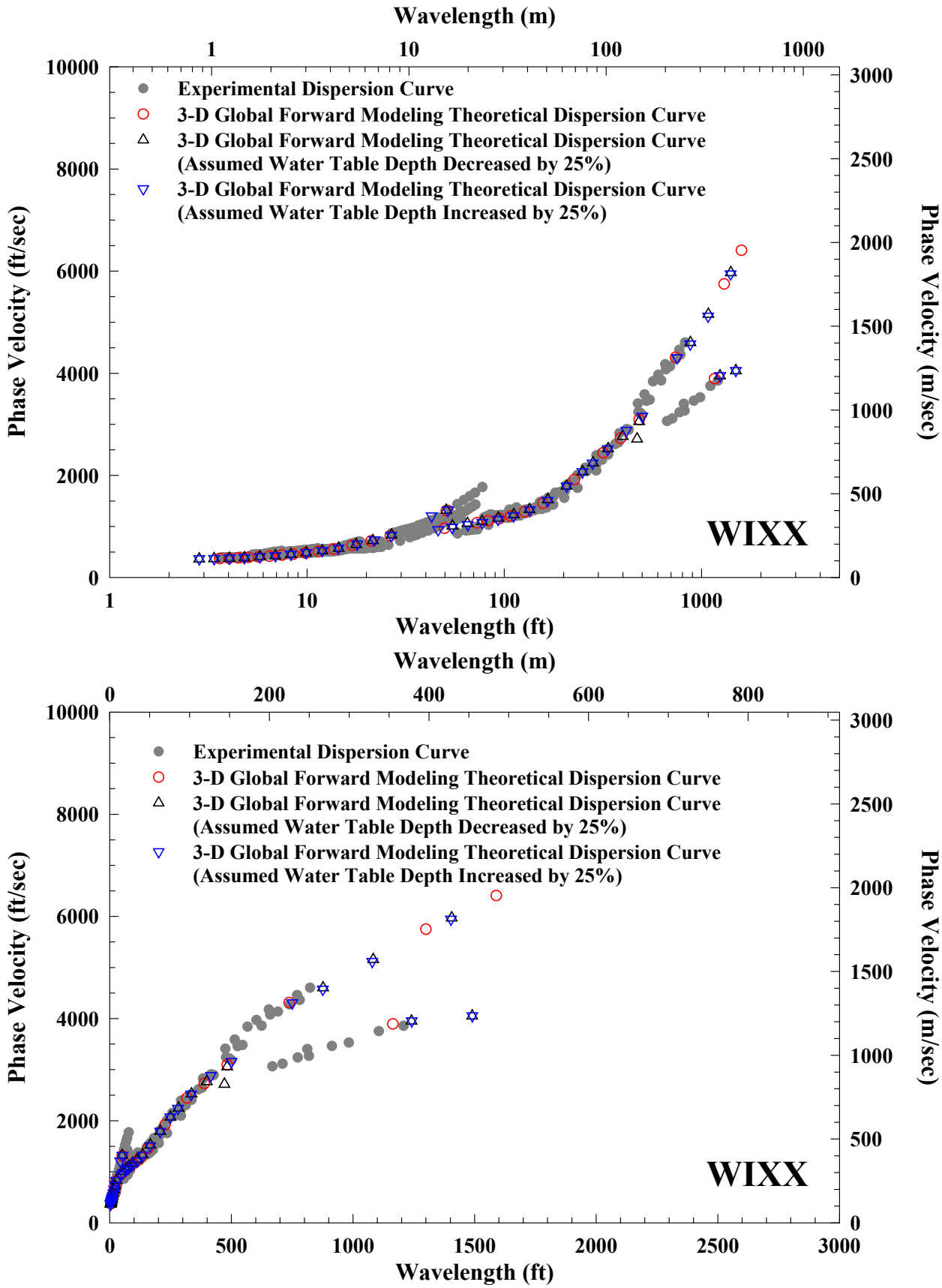

Figure C.6.1 Comparison of Experimental (Field) and Global Forward Modeling Theoretical Dispersion Curves from Site WIXX Before and After Changing the Water Table Depth by +/- 25%; Logarithmic (Top) and Linear (Bottom) Wavelength Axes

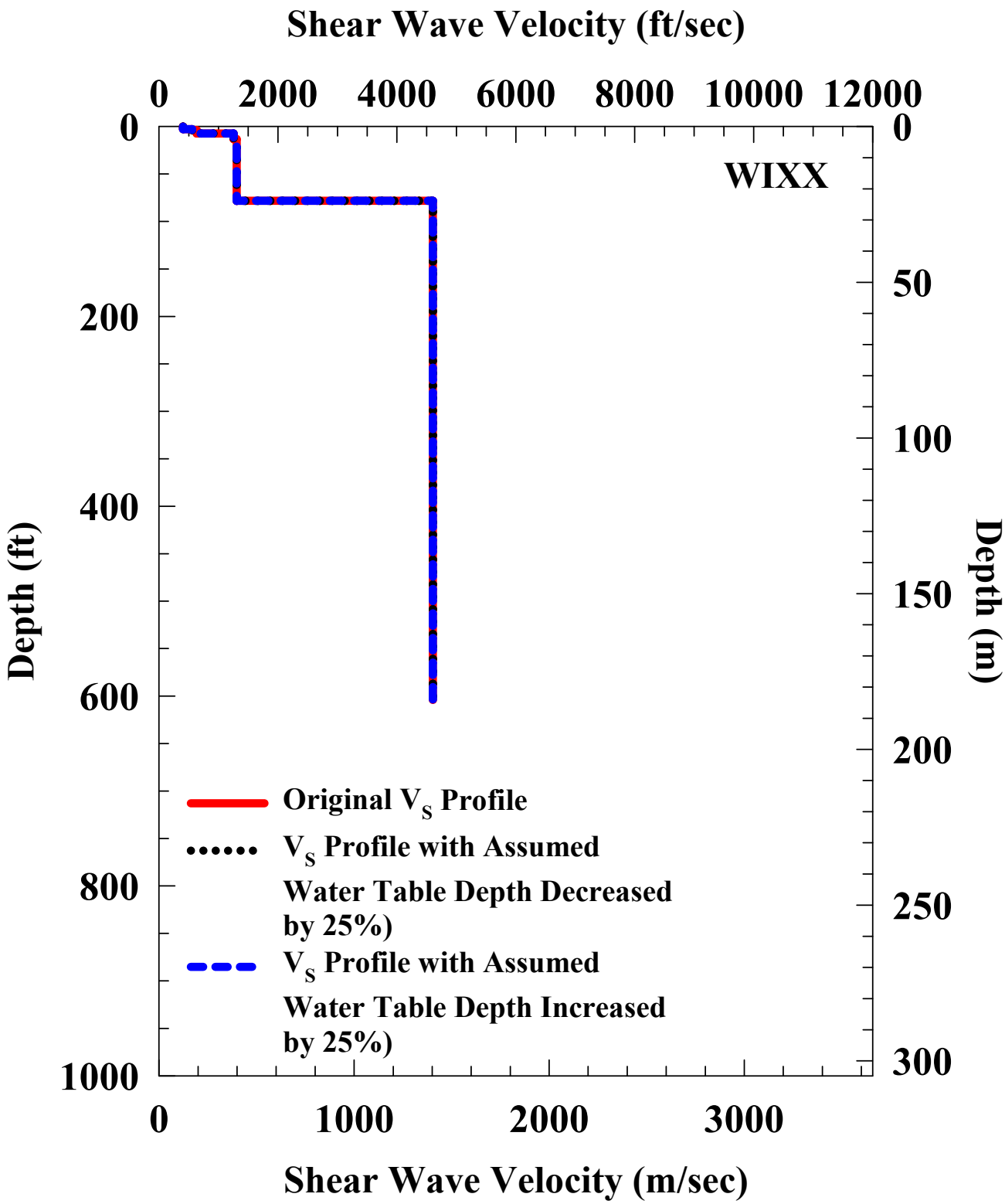

Figure C.6.2 Comparison of V_S Profiles from Site WIXX Before and After Changing the Water Table Depth by +/- 25%

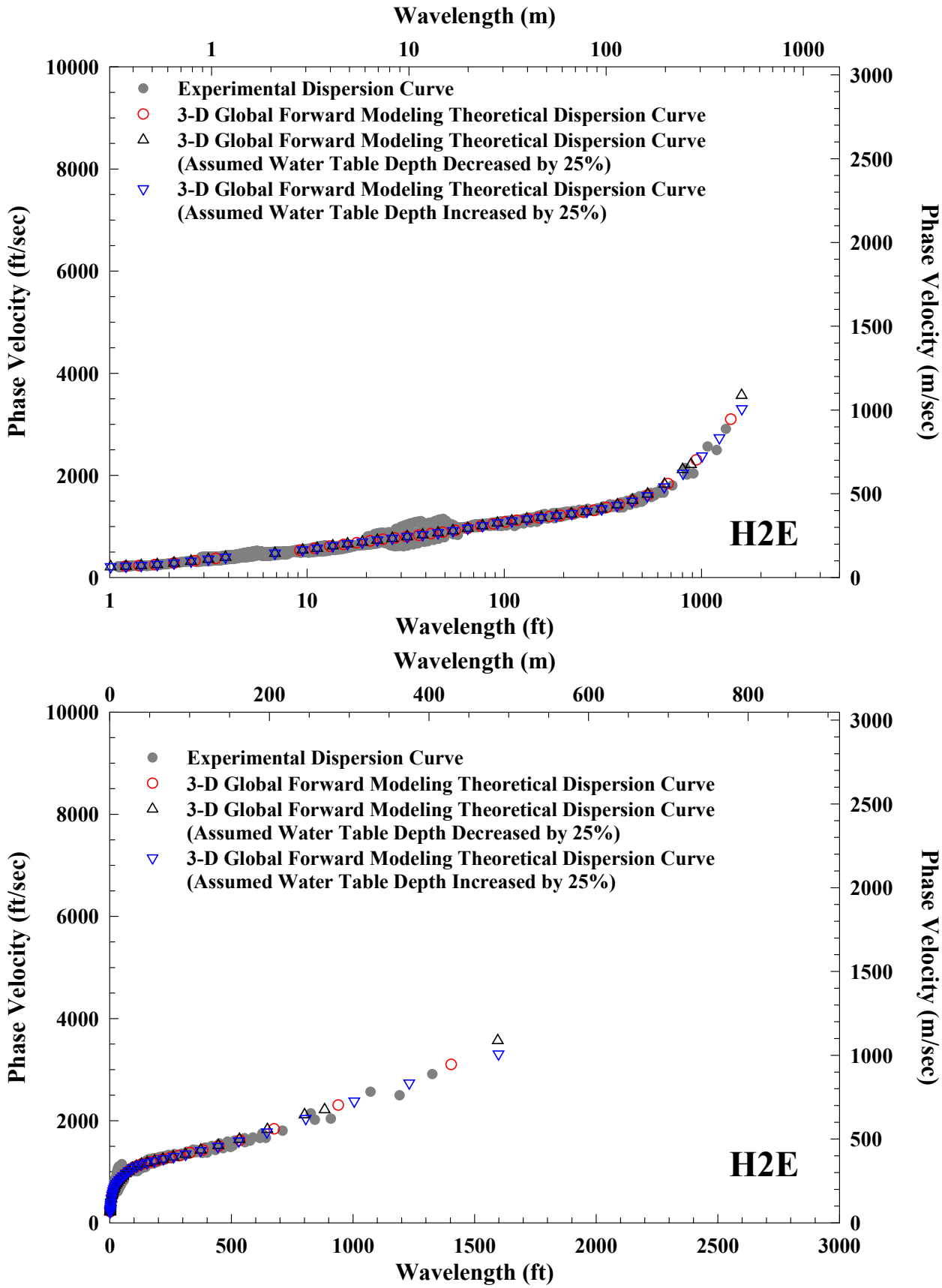

Figure C.7.1 Comparison of Experimental (Field) and Global Forward Modeling Theoretical Dispersion Curves from Site H2E Before and After Changing the Water Table Depth by +/- 25%; Logarithmic (Top) and Linear (Bottom) Wavelength Axes

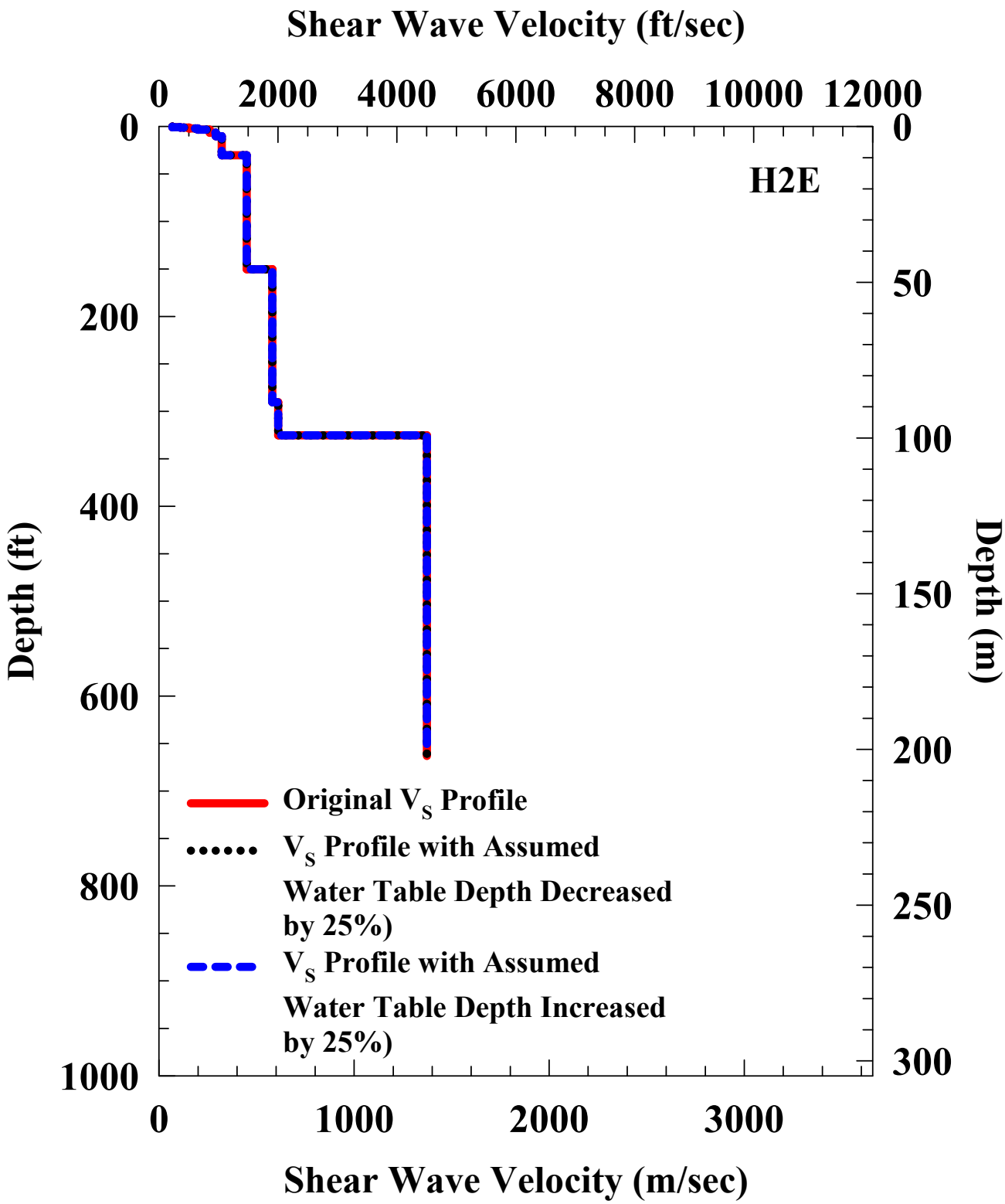

Figure C.7.2 Comparison of V_S Profiles from Site H2E Before and After Changing the Water Table Depth by +/- 25%

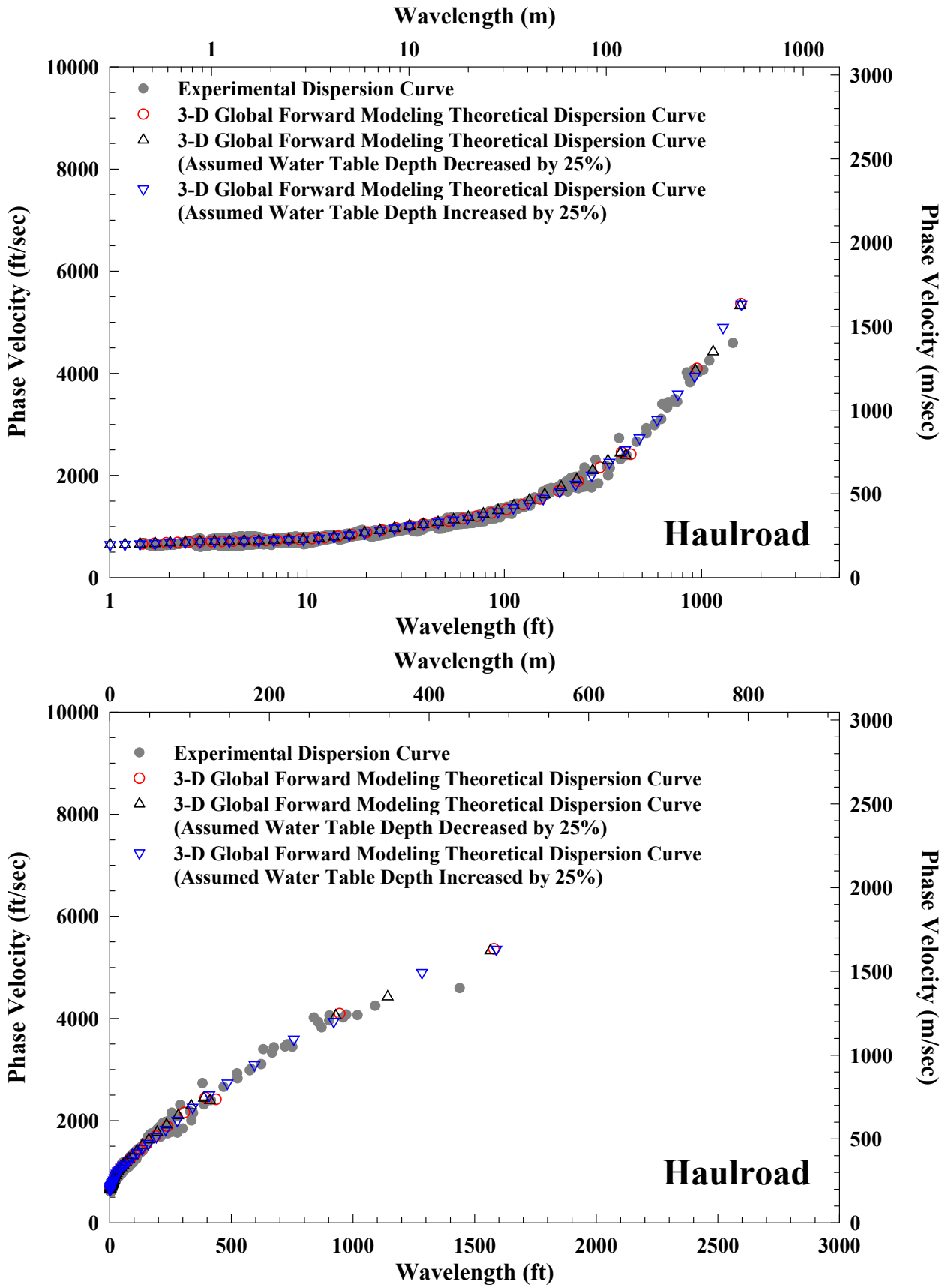

Figure C.8.1 Comparison of Experimental (Field) and Global Forward Modeling Theoretical Dispersion Curves from Site Haulroad Before and After Changing the Water Table Depth by +/- 25%; Logarithmic (Top) and Linear (Bottom) Wavelength Axes

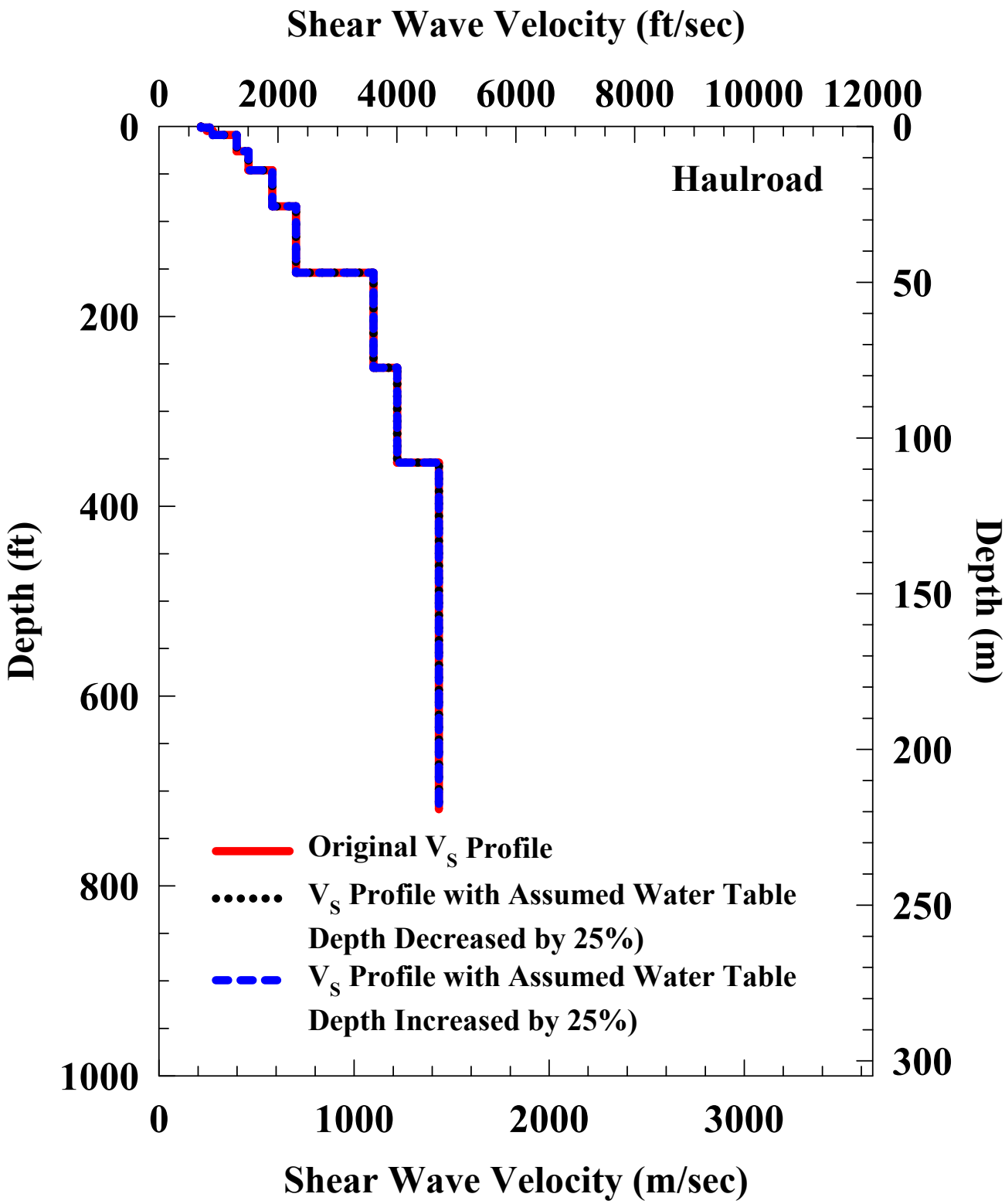

Figure C.8.2 Comparison of V_S Profiles from Site Haulroad Before and After Changing the Water Table Depth by +/- 25%

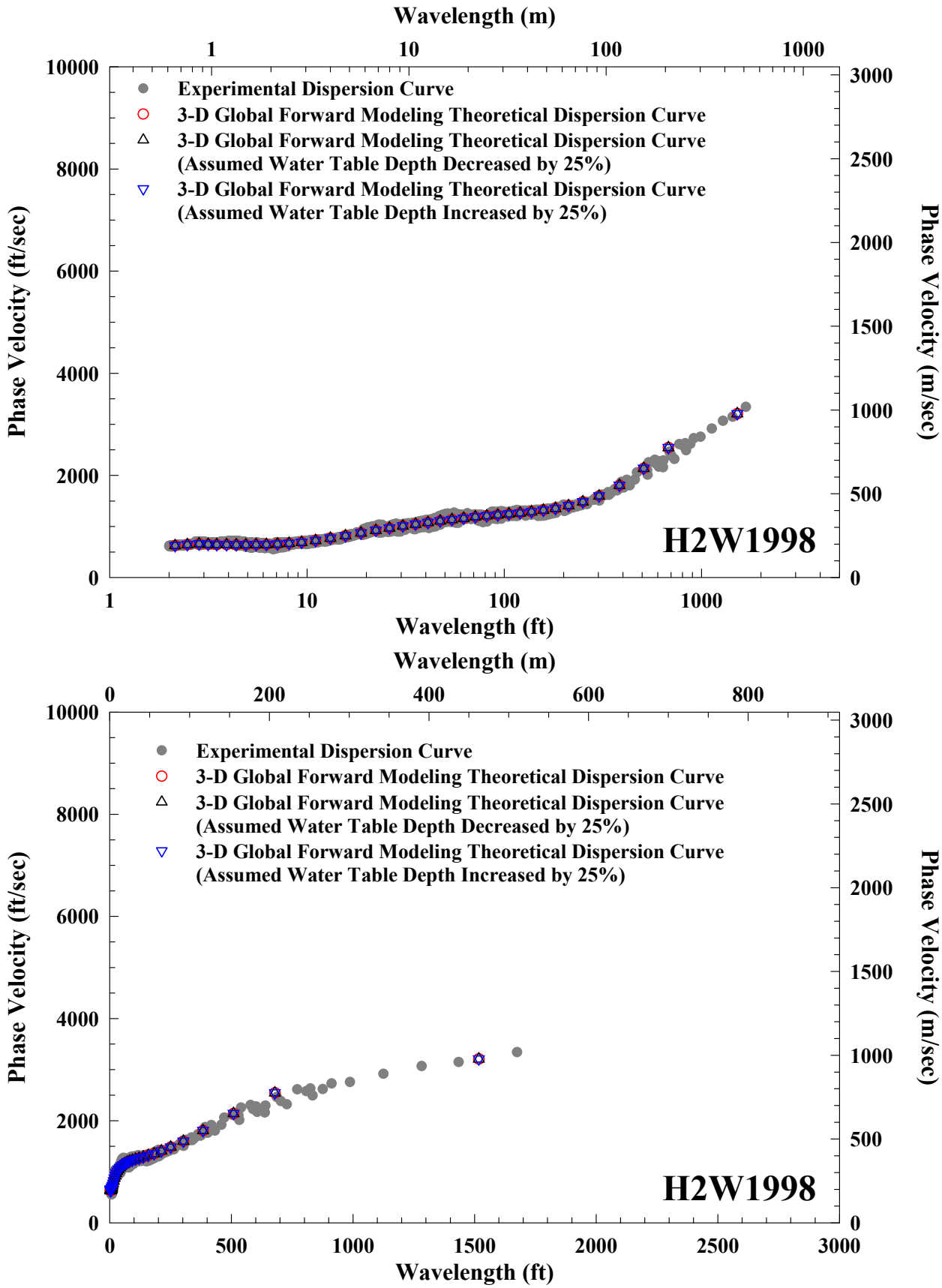

Figure C.9.1 Comparison of Experimental (Field) and Global Forward Modeling Theoretical Dispersion Curves from Site H2W1998 Before and After Changing the Water Table Depth by +/- 25%; Logarithmic (Top) and Linear (Bottom) Wavelength Axes

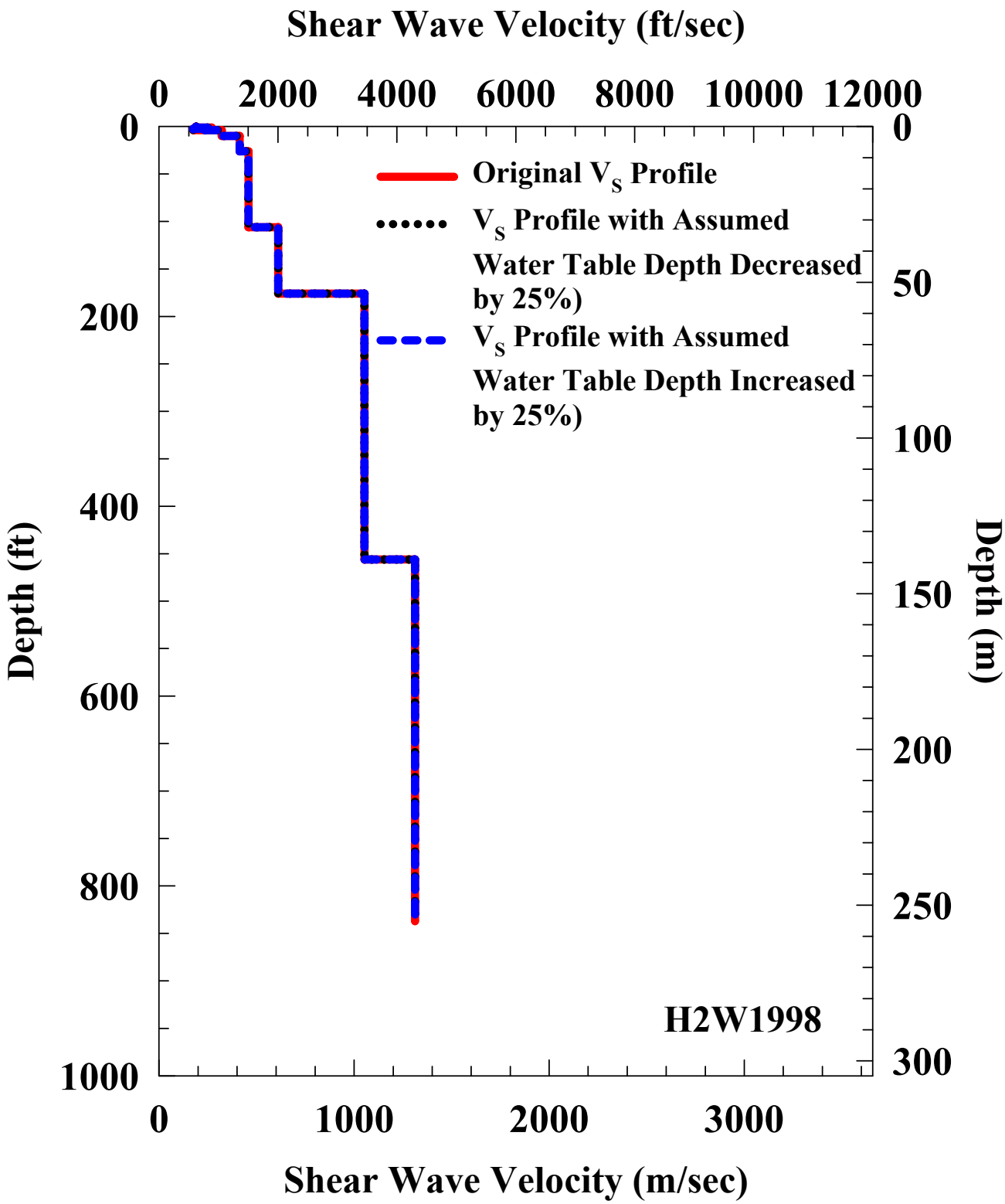

Figure C.9.2 Comparison of V_S Profiles from Site H2W1998 Before and After Changing the Water Table Depth by +/- 25%

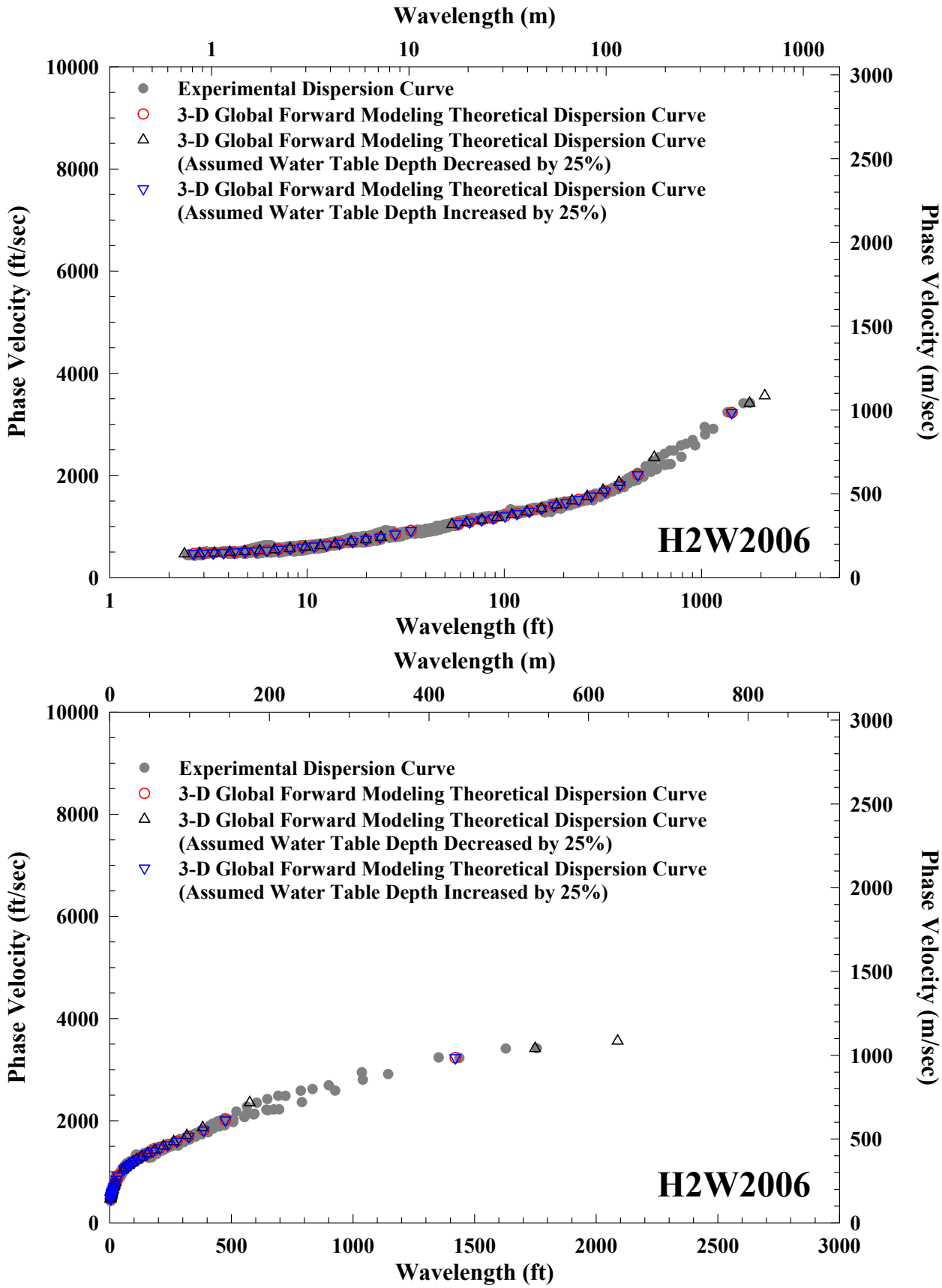

Figure C.10.1 Comparison of Experimental (Field) and Global Forward Modeling Theoretical Dispersion Curves from Site H2W2006 Before and After Changing the Water Table Depth by +/- 25%; Logarithmic (Top) and Linear (Bottom) Wavelength Axes

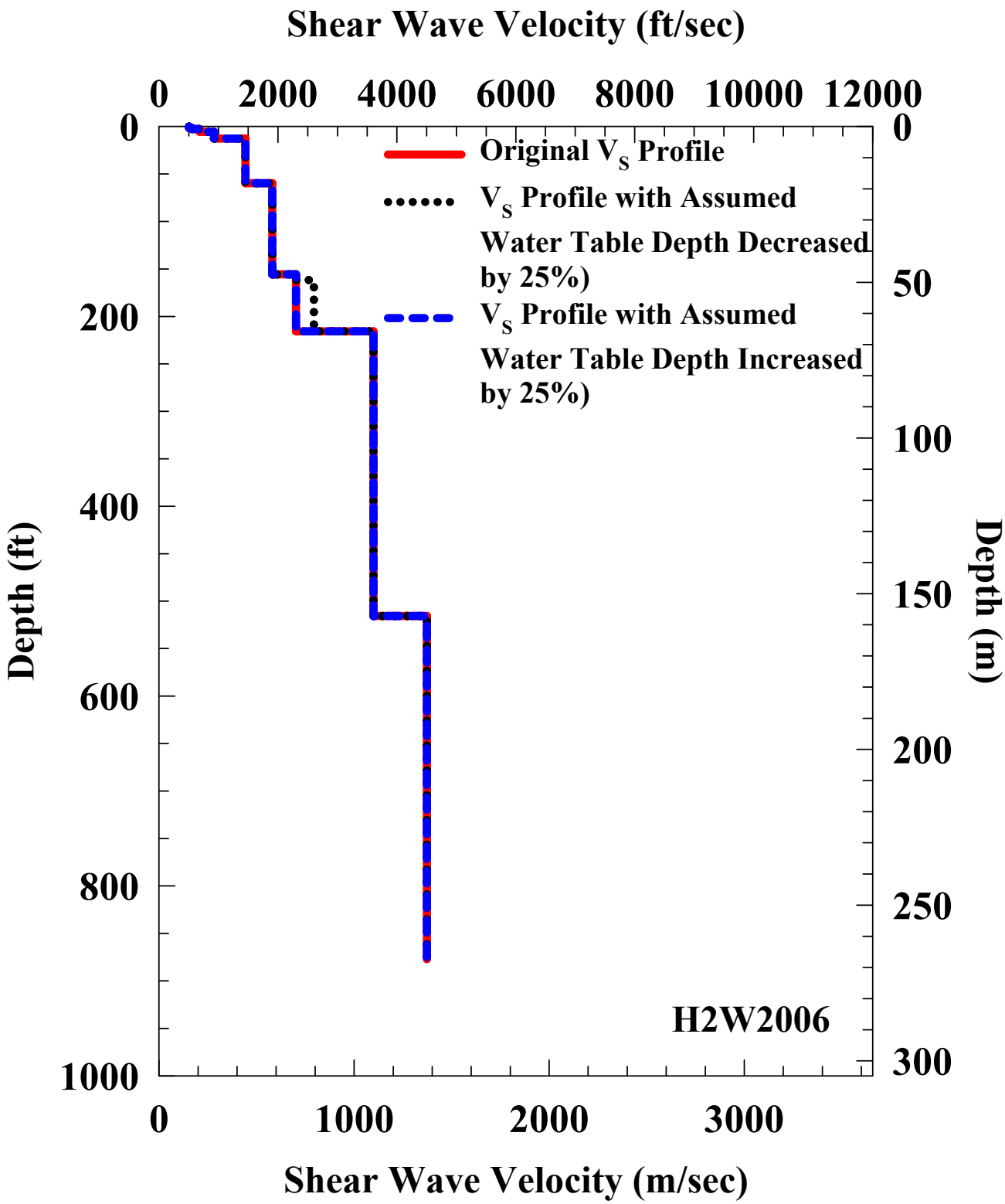

Figure C.10.2 Comparison of V_S Profiles from Site H2W2006 Before and After Changing the Water Table Depth by +/- 25%

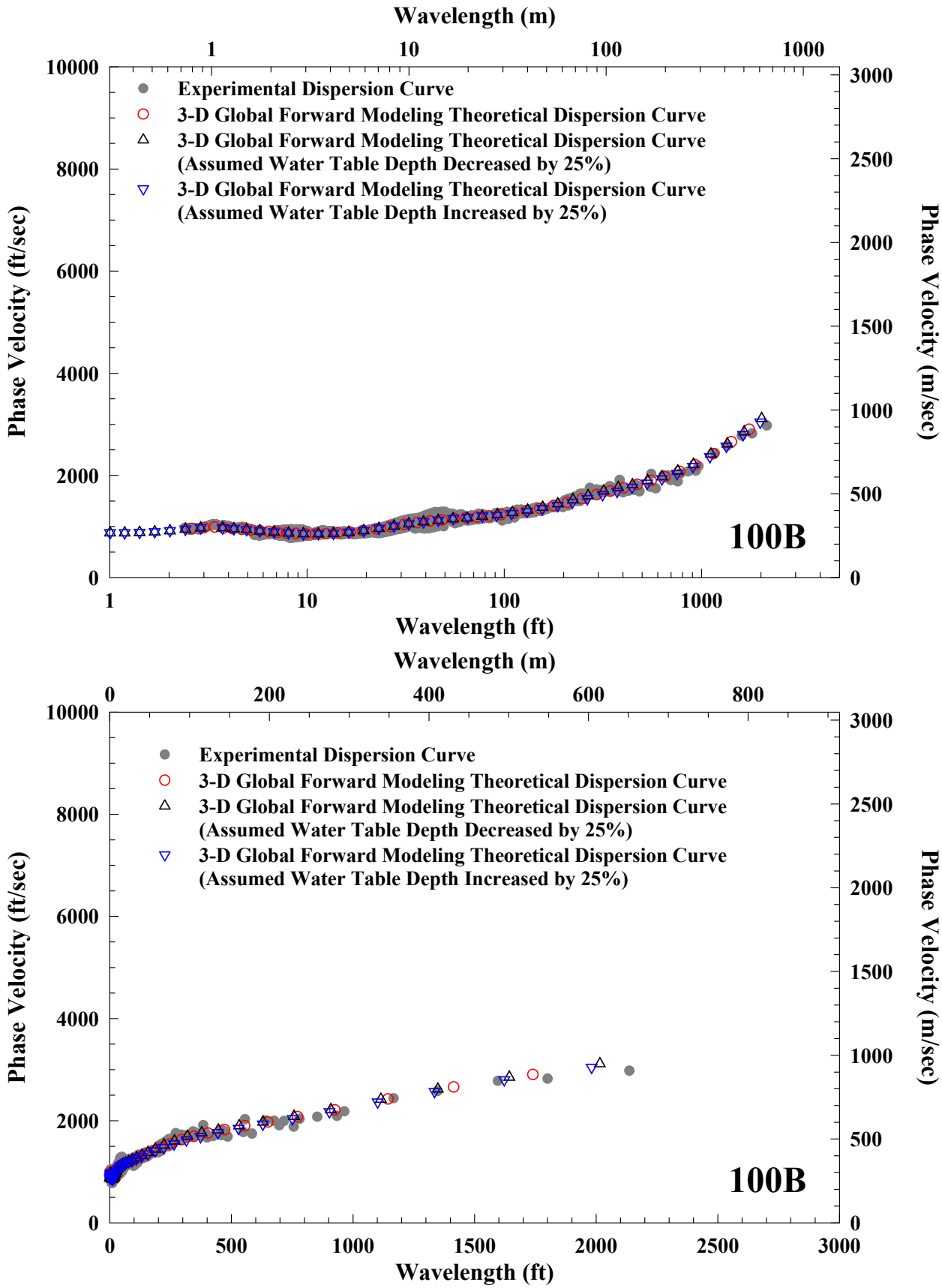

Figure C.11.1 Comparison of Experimental (Field) and Global Forward Modeling Theoretical Dispersion Curves from Site 100B Before and After Changing the Water Table Depth by +/- 25%; Logarithmic (Top) and Linear (Bottom) Wavelength Axes

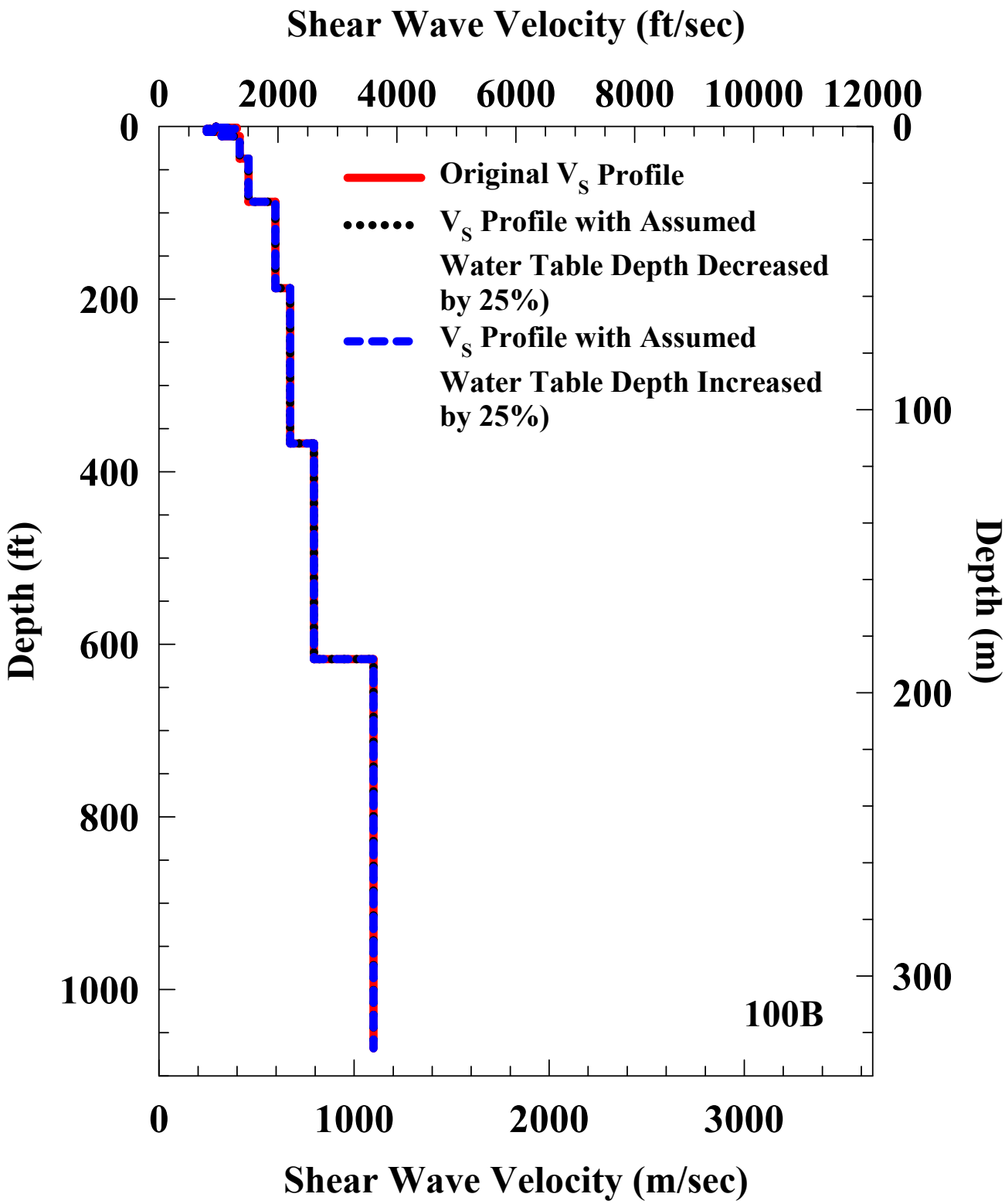

Figure C.11.2 Comparison of V_S Profiles from Site 100B Before and After Changing the Water Table Depth by +/- 25%

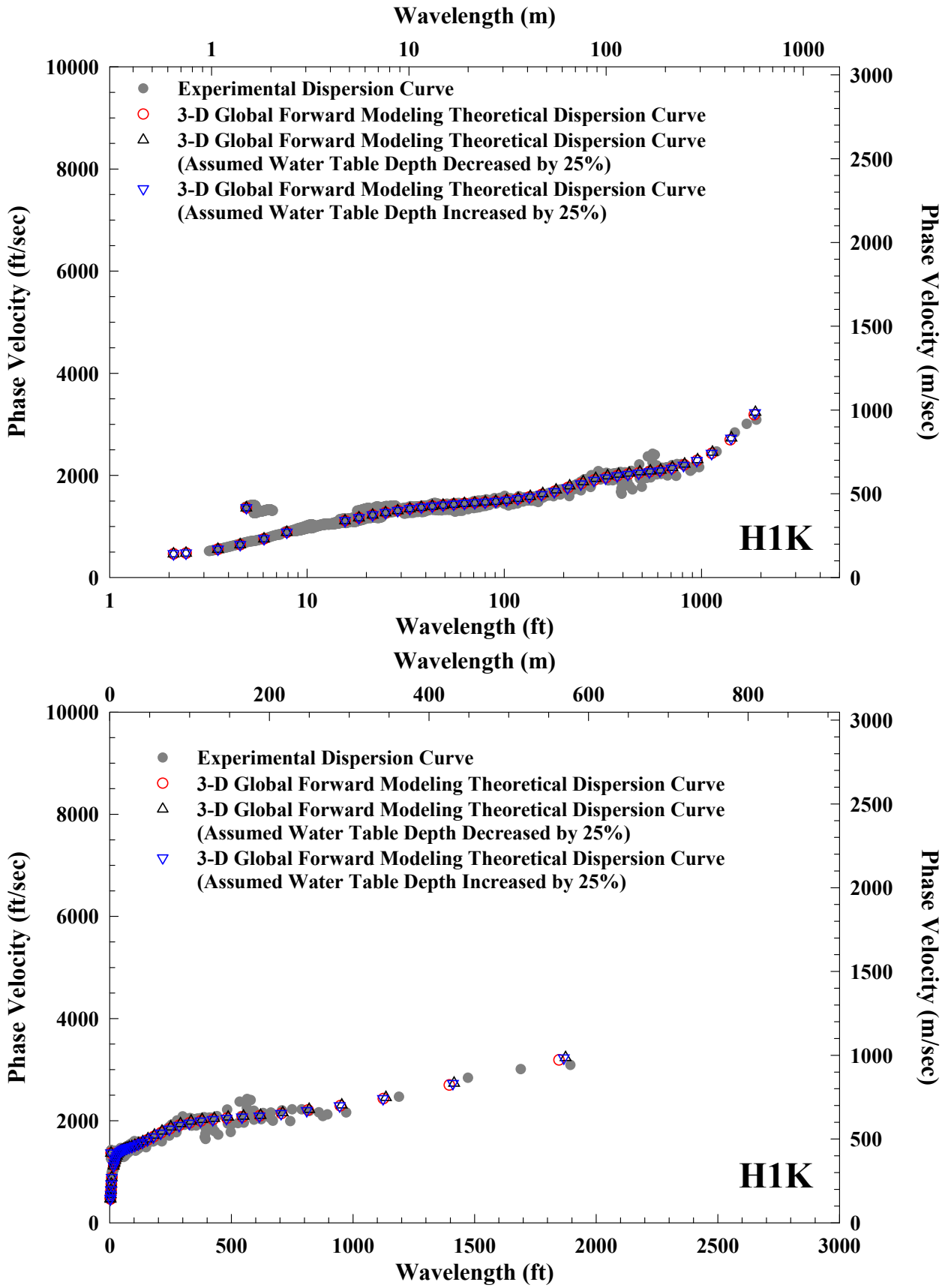

Figure C.12.1 Comparison of Experimental (Field) and Global Forward Modeling Theoretical Dispersion Curves from Site H1K Before and After Changing the Water Table Depth by +/- 25%; Logarithmic (Top) and Linear (Bottom) Wavelength Axes

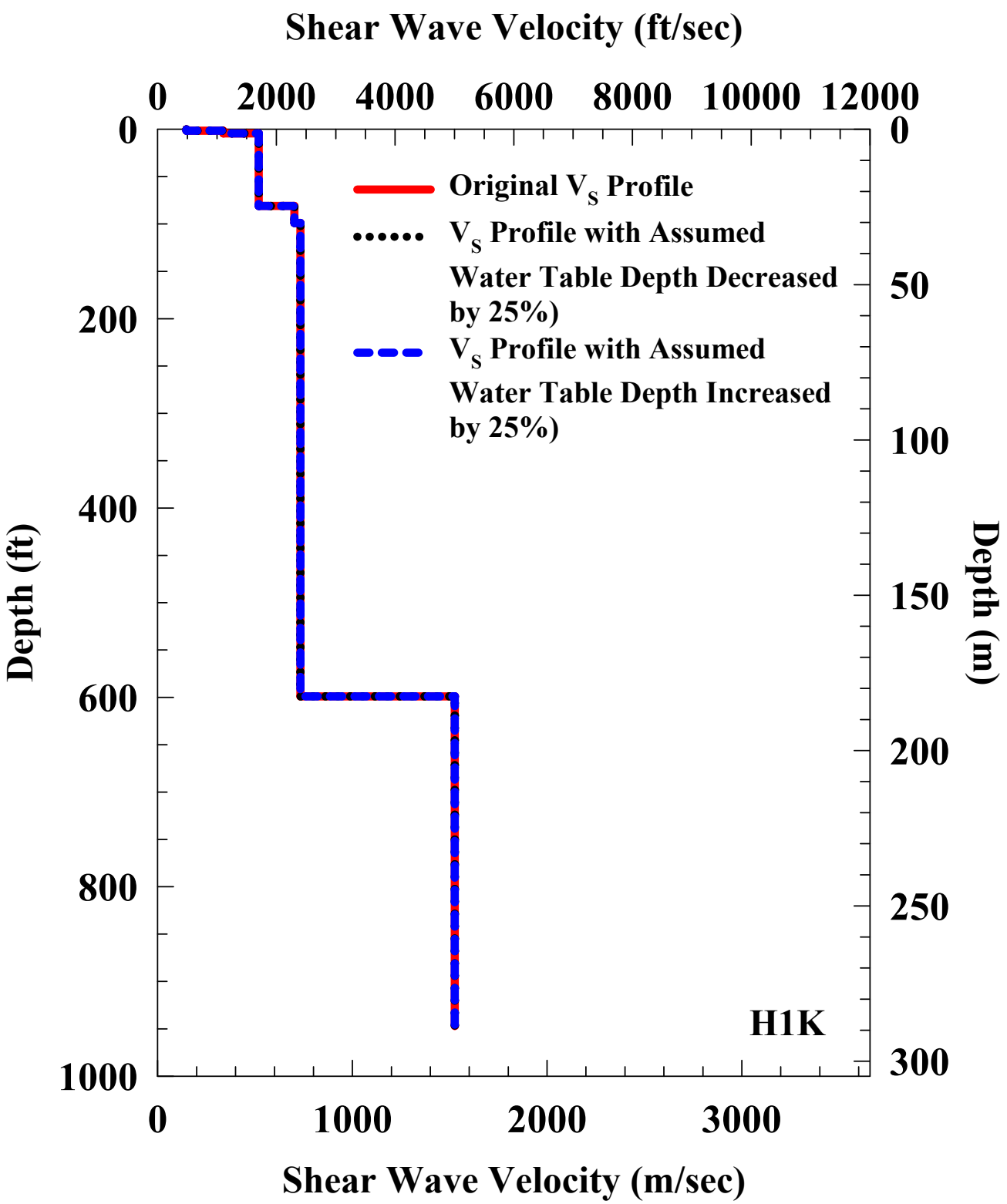

Figure C.12.2 Comparison of V_S Profiles from Site H1K Before and After Changing the Water Table Depth by +/- 25%

Appendix D

Responses to Questions from Technical Integration Team
Related to Development of V_s Profiles
from SASW Testing at Hanford Site

DCN: GR14-1
Revision 0, May 7, 2014

Question #1

Please explain/provide justification for the assumed Poisson ratios in the analysis and indicate whether reported water table depths are considered. It would be useful if you could provide a sensitivity analysis to demonstrate that the assumed value is unimportant to the final result if that is the case.

Response:

In SASW forward modeling, the following assumptions are made. First, the unit weight and Poisson's ratio of the material are assumed. Poisson's ratio is assumed to be 0.25 for all soils above the water table. (Soil is defined as $V_s < 2500$ fps.) This value of Poisson's ratio is a reasonable assumption for soil when no water table exists in the profiling depth; hence, the degree of saturation is less than ~ 97%. When no water table is present, the value of Poisson's ratio (which may vary from 0.22 to 0.35) has a minor influence on the calculated dispersion curve. The unit weight of the soil is assumed to be 125 pcf. Relative changes in unit weight with depth affect the dispersion curve, but the effect on the final shear wave velocity profile is minor. Therefore, precise knowledge of the unit weights at all depths is not required.

When soils are beneath the water table and are nearly saturated or saturated (or $S_r > 99\%$), values of Poisson's ratio are calculated in the WinSASW forward-modeling process. The P-wave velocities of soil layers beneath the water table are assumed to be 5000 fps. Sometimes higher values in the range of 5500 to 6000 fps are used at significant depths. Values of Poisson's ratio are then calculated from the assumed P-wave velocity and the S-wave velocity at each step in the forward model. The unit weight of the soil beneath the water table is assumed to be 135 pcf.

For rock layers ($V_s \geq 2500$ fps), Poisson's ratio is assumed to be 0.33 and the unit weight is assumed to be 145 pcf.

As an example, consider Site H3A. The parameters that were used to obtain the final shear wave velocity profile in the forward modeling process are presented in Table D.1.1 of Site H3A. The V_s profile at Site H3A is presented in Figure D.1.1. The water table depth of 44 ft that was given by George Last was used in the analysis.

The water table depths that were given by George Last were always used in forward modeling of the field dispersion data. To study the (lack of) sensitivity of the final V_s profile to water table depth in a soil profile, the original depth of 44 ft was varied by +/- 25% as requested by the Technical Integration Team. The best fits to the field dispersion curve of Site H3A for the three water table depths are shown in Figure D.1.2. The best fits for ± 25% involved some additional forward modeling. However, the resulting three V_s profiles are nearly the same as shown in Figure D.1.3. Clearly, there is little sensitivity to the water table depth at Site H3A.

In Question #1, it was not clear if the Technical Integration Team also meant to have us investigate changes in Poisson's ratio. Therefore, the value of Poisson's ratio was also varied. The following three cases were considered: (1) original values of ν (Table D.1.1), (2) assuming a constant value of ν equal to 0.33 throughout the profile, and (3) assuming a constant value of ν equal to 0.25. As seen in Figure D.1.4, good fits are found for all three cases. The sensitivity of the final V_s profile of Site H3A to these changes in Poisson's ratio is presented in Figure D.1.5 which shows an insignificant sensitivity over the range in V_s values studied. Although it could be argued that the value of Poisson's ratio could vary over a much larger range, that large range would be unrealistic for this site in which the water table remained in the soil

Table D.1.1 Parameters Used to Obtain the V_s Profile of Site H3A Shown in Figure D.1.1

Layer No.	Layer Thickness, ft	Depth of the Top of the Layer, ft	V_S, fps	Poisson's Ratio	V_P, fps	Total Unit Weight, pcf
1	1	0	310	0.25	537	125
2	0.9	1	370	0.25	641	125
3	2.8	1.9	650	0.25	1126	125
4	2.2	4.7	750	0.25	1299	125
5	22.5	6.9	1350	0.25	2338	125
6	15	29	1450	0.25	2511	125
7	18	44	1500	0.46	5000	135
8	30	62	1600	0.45	5000	135
9	50	92	2200	0.40	5000	135
10	120	142	4000	0.33	7941	145
11	100	262	4500	0.33	8934	145
12	279	362	5500	0.33	10919	145
13*	Half Space	641	5500	0.33	10919	145

* Layer extends below maximum depth of the V_s Profile.
▽ Water table reported at a depth of 44 ft
+ Not assumed but back-calculated from V_p = 5000 fps and V_s

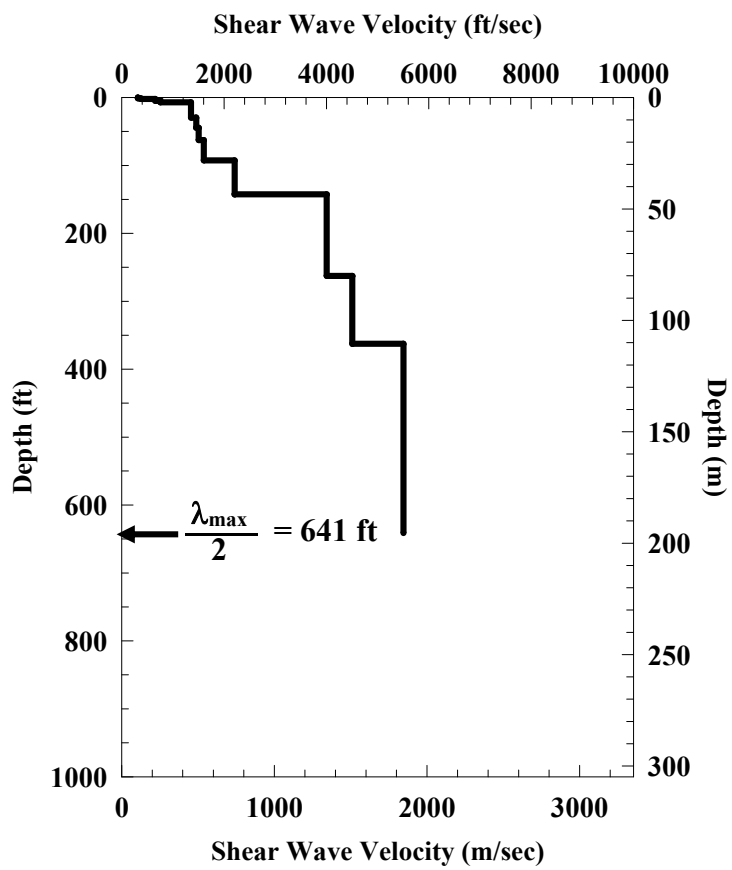

Figure D.1.1 Final Shear Wave Velocity Profile Determined at Site H3A

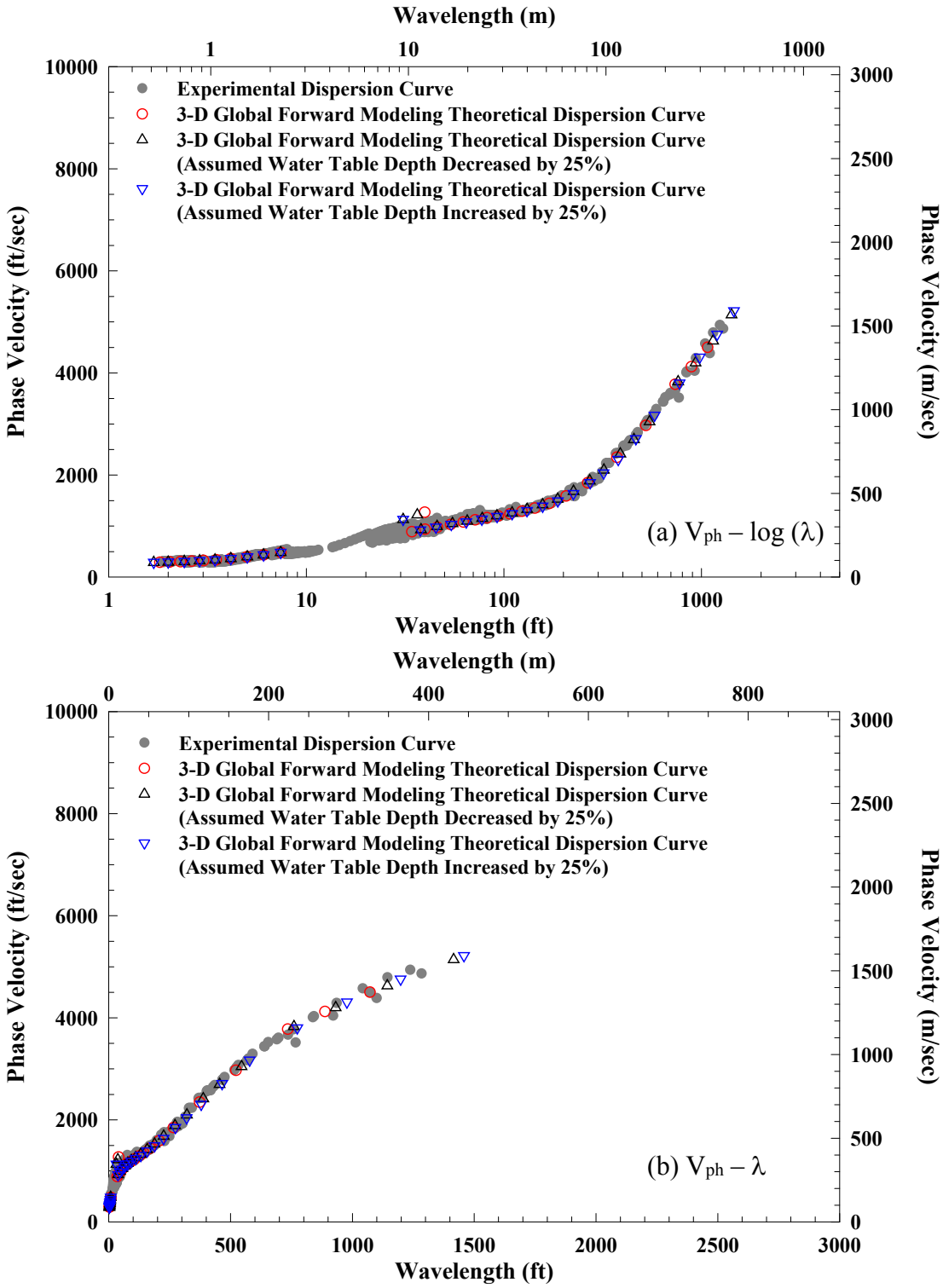

Figure D.1.2 Field Dispersion Curves for Site H3A for Three Water Table Depths

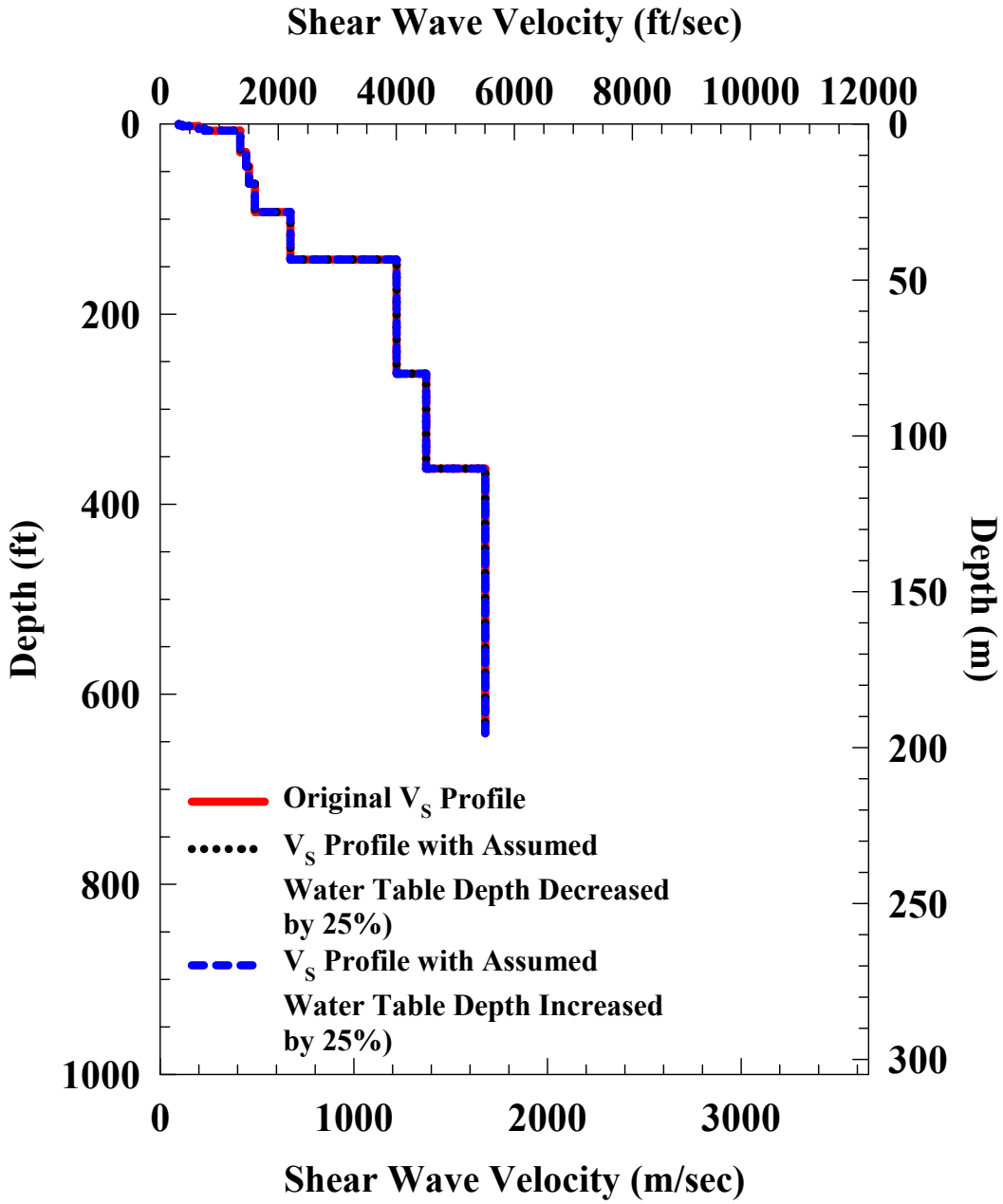

Figure D.1.3 V_s Profiles for Site H3A for Three Water Table Depths

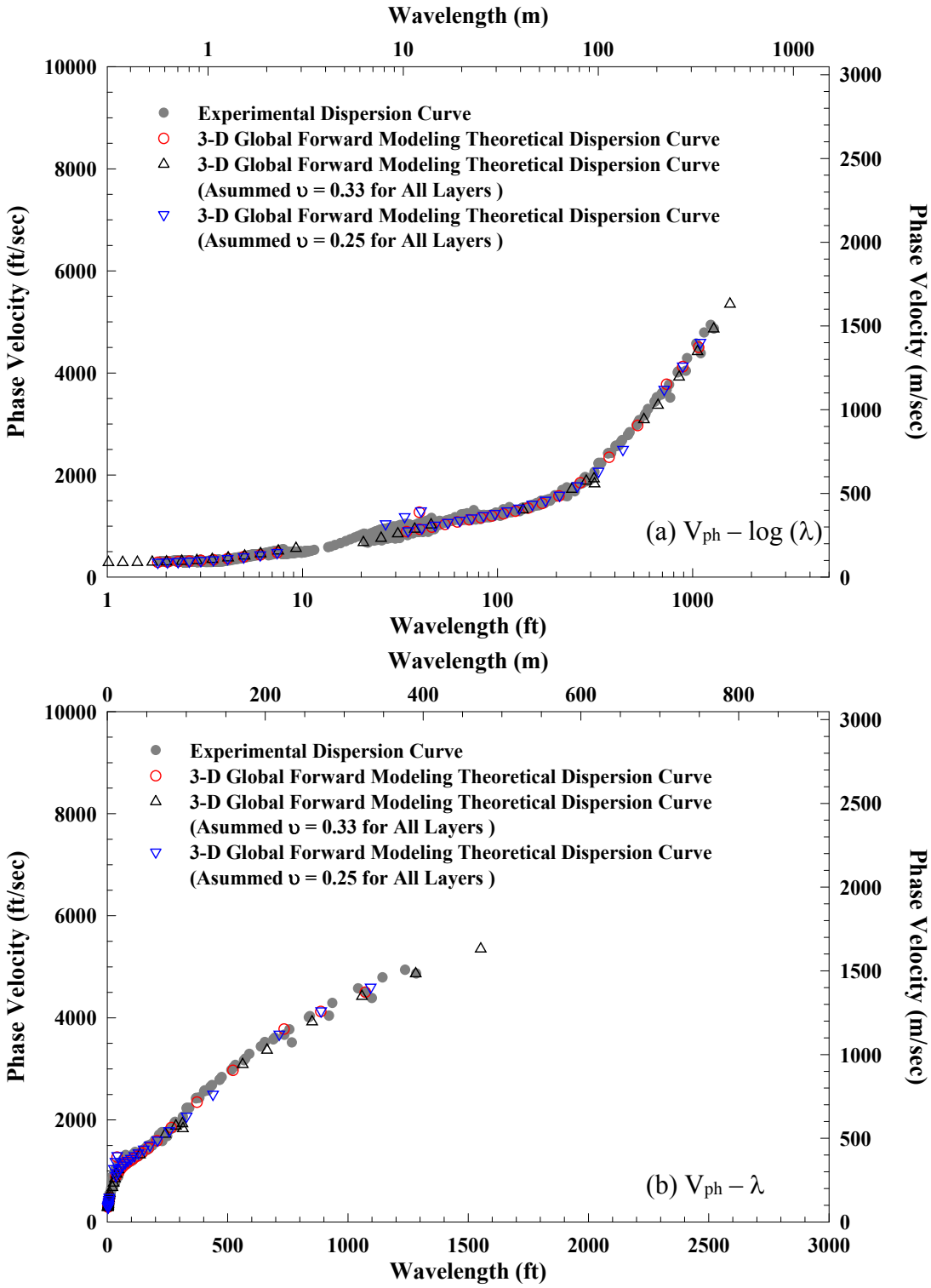

Figure D.1.4 Field Dispersion Curves for Site H3A using Different Assumptions for Poisson's Ratio

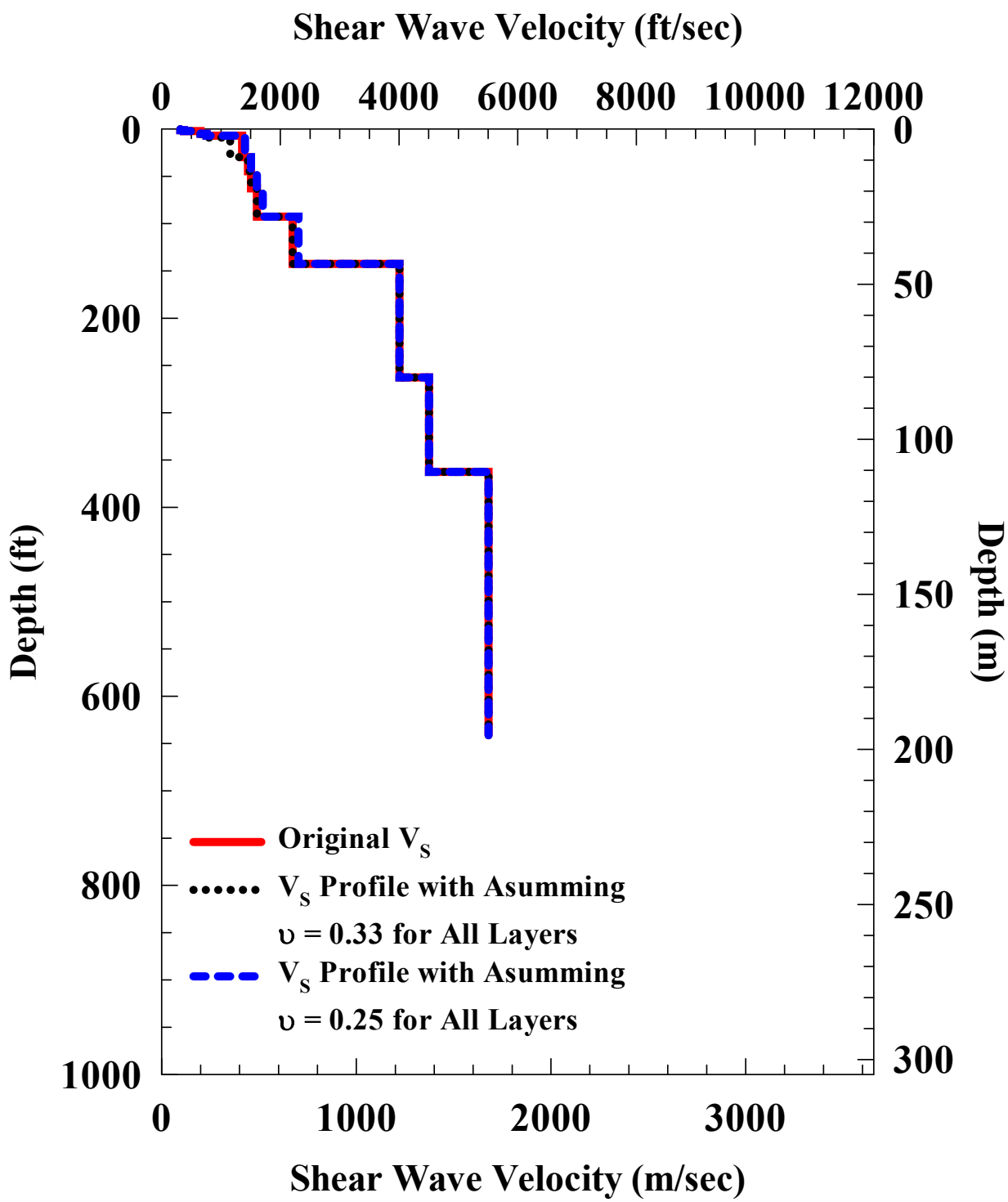

Figure D.1.5 V_s Profiles for Site H3A using Different Assumptions for Poisson's Ratio

Question #2

Please provide discussion and insight regarding dispersion curves and the differences in the Vs profiles at HAWA. One of the two long lines was run parallel to the slope (HAWA1) and another ran downslope past the underground bunker (HAWA3). Can you comment about the possible two-dimensional effect of thickening layers downslope that might account for the difference between these (nearly) perpendicular lines? Also please show how changing the deep velocity layer between 6000 and 9000 fps affects the calculated dispersion curves in comparison to the measured dispersion (see below).

Response:

The response to this question is covered in large part in the response to Question #4. The dispersion curves presented in Figure D.2.1 (same figure as Figure D.4.2) show the effect of reducing V_s of the bottom layer at Site HAWA 1 from 9000 fps to 7200 fps. The difference in the field (experimental) dispersion curve and the theoretical dispersion curve is significant at long wavelengths. As noted in Response #4, uncertainty arises in the value of 9000 fps due to possible shifting in modes which requires measurements at wavelengths longer than captured in the field test.

In terms of Site HAWA 2+3, the dispersion curves are shown in Figure D.2.2 (same figure as Figure D.4.1). If the V_s value of the bottom layer is increased from 6100 to 7625 fps (V_s bottom layer $\times$ 1.25), a significant difference between the field dispersion curve and the theoretical dispersion curve occurs at long wavelengths. However, the lack of long wavelengths in the field data increase the uncertainty in the V_s of the bottom layer.

The thickening of layers downslope would only be important if it occurred more locally in the area along Site HAWA 1. George Last can possibly address this situation. However, a wide gully with softer soil along the line of Site HAWA 2+3 would lower the velocity at this site. Again we need George Last's input.

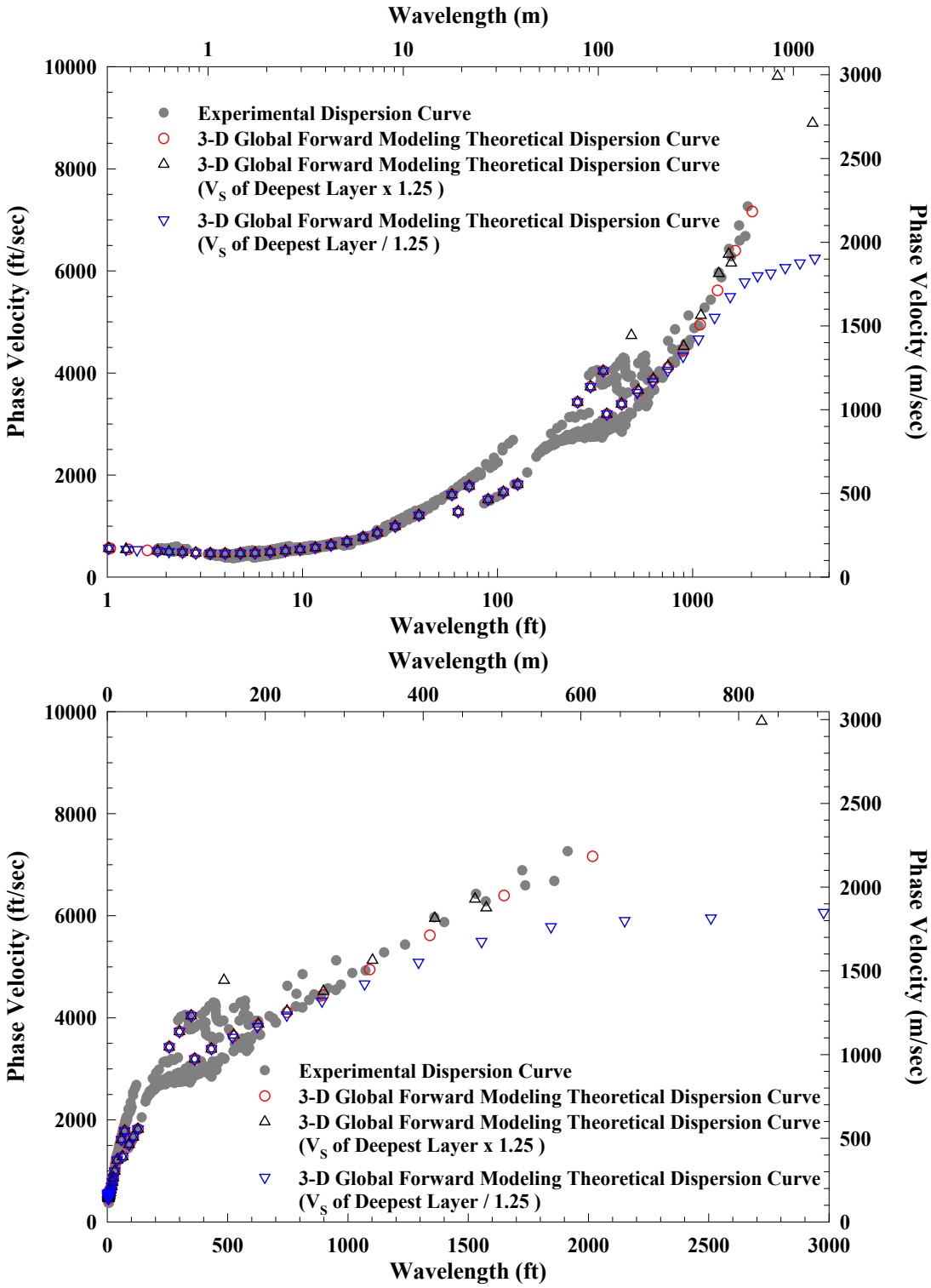

Figure D.2.1 Field Dispersion Curves for Site HAWA 1 using Different Assumptions for the V_s Value of the Bottom Layer

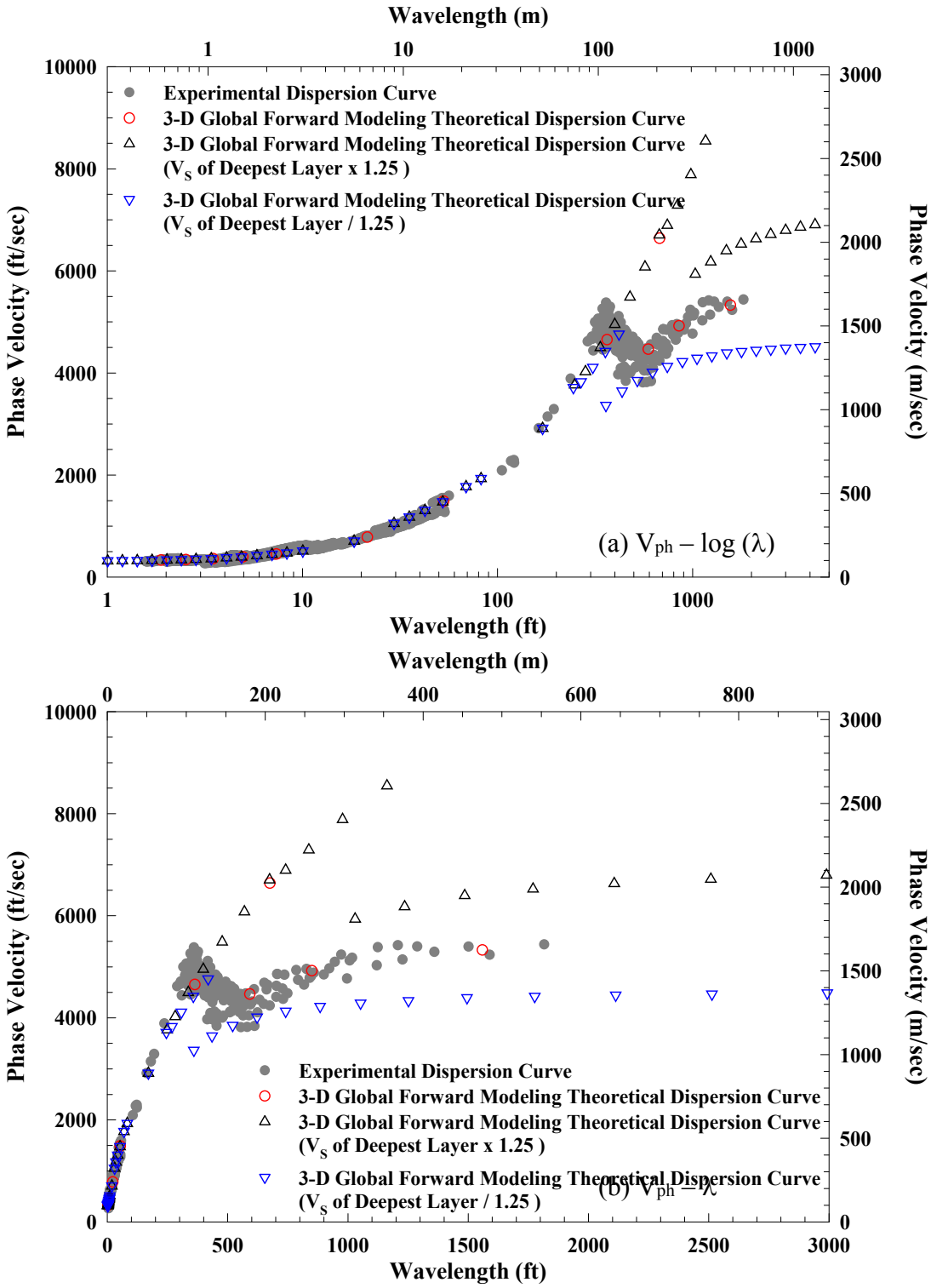

Figure D.2.2 Field Dispersion Curves for Site HAWA 2+3 using Different Assumptions for the V_s Value of the Bottom Layer

Question #3

We received your revised Bunker interpretation, but we do not have an explanation for surface differences or do not fully understand when you indicated that near-field data have been removed - it appears that the data from longer station spacing was removed. The result seems more reasonable now that the "concrete" layer is 3 or so feet thick - can you give a range of possible uncertainty? What do you think of the unusually low Vs for this concrete layer?

Response:

The original field dispersion data from the Bunker site included the normal SASW dispersion data plus some near-field data. Normal includes V_{ph} for wavelength (λ) ranging from $2\Delta X$ to ΔX / (2 to 3). The value of ΔX is equal to the distance between the two receivers used in the measurement and also the distance from the source to the first receiver. In an attempt to go deeper in the confined space of the Bunker complicated by exterior and interior walls, V_{ph} data for longer wavelengths were (unwisely) included. These data involved λ ranging up to $3\Delta X$ or more. The longer wavelength data (from $\lambda > 2\Delta X$) are termed near-field data. The measurements were further complicated by having to use 4.5 Hz geophones which could not measure frequencies above 800 Hz; hence no short wavelengths that sampled only the concrete floor slab were measured.

In the second set of tests, accelerometers were used to measure wavelengths ranging from 0.3 to 12 ft and no near-field data were included. The concrete was well characterized with short wavelengths (0.3 ft $> \lambda >$ 5 ft). The values of V_s of the concrete are low and quite variable. We have reviewed the raw field data. It is robust and I feel that the V_s values of the concrete in the upper portion of the floor slab are correct. However, this concrete is the poorest and most variable I have ever measured. My experience with concrete covers almost 20 years and includes concrete highway pavements, airport pavements, floor slabs, beams, thick concrete fills and tunnel liners.

With regard to uncertainty in the measurements, the situation of a stiff surface layer over softer geological materials is difficult and requires wavelengths many times (3 to possibly as much as 10 times) the surface layer thickness. We were unable to

generate these wavelengths in the confined space at the Bunker site. Therefore, the upper portion of the concrete is well defined but there is uncertainty in the thickness of the concrete, the stiffness near the bottom of the concrete, and the stiffness of the geologic materials over some depth below the concrete floor. The uncertainty also arises from the mode jumping that occurs in this type of layered system with a significant inversion.

Question #4

Please also include your estimates of uncertainty in the profiles; The team suggests exploring this by applying +/- 25% (logarithmic – multiplicative factor) to the deeper velocities and seeing the impact this has on the dispersion curves. It is suggested that this sensitivity study be conducted on both the HAWA1 and HAWA2/3 deep profiles mentioned in Question 2. (Note: Dr. Rohay clarified that the profiles should simply be evaluated using $V_s \times 1.25$ and $V_s / 1.25$.)

Response:

The effect of changing the V_s value of the bottom layer by $V_s \times 1.25$ or $V_s / 1.25$ many times falls into one of three categories: (1) very sensitive to this change so that neither theoretical dispersion curve ($V_s \times 1.25$ or $V_s / 1.25$) would be considered after one or two iterations in the fitting process, (2) sensitive which means that the original fitting process was continued until it converged to a best fit that was within the range of $V_s \times 1.25$ and $V_s / 1.25$, or (3) the theoretical dispersion curve with $V_s \times 1.25$ is close to the field dispersion curve and long enough wavelengths have not been measured in the field test to allow a more precise value of V_s to be resolved for the deepest layer, but the lowest V_s value ($V_s / 1.25$) falls below the field dispersion curve. As an example of Category #1, consider Site H2W2006. The theoretical dispersion curves for Site H2W2006 are shown in Figure D.4.1. Neither the theoretical curve for $V_s \times 1.25$ nor the theoretical curve for $V_s / 1.25$ in the model come close to approximating the field dispersion data at longer wavelengths, λ greater than about 1000 ft. Another example of a Category #1 site is Site WIAB. The theoretical dispersion curves for Site WIAB are compared with the field dispersion curve in Figure D.4.2.

An example of a site with a field dispersion curve that falls in Category #2 is Site H4A. As seen in Figure D.4.3, the theoretical dispersion curve determined with $V_s / 1.25$ data is below the field dispersion curve at long wavelengths, $\lambda > 1200$ ft. Also, the $V_s \times 1.25$ forward modeling data are above the field dispersion curve for $\lambda > 1500$ ft.

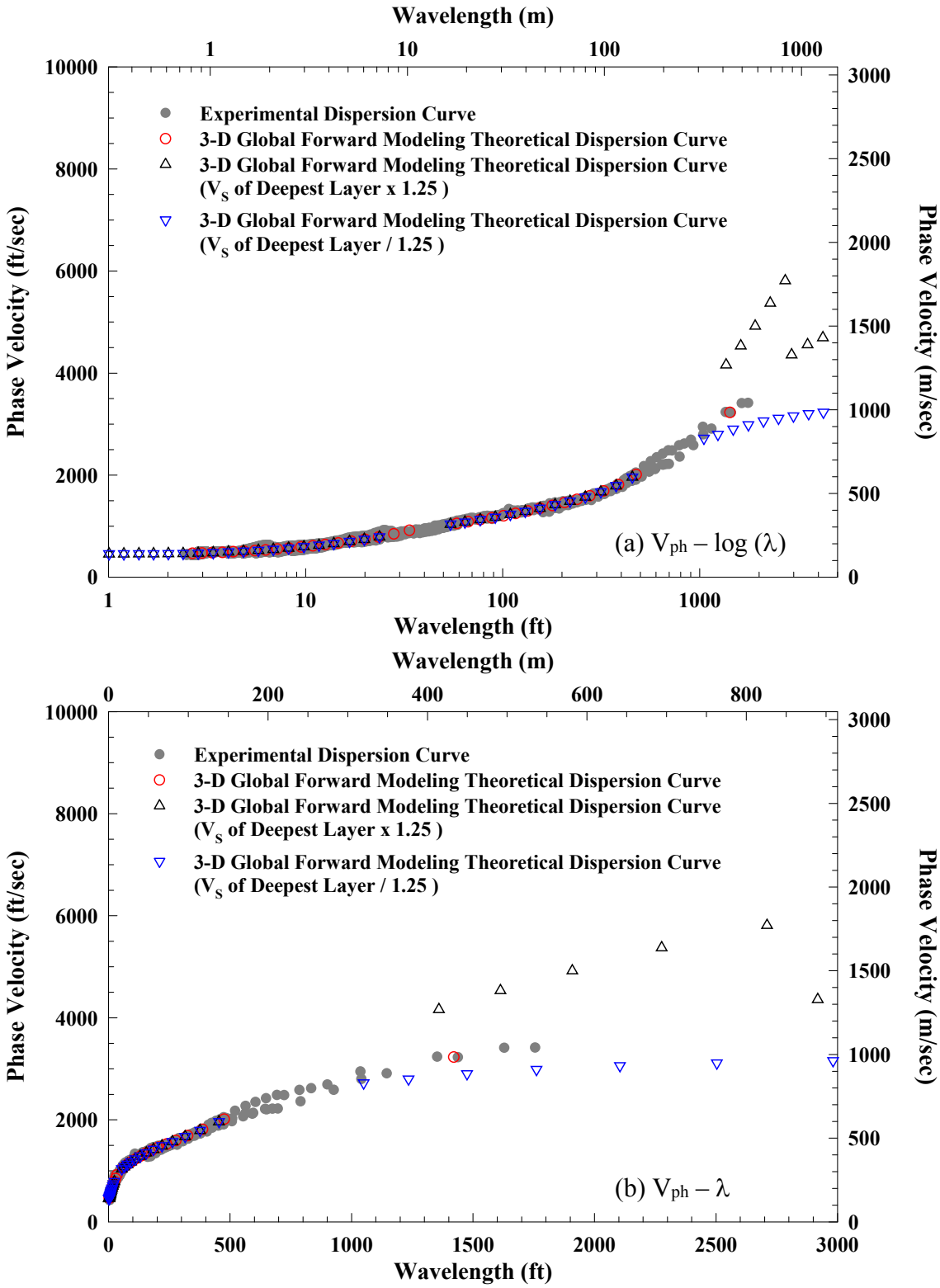

Figure D.4.1 Field Dispersion Curves for Site H2W2006 using Different Assumptions for the V_s Value of the Bottom Layer

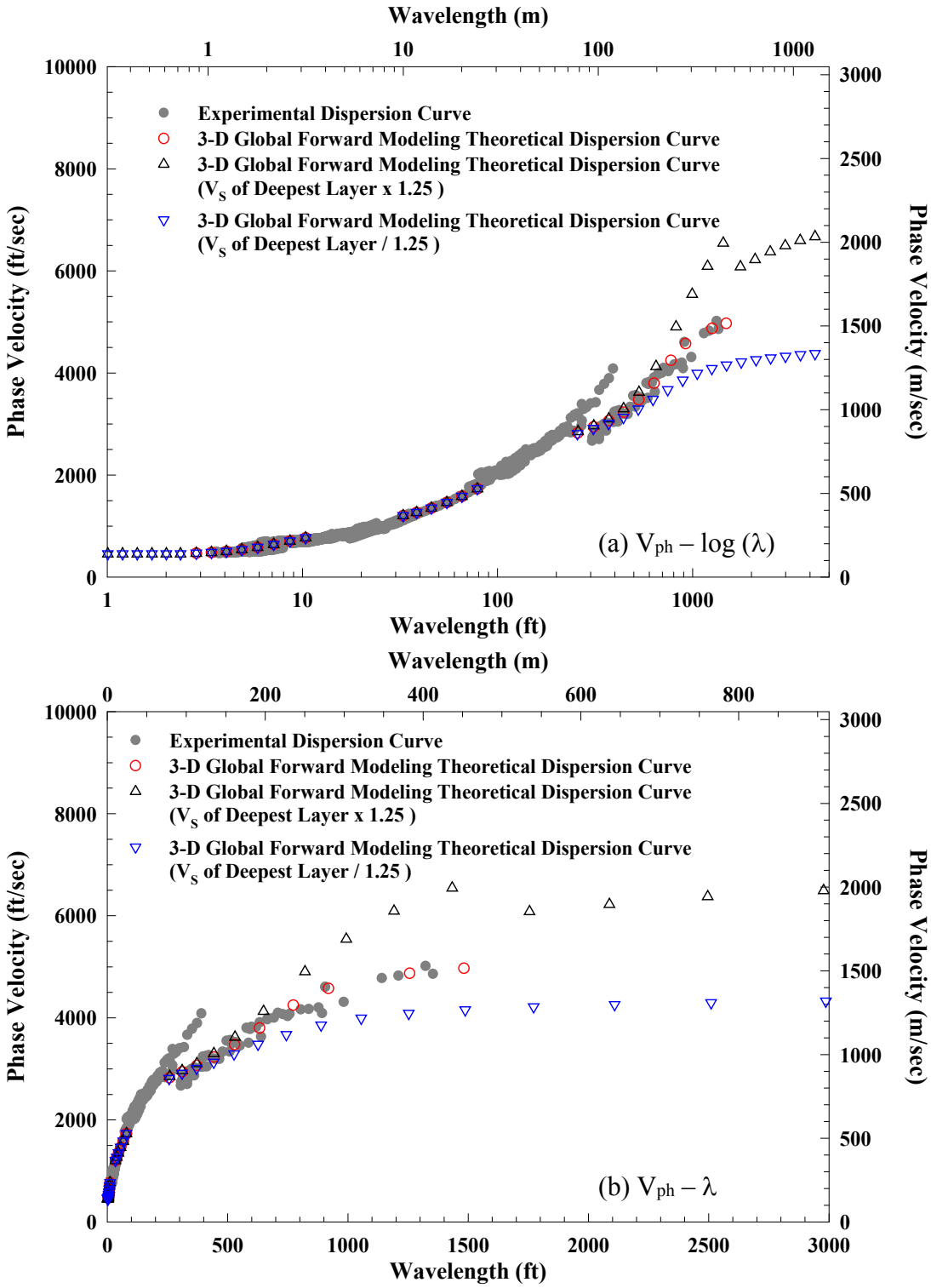

Figure D.4.2 Field Dispersion Curves for Site WIAB using Different Assumptions for the V_s Value of the Bottom Layer

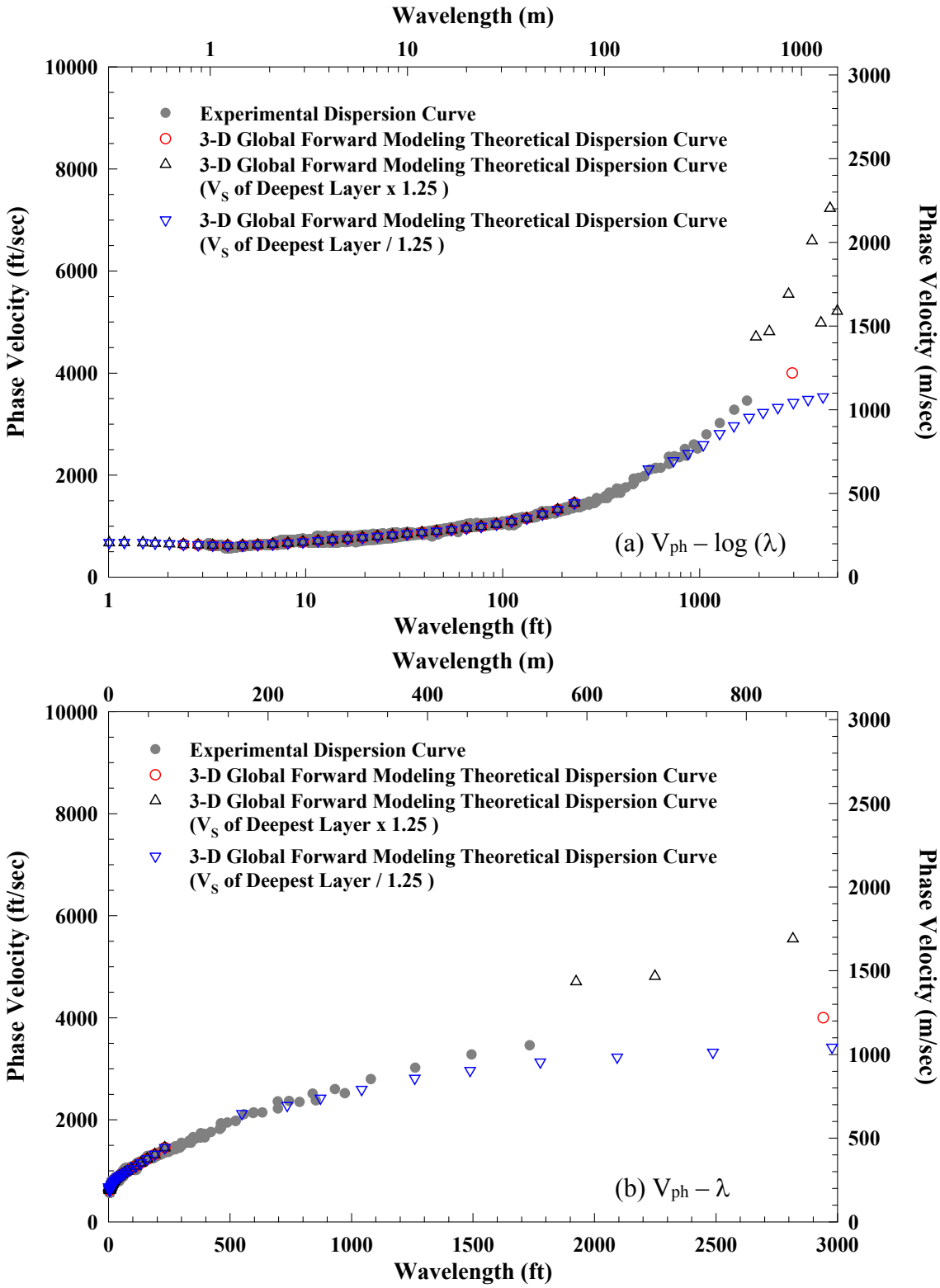

Figure D.4.3 Field Dispersion Curves for Site H4A using Different Assumptions for the V_s Value of the Bottom Layer

An example of a site that falls in Category #3 is H2E. Comparison of the dispersion data is presented in Figure D.4.4. The theoretical dispersion curve for V_s / 1.25 is trending below the field dispersion curve. On the other hand, the theoretical dispersion curve for $V_s \times 1.25$ is just slightly above the field dispersion curve at the longest wavelengths. To improve the sensitivity of the deepest part of the V_s profile, measurements of the dispersive characteristics of longer wavelengths are needed.

Now to the sensitivity study of Sites HAWA 1 and HAWA 2+3 requested by the Technical Integration Team. Both sites are Category #3 sites. The field (experimental) dispersion curve of Site HAWA 1 is compared with the theoretical dispersion curves ($V_s \times 1.25$ and V_s / 1.25) in Figure D.4.5. It appears that the lower velocity (V_s / 1.25) does not fit and the higher velocity is not well defined. The possible complication is that the rapidly increasing value in V_{ph} with λ in the range of the longest wavelengths ($\lambda > 1100$ ft) may represent a transition to a higher mode. Therefore, there is uncertainty and the measurements of longer wavelengths in the field would be required to resolve this issue.

The field dispersion curve of Site HAWA 2+3 is compared with the theoretical dispersion curves ($V_s \times 1.25$ and V_s / 1.25) in Figure D.4.6. The apparent shift from a higher mode to the fundamental mode as λ goes from 400 ft to 600 ft requires the bottom layer to have V_s at least equal to 6100 fps. However, the data are sparse for wavelengths greater than 1200 ft. Measurements of longer wavelengths are required to determine if the trend exhibits a V_{ph} increasing more rapidly than implied; hence V_s is larger than 6100 fps.

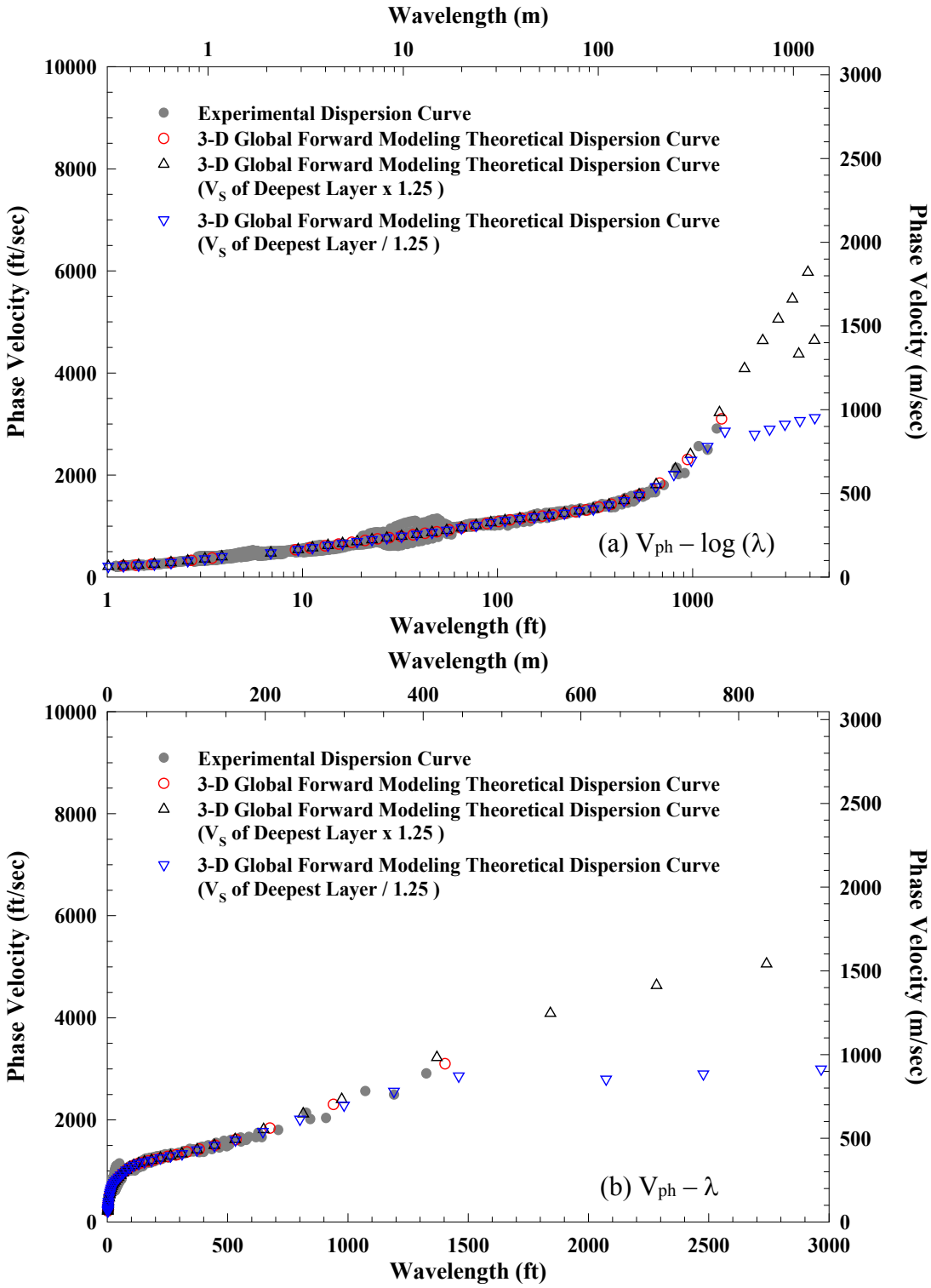

Figure D.4.4 Field Dispersion Curves for Site H2E using Different Assumptions for the V_s Value of the Bottom Layer

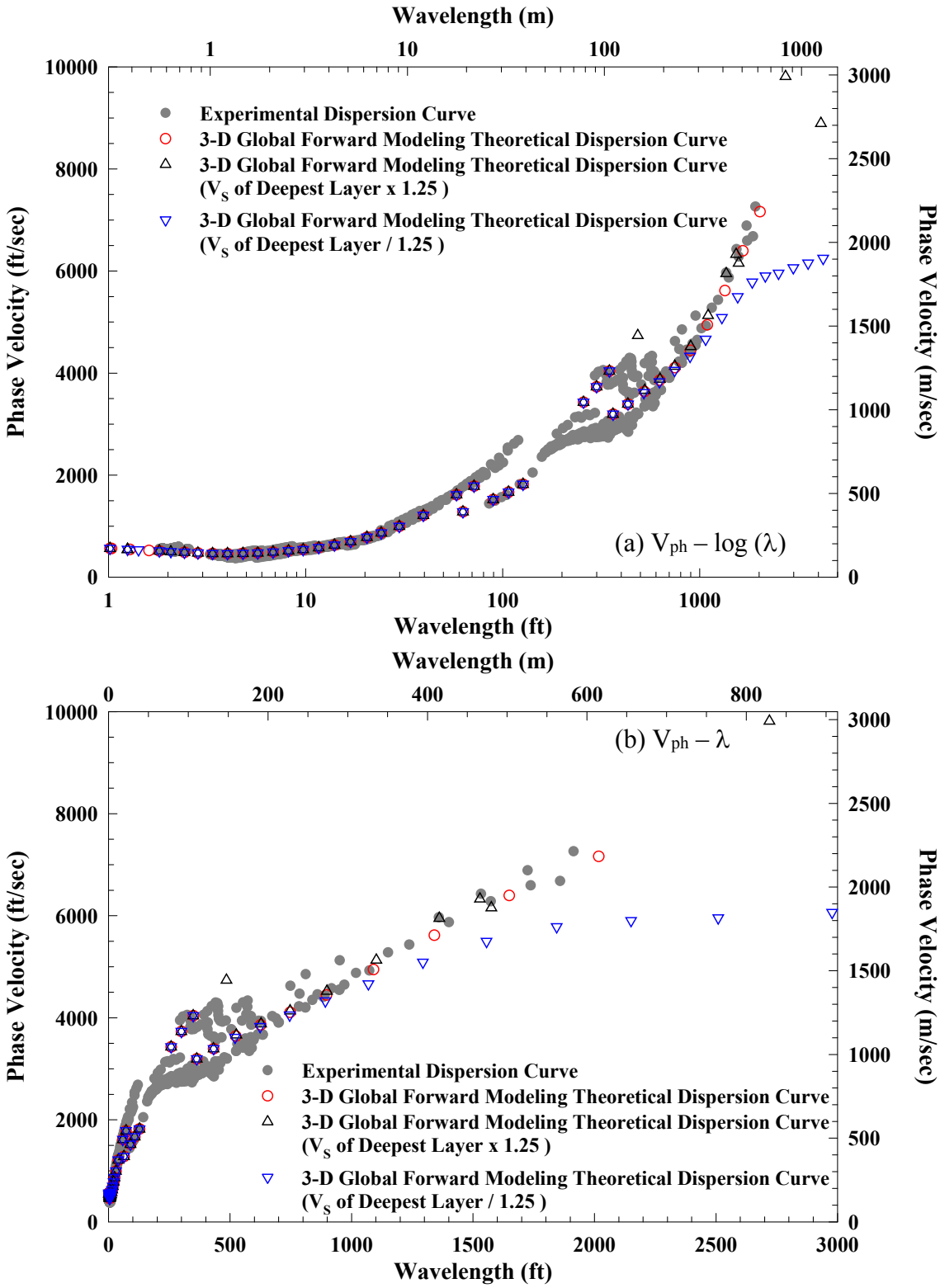

Figure D.4.5 Field Dispersion Curves for Site HAWA 1 using Different Assumptions for the V_s Value of the Bottom Layer